Design and Synthesis of Molecular Probes for Biological and Environmental Significant Ions

Thesis Submitted to AcSIR for the Award of the Degree of

DOCTOR OF PHILOSOPHY

In Chemical Science

(Academy of Scientific and Innovative Research)

By

Hridesh Agarwalla
(Reg.No. 10CC12J26034)

Under the guidance of

Dr. Amitava Das

CSIR-National Chemical Laboratory
Pune, Maharashtra, India– 411008

August 2016

CANDIDATE'S STATEMENT

I hereby declare that the work incorporated in the present thesis is original and has not been submitted to any University/Institution for the award of a Diploma or a Degree. Research material obtained from other sources has been duly acknowledged in the thesis. Any text, illustration, table etc., used in the thesis from other sources, have been duly cited and acknowledged." further declare that the results presented in the thesis and the considerations made therein, contribute in general to the advancement of knowledge in chemistry and in particular to **"Design and Synthesis of Molecular Probes for Biological and Environmental Significant Ions"**.

Hridesh Agarwalla

Hridesh Agarwalla

AcSIR

वैज्ञानिक तथा नवोन्मेषी अनुसंधान अकादमी
ACADEMY OF SCIENTIFIC & INNOVATIVE RESEARCH
अनुसंधान भवन, 2, रफी मार्ग, नई दिल्ली - 110 001
Anusandhan Bhawan, 2, Rafi Marg, New Delhi - 110 001

CERTIFICATE BY SUPERVISOR

This is to certify that the contents of this thesis entitled **"Design and Synthesis of Molecular Probes for Biological and Environmental Significant Ions."** is the original research work of **Mr. Hridesh Agarwalla,** carried out under my supervision at CSIR-National Chemical Laboratory, Pune, India.

Further, I hereby certify that the work has not been submitted either partly or fully to any other University or Institution for the award of any degree.

Signature of Supervisor

(Dr. Amitava Das)

Phone: 011-2370 8387, 2335 2097 (direct), EPABX: 2371 0138, 2371 0144, 2371 0158, 2371 0468, 2371 1251
Ext.: 301, 331, Fax: 91-11-2371 0340, Website: http://acsir.res.in

ACKNOWLEDGEMENTS

I whole heartedly express my deep sense of gratitude to **Dr. Amitava Das** – My Guide. I am extremely grateful to him for his continuous encouragement, timely advise, scholarly monitoring and invaluable suggestions. I am really thankful for the freedom that he gave to my research life. I grew as a research student watching him working till late night every day, which has been the source of inspiration to me.

I wish to convey my gratefulness to ***Dr. Biswajit Ganguly, Dr. Arindam Chaudhury, Dr. Santosh Mhaske, Dr. Samit Chattopadhyay, Dr. Sameer Jadav, and Dr. Divesh Srivastava*** for fruitful discussions on research problems, appreciative comments, and continuous guidance whenever I approached which helped me to explore various aspects of the chemistry.

I am also thankful to ***Prof. Kyo Han Ahn*** (POSTECH, Korea), Yong Woong Jun and Juryang Bae who helped me to explore the Two-photon microscopy technique.

I wish to express my sincere thanks to my Doctoral advisor committee ***Dr. J Nithyanandan, Dr. Santosh Mhaske*** and ***Dr. Sakya Singha Sen*** for their continued encouragement and valuable suggestions.

I wish to express my word of thanks to ***Dr. P. K. Ghosh*** (Former Director, CSMCRI, Bhavnagar), ***Dr. Sourav Paul*** (Former Director, NCL-Pune), ***Dr. Ashwini K. Nangia*** **(**Director, NCL), ***Dr. Parimal Paul*** (Discipline Coordinator, CSMCRI) ***Dr. Pradeep Kumar***, Head, Division of Organic Chemistry for providing me opportunity and all necessary facilities to carry out my research work.

My sincere thanks to ***Dr. D. S. Reddy***, ***Dr. S. B. Sukumaran***, ***Dr. R. A. Joshi, Dr. Rahul Banerjee, Dr. Sayam Sengupta***, ***Dr. B. L. V. Prasad***, ***Dr. P. S. Subramaniayan, Dr. S. P. Mukherjee, Dr. A. K. Siddhanta, Dr. R. I. Kureshi and Dr. Adimurthy*** and all other scientists of NCL and CSMCRI for their motivation, constant encouragement and support.

I would like to express my special thanks to my seniors ***Dr. Moorthy Suresh, Dr. Prasenjit Mahato, Dr. Amal Kumar Mandal, Dr. Priyadip Das, Dr. Sukdeb Saha, Dr. Tanmay Banerjee***. They all taught me in my initial days of my research carrier and took me along with them.

I feel fortunate enough to have wonderful group of colleagues ***Ramu***, ***Upendar***, ***Monalisa, Arunava, Firoj, Dr. Praveen L., Dr. Sovan Roy, Dr. Shilpi Kushwaha, Dr. Ketan Patel, Dr. Suman Pal, Dr. Ajoy Paul, Sunil, Anil, Koushik, Sanjukta and Ananta*** with whom I worked all these five year. Each one of them equally contributed in different

way to take up my course so fruitfully throughout these five years. I thank all of them individually from the bottom of my heart.

My Sincere thanks to my friends and collaborators ***Manoj Kesharwani, Kalyanashis Jana, Debashis Ghosh, Nandaraj Taye, Dharmendar Sharma, Santanu Basu, Pankaj Mahajan, Subhas Tanpure, Anirban Paul*** who are an important part of my journey.

My sincere thanks to all my friends for their support and to my make my journey joyful and a memorable one. I thank all of you ***Dibyendu, Milan, Jaswanta, Supratim, Pritam, Arnab, Debashis, Debdeep da, Mukesh, Anup, Santi, Pravat da, Partha da, Kanak da, Achintya da, Susanta da, Arpan da, Arya da, Pati da, Saikat da, Shyam da, Chandan da, Himadri da, Krishanu da, Siba, Manzoor, Saibal, Subrata, Avijit, Sandeepan, Mohitosh, Somsuvra, Indrwadeep, Sutanu, Manik, Santanu, Tapas, Tamal, Debu, Subhrasis, Pranab, Anirban, Sudip, Suman, Bittu, Atanu, Tamal, Somnath, Indranil, Monotosh, Pritam, Avik.***

I would like to extend my sincere thanks to my teachers Subodh Sir, Prabir Sir and Late Mohit Babu for their sincere efforts and patience in guiding me from my school days.

My sincere thanks to Dr. Kishan Chand Gupta for his encouragement and guidance.

I wish to thank **CSIR** for financial assistance and **AcSIR** for allowing me to submit my work in the form of thesis.

At this moment, I invariably feel short of words to express my sincere thanks to My Grand Parent Late ***Gobinda Agarwalla*** *and* ***Gita Agarwalla***, my father ***Sri. Ashoke Kumar Agarwalla*** and mother ***Smt. Renu Agarwalla*** and beloved sister ***Priyanka*** and brother-in-law ***Ashish*****,** for their love, prayers and support which inspired me and strengthen throughout my life. I thank all my well-wishers whose continuous encouragement and support in completion of this tough task.

I am also thankful to *Almighty God* for all your blessings to me and for the strength you give me each day.

List of Abbreviation

CD_2Cl_2	Deuterated dichloromethane
$CDCl_3$	Deuterated chloroform
CD_3OD	Deuterated Methanol
DMSO-d_6	Deuterated Dimethyl sulfoxide
CD_3CN	Deuterated acetonitrile
DMF	N,N'-dimethylformamide
DMSO	Dimethyl sulfoxide
THF	Tetrahydrofuran
ACN	Acetonitrile
ESI	Electrospray Ionization
ET	Energy Transfer
HOMO	Highest Occupied Molecular Orbital
LUMO	Lowest Unoccupied Molecular Orbital
MLCT	Metal to Ligand Charge Transfer
ICT	Intranolecular Charge Transfer
TICT	Twisted Intramolecular Charge Transfer
PET	Photo-induced Electron Transfer
ESIPT	Excited State Intramolecular Proton Transfer
ESICT	Excited State Intramolecular Charge Transfer
TBET	Through Bond Energy Transfer
NIR	Near Infrared
HEPES	4-(2-hydroxyethyl)-1-piperazineethanesulfonic acid

List of Abbreviation

NMR	Nuclear Magnetic Resonance
FTIR	Fourier Transform Infrared
MTT	3-(4,5-dimethylthiazol-2-yl)-2,5-diphenyltetrazolium bromide
CLSM	Confocal Laser Scanning Microscope
DFT	Density Functional Theory
CTAB	Cetyltrimethylammonium Bromide
TIRF	Total Internal Reflection Fluorescence
TPM	Two Photon Microscopy
TPACS	Two Photon Action Cross Section
ISE	Ion-Selective Electrode
PBS	Phosphate Buffer Saline
HSA	Human Serum Albumin
NEM	N-ethylmaleimide
NAC	N-acetylcystiene

Contents

CHAPTER 1

INTRODUCTION

1. A Brief Introduction of Synthetic Chemosensor of Important Analytes

Many important analytes such as cations, anions and neutral molecules play multifarious roles in various chemical, biological and environmental events. At times, it can exceed its maximum tolerable limit and can be toxic in the environment, water supplies, food chain, industrial products and wastes. Consequently, serious efforts have been made to develop molecules for qualitative and quantitative detection of these ions in aqueous and non-aqueous medium.[1] Thus, detection and specific recognition of ions have indeed become an important topic of research in supramolecular chemistry, diagnostics, clinical biology, biomarkers and environmental sample analysis.[2] Hence the design of purpose-built molecules or methods for specific recognition and quantification of analytes are of fundamental importance.

Among the numerous traditional analytical methods available, techniques like titrimetric, atomic absorption spectrometry, ion sensitive electrodes, High Performance Liquid Chromatography (HPLC) *etc.* are common.[3] However, most of these above mentioned techniques are expensive and often require samples of large size and involve pre-treatment for sample preparation which is neither well-suited for quick *in-field* detection nor for *in vivo* studies.[4]

Purpose built designer molecules which show specificity and selectivity towards particular analytes, have gained significant interest in the field of host-guest chemistry. These colorimetric/fluorogenic receptor molecules produce optical response(s) in the form of electronic and fluorescence spectral changes upon interaction with the targeted analyte. Chromogenic receptors offer the possibility for naked eye detection along with the quantitative estimation of the analyte, whereas fluorescence-based receptors offer higher sensitivity as well as the option for imaging application and non-invasive measurement in biological system.[5]

Designing an efficient chemosensor involved an appropriate choice of receptor unit that is covalently bound to a signaling unit through a conduit for effective signal transduction upon receptor-analyte binding. Choice of receptor depends on the nature of the target analyte; while that for signaling unit, it is about the nature of the optical responses that is desired. Chemosensors can be broadly classified into three different categories depending upon receptor analyte interaction namely, (i) Binding-site signaling approach (ii) displacement approach (iii) chemodosimetric approach (Figure 1.1). In binding-site signaling approach, receptor and signaling unit are covalently bonded, and induces a change in electronic or optical properties of signaling unit on interaction with the analyte. The binding interaction

involves mostly electrostatic interaction,[6] π-π interaction,[7] various non-bonded interactions—including hydrogen bonding (H-bonding).[8] Displacement approach relies on a much higher receptor-analyte affinity as compared to the affinity of the receptor for the signaling unit and this relative difference thermodynamically favors the displacement of the signaling unit form the receptor-signaling unit assembly to generate a free signaling unit with modified optical output.[9] Finally, in chemodosimeter approach, receptor molecule reacts specifically with an analyte to generate a product with entirely new optical responses, which could be monitored for recognition and simultaneous quantification of that analyte.[10]

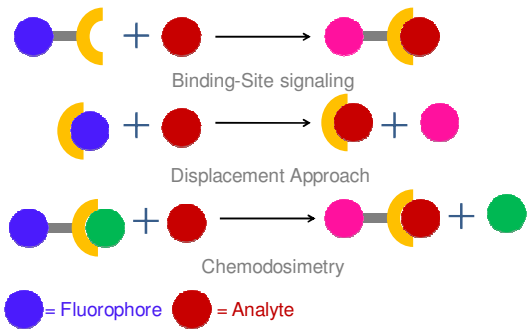

Figure 1.1. Schematic representation of different approaches of chemosensor.

1A. Artificial receptors for anion recognition

1A.1. Introduction

Anions are ubiquitous in nature and play an important role in human physiology as well as in various industrial and natural processes. Presence of such anions is good for human health or environment till concentration of the respective anionic analyte is restricted to a permissive level. Beyond this concentration, each of such anion has a deleterious influence. These led to the necessity for design and synthesis of a receptor that is specific towards a particular anionic species and capable of producing binding induced changes in optical responses.[11] The very first report of synthetic receptor describes size selective binding of Cl^- anions by diprotonated 1,1,1-diazabicyclo-[9.9.9] nonacosane in 1968.[12] In 1976 Graf and Lehn reported a protonated cryptate, which could encapsulate F^-, Br^- and Cl^- ions.[13] Since then several receptors have been reported and most of these rely on electrostatic attraction[14] and metal-anion complexation,[15] π-anion interaction,[16] hydrophobic effects,[17] H-bonds and chemodosimetric reactions.[10a]

The design of anion receptors is particularly challenging due to a number of reasons, e.g. (i) anions are larger than isoelectronic cations, so they have a lower charge to radius ratio than the cations and results a less effective electrostatic interaction, (ii) anions possess a variety of sizes and shape (e.g. spherical, linear, tetrahedral, trigonal planar), which makes the design of the receptor more complicated, (iii) anions are generally sensitive to media pH and the receptor must function within the pH window of their target anion. Despite these challenges several receptors were reported for recognition anions.

1A.2. Various receptors for Fluoride

Owing to its duplicitous nature fluoride (F^-) is one of the most studied anions. Fluoride plays an important role in several biological processes and also can have the detrimental effect on human physiology. Fluoride primarily used in prevention of dental caries and osteoporosis; however, it has been also used in military nerve gasses and anesthetic drugs.[18] Excess intake of fluoride causes fluorosis, neurological and metabolic dysfunction.[19] Concerns are also raised by the fact that fluoride is introduced into the environment through use of fertilizers and use of its various salts in aluminum industries.[20] Fluoride contamination in drinking water is one of the major sources for water pollution. It is also estimated that more than 100 million people are using drinking water which contains F^-, in concentration over the limit suggested by the World Health Organization guidelines (WHO). Hence, there is a need for efficient detection and quantification of F^-.

The most well studied binding motifs for recognition of fluoride ion are those which contain hydrogen bonding units, like urea, thiourea, amides, pyrroles, imidazole, and amines. Depending on the basicity of the anion, both hydrogen bonding interaction and anion induced deprotonation are involved in the recognition event. In some cases, both hydrogen bonded interaction followed by deprotonation at high anion concentration can be observed. Fluoride being the most basic anion in an organic medium often behaves as a Brönsted base and this was explored for sensing purpose.

1A.2.1. Hydrogen bonding based receptors

In this context, Das and coworkers described two anthraquinones based chromogenic receptor for fluoride ion with urea (**1**) and thiourea (**2**) as H-bonding unit (Figure 1A.1).[21] These receptors show high selectivity towards F^- over other halides ions and produce

visual color change with F^- in DMSO/CH_3CN medium. The experimental observation was also corroborated with theoretical calculation.

Figure 1A.1. The structure of receptor **1, 2** and **3** (i) change in color of **1** (top) and 2(bottom) in the presence of different ions F^- (B), Cl^- (C), Br^-(D), I^-(E). (ii) The 1D polymer of **3**.

A number of tripodal receptors consist of amide; urea or thiourea groups are reported which binds fluoride inside the cavity of a tripod. Ghosh and co-workers reported an amide based receptor **3,** (Figure 1A.1) in conjugation with K^+ specific 18-crown-6, which could be used to extract KF from aqueous medium.[22] Receptor **3** is found to bind with F^- and Cl^- in 1:1 fashion and crystal structure of the complexes were shown. N-H_{Amide} acts as H-bond donor and forms a hydrogen bonded adduct with the anions (F^- and Cl^-). KF and KCl were extracted with **3** in the presence of crown ether and subsequent complexes were crystallized in 1D coordination polymer, with F^- encapsulated in the tripodal cavity and K^+ in the crown cavity.

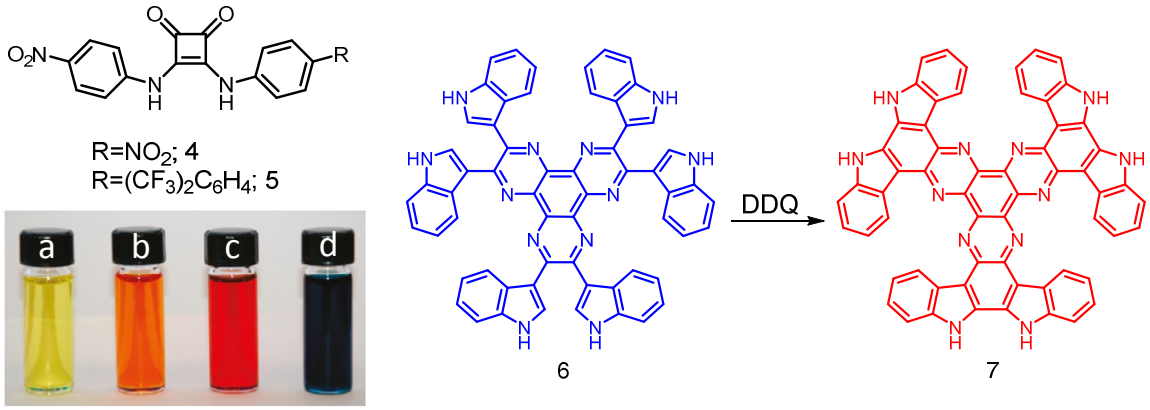

Figure 1A.2. Molecular Structures of the receptor **4-7**. Change in colour of receptor **5** in the presence of (a) Bu_4NOTs (b) No analyte (c) Bu_4NOAc (d) Bu_4NF.

Squaramide derivatives were found to be a better receptor than the urea. The solutions of receptor **4** (Figure 1A.2) in CH_3CN showed weakly red shifted absorption spectra upon

addition of Cl^-, Br^-, I^-, NO_2^-, NO_3^-, $H_2PO_4^-$ and HSO_4^- due to the formation of 1:1 H-bonded adducts.[23] However, interaction of **4** with F^- or AcO^- was quite different; both anions induced a red shift of 30 nm of the 395 nm band, with the appearance of a new absorption band with maximum at 500 nm. This change was ascribed to an anion-induced deprotonation of the receptor. Squaramide receptor **5** (Figure 1A.2) was also reported to be an efficient colourimetric receptor for F^-. It showed an intense blue color on the addition of TBAF and was attributed to double deprotonation of the receptor molecule **5**.[24]

Bu *et al*. reported, two receptors containing biindole and indolecarzole NH for recognition of F^- was reported.[25] Both **6** and **7** (Figure 1A.2) displayed yellow to golden-red colour change on addition of F^-. On addition 21 mole equivalents of F^-, no colour change was observed for **6** and then on further addition of F^- colour turned golden-red. Receptor **7** with a more rigid structure, showed two distinct changes in emission spectral pattern on gradual increase on [F^-]. Initial fluorescence quenching (till 10 mole equivalents of F^- was added) was attributed to an effective photoinduced electron transfer (PET) process. On further addition (≤100 mole equivalent) of F^-, a new band with a maximum at 602 nm appeared. This was ascribed to the deprotonation of the receptor **7** and this deprotonated species favored an intramolecular charge transfer (ICT) process with indole phenyl ring as the donor moiety and was accounted for this new band at 602 nm.

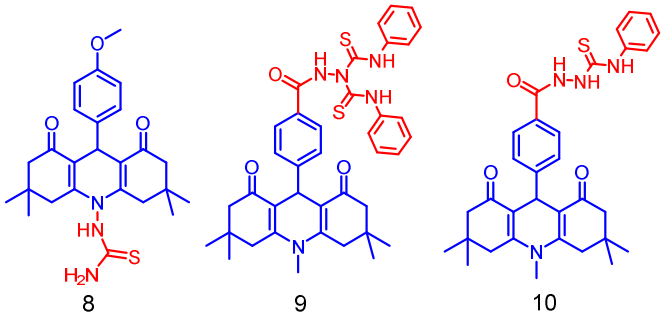

Figure 1A.3. Structures of chemosensor **8-10**.

Ramamurthy and co-workers reported thiourea-linked acridinedione derivatives **8** (Figure 1A.3) for detection of F^- by fluorescence spectroscopy.[26] Compound **8** showed a change in absorption and emission spectra in the presence of F^-, OAc^- and $H_2PO_4^-$. In presence of OAc^- and $H_2PO_4^-$, red shifted absorption spectrum and fluorescence enhancement at 484 were observed and these changes were attributed the to the H-bonded adduct formation. For F^- two distinct changes were observed in both absorption and emission spectra. At

lower [F⁻], a redshifted absorption band and emission band at 473 nm appears due to H-bonded complex. However, in presence of higher [F⁻], new absorption and emission spectra with respective maximum at 459 and 502 nm is observed due to deprotonation.

They also reported receptors **9** and **10** (Figure 1A.3) for F⁻ recognition.[27] For Compound **9**, an initial blue shift in the absorption spectrum was observed in presence of relatively lower [F⁻] and then a red shift on further increase in [F⁻]. These changes in absorption spectra were attributed to the formation of H-bonded complex and its subsequent deprotonation of the receptor, respectively. At low concentration for F⁻, fluorescence quenching occurred due to an efficient PET process, but further addition of F⁻ led to a new emission peak at 600 nm due to the formation of new CT State of the deprotonated receptor. Amidothiourea **10** in acetonitrile showed an emission quenching on addition of F⁻ without any spectral shift—a typical response of a classical PET sensor, which emphasized the importance of the bisthiourea derivative in the formation of new CT emission state.

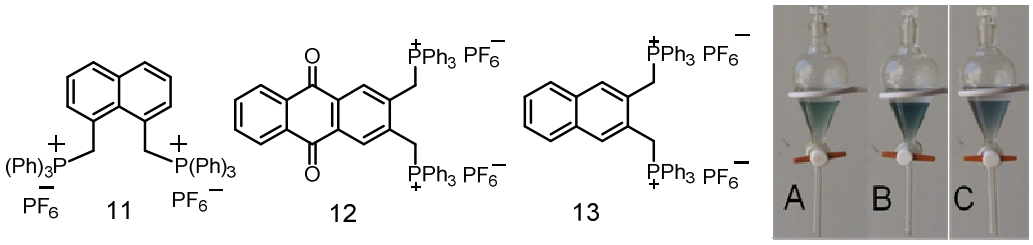

Figure 1A.4.The structure of chemosensors **11-13**. Photograph of the solvent extracted **13** in CH_2Cl_2 layer from (A) 2 ppm aq. a solution of NaF, (B) 2 ml sea water from Okha and (C) 3 ml water from Sambhar Lake.

A New type of receptor unit, bistriphenyphosphine derivatives **11** (Figure 1A.4) was employed for selective detection and extraction of F⁻ from the water. A new phosphonium derivative **11** (Figure 1A.4), was reported by Nam et al.[28] This receptor showed a visually detectable color change from colorless to yellow only in the presence of fluoride ion. The high selectivity for F⁻ can be attributed to the acidity of the methylene protons and the small size of fluoride ions. In a similar line, Das *et al*. reported **12** which were used for selective extraction of inorganic fluoride from aqueous solution with an associated change in solution colour (Figure 1A.4).[29] Hydrogen bonding interaction of the fluoride ion with active methylene group was strong enough to perturb the energies of the frontier orbitals, which accounted for the change in colour. This interaction was well established by ^{1}H, ^{31}P NMR spectroscopic studies. Further, the reagent was also used for detection of F⁻ in sea water for real application and it was found that the reagent was able to detect F⁻ as low as

0.06 ppm which was much lower than the W HO norm for drinking water. Similarly, analogous molecular receptor **13** was reported, which showed a dual response in the presence of F^- (Figure 1A.4).[30] Apart from F^-, CN^- and $H_2PO_4^-$ were also found to bind to the receptor **13** and could induce changes in the optical spectra; however, the binding affinity was found to follow the order $F^- > CN^- \sim H_2PO_4^-$. In the presence of F^-, **13** showed a turn on emission response, this was attributed to the increased molecular rigidity upon F^- binding.

1A.2.2 Chemodosimetric approach

Most of the reported chemodosimetric sensors for detection of F^- involve cleavage of silyl ethers by fluoride as bond strength of Si-F bond is much higher than the Si-O bond. Wang and coworkers reported a new coumarin-BODIPY based probe **14** (Figure 1A.5) for ratiometric detection of fluoride ion.[31] A large red shift in absorption spectra upon desilylation attributed to the better electron donating effect of phenolate group than the silyl ether. Accordingly, fluorescence spectra showed increase in emission band intensity at 472 nm with simultaneous decrease in 606 nm band.

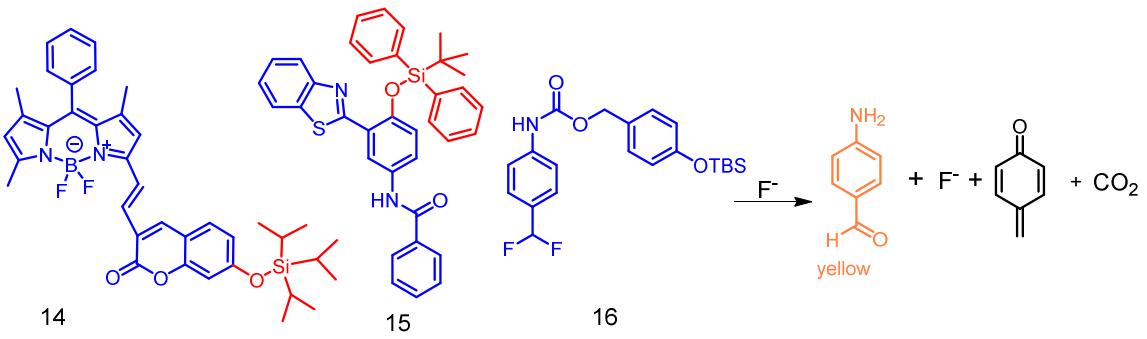

Figure 1A.5. Structures of chemosensor **14-16**. Signal amplification and colour change of **16** in presence F^-.

In another report, yang and coworkers revealed that probe **15** (Figure 1A.5) could be used for selective detection of F^- and optical responses were observed due to the excited state intramolecular proton transfer (ESIPT) process.[32] Receptor **15** was designed in such a way that following Si-O bond cleavage, enol form of the fluorophore predominated and exhibited different emission property than the probe. It is worth noting that experiments with this reagent were performed in micellar solution of CTAB. Reagent **15** was trapped inside the hydrophobic core of the micelles and this had helped not only in solubilizing the reagent in aqueous medium, but also provided a favorable environment for the reaction

between receptor **15** and F^-. Further, the system was improved to test paper system for convenient and reliable detection of fluoride for in everyday application.

A new type of signal amplification approach was adopted by Philips *et al* for selective sensing of fluoride that produced unambiguous colourimetric readout.[33] The reagent **16** (Figure 1A.5) was designed in such a way that F^- induced desilylation, generated two more fluoride anion which could be used for signal amplification and generation of p-aminobenzaldehyde, which was responsible for yellow colour. The newly generated fluoride will amplify the signal and it was found that only 30% of the reagent used was capable of colorimetric readout. Further, the reagent was used successfully for semi-quantitative and quantitative detection of F^- in aqueous medium.

1A.3. Various receptors for Cyanide

Cyanide is one of the most potent neurotoxin and has a huge biological significance.[34] Its toxicity in human arises from the fact that it can form stable complex with Cytochrome *c* oxidase, which leads to cytotoxic hypoxia.[35] LD_{50} value of HCN for human is 1 mg/kg.[36] Keeping this in mind, the World Health Organization (WHO) set, 1.9 μM as the maximum acceptable concentration level of cyanide in drinking water.[35] Despite being toxic, cyanide is used in several industries and also present in some foods and plants. Hence, development of chemosensors for specific detection of cyanide ion is important and several fluorogenic chemosensors for cyanide ion were reported. However, significance of such sensor molecules lies in their ability to detect cyanide species either in aqueous medium having physiological relevance or in biofluids. Importantly, such fluorogenic molecular sensors also offer the possibility of using such reagent for in-vitro or in-vivo imaging applications.

1A.3.1. Designing receptors based hydrogen bonding interaction

Cyanide acts as a strong H-bond acceptor this has been explored by several research groups for designing receptors that are specific for cyanide ion. Das and coworkers reported two imidazole based colorimetric sensor **17-18** for CN^- ion recognition in aqueous medium (Figure 1A.6 (i)).[37] These probes could be used as a colorimetric and fluorescence based sensor for detection of cyanide ion in aqueous environment and could detect CN^- as low as 0.2 ppm. This probe was further used for detection of CN^- ion uptake in organism *Pseudomonas putida.*

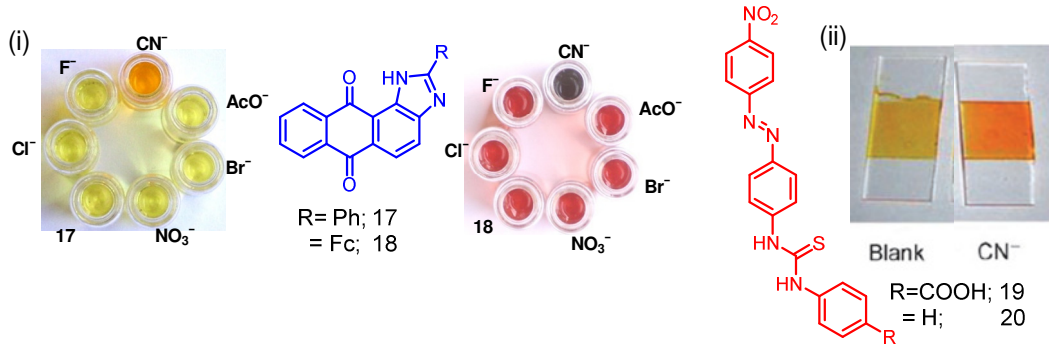

Figure 1A.6. (i) Molecular structure and change in solution colour for chemosensors **17-18** in presence of different anions, (ii) The molecular structure for **19-20** and change in colour of Al_2O_3 film in absence and presence of CN^-.

Vilar and coworkers had reported azophenylthiourea dye **19-20**, for colorimetric detection of cyanide ion (Figure 1A.6 (ii)).[38] Interestingly, these dyes showed selectivity towards CN^- in methanol solution; however, in DMSO medium other anions also induced visually detectable change in solution color. This could be attributed to the fact that with increase in solvent polarity basicity of anions increases. Pendant –COOH group could be used for anchoring the receptor molecule to Al_2O_3 or TiO_2 surfaces and these modified surfaces were to detect cyanide ion in aqueous medium with a detection limit of 2.6 ppm. As associated change in solution or film color from yellow to orange was observed.

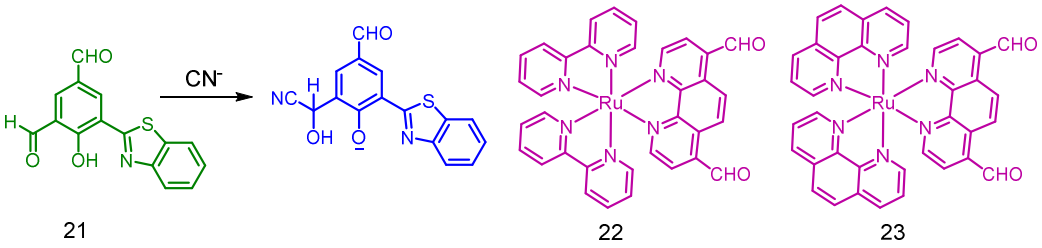

Figure 1A.7. Molecular structures of chemosensor **21-23**.

1A.3.2. Chemodosimeter approach

Though H-bonding receptors were used for recognition of CN^-, its use or possibility of suing such reagents for analysis of any environmental/biological samples is rather limited owing to the deleterious hydration enthalpy of the CN^- in aqueous or physiological medium. To get around this problem, researchers have moved towards enthalpy driven probes, which undergo chemical reaction with cyanide species with an associated enthalpy changes higher than the aquation enthalpy for the CN^-. It is well documented that carbonyls undergo a facile nucleophilic reaction with cyanide species to form the

corresponding cyanohydrin species and this has been used successfully for designing various chemodosimetric reagents for cyanide species.

Goswami et al. developed an aldehyde derivative **21** (Figure 1A.7) for ESIPT based ratiometric detection of CN^- in CH_3CN:Water (1:1, v/v) medium.[39] Cyanide preferentially reacted with the *orhto*-aldehyde group and on cyanohydrins formation interrupted the ESIPT process which led to an emission enhancement at 436 nm with simultaneous decease in 521 nm. Participation of the ESIPT process was further corroborated from results of the DFT studies. In another report, ruthenium bipyridyl complex **22-23 (**Figure 1A.7) with two appended aldehyde groups reacted specifically with CN^-.[40] This resulted a visually detectable change in solution colour as well as fluorescence enhancement for the ^{3}MLCT transition for the Ru(II)-species. Emission enhancement was attributed to the partial switching of MLCT band, which was also corroborated by DFT studies. Two aldehyde groups react in a stepwise manner unlike other reported probes, and have a very low detection limit of 0.18 μM in acetonitrile.

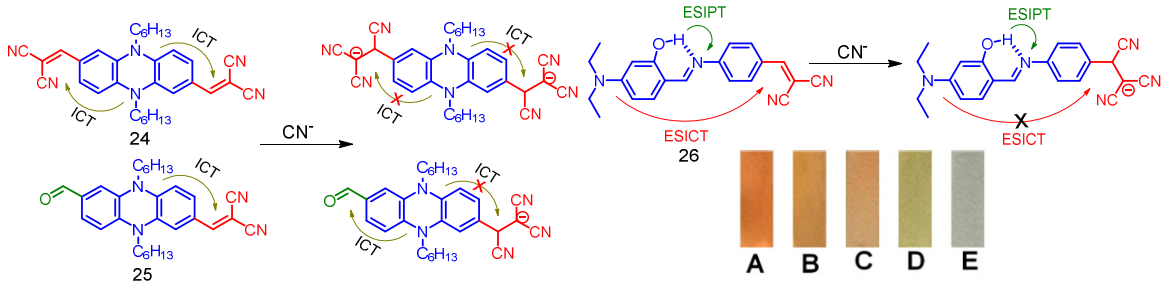

Figure 1A.8. Structure and sensing mechanism of **24-26**. [inset test strips of **26** at various concentrations of CN^- (mM): (A) 0, (B) 20.0, (C) 40.0, (D) 60.0, and (E) 80.0.

Apart from carbonyl based receptors, Michael addition reaction is also explored for detection of CN^- by virtue of its nucleophilicity. Hua and group reported two dihydrophenazine **24-25** (Figure 1A.8 (i)) based NIR probes for detection of cyanide by utilizing this reaction pathway.[41] Probe was designed in such a way that ICT process was altered on formation of cyanide adduct. For the reagent **24** (with two dicyanovinyl groups), ICT process was interrupted to result an on-off fluorescence response in acetonitrile medium. However, for reagent **25** having an aldehyde and dicyanovinyl group, CN^- was found to react preferentially to the dicyanovinyl group. This resulted in a modified ICT process with a ratiometric fluorescence response. Both these probes are reported to be efficient for CN^- and spectroscopic experiments are well supported by theoretical calculation.

A new receptor **26** (Figure 1A.8 (ii)) was reported by Chen *et al.* for detection of CN^- ion in aqueous medium.[42] The probe **26** was purposefully designed to have the diethyamino salicylideneaniline as ESIPT group and a dicyanovinyl group as the electron withdrawing group. ESICT to ESIPT switching occurs following an addition reaction of CN^- at dicyanovinyl group, which resulted absorptions spectrum to show a blue shift of 96 nm, while a blue shift of 103 nm was observed for the fluorescence spectrum. Further, DFT studies were carried out in support of experimental observations also this reagent could be used as test strip for detection of CN^- in aqueous medium.

1A.3.3. Displacement assay based receptor

Schiller and co-workers had developed an allosteric indicator displacement assay with boronicviologen derivatives for specific detection of CN^- in aqueous medium and they could successfully use this reagent for developing an enzymatic assay for an important enzyment like β-glucosidase.[43] Fluorescence of the indicator (8-hydroxypyrene-1,3,6-trisulfonic acid trisodium salt (HPTS)) was quenched by three viologen derivatives **27-29** (Figure 1A.9). Negatively charged CN^- was found to displace indicator and consequently fluorescence was enhanced. This was further extended for monitoring the release of cyanide specie from amygdalin through an enzymatic reaction of β-glucosidase. Finally, they coud even reveal the possibility of monitoring CN^- content in commercial amygdalin.

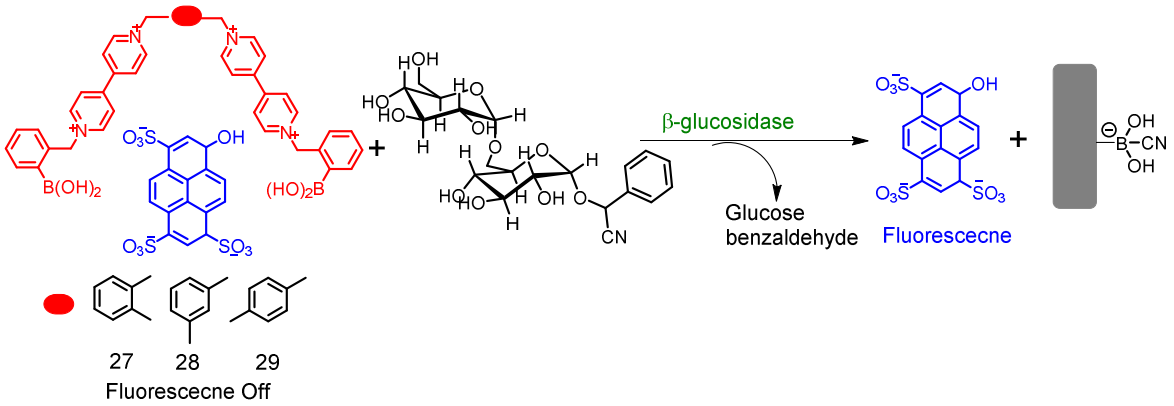

Figure 1A.9. Chemosensor **27-29** and their Indicator displacement assay. Schematic presentation of enzymatic assays between amygdalin and β-glucosidase.

More recently, Das and his co-workers have reported a Ir^{III}-cyclometallated complex **30** (Figure 1A.10) with a pendent Cu(II) moiety for the recognition of CN^- through an analogous displacement approach in aqueous HEPES buffer-CH_3CN, (99.6:0.4, v/v) with associated *turn on* phosphorescence response.[44] Reagent **30** was used for the

development of an assay for probing the *in-situ* release of cyanide from mandelonitrile by another enzyme, hydroxynitrilelyase (HNL) under physiological condition. The probe could detect very low concentration of CN^- in an aqueous medium and further utilized the reagent for the detection of CN^- uptake of as low as 0.2 ppm in live HeLa cells.

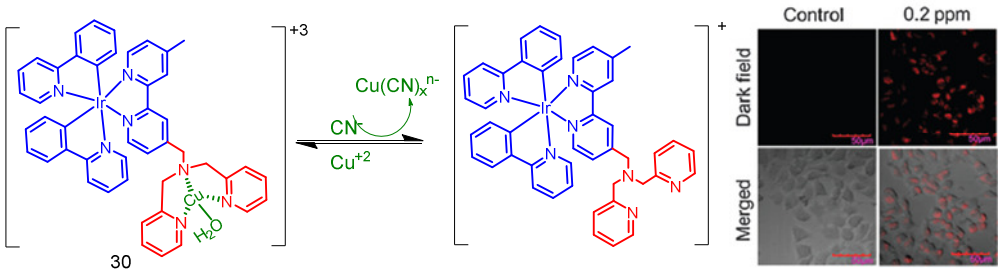

Figure 1A.10. The structure of chemosensor **30**. [Inset cellular uptake of CN^- in Hela cell].

1A.4. Various receptors for Bisulfite

Sulfur dioxide (SO_2) is one of the most common air pollutants and this is primarily released in environment due to burning of fossil fuels. Studies revealed that SO_2 induces respiratory problems, cardiovascular diseases and neurological disorder.[45] On inhalation of SO_2, it gets hydrated and leads to the generation of bisulfite. On the other hand, bisulfite has antioxidant and antimicrobial properties which lead to its use in various industries like pharmaceuticals, wine industry, and food storage. [46] Moreover, sulphite/bisulphite is also endogenously generated from sulphur-containing amino acids, and plays a very important role in the biological sulfur cycle.[47] HSO_3^-/SO_3^{2-} have toxicological effects at higher concentrations, but at low concentration these species are expected to have a physiological role in the regulation of cardiovascular function. Hence, US food and drug administration allow 10 ppm of sulfite in food and beverages.[48] So, developing a chemosensor for bisulfite at low concentration will not only be useful in environment but also in food/pharmaceuticals. Most of the receptors till now for HSO_3^-/SO_3^{2-} used nucleophilic reaction towards aldehyde, Michael acceptors or by a levulinate group.

1A.4.1. Aldehyde based receptors

Bisulfite addition reaction to carbonyl is a well-known reaction in organic chemistry is very common process for purification of aldehydes. This reaction is utilized for developing several receptors for fluorgenic detection of bisulfite ion. Two different groups had reported the probe **31** for detection of bisulfite ion in aqueous medium (Figure 1A.11).[49] Both the

group found it to be selective for bisulfite ion and fluorescence change was attributed to a modified ICT-based response. Li and co-workers further used this probe for detection of bisulfite ion uptake in cells.

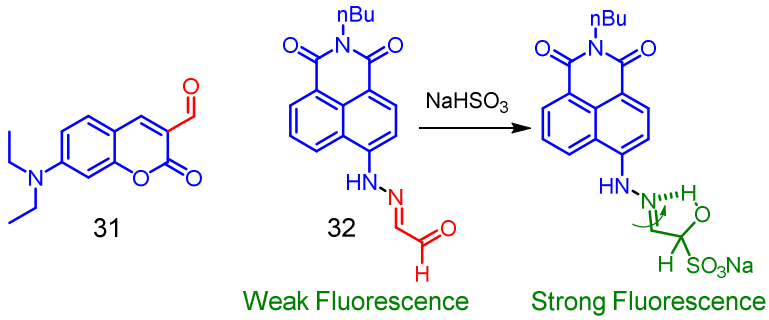

Figure 1A.11. Molecular structure of chemosensor **31-32**. Interruption of C=N isomerization after formation of the bisulfite adduct of **32**.

Guo *et al.* reported a naphthalimide-glyoxal derivative **32** for detection of bisulfite ion in DMSO:buffer (1:1, v/v) at pH 5 (Figure 1A.11).[50] The fluorescence on signal was due to the inhibition of C=N isomerisation process. Upon reaction with HSO_3^-, a new H-bond donor functionality (–OH) was generated, which formed an intramolecular H-bond to restrict the cis-trans isomerization—a major de-excitation process. This accounted for the significant emission enhancement at 535 nm.

1A.4.2. Receptors based on levulinate group

In another approach phenol protected by levulinate groups were employed for designing sulphite sensors. Sulfites were known to deprotect levulinate group under mild and neutral condition. Chang and group used this strategy and synthesised a resorufin-levulinate derivative **33** (Figure 1A.12), which provided a naked-eye detectable chromogenic and fluorogenic response in presence of sulfite.[51] On reaction with sulphite ion, the carbonyl carbon at the 4-position of levulinate formed a tetrahedral intermediate, which underwent a cyclization reaction to cleave the ester linkage and accounted for the release of resorufin. This resulted a change in the ICt process and produced a change in solution colour from yellow to pink with subsequent fluorescence enhancement at 588 nm in H_2O-CH_3CN (98:2, v/v) medium. Zhu *et al.* utilized similar strategy for construction of BODIPY derivative **34** (Figure 1A.12) appended with levulinate group for detection of bisulfite ion in H_2O/DMSO solution (1:1, v/v).[52] In indole-based BODIPY derivative, the OH group was protected by levulinate which on reaction with sulfite produced corresponding phenolate derivative with altered ICT process. A red shift of 110 nm was observed for the absorption spectrum with

an associated change in solution color from orange to red, whereas fluorescence spectra showed a ratiometric change with increase in emission at 674 nm and a simultaneous decrease at 570 nm.

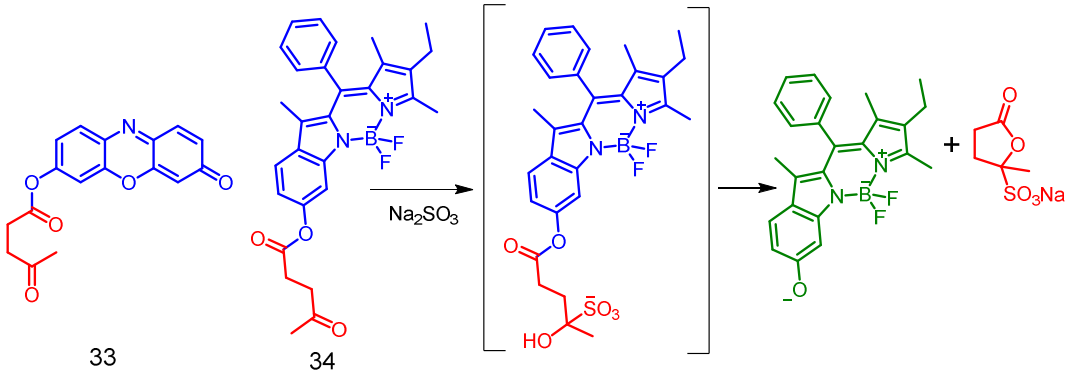

Figure 1A.12. Structure of chemosensor **33-34**. Mechanism for deprotection of levulinate group of **34**.

1A.4.3. Michael reaction based receptors

Li and coworkers had developed two probes **35-36** using a positively charged benzo[*e*]indolium moiety (Figure 1A.13). 1,4-addition of bisulfite took place at C=C bond and this was activated by positive charge. On addition of bisulfite, conjugation was disrupted and produced a change in optical response. For **35**, absorption band at 370 nm was found to decrease and solution color changed from yellow to colorless. For emission spectrum band at 463 nm, an increase in intensity with increasing concentration of bisulfate was observed.[53] In case of **36**, solution colour changed from orange to cyan, but for emission spectrum a ratiometric change, with increase in emission at 465 nm and a concomitant decrease in emission at 571 nm was observed.[54]

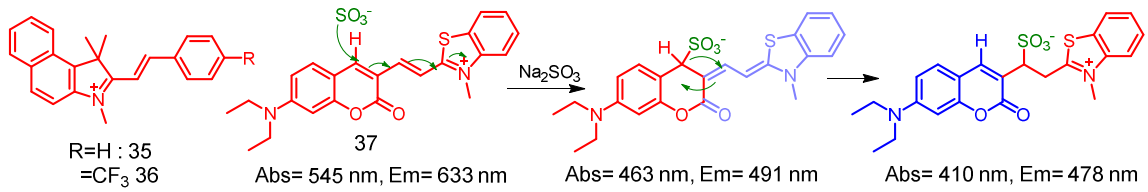

Figure 1A.13. Molecular structure of chemosensor **35-37**. Mechanism of sulfite addition to the receptor **37** and 1,3 rearrangement.

Guo and coworkers employed addition reaction of sulfite in α,β-unsaturated compounds for designing specific sensors for sulfite. They had prepared a coumarine-hemicyanine derivative (**37**) and tested its reactivity against sulfite.[55] Both time dependent absorption

and fluorescence study indicated that reaction happened via a two-step process. Initially sulfite reacted with coumarine and then participated in an intramolecular 1-3 rearrangement (Figure 1A.13) reaction. They could detect an intermediate by ^{1}H NMR, Uv-vis and fluorescence spectroscopic studies. For absorption spectrum, a new band at 463 nm emerged on addition of sulfite and then quickly disappeared to give a new band at 410 nm. Similarly, in fluorescence spectra for intermediate with maximum at 498 nm band disappeared with emergence of a new emission band at 478 nm.

In a novel approach, chao and coworkers employed cyclometalated iridium(III) complexes bridged via an azo group (**38-41**) for selective detection of bisulfite ion in aqueous medium and in cells (Figure 1A.14). Bisulfite reduced the azo group, which in turn altered the luminescence property of metal complex. Receptor **38** showed enhancement in phosphorescence intensity at 600 nm on addition of sulfite in DMSO:aq.HEPES buffer (3:7, v/v) medium.[56] Probe was found to be very selective towards sulfite and bisulfite, however insignificant interference occurred in presence of high concentration of biological reducing agents like Cys, GSH, and DTT. Further the reagent was used for detection of exogenous and endogenous sulfite/bisulfite in live cells.

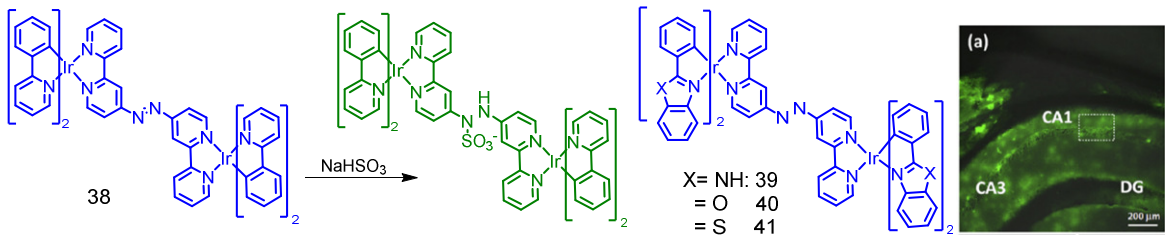

Figure 1A.14. Molecular structure of chemosensor **38-41**. TPM image of endogenous bisulfite in rat hippocampal tissue.

Same group extended their work, and prepared three new derivatives (**39-41**) and showed high selectivity towards sulfite and bisulfite with enhanced phosphorescence responses.[57] However among these receptors, **41** showed best two photon cross-section absorption (TPA) and used further for cellular imaging studies. Probe **41,** preferentially targeted mitochondria and allowed direct visualization of intracellular sulfite/bisulfite levels. This could be used for real time imaging of endogenous sulfite/bisulfate generation in model organism *C. elegans* by TPM. Finally, more strikingly, in vivo deep-tissue imaging of fresh slices of rat hippocampal tissue, demonstrates sulfite distribution in rat brain using TPM (Figure 1A.14) was also performed.

1A.5. References

1. (a) Lee, M. H.; Kim, J. S.; Sessler, J. L. *Chem. Soc. Rev.,* **2015***, 44*, 4185. (b) Kim, J. S.; Quang, D. T. *Chem. Rev*., **2007**, *107*, 3780.

2. (a) Yang, Y.; Zhao, Q.; Feng, W.; Li, F. *Chem. Rev*., **2013**, *113*, 1, 192. (b) Lou, X.; Ou, D.; Li, Q.; Li, Z. *Chem. Commun*., **2012**, *48*, 8462.

3. (a) Leermakers, M.; Baeyens, W.; Quevauviller, P.; Horvat, M. *Trends Anal. Chem*. **2005**, *24*, 383. (b) Chen, C.; Li, B.; Sun, J.; Wang, J.; Gao, Y.; Zhao, Y.; Chai, Z. J. *Anal. At. Spectrom*., **2006**, *21*, 94.

4. Chen, X.; Pradhan, T.; Wang, F.; Kim, J. S.;Yoon, J. *Chem. Rev.,* **2012**, *112*, 1910.

5. (a) Silva, de, A. P.; Gunaratne, H. Q. N.; Gunnlaugsson, T.;Huxley, A. J. M.; McCoy, C. P.; Rademacher, J.; Rice, T. E. *Chem. Rev.,* **1997,** *97,* 1515. (b) Fabbrizzi, L.; Poggi, A. *Chem. Soc. Rev*., **1995,** *24,* 197. (c) Kim, H. M.; Cho, B. R. *Chem. Rev.,* **2015**, *115*, 5014.

6. (a) Bissell, R.; de Silva, A. P.; Gunaratne, P. H. Q. N.; Lynch, P. L. M.; Maguire, G. E. M.; Sandanayake, K. R. A. S. *Chem. soc. Rev*., **1992**, 187. (b) Mangani, S.; Ferraroni, M. *Supramolecular Chemistry of Anions* (Eds.: A. Bianchi, K. Bowman-James, E. Garcia-EspanÄ a), WILEYVCH, New York, **1997**, p. 63

7. Lambert, J. B.; Taba, K. M., *J. Org. Chem*., **1980**, *45*, 452.

8. Pu, L. *Chem. Rev*., **2004**, *104*, 1687.

9. (a) Wiskur, S. L.; Aït-Haddou, H.; Lavigne, J. J.; Anslyn, E. V. *Acc. Chem. Res*., 2001, 34, 963. (b) Xue, L.; Liu, Q.; Jiang, H. *Org. Lett*., **2009**, *11,* 15, 3454.

10. (a) Yang, Y.; Zhao, Q.; Feng, W.; Li, F. *Chem. Rev*., **2013**, *113*, 1, 192. (b) Martínez-Máñez, R.; Sancenón, F. *Coord. Chem. Rev.,* **2006**, *250*, 3081.

11. (a) Wenzel, M.; Hiscock, J. R.; Gale, P. A. *Chem. Soc. Rev.,* **2012**, *41*, 480. (b) Steed, J. W. *Chem. Commun*., **2006**, *2637*.

12. Pedersen, C. J. *J. Am. Chem. Soc.,* **1967**, *89*, 7017.

13. Graf, E.; Lehn, J. M. *J. Am. Chem. Soc.,* **1976**, *98*, 6403.

14. (a) Ballester, P.; *Chem. Soc. Rev*., **2010**, *39*, 3810. (b) Bazzicalupi, C.; Bencini A.; Lippolis, V. *Chem. Soc. Rev*., **2010**, *39*, 3709.

15. Mercer D. J.; Loeb, S. J. *Chem. Soc. Rev*., **2010**, *39*, 3612.

16. Schottel, B. L.; Chifotides H. T.; Dunbar, K. R. *Chem. Soc. Rev*., **2008**, *37*, 68.

17. Steed, J. W.; Juneja, R. K.; Atwood, J. L.; *Angew. Chem., Int. Ed*., **1994**, *33*, 2456.

18. (a) Krik, K. L. *Biochemistry of Halogens and Inorganic Halide*s; Plenum Press: New 468 York, **1991**; p 59l. (b) Ayoob S.; Gupta, A. K. *Crit. Rev. Environ. Sci. Technol*., **2006**, *36*, 433. (c) Dreisbuch, R. H. *Handbook of Poisoning*; Lange Medical Publishers: Los 478 Altos, CA, **1980**.

19. Spittle, B. *Fluoride*, **2011**, *44*, 117. (b) Gazzano, E.; Bergandi, L.; Riganti, C.; Aldieri, E.; Doublier, S.; Costamagna, C.; Bosia, A.; Ghigo, D. *Curr. Med. Chem*., **2010**, *17*, 2431.

20. Clark, J. H. *Chem. Rev*., **1980,** *80*, 429.

21. Jose, D. A.; Kumar, D. K.; Ganguly, B.; Das, A.; *Org. Lett*., **2004**, *6*, 3445.

22. Ravikumar, I.; Saha, S.; Ghosh, P. *Chem. Commun*., **2011**, *47*, 4721.

23. Amendola, V.; Bergamaschi, G.; Boiocchi, M.; Fabbrizzi, L.; Milani, M.; *Chem. Eur. J*., **2010**, *16*, 4368.

24. Rostami, A.; Colin, A.; Li, X. Y.; Chudzinski, M. G.; Lough, A. J.; Taylor M. S. *J. Org. Chem.,* **2010**, *75*, 3983.

25. Liu, X-M.; Zhao, Q.; Song, W-C.; Bu, X-H.; *Chem. Eur. J.,* **2012**, *18*, 2806.

26. Ashok, P.; Ramakrishnan, V. T.; Ramamurthy P. *Chem. Eur. J.,* **2010**, *16*, 13271.

27. Koteeswari, R.; Ashokkumar, P.; Ramakrishnan, V. T.; Malarz, E. J. P.; Ramamurthy P. *Chem. Commun*., **2010,** *46*, 3268.

28. Yeo, H. M.; Ryu, B. J.; Nam, K. C. *Org. Lett*., **2008**, *10*, 2931.

29. Das, P.; Mandal, A. K.; Keshwarwani, M. K.; Suresh, E.; Ganguly, B.; Das A., *Chem. Commun*., **2011**, *47*, 7398.

30. Das, P.; Keshwarwani, M. K.; Mandal, A. K.; Suresh, E.; Ganguly, B.; Das A. *Org. Biomol. Chem.,* **2012**, *10*, 2263.

31. Cao, X.; Lin, W.; Yu, Q.; Wang, J. *Org. Lett.,* **2011**, *13*, 6098.

32. Hu, R.; Feng, J.; Hu, D.; Wang, S.; Li S.; Li Y.; Yang, G., *Angew. Chem*., **2010**, *122*, 5035.

33. Baker, M. S.; Phillips, S. T. *Org. Biomol. Chem*., **2012**, *10*, 3595.

34. Vennesland, B.; Comm, E. E.; Knownles, C. J.; Westly, J.; Wissing, F. *Cyanide in Biology*, Eds.; Academic Press: London, **1981.**

35. (a) R. Takano, *J. Exp. Med.*, **1916,** *24*, 207. (b) Wang, F.; Wang, L.; Chen, X.; Yoon, J. *Chem. Soc. Rev.,* **2014**, 43, 4312.

36. Baskin S. I.; Brewer, T. G. *Medical Aspects of Chemical and Biological Warfare*, ed. F. Sidell, E. Takafuji, T.; Franz, D. R. TMM Publication, Washington, DC, **1997**, ch. 10, pp. 271–286.

37. Saha, S.; Ghosh, A.; Mahato, P.; Mishra, S.; Mishra, S. K.; Suresh, E.; Das, S.; Das, A. *Org. Lett.,* **2010,** *12*, 15, 3406.

38. Gimeno, N.; Li, X.;Durrant, J. R.;Vilar, R. *Chem. Eur. J.,* **2008**, *14*, 3006.

39. Goswami, S.; Manna, A.; Paul, S.; Das, A. K.; Aich, K.; Nandi P. K. *Chem. Commun.,* **2013**, *49*, 2912.

40. Khatua, S.; Samanta, D.; Bats, J. W.;Schmittel, M. *Inorg. Chem.*, **2012**, 51, 7075.

41. Yang, L.; Li, X.; Yang, J.; Qu, Y.; Hua, J. *ACS Appl. Mater. Interfaces*, **2013,** *5*, 1317.

42. Lin, W. C.; Fang, S. K.; Hu, J. W.; Tsai, H. Y.; Chen K. Y. *Anal. Chem.*, **2014**, *86*, 4648.

43. Jose, D. A.; Elstner, M.; Schiller, A. *Chem. Eur. J.,* **2013**, *19*, 14451.

44. Reddy, U. G.; Das, P.; Saha, S.; Baidya, M.; Ghosh, S. K.; Das, A. *Chem. Commun.,* **2013**, *49*, 255.

45. Sang, N.; Yun, Y.; Li, H.; Hou, L.; Han, M.; Li, G. K. *Toxicol. Sci.*, **2010**, *114*, 226.

46. (a) Yang, X.; Guo, X.; Zhao, Y. *Anal. Chim. Acta*, **2002**, 456, 121–128. (b) Fazio, T.; Warner, C. *Food Addit. Contam.,* **1990**, 7, 433–454. (c) McFeeters, R. F. *J. Food Prot.,* **1998**, 61, 885.

47. (a) Stipanuk, M. H.; Rosa, J. D.; Hirschberger, L. L.; *J. Nutr.,* **1990**, *120*, 450. (b) Stipanuk, M. H. *Annu. Rev. Nutr.,* **1986**, *6*, 179.

48. Kalimuthu, P.; Tkac, J.; Kappler, U.; Davis, J. J.; Bernhardt, P. V. *Anal. Chem.,* **2010**, 82, 7374.

49. (a) Yang, Y.; Huo, F.; Zhang, J.; Xie, Z.; Chao, J.; Yina, C.; Tong, H.; Liu, D.; Jin, S.; Cheng, F.; Yan, X. *Sens. Actuators B*, **2012**, *166–167*, 665. (b) Cheng, X.; Jia, H.; Feng, J.; Qin, J.; Li Z. *J. Mater. Chem. B*, **2013**, *1*, 4110.

50. Sun, Y. Q.; Wang, P.; Liu, J.; Zhang, J.; Guo, W. *Analyst*, **2012**, *137*, 3430.

51. Choi, M. G.; Hwang, J.; Eor, S.; Chang S. K. *Org. Lett.,* **2010,** 12, 24, 5624.

52. Gu, X.; Liu, C.; Zhu, Y. C.; Zhu, Y. Z. *J. Agric. Food Chem.*, **2011**, *59*, 11935.

53. Suna, Y.; Fana, S.; Zhang, S.; Zhao, D.; *Sens. and Actuators B*, **2014**, *193*,173.

54. Sun, Y.; Zhao, D.; Fan, S.; Duan, L.; Li, R. *J. Agric. Food Chem.*, **2014**, *62*, 3405.

55. Sun, Y. Q.; Liu, J.; Zhang, J.; Yang, T.; Guo, W. *Chem. Commun.,* **2013**, *49*, 2637.

56. Li, G.; Chen, Y.; Wang, J.; Lin, Q.; Zhao, J.; Jia, L.; Chao, H. *Chem. Sci.,* **2013**, *4*, 4426.

57. Li, G.; Chen, Y.; Wang, J.; Wu, J.; Gasser, G.; Ji, L.; Chao, H. *Biomaterials,* **2015**, *63,*128.

1B. Artificial receptors for cation recognition

1B.1. Introduction

Metal ions play important role in living systems. Sodium, potassium, magnesium and calcium ions are involved in various biological processes; whereas Copper and Zinc are generally associated with metalloenzymes.[1] On the contrary certain metal ions exhibit toxicity in living organism, such as heavy metals ions like Mercury, Lead, Cadmium, Chromium etc.[2] Moreover, these metals are heavily used in various industries and subsequently released in environment which causes environmental pollution.[3] Therefore early detection and sensing of these metal ions is desired and this has attracted much attention not only among chemists, but also biologists and environmentalist. In recent years, number of reports describes specific detection of metal ions for various applications among them fluorogenic receptors are the most important ones.[4]

1B.2. Various receptors for mercury ion (Hg^{+2})

Among the heavy metals ions, mercury is one of the most important analyte because of its toxic influence on the environment and the human physiology.[5] Despite its adverse influences, mercury is still known to be used in various industries like gold mining, coal burning etc.[6] Mercury contamination in water leads to formation of methyl mercury in lower aquatic organisms and is known to be a potent neurotoxin. Bioaccumulation of methyl mercury via aquatic food chain in humans causes damage to central nervous system and minamata disease.[7] Moreover, inorganic mercury does not have metabolic pathway for excretion from the human body and targets the epithelial cells on kidney.[8] Considering this, Environmental Protection Agency (EPA, US) has set 2 ppb (10 nM) as the maximum allowed concentration for Hg^{2+} in drinking water.[9] In this chapter, various receptors for Hg^{2+} were briefly discussed, and special attention were given to NIR based probes.

1B.2.1. Rhodamine based receptor

Among long emitting fluorophores, rhodamine derivatives were extensively used for developing chemosensors that are specific towards Hg^{+2}. Das *et al.* reported a new quinoline-rhodamine-based probe **1**, (Figure 1B.1) which showed remarkable preference toward Hg^{2+} and Cr^{3+}.[10] Upon binding to these metals, a visually detectable change in the color and emission were observed due to conversion of the lactam to the acyclic xanthene

form. More importantly, probe **1** could be used as cell imaging reagent for detection of these ions in breast cancer cell MCF7.

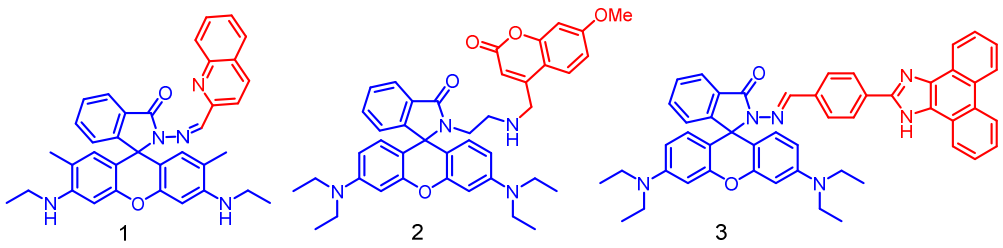

Figure 1B.1. Molecular structures of rhodamine based receptors (**1-3**), specific towards Hg^{2+}.

Das and co workers have also reported a coumarin–rhodamine conjugate **2** (Figure 1B.1) utilizing a unique PET-coupled TBET based photo-induced process for detection of Hg^{2+} ion.[11] On addition of Hg^{2+} both emission band at 402 nm (due to coumarine) and 560 nm (xanthenes form) were found to increase, when excited at 320 nm. This was attributed to the interruption of PET process as well as the energy transfer process. Same group reported another TBET based probe **3** for detection Hg^{2+} ion (Figure 1B.1).[12] A suitably designed receptor molecule revealed Hg(II)–Π^2-arene-π–interaction, which helped in achieving the TBET process with a pseudo-Stokes shift of 200 nm.

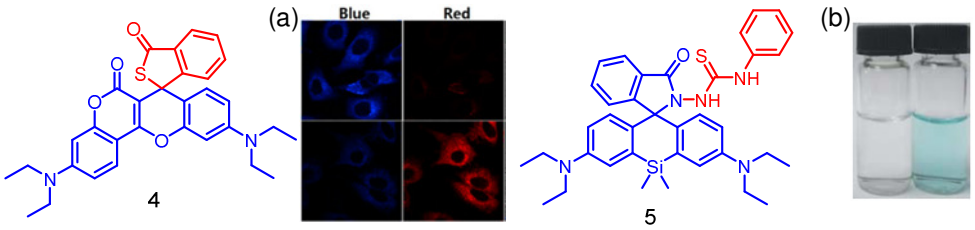

Figure 1B.2. Molecular structure of the probes **4** and **5**; (a) confocal image of **4** in presence and absence of Hg^{+2} in blue and red channel and (b) change in solution colour of **5** from colourless blue in presence of Hg^{+2}.

Wang and coworkers used rhodamine platform in conjugation with coumarin to construct NIR emissive probe **4** for detection of Hg^{2+} localized in the mitochondria of the cells (Figure 1B.2).[13] They have constructed new deep red emitting dyes with high photostabilty and less toxicity. Their studies revealed excellent selectivity towards Hg^{+2} and emission enhancement occurred upon ring opening in presence of Hg^{+2}. Colocalization study showed that probe can detect Hg^{+2} that were localized in mitochondria.

Another approach to construct NIR emissive rhodamine derivative was to replace O with Si. Wu *et al.* reported a spirolactomized Si-rhodamine **5** for detection of Hg^{+2}, (Figure 1B.2) which underwent a ring opening process to produce chromogenic and fluorogenic turn on NIR signals.[14] In presence of Hg^{2+}, colourless solution was changed to blue and new absorption band at 664 nm and emission band at 680 nm appeared. Further, the probe was also used for imaging Hg^{2+} in cells.

1B.2.2. Cyanine based NIR probes

Cyanin dyes are popular NIR emissive dyes and suitably derivatized for detection of Hg^{2+} ion. Tang and co-workers synthesized a fluorescent probe **6** having a NIR active tricarbocyanine moiety (Figure 1B.3).[15] Probe showed weak fluorescence intensity with a fluorescence quantum yield of 0.02 in buffered aqueous solution (10 mM PBS, pH 7.40, 1% acetonitrile as co-solvent) due to an effective PET process. Upon addition of Hg^{2+}, PET was interrupted and fluorescence enhancement was observed. Moreover, probe was used to monitor cellular uptake of Hg^{+2} in cells and zebra fish. Zhu and co-workers had also used tricarbocyanine dye for developing NIR-active ratiometric fluorescent probes (**7-9**) for Hg^{2+} and $MeHg^{+}$ by using mercury mediated desulfurization and cyclization (Figure 1B.3) process.[16] Probe **7** displayed ratiometric response with both dual emission and dual excitation. It is also used for imaging Hg^{+2} and $MeHg^{+}$ in biological system.

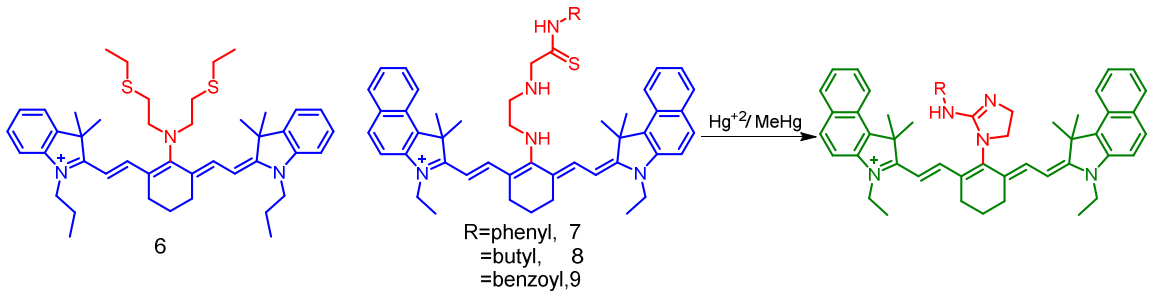

Figure 1B.3. Molecular structures of tricarbocyanine based receptors for Hg^{+2} (**6**-**9**) and example of the chemodosimeter sensing of Hg^{+2} by eceptors (**7**-**9**).

Li *et al.* designed a naphthalenedimide coupled dipycolylamaine (DPA) based receptor **10** for detection of Hg^{2+}.[17] This probe showed a turn on response in NIR region in presence of Hg^{2+} ion and the fluorescence response was attributed to the twisted intramolecular charge transfer (TICT) mechanism (Figure 1B.4). Probe **10** shows very weak fluorescence due to effective TICT process involving the DPA moiety. However, on addition of Hg^{+2}, DPA formed a complex which restrained the formation of TICT state and this attributed to an

emission enhancement at 610 nm. TICT state was further evident from DFT studies and cellular uptake of Hg^{+2} was also carried out.

1B.2.3. BODIPY based NIR probes

BODIPY dyes are important due to their photostability and ease of synthetic modification. Wu et al. reported a monostyryl BODIPY derivative **11** having two triazole units (Figure 1B.4).[18] In presence of Hg^{+2}, a visual change in solution colour from blue to purple occured with simultaneous blue shift of the absorption band maximum by 29 nm due to the interruption of ICT band in acetonitrile-water (9:1, v/v; pH 7.0). Emission intensity at 650 nm was found to increase with increase in Hg^{+2} concentrations and a detection limit of 0.22 μM was evaluated. Probe **11** was also used for imaging cellular uptake of Hg^{+2}.

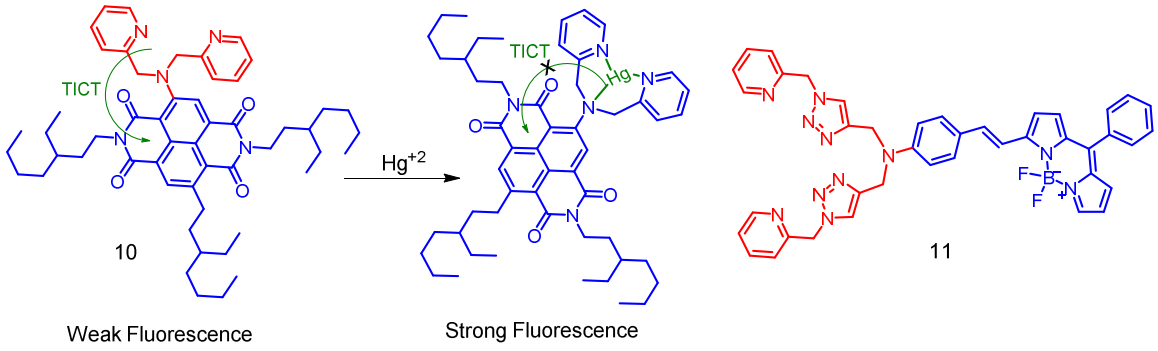

Figure 1B.4. Structures of chemosensors **10-11**.

Guo and coworkers designed a PET based BODIPY-styryl derivative (**12**) with a known Hg^{2+} binding unit (Figure 1B.5).[19] Probe **12** showed a strong $S_0 \rightarrow S_2$ transition which was exploited to enhance the brightness of dye. The probe showed very weak emission due to PET process involving the aniline group. However, on addition of Hg^{+2}, lone pair of electron was no longer available and PET process was suppressed to give emission enhancement. Importantly, when excited at high energy absorption band (λ_{ex} 370 nm), the fluorescence intensity of Hg^{2+} complex was found to be considerably enhanced (2.5-fold) than the direct excitation of Bodipy dye (λ_{ex} 640 nm) and this helped in achieving higher sensitivity. Atilgan *et al.* synthesized a NIR based ratiometric fluorescent probe **13** (Figure 1B.5) using a distyryl-BODIPY derivative having an appended dithia-dioxa-aza macrocycles for specific detection of Hg^{+2}.[20] The probe showed an absorption band at 720 nm due to ICT process, which underwent 90 nm hypsochromic shift on addition of Hg^{+2}. Weak emission intensity at 740 nm for the receptor **13** in THF was attributed to an effective

ICT process, which was interrupted and enhanced emission was observed at 650 nm in presence of Hg^{+2}.

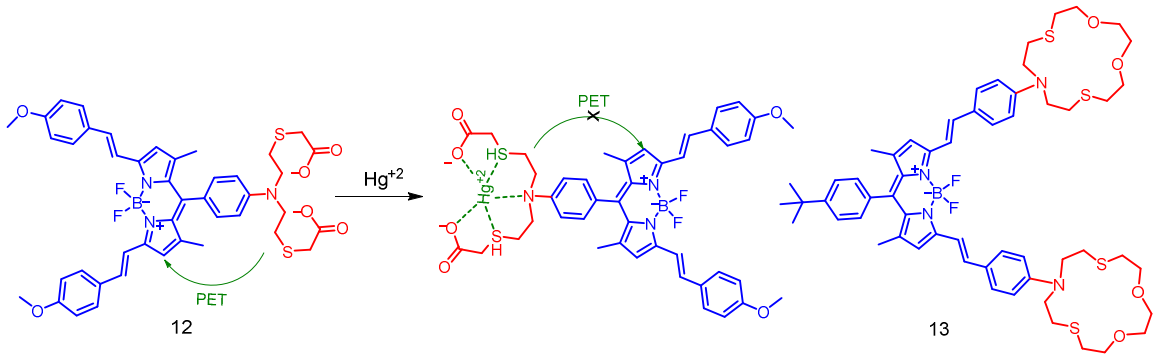

Figure 1B.5. Molecular structures of receptors **12-13**.

Akkaya *et al.* reported probe **14**. For this they had utilized the resonance energy transfer for achieving the signal ratio amplification. They synthesized BODIPY derivative with appended azadioxadithia-15-crown-5 moiety as specific receptor for Hg^{2+} (Figure 1B.6).[21] Probe molecule showed two different emission bands at 540 and 670 nm. The hypsochromic shift upon binding of Hg^{+2} improved the spectral overlap between the emission spectrum of donar BODIPY and modified acceptor BODIPY in **14**. This helped to increase in efficiency of the FRET process and a large increment in signal ratio.

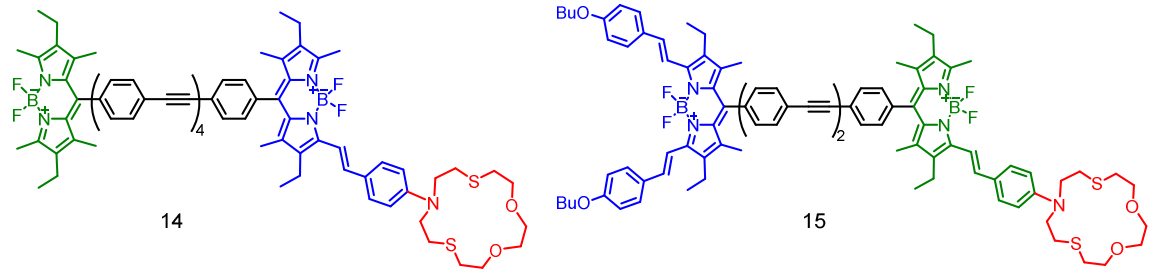

Figure 1B.6. Molecular structures of energy transfer dyad **14-15**.

Subsequently, Akkaya's group also introduced another strategy for designing ratiometric probes by modulation of excitation energy transfer efficiency at the energy donor site. They had reported ratiometric probe using similar strategy and constructed probe **15** (Figure 1B.6) composed of a monostyryl BODIPY-distyryl BODIPY dyad and an azadioxadithia-15-crown-5 attached to donor BODIPY in contrast to acceptor in **14**.[22] The probe **15** exhibited a single broad absorption/excitation band at around 635 nm in THF due to the significant overlap of the absorption/ excitation spectra of the distyryl and monostyryl-

BODIPY chromophores. However, upon addition of Hg^{+2}, blue-shift in the monostyryl-BODIPY chromophore occurred, which resulted in separation of the overlapping absorption/or excitation bands. This could be attributed to the decrease in the electron-donating character of the azathiacrown moiety upon metal ion binding. The attributed to a poorer energy transfer on binding of Hg^{+2} to the receptor **15**.

1B.3. Reference

1. (a) Baker, S. B.; Worthley, L. I. G. *Critical Care and Resuscitation*, **2002**; *4*, 301. (b) Morth, P.; Pedersen, B. P.; Toustrup-Jensen, M. S.; Sørensen, T. L. -M.; Petersen, J.; Andersen, J. P.; Vilsen, B.; Nissen, P. *Nature*, **2007**, *450*, 1043. (c) Watts, D. L. *J. Orthomolecular Medicine*, **1988**, *3*, 197.

2. Vries, W. d.; Römkens P. F.; Schütze, G. *Rev. Environ. Contam. Toxicol*., **2007**, *191*, 91.

3. (a) Natale, F. D.; Lancia, A.; Molino, A.; Natale, M. D.; Karatza, D.; Musmarra, D. *J. Hazard. Mater.,* **2006**, *132*, 220. (b) Flegal, A. R.; Smith, D. R. *Environ. Res.,* **1992**, 58, 125.

4. (a) Kim, H. N.; Ren, W. X.; Kim, J. S.; Yoon, J. *Chem. Soc. Rev.,* **2012**, *41*, 3210. (b) Quang, D. T.; Kim, J. S. *Chem. Rev.* **2010,** *110,* 6280.

5. Harris, H. H.; Pickering, I. J.; George, G. N. *Science*, **2003**, *301*, 1203.

6. Clarkson, T. W.; Magos, L.; Myers, G. J. N. *Engl. J. Med.* **2003**, *349*, 1731.

7. (a) *Toxicological profile for Mercury*, **1999**. U.S. Department of Health and Human Services, Centers for Disease Control and Prevention, Agency for Toxic Substances and Disease Registry, Atlanta (GA). (b) B. Weiss, *Toxicol. Sci.,* **2007**, *97*, 223.

8. Nolan, E. M.; Lippard, S. J. *Chem. Rev*., **2008**, *108*, 3443.

9. Mercury Update; Impact of fish Advisories. EPA fact Sheet EPA-823-F-01-011; EPA, office of water; Washington, DC, 2741.

10. Saha, S.; Mahato, P.; Reddy, U. G.; Suresh, E.; Chakrabarty, A.; Baidya, M.; Ghosh, S. K.; Das, A. *Inorg. Chem.* **2012**, *51*, 336.

11. Saha, S.; Mahato, P.; Baidya, M.; Ghosh, S. K.; Das, A. *Chem. Commun.,* **2012**, *48,* 9293.

12. Reddy, U. G.; Ramu, V.; Roy, S.; Taye, N.; Chattopadhyay, S.; Das, A. *Chem. Commun.,* **2014**, *50*, 14421.

13. Chen, J.; Liu, W.; Zhou, B.; Niu, G.; Zhang, H.; Wu, J.; Wang, Y.; Ju, W.; Wang, P. *J. Org. Chem.,* **2013**, *78*, 6121.

14. Wang, T.; Zhao, Q. J.; Hu, H. G.; Yu, S. C.; Liu, X.; Liu, L.; Wu, Q. Y. *Chem. Commun*., **2012**, *48*, 8781.

15. Tang, B.; Cui, L. J.; Xu, K. H.; Tong, L. L.; Yang, G. W.; Guo, L. A. *ChemBioChem.,* **2008**, 9, 1159.

16. Guo, Z.; Zhu, W.; Zhu, M.; Wu, X.; Tian, H. *Chem. Eur. J.*, **2010**, *16*, 14424.

17. Li, Q.; Peng, M.; Li, H.; Zhong, C.; Zhang, L.; Cheng, X.; Peng, X.; Wang, Q.; Qin, J.; Li, Z. *Org. Lett.*, **2012**,*14*, 8, 2094.

18. Vedamalai, M.; Wu, S. P. *Org. Biomol. Chem.,* **2012**, *10*, 5410.

19. Zhao, Y.; Lv, X.; Liu, Y.; Liu, J.; Zhang, Y.; Shi, H.; Guo, W. *J. Mater. Chem.,* **2012**, *22*, 11475.

20. Atilgan, S.; Kutuk, I.; Ozdemir, T. *Tet. Lett.*, **2010**, *51*, 892.

21. Coskun, A.; Akkaya, E. U. *J. Am. Chem. Soc.,* **2006**, *128*, 14474.

22. Guliyev, R.; Coskun, A.; Akkaya, E. U. *J. Am. Chem. Soc.,* **2009**, *131*, 9007.

1C. Artificial receptors for Biothiol recognition

1C.1. Introduction

Thiols play important role in biological systems and among them Cysteine (Cys), Homocysteine (Hcy) and Glutathione (GSH) are the most important one. They have very similar structure and reactivity. These biothiols are linked with many diseases such as leukocyte loss, psoriasis, liver damage, cancer, and AIDS.[1] Abnormal levels of Cys causes liver damage, slow growth in children, skin lesions, hair depigmentation, edema, and loss of muscle.[2] Accumulation of abnormal level of Hcy in plasma is a risk factor for Alzheimer's disease,[3] folate and cobalamin (vitamin B12) deficiency,[4] and cardiovascular disease (CVD).[5] These are also related to cognitive impairment in the elderly and birth defects.[6] GSH, a non-protein thiol is most important and abundant in human physiology. It maintains oxidative stress of cells, and ratio of GSH in its reduced to oxidized form indicates the redox state of the cell.[7] Hence, it is important to detect and monitor intracellular thiols for both diagnostics and also for assessing the health risk factor. Fluorescence based technique offer simple methodology, with low detection limit and most importantly it can be used for mapping distribution of intracellular thiols. Among those reported fluorescent sensor for biothiols, majority of them relied on the strong nucleophilicity of the corresponding thiolate form or on the high affinity of these thiols towards certain metal ions. Few such important receptors were briefly described.

1C.2. Various receptors for Biothiol

1C.2.1 Michael Acceptor based receptors

Due to strong nucleophilicity of the thiols, Michael addition reaction to an α,β-unsaturated carbonyl moiety, has been widely used as a basis for fluorescent probes for biothiols. maleimide, squarine, acrylamide, nitroolefins were widely used Michael acceptors for biothiols. Maleimide moiety is known to quench fluorescence by PET mechanism and interruption of PET on addition of thiols has been a popular mechanism for biothiol detection. Langmuir et al. reported a naphthopyranone based fluorescent probe **1**-**3** with maleimide group, which was found to quench its fluorescence (Figure 1C.1).[8] Addition reaction of the thiol molecule to the unsaturated double bond led to the formation of a saturated compound and thus, nullifying PET, which caused the revival of the fluorescence. They had also reported probe **2** and **3** for specific detection of GSH. Nagano

and coworkers employed maleimide in conjugation with BODIPY as for developing the receptor **4** (Figure 1C.1).[9] BODIPY emission was effectively quenched by donor-excited photoinduced electron transfer (d-PeT), from BODIPY to maleimide group. On addition of thiols, d-PeT was interrupted and emission response occurred with an increase in quantum yield by 350 folds. On the other hand, d-PeT mechanism also depends on distance between the fluorophore and electron acceptor and so meta- and para- substituted derivative were found to be less effected by d-PeT quenching and shows less significant emission enhancement upon thiol addition.

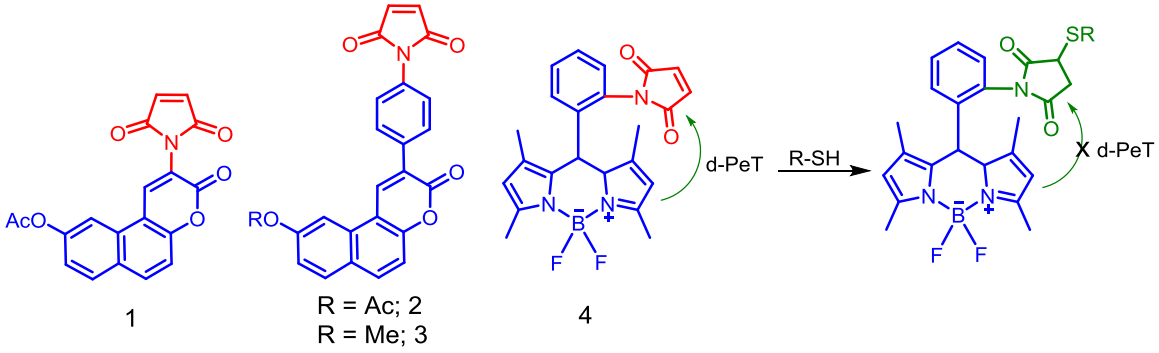

Figure 1C.1. Structure of the probes **1-4**. Sensing mechanism of **4**.

Kim *et al.* reported a coumarin-based probe **5**, which could recognize thiols effectively and selectively with *switch on* fluorescence response (Figure 1C.2) .[10] The reagent **5** could specifically detect Cys in presence of other interfering thiols like, Hcy and GSH. On reaction with thiols, **5** showed fluorescence enhancement due to an interrupted ICT process, which was further corroborated from the results of the DFT studies. The preference for Cys over Hcy and GSH in the cellular metabolite was also confirmed from the results of the LC-MS spectroscopic studies. This reagent **5** could also be used as an imaging reagent for detection of the intracellular distribution of thiols in HepG2 cell line using laser confocal microscopic studies.

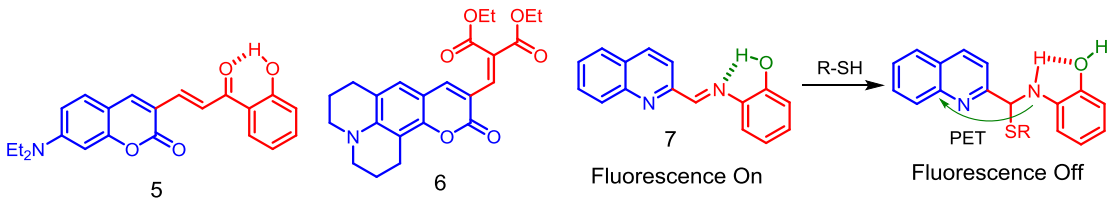

Figure 1C.2. structures of chemosensor **5-7**.

Kim *et al.* reported a probe **6** with an α,β-unsaturated carbonyl group (Figure 1C.2).[11] They had shown that H-bonding played a key role in enhancing the rate of reaction. Probe **6** show ratiometric response towards thiols and also used for detection of thiols in cells by confocal imaging. In similar line Das *et al.* reported a probe **7** with polar imine bond as a receptor for thiols in conjugation with a H-bonding unit (Figure 1C.2).[12] Kinetic studies revealed that the resonance assisted H-bonding facilitated nucleophilic reaction of thiols towards **7**. Fluorescence off response in presence of thiols was ascribed to the PET mechanism. Probe **7** was further used to measure thiols in blood serum and for detection of intracellular distribution of thiols.

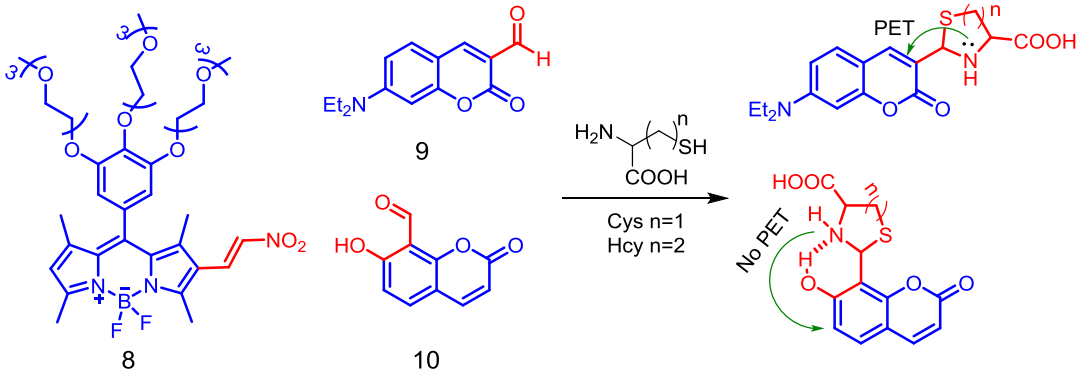

Figure 1C.3. Molecular structures for nitro olefin and aldehyde based receptors **8-10** for thiols.

Akkaya *et al.* reported nitro olefin as Michael acceptor and designed an ethylene glycolated BODIPY derivative **8**, for detection of thiols in aqueous medium (Figure 1C.3).[13] Nitro olefins involved in ICT process as well as in PET process. On reaction with the thiol moieties, a 15 nm hypsochromic shift with simultaneous change in colour from red orange were observed, which signified the interruption of ICT process. Increase in emission intensity was attributed to the reduction in PET efficiency in thiol-adducts.

1C.2.2 Aldehyde based receptors

Aldehydes react with N-terminal cysteines to form thiazolidines via a cyclization reaction. This has been utilized by many to prepare fluorescent probes for thiol detection. Kim et al. reported a coumarin derivative **9** thatbhad an aldehyde group in conjugation with a diethylamino functionality (Figure 1C.3) for a facile push-pull effect.[14] Though the probe molecule showed high selectivity towards Cys/Hcy, on addition of Cys/Hcy it formed corsponding cyclised derivative and fluorescence was quenched due to an effective PET process. Hong and coworkers designed a similar type of coumarine derivative (**10**),

functionalized with a salicyldehyde unit as reactive centre (Figure 1C.3).[15] In contrast to the previous molecule it showed emission enhancement in aqueous medium on reaction with Cys. This emission enhancement could be attributed to the reduced PET process due to formation of intramolecular H-bond.

1C.2.3 Sulfonamide, sulfonate ester and disulfide bond cleavage based receptors

Peng *et al.* reported an imminocoumarine sulfanomide derivative (**11**) for detection of biothiols in aqueous medium (Figure 1C.4).[16] 2,4-Dinitrobenzensulfonyl (DNBS) moiety is electron withdrawing group and reduces emission of fluorophore by ICT process. On reaction with biothiols it releases iminocoumarine and shows a turn on emission response at 525 nm. They also observed that cys reacts better than the Hcy and GSH. Finally, it was used for detection of biothiols in blood serum. Govindraju and coworkers reported a NIR emissive cyanine derivative (**12**) (Figure 1C.4) following similar method but used a sulfonate ester moiety.[17] Cleavage of DNBS led to the formation of a phenolate ion, which rearranged to produce a heptamethine cyanine-like extended π-electron conjugation pattern and was responsible for the turn-on NIR fluorescence response. Moreover, the probe **12** was used to detect thiols in fetal bovine serum (FBS) and also to monitor the GSSG/GSH redox process in the presence of glutathione reductase enzyme and NADPH.

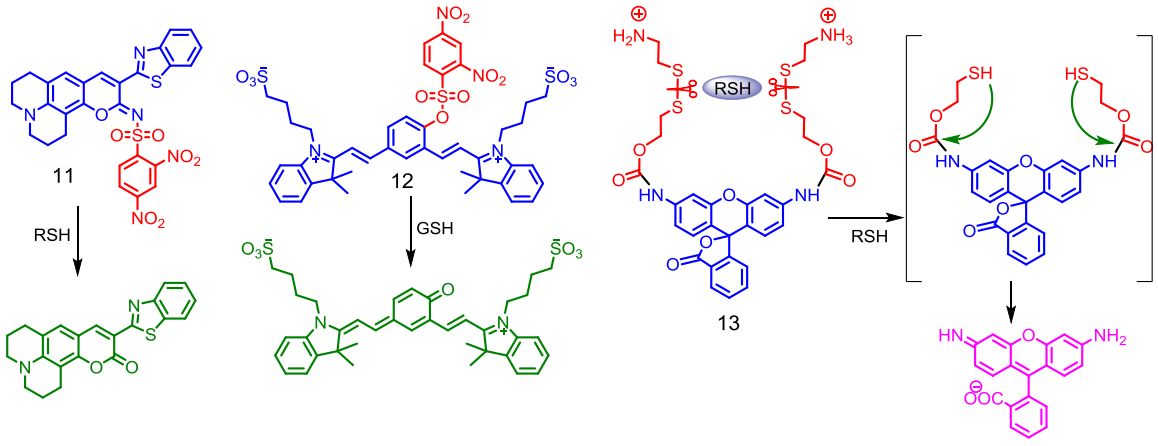

Figure 1C.4. Molecular structures for receptors **11-13**.

Disulfide bond cleavage is also a popular method for detection of thiols. Chmielewski et al. synthesized a new rhodamine derivative (**13**) having a disulfide unit, which displayed fluorescent enhancement upon reduction by cellular thiols (Figure 1C.4).[18] Nucleophilic

sulfhydryl groups reduced the disulfide bonds and the cleavage of the neighboring carbamate bonds. This unmasked the rhodamine 110. In addition, probe **13** was also demonstrated to respond to changing levels of intracellular GSH in live HeLa cell.

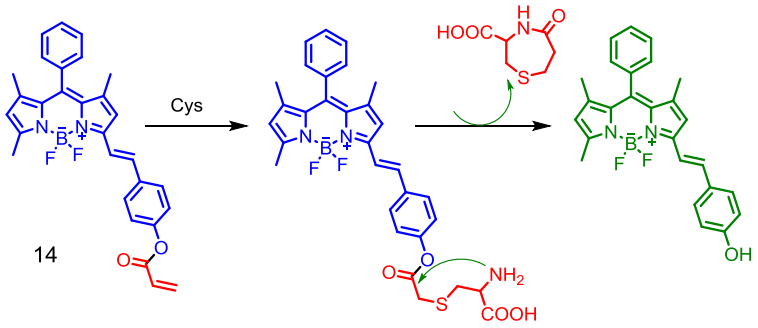

Figure 1C.5. Structure and sensing mechanism of acrylate based receptor **14**.

1C.2.4 Receptors based on addition followed by cyclization reaction

Addition followed by cyclization reaction of Cys with acrylates provided a method for selective detection of Cys among thiols. Das et al. reported a monostyryl BODIPY derivative **14**, appended with an acrylate group for this purpose.[19] Nucleophilic addition reaction involving free sulfhydryl group of Cys moiety with α,β-unsaturated ester resulted an intermediate, which participated in an intramolecular cyclization reaction to regenerate phenolate BODIPY with luminescence *ON* response. The probe was further used for detection of Cys in blood plasma, intracellular Cys and also in situ generated Cys produced through enzymatic reaction of aminoacylase-1 and N-acetyl cysteine.

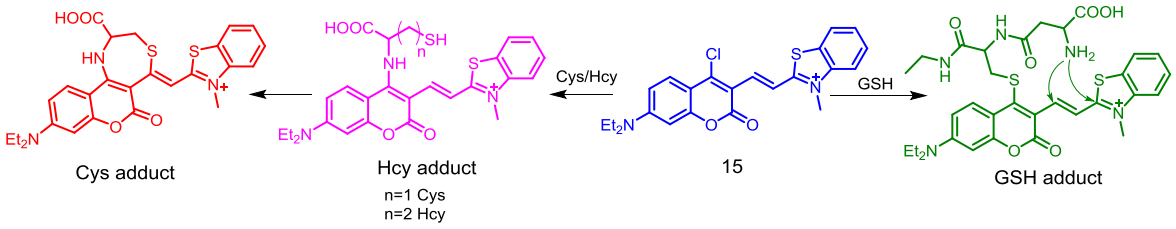

Figure 1C.6. Structure of **15** and different products obtained on reaction with Cys/Hcy/GSH.

Though there are many reports for detection of biothiols, discrimination between biothiols is still a challenge as Cys, Hcy and GHS possess similar reactivity. Recently Guo *et al.* reported a coumarine-cyanine receptor (**15**), which could discriminate between Cys, Hcy and GSH.[20] Presence of other reactive sites in close proximity to the addition reaction site provided way to discriminate thiols. They proposed that initial addition reaction would

replace Cl^- by sulfahydryl group and this was followed by rearrangement process involving free amine. Free SH of Cys then initiated addition reaction to the C=C bond via a favourable 7-member ring, while Hcy and GSH failed to do so. On the other hand, GSH could form large ring and this led to different products after addition-cyclization reaction with distinctly different absorption and fluorescence spectral responses. Reaction with Cys accounted for a new absorption and emission band at 360 nm 420 nm, respectively. GSH showed absorption and emission band at 450 and 512 nm, respectively. However, Hcy could only show absorption band at 500 nm with no fluorescence enhancement.

1C.3. References

1. (a) Townsend, D. M.; Tew K. D.; Tapiero, H.; *Biomed. Pharmac-other.* **2003**, *57*, 145. (b) Herzenberg, L. A.; De Rosa, S. C.; Dubs, J. G.; Roederer M.; Anderson, M. T.; Ela, S. W.; Deresinski S. C.; Herzenberg, L. A.; *Proc. Natl. Acad. Sci. U. S. A.* **1997**, *94*, 1967.

2. Shahrokhian, S.; *Anal. Chem*., **2001**, *73*, 5972.

3. Seshadri, S.; Beiser, A.; Selhub, J.; Jacques, P. F.; Rosenberg, I. H.; D'Agostino, R. B.; Wilson, P. W. F.; Wolf, P. A. *N. Engl. J. Med*., **2002,** *346*, 476.

4. (a) Savage, D. G.; Lindenbaum, J.; Stabler S. P.; Allen, R. H.; *Am. J. Med*. **1994**, *96*, 239. (b) Klee, G. G. *Clin. Chem.,* **2000**, *46*, 1277.

5. Refsum, H.; Ueland, P. M.; Nygard, O.; Vollset, S. E.; *Annu. Rev. Med*., **1998**, *49*, 31.

6. (a) Smith, A. D. *Am. J. Clin. Nutr*. **2002**, *75*, 785. (b) Ray, J. G. Laskin, C. A.; *Placenta*, **1999**, *20*, 519.

7. Dalton, T. D.; Shertzer, H. G.; Puga, A. *Annu. Rev. Pharmacol. Toxicol.,* **1999**, *39*, 67.

8. Langmuir, M. E.; Yang, J.-R.; Moussa, A. M.; Laura R.; LeCompte, K. A. *Tetrahedron Lett*., **1995**, *36*, 3989.

9. Matsumoto, T.; Urano, Y.; Shoda, T.; Kojima, H.; Nagano, T. *Org. Lett*. **2007**, *9*, 3375.

10. Jung, H. S.; Ko, K. C.; Kim, G.-H.; Lee, A-R.; Na, Y-C.; Kang, C.; Lee, J. Y.; Kim, J. S. *Org. Lett*. **2011**, *13*, 1498.

11. Kim, G. J.; Lee, K.; Kwon, H.; Kim, H. J. *Org. Lett.,* **2011**, *13*, 11, 2799.

12. Das, P.; Mandal, A. K.; Reddy U. G.; Baidya, M.; Ghosh, S. K.; Das, A. *Org. Biomol. Chem*., **2013**, *11*, 6604.

13. Isik, M.; Ozdemir, T.; Turan, I. S.; Kolemen, S.; Akkaya, U. G. *Org. Lett.,* **2013**, *15*, 1, 216.

14. Kim, T. K.; Lee, D. N.; Kim, H. J. *Tet. Lett.,* **2008**, *49*, 4879.

15. Lee, K.-S.; Kim, T.-K.; Lee, J. H.; Kim H.-J.; Hong, J.-I. *Chem. Commun*., **2008**, 6173.

16. Yang, Y. -L.; Zhang, F. M.; Wang, Y. W.; Zhang, B. X.; Fang, R.; Fang, J. G.; Peng, Y. *Chem. Asian J.,* **2015**, *10*, 422.

17. Maity, D.; Govindaraju, T. *Org. Biomol. Chem*., **2013**, *11*, 2098.

18. Pires, M. M.; Chmielewski, J.; *Org. Lett*., **2008**, *10*, 837.

19. Ali, F.; Anila H. A., Taye, N.; Gonnade, R. G.; Chattopadhyay, S.; Das, A. *Chem. Commun*., **2015**, *51*, 16932.

20. Liu, J.; Sun, Y. Q.; Huo, Y.; Zhang, H.; Wang, L.; Zhang, P.; Song, D.; Shi, Y.; Guo, W. *J. Am. Chem. Soc.,* **2014**, *136*, 574.

CHAPTER 2

HYDROGEN BONDING INTERACTION BETWEEN ACTIVE METHYLENE HYDROGEN ATOMS AND AN ANION AS A BINDING MOTIF FOR ANION RECOGNITION: EXPERIMENTAL STUDIES AND THEORETICAL RATIONALIZATION

Publication:

J. Phys. Chem. A, ***2014,*** *118, 14, 2656–2666*

2.1. Introduction

Anions plays important role in chemical and biological events and among them most important individual is F^- ion owing to its duplicitous nature.[1] F^- is essential for the prevention of dental caries and treatment of osteoporosis[2] and it is used in anesthetic, hypnotic, psychiatric drugs and military nerve gases.[3] Fluorosis, neurological and metabolic disorders are reported to be caused by an exposure to a higher amount of F^- and this even lead to cancer.[4] All these have contributed to an exponential growth in research for specific recognition of fluoride ion, and the most common methodology adopted for designing receptor molecule for recognition of fluoride ion is based on hydrogen bonding interactions. For such interactions, geometry and spatial orientation(s) of the hydrogen bond donor fragment(s) with respect to the fluoride ion play a very crucial role.[5] Despite several reports, the basic understanding that governs such interaction and thus the binding efficiency is not very well understood.

Recently, it has been argued that a dual approach, having both H-bond donor group along with a nearby positively charge centre would enhance the recognition process. Positive charge increases the acidity of the protons and thus, is expected to enhance the hydrogen bond donating ability as well as is expected to provide an additional electrostatic interaction for anions.[6] Two recent reports from the our group reveal that the active methylene functionality, adjacent to the cationic triphenyl phosponium ion, could act as efficient hydrogen bond donor functionality for selective binding to fluoride ion.[6f,g] However, results of our previous study reveal that a subtle difference in the relative spatial orientations could actually influence hydrogen bonding interaction of these methylene hydrogen atoms and the fluoride ion.

In order to have a better insight in such hydrogen bonding interactions and also to utilize the electrostatic interaction with the cationic phosponium ions, a new terpyridyl derivatives having triphenylphosphonium moiety adjacent to the hydrogen bond donor active methylene moiety was designed and synthesized. More importantly, to envisage the role of the acidity of the active methylene hydrogen atoms, while maintaining the identical relative spatial arrangement, a corresponding Ru(II)-bisterpyridyl complex was synthesized and used for hydrogen bonding interaction studies with different anionic analytes.

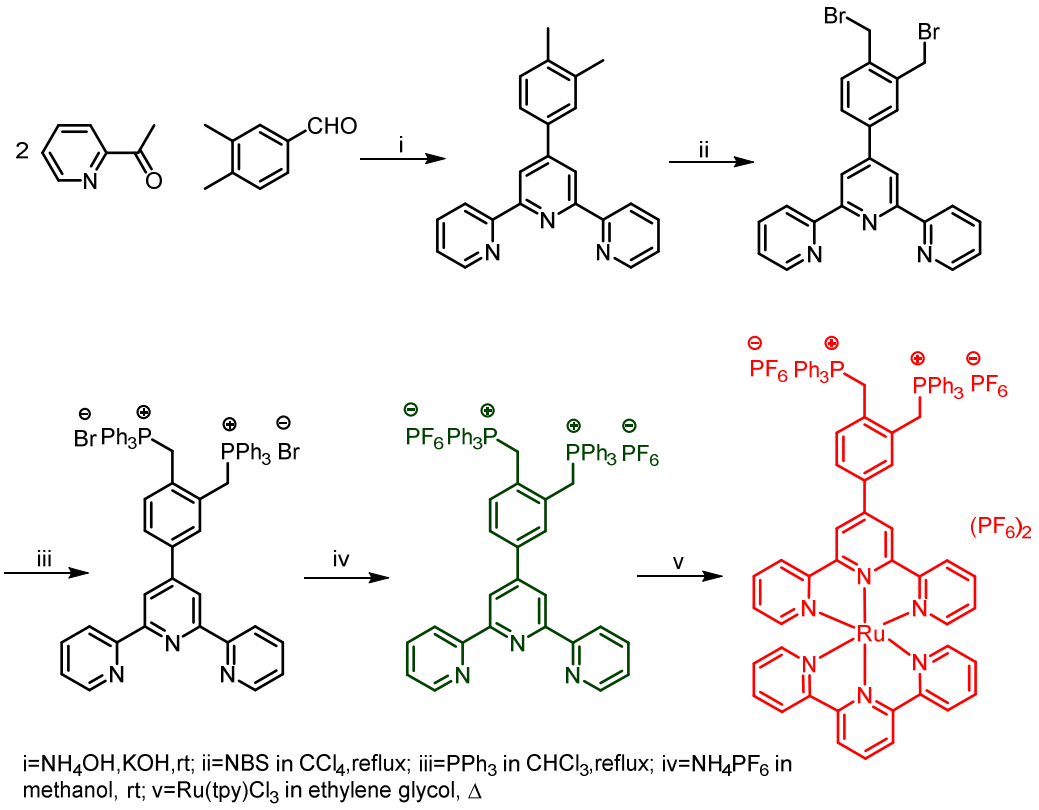

Scheme 2.1: Methodology adopted for synthesis of the reagents.

2.2. Experimental section

2.2.1. Materials

3,4-dimethyl benzaldehyde, 2-acetyl pyridine, N-bromosuccinimide (NBS), triphenylphosphine, ammonium hexafluorophosphate (NH_4PF_6), 2,2':6',2''-terpyridine, ruthenium(III) trichloride hydrate and tetrabutylammonium salts of various anions were purchased from Sigma-Aldrich and were used as received. Dibenzoyl peroxide and all other reagents used were of reagent grade (S. D. Fine Chemical, India) and were used as received. All solvents like ethanol, chloroform and carbon tetrachloride were dried and distilled prior to use. HPLC grade acetonitrile (Fischer Scientific, India) was used for recording all spectrophotometric data.

2.2.2. Analytical Methods

^{1}H, ^{13}C and ^{31}P NMR spectra have been recorded on a Bruker 200/500 MHz FT NMR (Model: Avance-DPX 200/500). FTIR spectra were recorded as KBr pellets in a cell fitted with a KBr window, using a Perkin-Elmer Spectra GX 2000 spectrometer. ESI-MS

measurements have been carried out on a Waters QTof-Micro instrument. Microanalyses (C, H, N) have been performed using a Perkin-Elmer 4100 elemental analyzer. Electronic spectra have been recorded using a Varian Cary 500 UV-Vis-NIR spectrophotometer.

2.2.3. Generalised methodology for spectroscopic studies

For electronic spectral studies, stock solutions of **4** and **5** (1.0×10^{-4} M) were prepared in dry and distilled acetonitrile and stored in dark. Stock solutions of the tetrabutylammonium salts of various anions (1.0×10^{-3} M) were prepared in acetonitrile and stored in cold and dark condition. Stock solutions of **4** and **5** were diluted to effective final concentration of 2.0 $\times 10^{-5}$ M for all spectroscopic studies. For titrations, anion concentration was varied in an incremental manner and the corresponding spectra were recorded at room temperature.

From Absorption titrations and their corresponding spectra, the association constant and binding stochiometry of **L** with Hg^{+2} was determined by using Benesi- Hildebrand analyses and related expression used for this purpose is shown in equation 1.[7]

$$1/(A-A_0) = 1/K(A_{max} - A_0)[F^-] + 1/[A_{max} - A_0) \qquad \text{Equation 1}$$

Where A_0 is the absorption of probes at a particular wavelength, A is the absorption obtained with externally added Hg^{+2} at that particular wavelength, A_{max} is the maximum absorption at the saturation point, *K* is the association constant (M^{-1}) and $[F^-]$ is the concentration of the externally added F^-.

2.2.4. Computational Details

Receptor **4**, **5** and its complexed geometries **(4.F$^-$**, **4.2F$^-$**, **4.OAc$^-$**, **4.2OAc$^-$, 5.F$^-$**, **5.2F$^-$**, **5.OAc$^-$**, and **5.2OAc$^-$**) with analytes have been fully optimized in the gas phase with density functional theory method using M05-2X[8] functional and 6-31G* basis set. We have considered M052X DFT function for its excellent agreement with the experimental results, especially for a system having anion as an analyte(s).[9] We have examined other orientations of receptor molecules and their interaction with analyte(s) and considered the geometries with lowest energies for comparison. The minima of all the geometries i.e. **4**, **4.F$^-$**, **4.2F$^-$**, **4.OAc$^-$**, and **4.2OAc$^-$** were confirmed by true diagonalizing their Hessian (force constant) matrices at the same level of theory with no imaginary frequency. Single point energy calculations were performed with higher basis set 6-31+G** and M06 DFT functional method.[10] Influence of solvent was also considered by using the self-consistent

reaction field (SCRF)[11] method and using the polarized continuum (PCM) model with M06/6-31+G** method.[12] Acetonitrile (ε = 35.688) was taken as solvent. All calculations were performed with Gaussian 09 program.[13]

We have also performed the DFT calculations for **5** and its corresponding complexes with **5.F⁻**, **5.2F⁻**, **5.OAc⁻**, and **5.2OAc⁻** using M05-2X functional and 6-31G(d)[14] basis set for the H, N, O, C, P, F and the transition metal ruthenium ion was treated with LANL2DZ basis set.[15] The minima of all the geometries i.e. **5**, **5.F⁻**, **5.2F⁻**, **5.OAc⁻**, and **5.2OAc⁻** were confirmed by Harmonic vibrational frequency analysis with real frequency. Single point energy calculations have been performed with M06 DFT functional and the higher basis set 6-31+G** was employed for the H, N, C, O, P, F elements. [16] Solvent effect was studied by SCRF-PCM solvent model with acetonitrile solvent (ε = 35.688) and M06 DFT functional method. M06 functional has been suggested to be one of the better models for Ru-containing systems.[17]

2.2.5. Synthesis

2.2.5.1. Synthesis of 1 (4'-(3,4-dimethylphenyl)-2,2':6',2''terpyridine)

A mixture of 2-acetyl pyridine (4.84 gm, 40 mmol) and 3,4-dimethyl benzaldehyde (2.68 gm, 20 mmol) was taken in 100 ml of ethanol. To it KOH pellets (3.08 gm, 85%, 40 mmol) and aqueous NH_3 (68 ml, 25 %, 50 mmol) were added and stirred for 4 h at room temperature. Colour changes to red and a thick residue appears. Excess solvent was filtered off. Residue was subjected to column chromatography on silica gel as stationary phase and hexane / chloroform (8:2 v/v) as eluent to get pale yellow crystalline solid. (1.33gm, 20 %). ^{1}H NMR (500 MHz, CD_2Cl_2, 25 ^{o}C, TMS) 8.64-8.73 (m, 6H, ArH), 7.88 (t, 2H, ArH), 7.61-7.66 (m, 2H, ArH), 7.26-7.38 (m, 3H, ArH), 2.37 (s, 3H, CH_3), 2.33 (s, 3H, CH_3). ^{13}C NMR (500 MHz, $CDCl_3$, 25 ^{o}C, TMS) 19.65, 19.87, 118.61, 121.40, 123.77, 124.70, 128.37, 130.20, 135.83,136.87, 137.19, 137.80, 149.11, 150.32, 155.79, 156.40. IR (KBr) ν_{max}/cm^{-1}: 3433, 1579, 1462, 789. ESI-MS (m/z): 338.49 $[M + H]^+$ Elemental analysis: $C_{23}H_{19}N_3$ calculated C (81.87), H (5.68), N (12.45); found C (81.9), H (5.65), N (12.42).

2.2.5.2. Synthesis of 2 (4'-(phenyl-(3,4-bisbromomethyl))-2,2':6',2''terpyridine)

200 mg of 4'-(3,4-dimethylphenyl)-2,2':6',2'' terpyridine (0.59 mmol) was dissolved in 20 ml of dry CCl_4. Then 253 mg of N-bromosuccinimide (NBS) (1.42 mmol) was added to it and heated to reflux. When the mixture starts to reflux a catalytic amount of freshly recrystalised dibenzoylperoxide was added and irradiated with a 100 W lamp. After 2.5 h reaction completion takes place. Cooled and decomposed product of NBS was filtered using G4 crucible. The filtrate was evaporated to dryness and precipitated from hexane to get product as white solid. (120 mg, 41%). ^{1}H NMR (500 MHz, $CDCl_3$, 25 ^{o}C, TMS) 8.72-8.75 (m, 4H, ArH), 8.67 (d, 2H, ArH), 7.85-7.91 (m, 4H, ArH), 7.52 (d, 1H, ArH), 7.36-7.38 (m, 2H, ArH), 4.77 (s, 2H, CH_2), 4.74 (s, 2H, CH_2). ^{13}C NMR (500 MHz, $CDCl_3$, 25 ^{o}C, TMS) 29.51, 29.76, 118.68, 121.45, 124.02, 128.26, 129.88, 131.85, 137.02,136.35, 137.39, 139.58, 149.13, 155.96, 156.07. IR (KBr) ν_{max}/cm^{-1} : 3431, 1533, 1381, 1033, 788. ESI-MS (m/z): 496.49 $[M + H]^+$. Elemental analysis: $C_{23}H_{17}Br_2N_3$ calculated C (55.78), H (3.46), N (8.49); found C (55.82), H (3.43), N(8.5).

2.2.5.3. Synthesis of 3 (4'-(phenyl-(3,4-bis-(triphenylphosphinomethyl)))-2,2':6',2'' terpyridine dibromide) [Tpy-$(PPh_3)_2$] Br_2

100 mg of **2** (0.2 mmol) was taken in 20 ml of dry $CHCl_3$ and 126 mg of triphenylphosphine was added and refluxed for 4 hr and then stirred at room temp for 12 h. the resulting solution was evaporated and precipitated from toluene. Filtered, and washed with toluene to afford white product.(150 mg, 73 %). ^{1}H NMR (200 MHz, $CDCl_3$, 25 ^{o}C, TMS) 8.81-8.70 (m, 4H, ArH), 8.32 (s, 1H, ArH), 8.06-7.98 (m, 2H, ArH), 7.89-7.83 (m, 6H, ArH), 7.70-7.64 (m, 25H, ArH), 7.52 (m, 3H, ArH), 7.37 (s,1H, ArH), 7.16 (d. 2H, ArH), 4.50 (s, 2H, CH_2), 4.25 (s, 2H, CH_2). ^{13}C NMR (500 MHz, $CDCl_3$, 25 ^{o}C, TMS) 21.67, 125.51, 128.44, 128.66, 128.76, 129.25, 130.46, 130.60, 130.70, 132.14,132.28, 132.36, 134.53, 134.61, 134.72, 134.79, 149.1135.34, 138.09 , IR (KBr) ν_{max}/cm^{-1}: 3427, 2363,1597, 1436, 1108, 688. ESI-MS (m/z): 429.76 $[M - 2Br^-]^{+2}$, 940.65 $[M - Br^-]^{+1}$ Elemental analysis: $C_{59}H_{47}Br_2N_3P_2$ calculated C (69.49), H (4.65), N (4.12); found C (69.43), H (4.64), N (4.1).

2.2.5.4. Synthesis of 4 (4'-(phenyl-(3,4-bis-(triphenylphosphinomethyl)))-2,2':6',2'' terpyridine di(hexafluorophophate)) [Tpy-$(PPh_3)_2$]$(PF_6)_2$

To a solution of **3** (100 mg, 0.098 mmol) in 10 ml of MeOH was added 317 mg of NH_4PF_6 (1.96 mmol) and stirred for overnight. Solvent was evaporated to dryness, and extracted

with water and DCM to get white solid. (90 mg, 80%). ^{1}H NMR (500 MHz, $CDCl_3$, 25 ^{o}C, TMS) 8.73 (d, $2H_{6,6'}$, J=4Hz), 8.62 (d, $2H_{3,3''}$,J=8Hz), 8.17 (s, $2H_{3',5'}$), 7.90 (t, $2H_{4,4''}$), 7.83 (t, $2H_{5,5''}$,,$1H_{PPh3}$), 7.78 (m, $2H_{PPh3}$), 7.70 (m, $13H_{PPh3}$), 7.58 (m, $7H_{PPh3}$) , 7.50 (m, $6H_{PPh3}$), 7.39 (m, $1H_{PPh3}$,$1H_c$), 7.18 (m, $2H_{a,b}$), 4.02 (d, $2H_m$, J=14 Hz), 3.92 (d, $2H_p$, J=14.5 Hz). ^{13}C NMR (500 MHz, CD_3CN, 25 ^{o}C, TMS) 30.97, 117.22, 117.31, 120.70, 120.83, 123.58, 126.96, 127.00, 129.33, 131.41,131.51, 132.47, 134.55, 135.15, 135.23, 135.31, 136.87, 1376.92. IR (KBr) ν_{max}/cm^{-1}: 3432, 1602, 1439, 1111, 839. ESI-MS (m/z): 429.98 $[M - 2PF_6]^{+2}$, 1005.20 $[M - PF_6]^{+1}$ Elemental analysis: $C_{59}H_{47}F_{12}N_3P_4$ calculated C (61.63), H (4.12), N (3.65); found C (61.6), H (4.11), N (3.63).

2.2.5.5. Preparation of 5 $[(Tpy)Ru(Tpy\text{-}(PPh_3)_2)](PF_6)_4$

62 mg of $Ru(Tpy)Cl_3$ (0.14 mmol) prepared by previously reported method, was suspended in 15 ml of glycol and heated to dissolve. Then 160 mg of compound **3** (0.14 mmol) was added to it and heated for 4h at 130-140 ^{0}C. After that it is cooled to room temperature and 10 ml of saturated KPF_6 solution was added to it, to get precipitate. Kept in fridge for complete precipitation and filtered with G4 crucible. The ppt was washed with excess of water to remove excess of KPF_6 and then with ether. Dried in vacuum and purified by column chromatography using neutral alumina (grade II) as stationary phase and CH_3CN:Toluene (30:70) mixture as eluent. (95 mg, 38 %). ^{1}H NMR (500 MHz, CD_3CN, 25 ^{o}C, TMS) 8.91 (s, $1H_{3'}$), 8.76 (d, $1H_h$,), 8.75 (d, $1H_j$,), 8.60 (d, $1H_i$,), 8.50 (m, $4H_{5'6,6'',c}$), 8.42 (m, $2H_{3,3''}$), 8.08 (m, $1H_g$), 7.99-7.90 (m, $10H_{PPh3,}1H_k$), 7.80-7.74 (m, $8H_{PPh3}$), 7.70-7.64 (m, $12H_{PPh3}$) 7.50 (d, $1H_b$), 7.37-7.32 (m, $6H_{5,5'',4,4'',f,l}$), 7.20-7.16 (m, $5H_{a,d,o,e,n}$), 4.73 (d, $2H_p$, J=15Hz), 4.64 (d, $2H_m$, J=15Hz) ^{13}C NMR (500 MHz, CD_3CN, 25 ^{o}C, TMS) 29.57, 120.96, 121.15, 123.97, 124.70, 127.67, 127.73, 127.78, 128.88, 128.98, 130.53, 130.63, 131.89, 131.97, 132.34, 134.46, 134.53, 134.64, 134.72, 135.82,137.87, 138.27, 138.33, 138.88, 152.47, 152.86, 155.40, 155.54, 158.26. IR (KBr) ν_{max}/cm^{-1}: 3435, 1611, 1442, 1114, 838. ESI-MS (m/z): 742.75 $[M\text{-}2PF_6]^{+2}$, 1223.19 $[M\text{-}1PF_6\text{-}PPh_3]^{+2}$ Elemental analysis: $C_{74}H_{58}F_{24}N_6P_6Ru$ calculated C (50.10), H (3.30), N (4.74); found C (50.15), H (3.29), N (4.76).

2.3. Results and Discussions

We have prepared two new receptor molecules **4** and **5** (scheme 2.1). Their binding affinity towards different anions was examined spectroscopically. It was found that the methylene

units of **4** and **5** were involved in the binding with anions which were evident from both NMR and DFT studies.

2.3.1. Spectroscopic studies

Electronic spectrum of **4** was recorded in acetonitrile medium (Figure 2.1(i)). The absorption spectra shows three characteristic bands at around 254 nm ($\varepsilon = 3.04 \times 10^4\ M^{-1}\ cm^{-1}$), 276 nm ($\varepsilon = 3.86 \times 10^4\ M^{-1}\ cm^{-1}$), and 323 nm ($\varepsilon = 6.99 \times 10^3\ M^{-1}\ cm^{-1}$). The weak band at 254 nm could be assigned to terpyridine based n-π^* transition, which is partly covered by terpyridine based stronger π-π^* band at 276 nm.[18] The weaker broad band at 323 nm could be assigned as (Tpy $\rightarrow$ PPh_3) based inter-ligand charge transfer (ICT) transition.

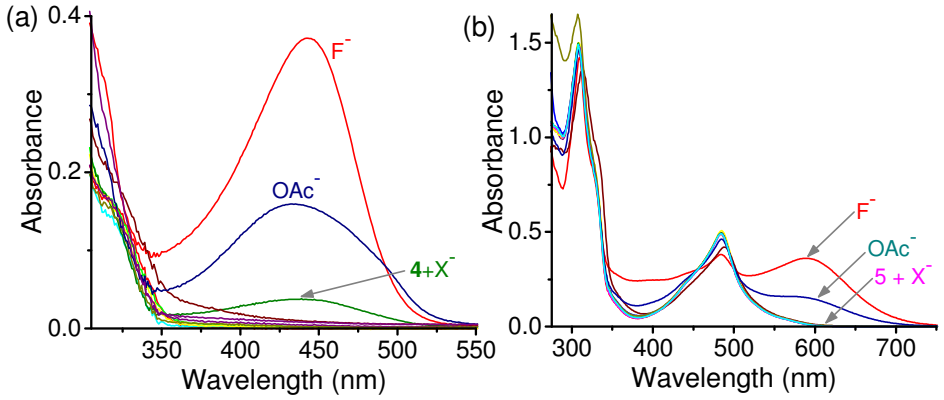

Figure 2.1. Absorption spectra of (a) **4** (2.0×10^{-5} M) and (b) **5** in (2.0×10^{-5} M) the presence of tetrabutylammonium salts of various anions (100 mole equivalent) (X = F^-, Cl^-, Br^-, I^-, $H_2PO_4^-$, HSO_4^- OAc^-, NO_3^-, IO_4^-, SCN^-) in acetonitrile.

In order to evaluate the specificity and sensitivity of **4** towards different anionic guests absorption spectra of **4** were recorded in presence of tetrabutyl ammonium salts of various anions such as F^-, Cl^-, Br^-, I^-, $H_2PO_4^-$, HSO_4^-, OAc^-, NO_3^-, IO_4^- and SCN^-. Among these anions, only F^- and OAc^- were able to induce detectable changes in absorption spectral pattern upon addition of 100 mole equivalents of these respective anions. A new broad absorption band appeared at 443 nm upon addition of the solution of TBA salt of F^- and OAc^- (Figure 2.1(a)); while this new spectral band was much stronger for F^- (Figure 2.1(a)). However, for F^- and OAc^- these changes in absorption spectra were significant enough to induce a visually detectable change in solution colour from colourless to yellow, which also reveal appreciable interaction between the receptor molecule **4** and F^- or OAc^-.

Other anions (Cl^-, Br^-, I^-, $H_2PO_4^-$, HSO_4^-, NO_3^-, IO_4^- and SCN^-) failed to induce any significant change in the absorption spectra, which suggests either an insignificant or no interaction between the receptor **4** and these anions. Thus all other anionic analytes, except F^- or OAc^-, failed to perturb the energies of the frontier orbital of the receptor **4** and consequently, no detectable change in spectral pattern could be observed.

The absorption spectra of **5** showed three characteristic bands in absorption spectra in acetonitrile medium (Figure 2.1(b)). The intense high energy bands at 275 nm ($\varepsilon = 5.37 \times 10^4\ M^{-1}\ cm^{-1}$) and 309 nm ($\varepsilon = 5.37 \times 10^4\ M^{-1}\ cm^{-1}$) were ascribed to a ligand centered π-π^* transition. The relatively broad low energy band at 484 nm ($\varepsilon = 2.46 \times 10^4\ M^{-1}\ cm^{-1}$) was attributed to the to the $Ru_{[d\pi]} \rightarrow Tpy_{[\pi^*]}/Tpy'_{[\pi^*]}$ (Tpy' is terpyridyl derivative used for this study, i.e. (**4**)) based metal to ligand charge transfer (MLCT) transition.[19] These transitions are primarily responsible for the intense red colour of the solution. On addition of 100 mole equivalents of tetrabutylammonium salt of various anions (F^-, Cl^-, Br^-, I^-, $H_2PO_4^-$, HSO_4^- OAc^-, NO_3^-, IO_4^- and SCN^-) to a solution of **5** (2.0×10^{-5} M) in acetonitrile, a new peak at 590 nm appeared only for F^- and OAc^-, (Figure 2.1(b)) with subsequent change in solution colour from red to violet-blue. Other anions failed to induce any detectable change in spectral pattern for **5**.

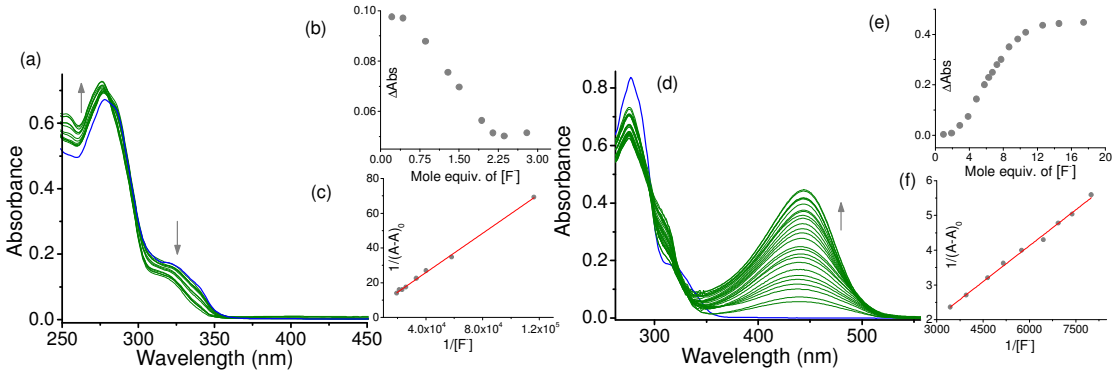

Figure 2.2. Systematic changes of UV-Vis spectra of **4** (2.0×10^{-5}M) in acetonitrile with varying [F^-] (a) 0 – 3 mole equivalent [inset: (b) change in Δabs. with [F^-] monitored at 323 nm) (c) Benesi-Hildebrand plot for 1st equilibrium] (d) with varying [F^-] of 2.5 - 20 mole equivalent [inset: (e) change in Δabs. with [F^-] monitored at 443 nm (f) Benesi-Hildebrand plot for 2nd equilibrium]

To understand the extent and nature of interactions involved in these receptors with F^- and OAc^-, systematic spectrophotometric titrations were carried out in acetonitrile medium with varying concentration of F^- and OAc^-, while maintaining the concentration of receptor **4** (2.0×10^{-5} M) unchanged. During the initial part of the titration, a decrease in the ICT band

at 323 nm with concomitant increase in absorbance at ~ 275 nm were observed till two mole equivalents of F^- or OAc^- was added. These spectral changes were associated with an isosbestic point at ~ 290 nm. On further increase in [F^-], a new band appeared at 443 nm and limiting gain in absorbance was achieved on addition of 20 mole equivalents of F^- (Figure 2.2) with an associated change in solution colour from colourless to yellow. These spectral changes were also associated with a decrease in absorbance at 275 nm and a slight increase in absorbance at around 308 nm, along with the appearance of isosbestic points at 296 and 326 nm.

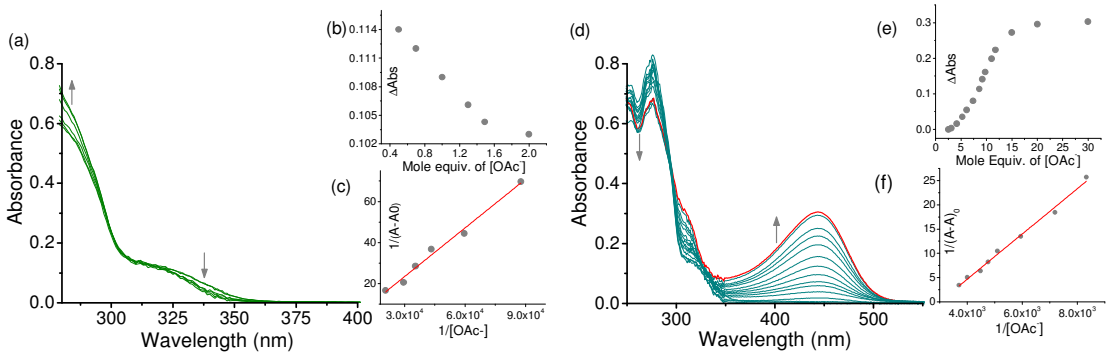

Figure 2.3. Systematic changes of UV-Vis spectra of **4** (2.0×10^{-5} M) in acetonitrile with varying [OAc^-] (i) 0 - 2 mole equivalent [inset: (ii) change in Δabs. with [OAc^-] monitored at 323 nm (iii) Benesi-Hildebrand plot of 1st equilibrium] (iv) 2.5 - 30 mole equivalent [inset: (v) change in Δabs. with [OAc^-] monitored at 443 nm (vi) Benesi-Hildebrand plot for 2nd equilibrium]

These observations tend to suggest that two different equilibriums were actually involved during the titration process with varying [F^-] (0 to 20 mole equivalents). It was presumed that initially for lower effective [F^-], a weak electrostatic and/or hydrogen bonding interaction(s) involving **4** and F^- could be attributed for the initial sets of spectral changes. Further increase in [F^-], presumably triggered the deprotonation from the methylene functionality, adjacent to the cationic PPh_3^+ moieties. F^- ion is known to act as a strong base in acetonitrile medium and the possibility of the formation of thermodynamically more stable HF_2^- was expected to initiate the deprotonation process.[20] Values for the first equilibrium constant for the hydrogen bonded adduct formation was evaluated from respective Benesi-Hildebrand plot for the data obtained from the first set of systematic titration data (Figure 2.2(a)) and it was found to be $(5.78 \pm 0.2) \times 10^3$ M^{-1} for a 1:1 binding stoichiometry. Good linear fit of the B-H plot for $1/A\text{-}A_0$ vs 1/[F^-] also confirmed the 1:1 binding stoichiometry. Using the data from the spectrophotometric titration for the second set of changes for relatively higher [F^-], which leads to the deprotonation equilibrium, value

for the deprotonation equilibrium process was evaluated as $(3.92 \pm 0.1) \times 10^3$ M^{-1}. It is worth mentioning here that the reaction between **4**.F^- + F^- was considered for the calculation of this second equilibrium constant, i.e, the deprotonation process.

Analogous studies were also performed with OAc^-, while similar spectral changes were observed (Figure 2.3). However, spectral changes associated with both equilibrium processes were less for AcO^-, as compared to those with F^-. For OAc^-, two respective equilibrium constants were evaluated as $(3.16 \pm 0.3) \times 10^2$ M^{-1} and $(7.09 \pm 0.2) \times 10^2$ M^{-1} for 1:1 hydrogen bonded adduct formation and the deprotonation process, respectively. Weaker binding of OAc^- with the reagent **4** and its efficiency as a base to induce the deprotonation process were also evident from the respective lower equilibrium constants as compared to those with F^-. These were further confirmed in the ^1H NMR studies and are discussed latter.

Presence of the cationic Ru(II)-center was expected to enhance the acidity of the methylene hydrogen atoms without altering the relative spatial orientations of the hydrogen bond donor methylene moieties and would allow us to study the role of acidity on the hydrogen bonded adduct formation. This was not possible in our earlier studies,[6f,g] where spatial orientations of the two methylene groups were different in the anthaquinone and naphthalene moities.

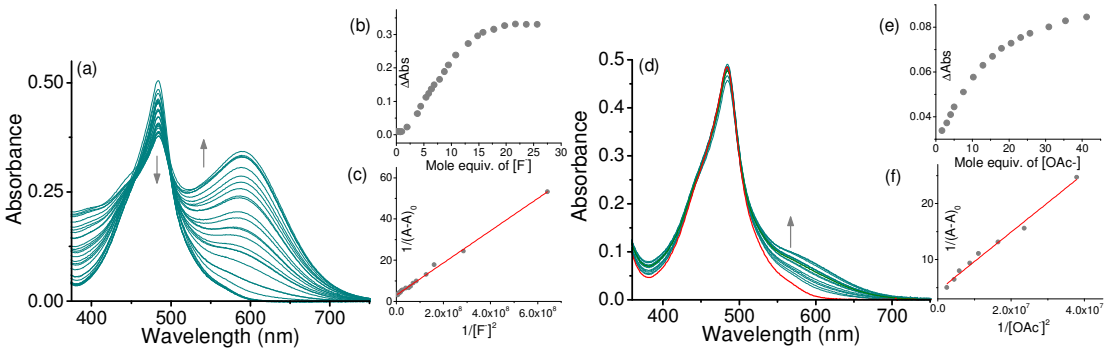

Figure 2.4. Changes in UV-Vis spectra of **5** (2.0×10^{-5}) in acetonitrile with varying (a) [F^-] [inset: (b) change in Δabs. with [F^-] (0 – 50.0×10^{-5} M) at λ_{Max} of 590 nm (c) Benesi-Hildebrand plot] and (d) [OAc^-] [inset: (e) Δabs. with [OAc^-] (0 – 80.0×10^{-5} M) at λ_{Max} of 590 nm (f) Benesi-Hildebrand plot].

Similar spectrophotometric titrations were also performed with metal complex **5** in order to find out its relative interaction with F^- and OAc^-. These spectral changes were also associated with two isosbestic points at 499 nm and 455 nm (Figure 2.4), along with a visually detectable change in solution colour from red to violet. However, for complex **5** it

was not possible to clearly distinguish two equilibrium processes and consequently, it was not possible to evaluate values for two individual equilibrium constants. As anticipated, extent of spectral changes was much less for OAc^- as compared to that for F^-. The composite equilibrium constants evaluated for F^- and OAc^- were $(3.97 \pm 0.3) \times 10^7$ M^{-2} and $(8.36 \pm 0.45) \times 10^6$ M^{-2}, respectively.

2.3.2. NMR Study

2.3.2.1. ^{1}H NMR

To understand the mode of interaction and any possible involvement of the cationic triphenylphosphine moiety in such interaction, detailed ^{1}H NMR spectral studies were carried out. Two sets of signals for methylene protons for **4** and **5** were observed at 3.8-3.85 ppm and 4.74-4.8 ppm, respectively (Figure 2.5). Due to the presence of the adjacent PPh_3^+ functionality, the observed *J* values for these methylene protons were found to be higher (~ 14 - 15 Hz), which was characteristics of coupling with adjacent phosporous atom and was rather anticipated.[6f] As expected, signals for these methylene protons for complex **5** (δ_5^{para} = 4.73 ppm) and δ_5^{meta} = 4.64 ppm) appeared at much higher ppm than that was observed for **4** (δ_4^{meta} = 3.84 ppm and δ_4^{para} = 3.81 ppm). These also supported the anticipated increase in acidity of methylene protons in **5** owing to the presence of the cationic Ru(II)-center.

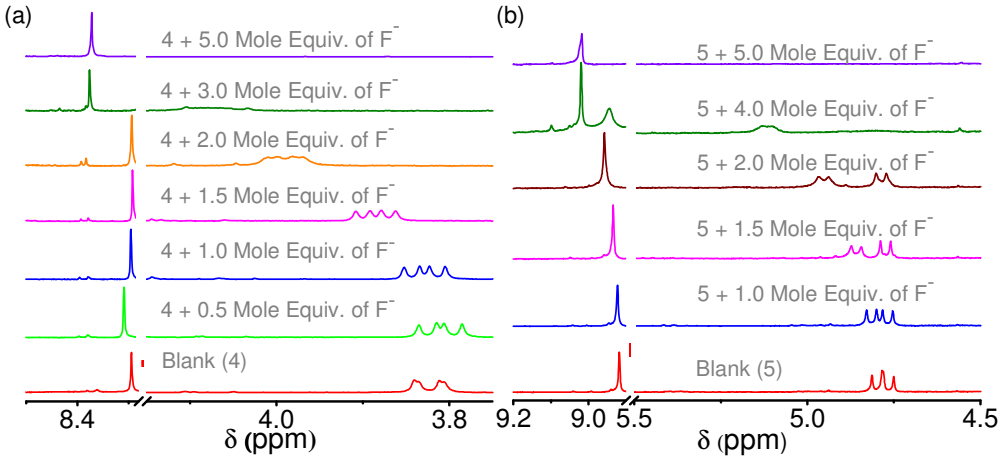

Figure 2.5. Partial ^{1}H NMR spectra of (i) **4** and (ii) **5** in CD_3CN with varying $[F^-]$. Signals at 8.29 and 8.91 ppm are due to 3'/5' protons in **4** and **5**. Methylene protons for **4** and **5** were observed at 3.8 - 3.85 ppm and 4.74 - 4.8 ppm, respectively.

^{1}H NMR titration studies for **4** and **5** were carried out in presence of varying [F^-] or [OAc^-]. A closer look at the ^{1}H NMR titration profile of **4** (Figure 2.5) revealed initial little upfield shifts for both methylene protons (unto [F^-] of 0.5 mole equivalent). These tend to suggest that initially an ion pair association between the cationic Ph_3P^+ moiety and the F^- could have been operational.[6g] Distinct downfield shifts for both methylene protons in **4** were observed on subsequent increase in [F^-]. This trend of the down field shift for methylene protons were prominent till 1.5 mole equivalents of F^- was added and this supported hydrogen bonding interactions involving methylene protons and F^-. These shifts were the result of the net deshielding effect induced by the hydrogen-bonding interaction between the methylene protons and the F^-. Higher $\Delta\delta$ ($\Delta\delta_4^{meta}$ = 0.066 ppm) for the *meta*-substituted methylene protons signified a stronger interaction with F^- than that of *para*-substituted ($\Delta\delta_4^{para}$ = 0.058 ppm) one. Thus, it would be reasonable to conclude that the observed shifts are actually the result of two opposing influences due to the ion-pair association of Ph_3P^+ moiety and the F^- as well as the hydrogen bonding interaction between methylene protons and F^-. Signals for methylene protons were found to be very broad and eventually disappeared for [F^-] ≥ 3.0 mole equivalents, which could be attributed to the deprotonation phenomena.

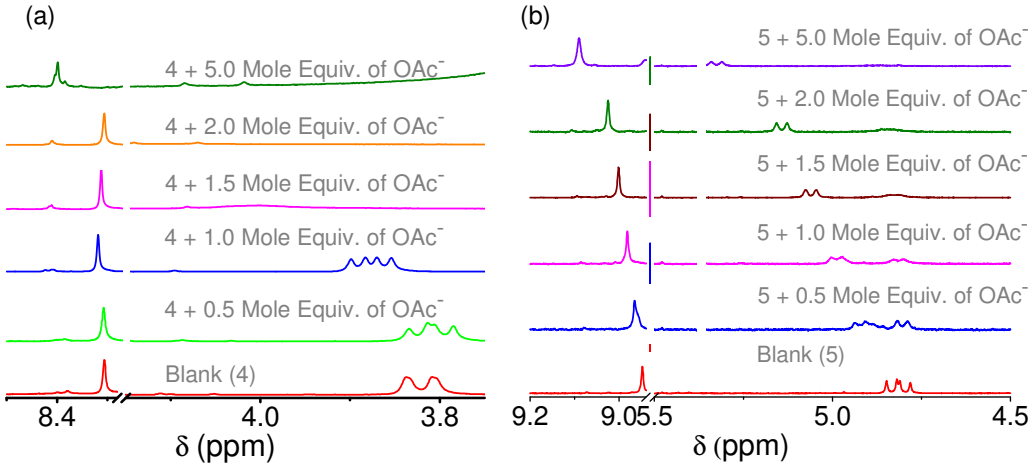

Figure 2.6. Partial ^{1}H NMR spectra of (i) **4** and (ii) **5** in CD_3CN with varying [OAc^-] in CD_3CN.

Analogous trend was observed for similar ^{1}H NMR titration studies with OAc^- (Figure 2.6). During initial addition of OAc^- (i.e. for lower [OAc^-], broad downfield shifted signals for methylene hydrogen atoms were observed for the 1:1 hydrogen bonded adduct formation. These signals were found to be shifted more downfield as well as broaden at higher [OAc^-]

and eventually disappear for relatively much higher [OAc^-]. Higher downfield shifts for meta-substituted methylene protons in **4** for hydrogen bonding interactions with F^- or OAc^- were also reflected a stronger interaction as well as the higher acidity of these protons. These presumptions were further confirmed from the results of the theoretical studies (*vide infra*).

Similar studies with **5** also revealed downfield shift of methylene proton on addition of F^- and OAc^-. On addition of 1.5 mole equivalents of [F^-], shift of methylene protons found to be $\Delta\delta_5^{para}$ = 0.06 ppm and $\Delta\delta_5^{meta}$ = 0.01 ppm. However on further increase in [F^-], the Bronsted acid-base equilibrium prevailed and signal for methylene proton disappear on addition of 5 mole equivalents of [F^-]. Deprotonation process that was evident for [F^-] beyond 2 mole equivalents also induced a detectable upfield shifts for phenyl ring protons, due to the overall increase in electron density on deprotonation. Similar trend of downfield shift of methylene proton was also observed for studies with [OAc^-] and **5** (Figure 2.6).

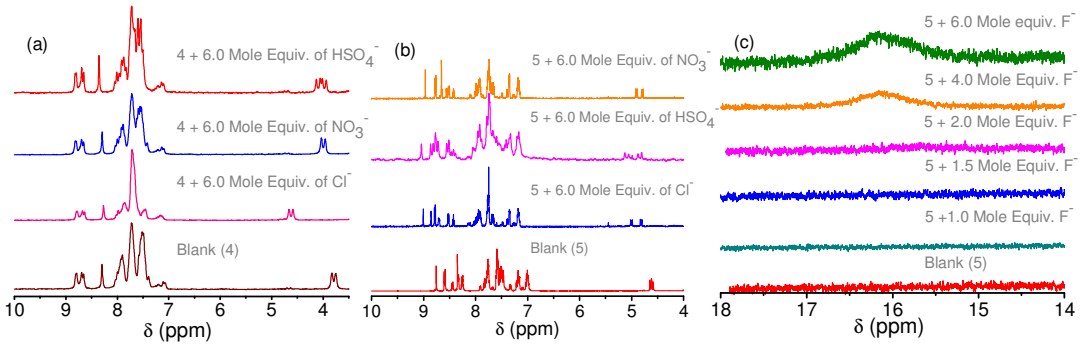

Figure 2.7. ^{1}H NMR spectra of (a) **4** and (b) **5** in presence of other anions. (c) Formation of signal for HF_2^- at 16 ppm for **5**.

These shifts in the ^{1}H NMR spectra for **4** and **5** were insignificant when recorded in presence of other anions studied (Figure 2.7). These minor shifts also confirmed weak interactions between **4** or **5** with these anions and also supported the fact that such weak interactions failed to perturb the energies of frontier orbitals for **4** or **5**. This was accounted for insignificant change in the HOMO-LUMO energy gap and thus, no detectable change in absorption spectra. Smaller size of the F^-, as compared to OAc^- would account for its higher charge density and thus, a more effective binding to the acidic methylene protons and the more pronounced shift.

2.3.2.2. ^{31}P NMR

^{31}P NMR spectra of **4** were also recorded with varying concentration of F^-. ^{31}P NMR spectra of the receptor **4** in CD_3CN show two signals at 22.09 ppm (for Ph_3P^+ attached to *para*-substituted methylene group) and 22.18 ppm (for Ph_3P^+ attached to *meta*-substituted methylene group). On addition of one mole equivalent of F^-, a little upfield shifts (21.95 and 22.08 ppm) were observed. However, on addition of excess of F^-, downfield shifts to 22.77 ppm and 27.24 ppm were observed for these two Ph_3P^+ groups, respectively (Figure 2.8).

Appreciable unsymmetrical shifts indicated that two P-atoms were certainly in different environment in presence of excess of F^-. These observations also indicated a difference in the nature of the interactions involving F^- and two different Ph_3P^+ ions for different [F^-]. Similar unsymmetric and appreciable downfield shifts to 22.83 and 27.22 ppm for two Ph_3P^+ groups were also observed when ^{31}P NMR spectra were recorded for **4** in presence of excess of OAc^- (Figure 2.8). However, such changes were only negligible when ^{31}P NMR spectra were recorded in presence of excess of other anionic analytes.

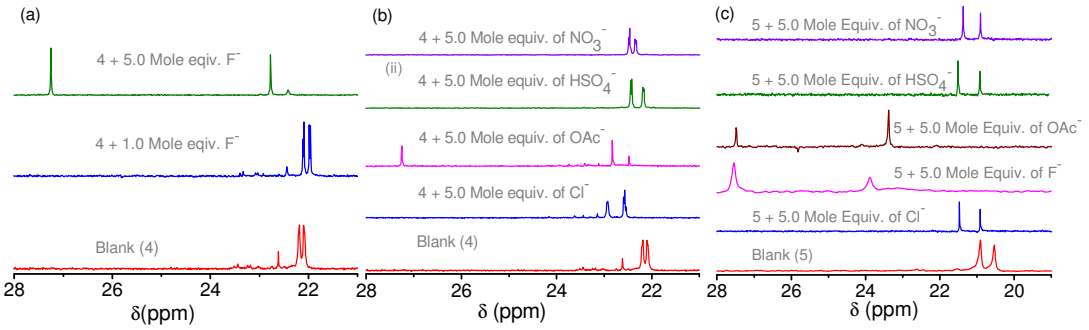

Figure 2.8. ^{31}P NMR spectra of (i) **4** in presence of F^- (ii) **4** in presence different anions (iii) **5** in presence of various anions.

^{31}P NMR spectra for **5** were also recorded in CD_3CN in presence of 5 mole equivalent of different anions at room temperature (Figure 2.8). ^{31}P NMR of receptor **5** in CD_3CN, clearly shows two signals at 20.54 (for Ph_3P^+ attached to *meta*-substituted methylene group) and 20.91 ppm (for Ph_3P^+ attached to *para*-substituted methylene group). In presence of different anions these peaks were found to be shifted downfield, while the extent of shifts varied based on the nature of anions. As it was observed for **4**, these shifts for **5** were significant for F^- ($\Delta\delta^{para}_{Ph3P+}$ = 6.66 ppm and $\Delta\delta^{meta}_{Ph3P+}$ = 3.34 ppm) or OAc^- ($\Delta\delta^{para}_{Ph3P+}$ = 6.5 ppm and $\Delta\delta^{meta}_{Ph3P+}$ = 2.8 ppm) and for all other anions these shifts were insignificant

($\Delta\delta^{para}_{Ph3P+}$ ~ 0.55 ppm and $\Delta\delta^{meta}_{Ph3P+}$ = 0.35 ppm). Observed unequal shifts of the signals for two Ph_3P^+ groups suggested an asymmetrical electronic environment for two P atoms in presence of excess F^-.

Thus, results of the ^1H NMR spectral data as well as the ^{31}P NMR spectral data corroborated observations of the spectrophotometric titration data, which suggested the presence of two equilibrium processes, namely the hydrogen bonded adduct formation for relatively lower [F^-] or [OAc^-] and a Bronsted acid-base equilibrium process at relatively higher concentration of respective ions. Deprotonation process at higher [F^-] or [OAc^-] was initiated through the formation of the thermodynamically stable higher aggregates HX_2^- (X being F^- or OAc^-). Formation of HF_2^- was evident from the appearance of the broad signal for HF_2^- at 16.1 ppm (Figure 2.7).

2.3.3. Computational Study

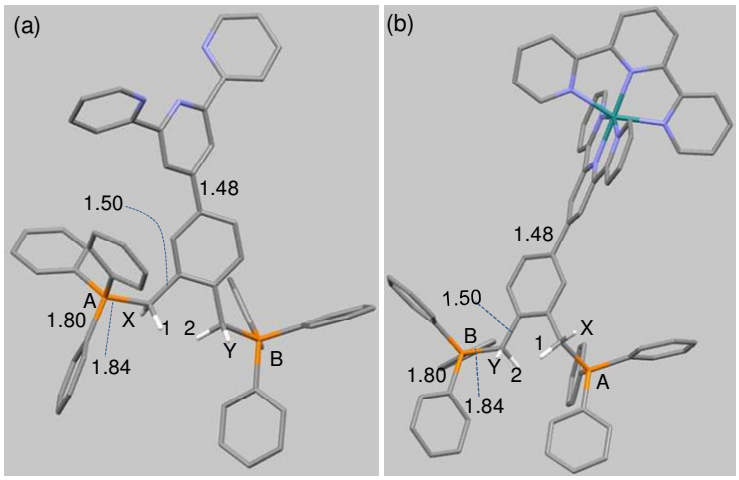

Figure 2.9. M05-2X/6-31G* optimized geometries and important distances (Å) of (a) **4** and (b) **5**; (Grey: C; green: Ru; orange: P; blue: N; white: H).

The optimized geometry of **4** and its possible fluoride ion complexes (1:1 and 1:2) are given in Figures 2.9 and 2.10. The calculated structure of **4** revealed that the arrangement of active methylene hydrogen atoms was different than the previously reported anthraquinone[6f] and naphthalene[6g] based receptors. Optimized structures (Figure 2.9) for receptors **4** and **5** suggested that the methylene hydrogen atoms (H_1 and H_2) were appropriately aligned to cooperate in binding with these two anionic analytes, whereas, the other two hydrogen atoms (H_x and H_y) are oriented away from each other (Figure 2.9). Such an arrangement of methylene groups in **4** presumably arose due the unsymmetrical

placement of triphenylphosphine group with respect to the terpyridyl group. We have also observed the similar arrangement of methylene hydrogen atoms in Ru(II)-terpyridyl complex **5** (Figure 2.9(b)).

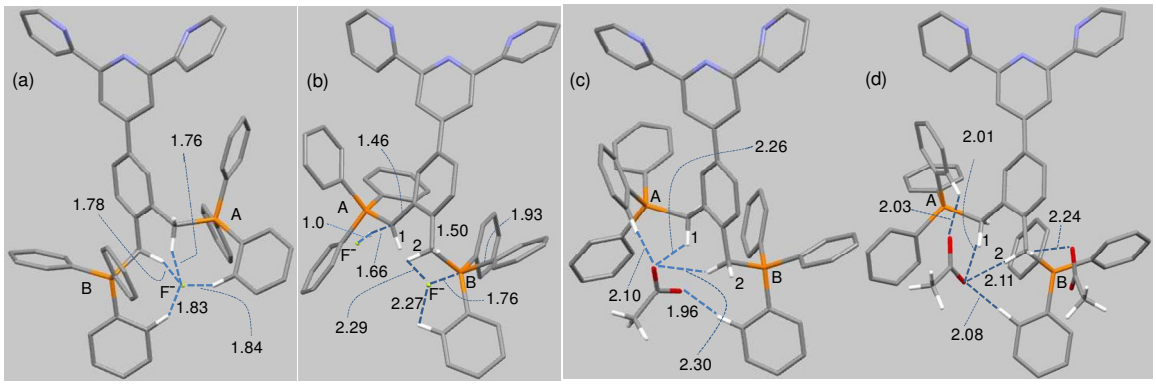

Figure 2.10. M05-2X/6-31G* optimized geometries and important distances (Å) of (a) **4.F⁻** and (b) **4.2F⁻** (c) **4.OAc⁻** and (d) **4.2OAc⁻**. In **4.2F⁻**, (Grey: C; orange: P; blue: N; white: H; Greenish yellow: F).

The asymmetrical arrangement of the active methylene hydrogen atoms were also supported by the ^{1}H NMR study, where two different signals were observed for H_1 and H_x, and H_2 and H_y. The interactions of F^- with **4** were calculated with both one (**4.F⁻**) and two fluoride (**4.2F⁻**) ions. The calculated geometry suggested that the active methylene hydrogen atoms were asymmetrically bound to the F^- ion, i.e., distances observed for F^-…H_1 and F^-…H_2 were 1.78 Å and 1.76 Å, respectively (Figure 2.10(a)). Phenyl hydrogen atoms were also found to interact with the F^-. The calculated binding energy of **4** with one F^- was found to be -176.9 kcal/mol at M06/6-31+G**//M05-2X/6-31G* level of theory. Further, interactions of receptor **4** with two fluoride ions have also been calculated. The optimized geometry of **4** with two fluoride ions (**4.2F⁻**; Figure 2.10(b)) revealed that one of the F^- interacted with active methylene hydrogen atom as well as with one of the two positively charged phosphorous center. Figure 2.10(b) also showed that F^- ion could abstract the H_x hydrogen atom from the carbon centre (1.66 Å). The calculated F^- affinity of **4.2F⁻** was found to be -275.1 kcal/mol, which was much higher than the F^- affinity of **4.F⁻.** Interestingly, the equilibrium constants calculated for **4.F⁻** and **4.2F⁻** show that the later has lower stability than the former one. We have further examined the stability of **4.F⁻** and **4.2F⁻** in acetonitrile medium. The calculated results show that the stability of **4.2F⁻** is lower compared to **4.F⁻** M06/6-31+G**//M05-2X/6-31G* level of theory (Table 2.1). Closer look at the optimized structure for **4.F⁻** also suggested that the abstraction of methylene hydrogen atom led to a partial double bond character C_{phenyl}-CH (1.46 Å) in the ring system

(Figure 2.10(b)). Consequently, the anisotropy was generated with the formation of the partial double bond and the positively charged phosphorus (A) atom was presumably placed in the deshielded zone, which could be attributed to the observed downfield shift in ^{31}P NMR signal. We have observed that this P-center (A) has a higher ($\delta_{31P}{}^{Para}$ = 27.24 ppm and ($\delta_{31P}{}^{Meta}$ = 22.77 ppm) chemical shift value in ^{31}P NMR spectra.

Table 2.1: Calculated binding energies of receptors **4** and **5** with F^- and OAc^- in the gas phase and in acetonitrile (ε = 35.688) using SCRF-PCM solvation model. Energies in kcal/mol.

Name	M06	PCM-M06
4.F$^-$ *a*	-176.9	-17.8
4.2F$^-$ *a*	-275.1	-11.6
4.OAc$^-$ *a*	-152.7	-16.0
4.2OAc$^-$ *a*	-228.4	-11.5
5.F$^-$ *b*	-233.0	-15.1
5.2F$^-$ *b*	-414.6	-22.1
5.OAc$^-$ *b*	-210.9	-15.9
5.2OAc$^-$ *b*	-357.1	-15.8

a: Single-point calculations with higher basis set 6-31+G** and M06 DFT functional using M05-2X/6-31G* optimized geometry. *b*: H, O, N, C, P, F elements were treated with 6-31+G** whereas ruthenium ion was treated with LANL2DZ basis set.

Similar types of interactions were also observed with acetate ion (OAc^-) and $2OAc^-$ (Figure 2.10). In presence of single acetate ion, O_{COO^-} centre of carboxylic acid was involved in hydrogen bonding interactions with two active methylene hydrogen atoms and with two phenyl ring hydrogen atoms (Figure 2.10(c)). However, the acetate ion affinity of **4.OAc$^-$** was found to be -152.7 kcal/mol, which is lower than the binding affinity of **4.F$^-$** complex. The solvent phase calculations also reveal that the binding energy of F^- with **4** is relatively higher than the binding energy of OAc^- with this receptor molecule (Table 2.1). The weaker interaction of OAc^- could be attributed to the steric interaction between the receptor unit and analyte compared to the F^- ion.

We have also extended our study with **5** in presence of fluoride and acetate ions to examine their interactions computationally. Optimized structure revealed that the two terpyridyl units were nearly perpendicular to each other in **complex 5** (Figure 2.9). Figure 2.11 reveals that the hydrogen bonding interactions of the F^- in complex **5.F$^-$** were strong with two active methylene hydrogen atoms. Also, an asymmetrical pattern in interaction i.e.

F^-…H_2 (1.86 Å) and F^-…H_1 (2.27 Å) was observed with two $H_{Methylene}$ atoms (Figure 2.11 (a)).

A strong interaction between F^- and positively charged phosphorus (A) atom was also evident for **5.2F$^-$**, which was not observed in **5.F$^-$**. The calculated fluoride ion binding affinity of **5.F$^-$** was found to be -233.0 kcal/mol with M06/6-31+G**//M05-2X/6-31G* level of theory. Nature of interactions of two fluoride ions and complex **5** (i.e. in **5.2F$^-$**) were found to be similar to that was observed for **4.2F$^-$** (Figures 2.10(b) and 2.11(b)). However, it is worth noting that the abstraction of a proton (H_y) with the second F^- ion took place from a different active methylene center than it was observed for **4.2F$^-$**. This result has been corroborated with the observed ^{31}P NMR data for **4** and **5** with F^- ion. H_y proton abstraction from methylene carbon centre leads to a significant conjugation in **5.2F$^-$** (Figure 2.11) and which is further observed in binding affinity calculations. The calculated binding affinity of complex **5** with fluoride ion was found to be -414.6 kcal/mol.

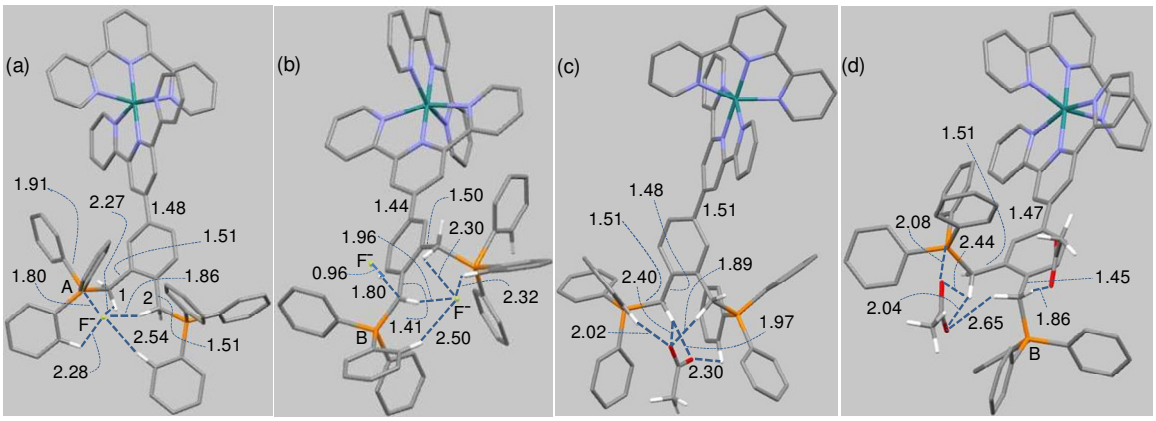

Figure 2.11. Optimized geometries and important distances (Å) of (a) **5-F$^-$** and (b) **5-2F$^-$** (c) **5.OAc$^-$** (d) **5.2OAc$^-$** . The interactions between two F^- and complex **5** are totally different from its analogous structures. Deprotonation is happening in presence of 2F^- and conjugation has been observed in **5-2F$^-$** . (Grey: C; green: Ru; orange: P; blue: N; white: H; Greenish yellow: F).

The interaction patterns for **5** with acetate ions (**5.OAc$^-$** and **5.2OAc$^-$)** were also examined with M06/6-31+G**//M05-2X/6-31G(d) level of theory. For **5.OAc$^-$**, acetate ion was found to interact with two phenyl hydrogen atoms and with two methylene hydrogen atoms, while the associated binding affinity was evaluated as -210.9 kcal/mol (Figure 2.11 and Table 2.1). The binding affinity of complex **5** towards the acetate ions in **5.2OAc$^-$** was evaluated as -357.1 kcal/mol, which was much lower than that was evaluated for **5.2F$^-$** complex. However, the binding energies calculated in solvent phase shows an interesting trend. The interaction energy of **5.F$^-$** is slightly lower than the corresponding binding energy of **5.OAc$^-$**

(Table 2.1). However, the interaction energy of **5.2F⁻** is much higher compared to the corresponding **5.2OAc⁻**. The experimental composite equilibrium constants evaluated for F^- and OAc^- were $(3.97 \pm 0.3) \times 10^7$ M^{-2} and $(8.36 \pm 0.45) \times 10^6$ M^{-2}, respectively, and this trend agrees well with that of the composite calculated binding energies (Table 2.1).

The previously reported receptors with acidic methylene hydrogen atoms were found to bind efficiently to F^- and also weakly to $H_2PO_4^{2-}$.[6f,g] The results of our experimental studies reveal that these two newly designed receptors (**4** and **5**) having acidic methylene hydrogen atoms are found to bind effectively to F^- and less effectively to OAc^-. We have not observed any affinity towards $H_2PO_4^{2-}$ for **4** and **5**. Relative spatial orientations of the active methylene hydrogen atoms could account for this difference and thus, the present study reveals how subtle changes in this as well as in acidity of these protons could influence the recognition process of relatively larger anions.

2.4. Conclusion

In this chapter we demonstrate that the presence of the positively charged phosphonium ion also contribute to the overall binding of F^- and OAc^- to the methylene functionality of the receptors **4** and **5**. Our earlier studies revealed that subtle difference in the relative special orientations could actually influence hydrogen bonding interaction of these methylene hydrogen atoms and the fluoride ion. To envisage the role of the acidity of the active methylene hydrogen atoms, while maintaining the identical relative spatial arrangement, a corresponding Ru(II)-bis terpyridyl complex was synthesized and used for hydrogen bonding interaction studies with different anionic analytes. Receptor **4** and **5** presented almost similar spatial orientations of the active methylene hydrogen atom and thus offered us the opportunity to reveal the role of the increase in acidity of the methylene protons on the affinities of the methylene hydrogen atoms towards F^-/OAc^-. Hydrogen bonding interactions at lower concentrations of these two anionic analytes and deprotonation equilibrium at higher concentration were observed with associated electronic spectral changes as well as visually detectable change in solution colour. DFT calculations substantiated the efficient hydrogen bonding interactions of F^- and OAc^- with receptor molecule **4**. The metal complex based receptor, **5** showed even stronger binding with these two analytes compared to the parent system **4**. Optimized geometries further revealed that extended conjugation in **5** was observed on deprotonation of one of the two methylene hydrogen atoms, which could help to facilitate the deprotonation process. The importance of hydrogen bonding interaction between the hydrogen atoms of the active

methylene groups and an anionic analyte as a motif for recognition of certain anionic analytes was explored and experimental results were rationalized based on the results of the detailed computational studies. Such unconventional binding motifs associated with appropriate reagent could be useful for design of new efficient receptors for molecular recognition studies.

2.5. References

1. (a) Sessler, J. L.; Gale, P. A.; Cho, W. S. *Anion Receptor Chemistry; Royal Society of Chemistry: Cambridge, UK,* **2006**. (b) Santos-Figueroa, L. E.; Moragues, M. E.; Climent, E.; Agostini, A.; Martínez-Máñezl, R.; Sancenón, F. C*hem. Soc. Rev.,* **2013**, *42*, 3489. (c) Duke, R. M.; Veale, E. B.; Pfeffer, F. M.; Kruger, P. E.; Gunnlaugsson, T. *Chem. Soc. Rev*., **2010**, *39*, 3936.

2. (a) Krik, K. L. *Biochemistry of Halogens and Inorganic Halide*s; Plenum Press: New York, **1991**; p 59l. (b) Kleerekoper, M. *Endocrinol Metab. Clin., North Am.* **1998**, *27,* 441. (c) Horowitz, H. S. *J. Public Health Dent.,* **2003**, *63*, 3.

3. *Ayoob S.; Gupta, A. K. Crit. Rev. Environ. Sci., Technol. **2006**, 36, 433s.*

4. (a) Gazzano, E.; Bergandi, L.; Riganti, C.; Aldieri, E.; Doublier, S.; Costamagna, C.; Bosia, A.; Ghigo, D. *Curr. Med. Chem.,* **2010**, *17*, 2431. (b) Friesen, M. C.; Benke, G.; Monaco, A. D.; Dennekamp, M.; Fritschi, L.; Klerk, N. D.; Hoving, J. L.; MacFarlane, E.; Sim, M. R. *Cancer Causes Control*., **2009**, *20*, 905. (c) Grandjean, P.; Landrigan, P. J. *Lancet*, **2006**, *368*, 2167. (d) Barbier, O.; Arreola-Mendoza, L.; Del Razo, L. M. *Chem. Biol. Interact*., **2010**, *188*, 319. (e) Sandhu, R.; Lal, H.; Kundu, Z. S.; Kharb, S. *Bio. Trace Elem. Res.,* **2011**, *144*, 1.

5. (a) Jose, A. D.; Kumar, D. K.; Ganguly, B.; Das, A. *Tetrahedron Lett*., **2005**, *46*, 5343. (b) Ghosh, A.; Ganguly B.; Das, A. *Inorg. Chem.,* **2007**, *46*, 9912. (c) James, K. B. *Acc. Chem. Res*., **2005**, *38*, 671. (d) Jose, A. D.; Kumar, D. K.; Kar, P.; Verma, S.; Ghosh, A.; Ganguly, B.; Ghosh H. N.; Das, A. *Tetrahedron*, **2007**, *63*, 12007. (e) Ghosh, A.; Jose, A. D.; Ganguly, B.; Das, A. *J. Mol. Model*., **2010**, *16*, 1441. (f) Wang J.; Bai F. Q.; Xia B. H.; Sun L.; Zhang H. X. *J. Phys. Chem. A*, **2011**, *115*, 1985.

6. (a) Shionoya, M.; Furuta, H.; Lynch, V.; Harriman, A.; Sessler, J. L. *J. Am. Chem. Soc*., **1992**, *114*, 5714. (b) Amendola, V.; Boiocchi, M.; Fabbrizzi, L.; Palchetti, A. *Chem. Euro. J*., **2005**, *11*, 120. (c) Amendola, V.; Boiocchi, M.; Fabbrizzi, L.; Palchetti, A. *Chem. Euro. J*., **2005**, *11*, 5648. (d) Mascal, M.; Yakovlev, I.; Nikitin, E. B.; J. Fettiger, C. *Angew. Chem., Int. Ed.,* **2007**, *46*, 8782-8784. (e) Arunachalam, M.; Suresh, E.; Ghosh, P. *Tetrahedron*, **2007**, *63*, 11371. (f) Das, P.; Mondal, A. K.; Kesharwani, M. K.; Suresh, E.; Ganguly, B.; Das, A. *Chem. Commun.,* **2011**, *47*, 7398. (g) Das, P.; Kesharwani, M. K.; Mandal, A. K. Suresh, E.; Ganguly, B.; Das, *Org. Biomol. Chem.,* **2012**, *10*, 2263. (h) Hamadi, A.; Num, K. C.; Ryu, B. J.; Kim, J. S.; Viceness, J. *Tetrahedron Lett.,* **2004**, *45*, 4689.

7. Shiraishi, Y.; Sumiya, S.; Kohono, Y.; Hirai, T. *J. Org. Chem*., **2008**, *74*, 8571.

8. Zhao, Y.; Schultz, N. E.; Truhlar, D. G. *J. Chem. Theory and Comput.,* **2006**, *2*, 364

9. (a) O'Reilly, R. J.; Karton, A.; Radom, L. *J. Phys. Chem. A,* **2013***, 117,* 460. (b) Yu, H-Z.; Yang, Y-M.; Zhang, L.; Dang, Z-M.; Hu, G-H. *J. Phys. Chem. A,* **2014***, 118,* 606.

10. Zhao, Y.; Truhlar, D. G. *Theor. Chem. Acc.,* **2008***, 120*, 215.

11. Wong, M. W.; Frish, M. J.; Weiberg, K. B. *J. Am. Chem. Soc.,* **1991**, *113*, 4776.

12. Cossi, M.; Barone, V. *J. Chem. Phys.,* **2000**, *112*, 2427.

13. Frisch, M. J.; Trucks, G. W.; Schlegel, H. B.; Scuseria, G. E.; Robb, M. A.; Cheeseman, J. R.; Scalmani, G.; Barone, V.; Mennucci, B.; Petersson, G. A.; et al. *Gaussian 09*, *Revision B01; Gaussian, Inc:* Wallingford, CT*,* **2010**.

14. Hariharan, P. C.; Pople, A. *J. Chem. Phys.*, **1974**, *27*, 209.

15. (a) Hay, P. J.; Wadt, W. R. *J. Chem. Phys.,* **1985**, *82*, 270. (b) P Hay, P. J.; Wadt, W. R. *Chem. Phys.*, **1985**, *82*, 299.

16. (a) Zhao, Y.; Truhlar, D. G. *J. Chem. Theory Comput.,* **2009**, *5,* 324. (b) Zhao, Y.; Truhlar, D. G. *Org. Lett.,* **2007**, *9*, 1967-1970. (c) Sieffert, N.; Bühl, M. *Inorg. Chem.,* **2009,** *48,* 4622.

17. (a) Wong, M. W.; Frish, M. J.; Weiberg, K. B. *J. Am. Chem. Soc.,* **1991**, *113*, 4776.

18. Das, P.; Ghosh, A.; Kesharwani, M. K.; Ramu, V.; Ganguly, B.; Das, *Eur. J. Inorg. Chem.,* **2011,** 3050.

19. Sauvage,J. P.; Collin, J. P.; Chambron J. C.; Guillerez, S.; Coudret, C.; Baltani,V.; Barigelletti, F.; Cola, L. D.; Flamign, L. *Chem. Rev.,* **1994**, *94*, 993.

20. (a) Xu, Z.; Kim, S.; Kim, H. N. S.; Han, J.; Lee, C.; Kim, J. S.; Quan, X.; Yoon, J. *Tetrahedron Lett.,* **2007**, *48*, 9151. (b) Caltagirone, C.; Bates, G. W.; Gale, P. A.; Light, M. E. *Chem. Commun.,* **2008**, 61. (c) Ghosh, A.; Verma, S.; Ganguly, B.; Ghosh, H. N.; Das, A. *Eur. J. Inorg. Chem.,* **2009**, 2496. (d) Esteban-Gómez, D.; Fabbrizzi, L.; Licchelli, M.; Monzani, E. *Org. Biomol. Chem.*, **2005**, *3*, 1495. (e) Das, S. K.; Misra, S. S.; Sahu, P. K.; Nijamudheen, A.; Mohan, V.; Sarkar, M. *Chem. Phys. Lett.*, **2012**, *546* , 90. (f) Liu, W.; Wang, B.; Zhang, C.; Yin, X.; Zhang, J. *Int. J. Quant. Chem.,* **2014**, *114*, 138.

CHAPTER 3

FLUORESCENT PROBE FOR DETECTION OF CYANIDE ION IN AQUEOUS MEDIUM: CELLULAR UPTAKE AND ASSAY FOR β-GLUCOSIDASE AND HYDROXYNITRILE LYASE

Publication:
J. Mat. Chem. B, ***2015,*** *3, 9148-9156*

3.1. Introduction

Among various toxic anions, cyanide ion (CN^-) is considered to be the most toxic and its acute toxicity towards mammals primarily arises from its adverse influences on the central nervous system.[1] Cyanide primarily binds to metallic cofactors in metalloenzymes, adversely influencing the enzyme and cell function. It inhibits the activity of Cytochrome-*c* oxidase and causes histotoxic hypoxia, which further adds to the toxicity by reducing the unloading gradient of oxyhemoglobin.[2]

Despite influences on living organisms, cyanide is extensively used in various industries like metal gold mining, electroplating, petrochemical, synthetic fibers and the resin industry.[3] Regardless of environmental consciousness, certain amount of this toxic ion escapes into the environment either as water soluble cyanide species or as HCN. Some fruits and vegetables such as cassava, lima beans, bitter almond, etc. also contain high level of cyanogenic glycosides which are potential source of cyanide in the presence of certain enzymes and can be lethal if not processed properly before consumption.[4] The World Health Organization (WHO) has set the maximum allowed cyanide contaminant in drinking water to be 1.9 μM.[5] Due to its extreme physiological toxicities, a suitable reagent for the efficient and preferential recognition of cyanide species in water, more specifically in physiological condition is a fundamental requirement.[6] If such reagent allows recognition process through fluorimetric response, the option of using such probe molecule as an imaging reagent for the detection of cellular uptake of cyanide species becomes a possibility.[7]

To address these researchers have put effort into designing new molecular probes that could show fluorescence response on reaction with CN^- and/or HCN in physiological conditions. The impact of such reagents will be greater if they could be used as an imaging reagent for the detection of cellular uptake of cyanide species. Such reagents could also be used to develop appropriate enzyme assay protocols for important industrial enzymes.[8,9] β-glucosidase is an important enzyme that plays an important role in a variety of fundamental biological processes like liberation of aromatic compounds from glucosidic precursors or detoxification of cyanogenic glycosides.[10] β-glucosidase, obtained from bitter almond, is known to have three different enzymes namely, amygdalin lyase, prunasin lyase and hydroxynitrile lyase (HNL),[11] each one is specific for one hydrolytic stage (*vide infra*). Thus, it is expected to release CN^- and/or HCN on reacting with amygdalin ([O-β-d-

gluco-pyranosyl-(1-6)-β-d-glucopyranosyloxy]benzeneacetonitrile), an important cyanogenic glycoside found in various fruits and seeds.[12] Hydroxynitrile lyases are the versatile group of enzymes, which play a significant defensive role in plant system against microbial attack and also cause the release of HCN or CN^- from biologically active cyanohydrin like mandelonitrile.[11]

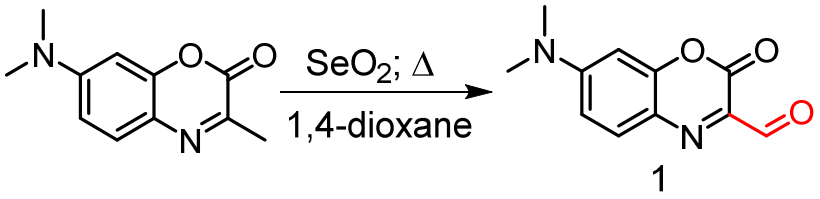

Scheme 3.1: Methodology adopted for synthesis of the reagent **1.**

3.2. Experimental section

3.2.1. Materials

3-(dimethylamino)phenol, hydrazine hydrate, ethyl pyruvate, selenium dioxide were purchased from Sigma-Aldrich and were used as received. Sodium salts of different anions and other reagents were used as received from S. D. Fine Chemical, India. Amygdalin, mandelonitrile, β-glucosidase and hydroxylnitrile lyase were purchased from Sigma-Aldrich and used as received. Dimethyl sulphoxide (DMSO) of HPLC grade was used for our studies.

3.2.2. Analytical Methods

^1H and ^{13}C NMR spectra were recorded on a Bruker 200/500 MHz FT NMR (Model: Avance-DPX 200/400/500) using trimethylsilane (TMS) as an internal standard. FTIR spectra were recorded as KBr pellets in a cell fitted with a KBr window, using a Perkin-Elmer Spectra GX 2000 spectrometer. ESI-Ms measurements were carried out on a Waters QTof-Micro instrument. Solution pH was evaluated using Mettler Toledo FEP20 pH meter. Absorption spectra were recorded using a Perkin Elmer Lambda 950 UV-Vis spectrophotometer equipped with cell holder having path length of 1 cm. Fluorescence spectra were recorded on PTI QuantaMaster 400 spectrophotometer.

3.2.3. Generalised methodology for spectroscopic studies

Deionised water and HPLC grade DMSO were used as solvent for spectroscopic studies. A stock solution of **1** (5.0×10^{-3} M) in DMSO was prepared and used for further studies. Another solution having 1.2 mM of CTAB (CMC for CTAB is 1 mM) in 10 mM aq. HEPES buffer (pH 7.2) was prepared. To a 5 ml of this 1.2 mM of CTAB solution, 20 µl of stock solution of the reagent **1** (5.0×10^{-3} M in DMSO) was added and the resulting aq. solution (aq. HEPES buffer:DMSO of 250:1, v/v; pH 7.2) having this reagent trapped inside the micellar structure of CTAB was used for all spectroscopic study. Different anions as their sodium salt were used for studies and all spectra were recorded at room temperature. For systematic titration studies, CN^- was added in an incremental manner.

The relative fluorescence quantum yields (ϕ_f) were estimated using equation 1 by using the integrated emission intensity of Coumarin-6 in ethanol (Φ = 0.78 at RT) as a reference.

$$\Phi_f = \Phi_f'(I_{sample}/I_{std})(A_{std}/A_{sample})(\eta^2_{sample}/\eta^2_{std}) \qquad \text{Equation 1}$$

where, Φ_f' is the absolute quantum yield for the Coumarin-6, used as standard; I_{sample} and I_{std} are the integrated emission intensities; A_{sample} and A_{std} are the absorbance at the excitation wavelength, and η_{sample} and η_{std} are the respective refractive indices of sample and standard.The lowest detection limit was calculated by following 2σ/k method; where σ is the standard deviation of blank measurement, k is the slope of intensity *vs.* [CN^-] plot.

3.2.4. Cell Culture and Confocal study

MDA-MB-231 human breast adenocarcinoma cells were cultured in complete medium at 37°C under 5% CO_2 atmosphere. The complete medium was comprised of DMEM, supplemented with 10% FBS, 1% antibiotics. For the experiments, after trypsinization, cells were seeded on to glass bottomed petridish at the density of 5000 cells per square cm and incubated for 24 hours. For fluorescence intensity imaging, MDA-MB-231 cells were fixed with 4% paraformaldehyde for 15-20 minutes, followed by incubation of the cells with 20 µL of **1** (10^{-3} M) in 1 mL of PBS in two different Petri-dishes for 30 minutes at 37℃ under 5% CO_2 atmosphere. After incubation, cells were washed twice with pre-warmed (37℃) phosphate-buffered saline (pH 7.4). For cyanide sensing these cells were incubated with 200 µM of CN^- for 15 minutes and then washed twice with PBS buffer, and visualized under inverted microscope (Olympus IX71) equipped with epifluorescence

optics using a 10× phase-contrast objective, and a halogen lamp as a light source (Olympus FITC filter 488 - 525 nm). Images were taken with Q Imaging camera controlled by Image pro plus software.

3.2.5. Spatially resolved fluorescence spectroscopy

A home-built objective-based epifluorescence/TIRF microscopy setup was used to perform intensity and spectrally-resolved imaging of Breast cancer cells.[13] In brief, a 458 nm cw Ar^+ laser was used to illuminate the sample (~30 mm diameter) of fixed cells under TIRF mode through an inverted microscope (Nikon Eclipse 2000U). The emerging fluorescence was collected by the same objective and separated from the excitation beam by using 488 nm dichroic mirror and a long pass filter, and imaged using a CCD camera (DVC 1412AM). Intensity images were collected at 10 Hz with excitation powers low enough (200 W/cm^2) to minimize photobleaching. To obtain the fluorescence emission profiles from submicroscopic regions (~0.25 μm^2) in a high-throughput manner, the entire emission in absence of filters was collected through a combination of an adjustable narrow slit and transmission grating (70 l/mm, Optometrics) mounted in front of the CCD. Different microscopic regions within a cell as well as different cells in the ensemble were selected by moving the sample stage laterally while maintaining the focus. The dispersed emission spectra collected via the narrow vertically oriented slits were integrated along 5 pixels in vertical direction, and pixel to wavelength conversion was performed using several laser lines. All spectral data, arbitrarily chosen from different subcellular regions or from various cells, were obtained at identical excitation powers (~200 W/cm^2) and 300 ms exposure time, and corrected for detector wavelength response. To construct statistically relevant distributions of emission peak positions and integrated intensities, more than 1000 spatially-resolved (0.25 μm^2) emission spectra were collected from ~15 cells in the absence and presence of cyanide, of which ~470 spectra were analyzed (for each) using Origin 8.0. All the measurements are carried out under ambient conditions at 295K.

3.2.6. Synthesis of Probe 1

(7-(dimethylamino)-3-methyl-2H-benzo[b][1,4]oxazine-2-one was prepared by a similar method as previously reported.[14] (7-(dimethylamino)-3-methyl-2H-benzo[b][1,4]oxazine-2-one (500 mg, 2.2 mmol) and selenium dioxide (333 mg , 3.0 mmol) was dissolved in 1,4-dioxan and heated at 75℃ for overnight. Then filtered over celite-545, evaporated to dryness and purified by column chromatography using silica (100-200 mesh) as stationary

phase and petether:ethylacetate (4:1) as eluent and further recrystalised from n-hexane to get pure product. (210 mg, 43 %). ^{1}H NMR (200 MHz, CD_3CN, 25 ^{o}C, TMS) 9.33 (s, $1H_e$,), 7.66 (d, $1H_c$, J = 8 Hz), 6.92 (dd, $1H_b$, J = 10 Hz, 2 Hz), 6.57 (d, $1H_a$, J =2 Hz), 3.20 (s, $6H_d$,). ^{13}C NMR (125 MHz, DMSO-d6, 25 ^{o}C, TMS) 55.37, 96.97, 112.27, 124.10, 132.75, 135.39, 151.18, 152.15, 155.67, 188.14. IR (KBr) ν_{max}/cm^{-1}: 2923, 2848, 1714, 1671, 1612, 1495, 1444, 1373. ESI-MS (*m/z*): 219.0764 $[M + H]^+$ Elemental analysis: $C_{11}H_{10}N_2O_3$ calculated C (60.55), H (4.62), N (12.84); found C (60.5), H (4.67), N (12.80).

3.3. Results and Discussions

Reagent **1** was prepared following a previously reported procedure, with necessary modification (Scheme 3.1). Oxidation of the methyl group with SeO_2 yielded the desired product **1**. After initial purification of the reagent (**1**) by column chromatography, using ethyl acetate-petether (1:4, v/v) as eluent and silica gel (100-200 mesh size) as the stationary phase, reagent **1** was further purified by recrystallization from n-hexane to ensure the desired purity. Proper characterization and purity of the isolated compound were ascertained based on the results of various analytical and spectroscopic (^{1}H & ^{13}C NMR and ESI-Ms) studies. For the present study, typically solutions having effective concentration of 1.2 mM for CTAB and 10 mM for aq. HEPES buffer with effective solution pH of 7.2 were used. Use of such micellar structure as “solubilizer" for organic molecules in water is not uncommon in the literature and we have adopted this ideology for our studies in physiological condition.[15]

3.3.1. Spectroscopic studies

The absorption spectrum of **1** (20 μM) in aqueous HEPES buffer medium (aq. buffer:DMSO of 250:1, v/v; pH 7.2) having 1.2 mM CTAB, showed a high energy band at 300 nm ($\varepsilon = 7.46\times10^3$ M^{-1} cm^{-1}) and a low energy band at 505 nm ($\varepsilon = 2.26\times10^4$ M^{-1} cm^{-1}) (Figure 3.1). The band at 300 nm can be attributed to a π-π^* transition, whereas the band at 505 nm was assigned to be intra-molecular charge transfer (ICT) process involving dimethylamino group as the donor and carbonyl group as an acceptor moiety. This solution shows a weak emission ($\Phi = 0.009$) when excited at 430 nm (Figure 3.1). Electronic spectra of the reagent **1** in identical solvent medium were recorded in absence and presence of all common amino acids (e.g. AAs: Ala, Ser, Trp, Met, Val, Arg, Phe, Pro, Thr, Gly, Lys, His, Asp, Ile, Leu, Glu, Tyr, Cys, Hcy), glutathione (GSH) and common anionic

analytes (e.g. F^-, Cl^-, Br^-, I^-, CN^-, CH_3COO^-, $H_2PO_4^-$, $P_4O_7^{4-}$, SO_4^{2-}, NO_2^-, NO_3^- & HSO_3^-) (Figure 3.1a). A distinct blue shift of 80 nm of the ICT band at 505 nm was observed in presence of added CN^- (Figure 3.1a) and HSO_3^- with an associated visually detectable change in solution colour from red to yellow.

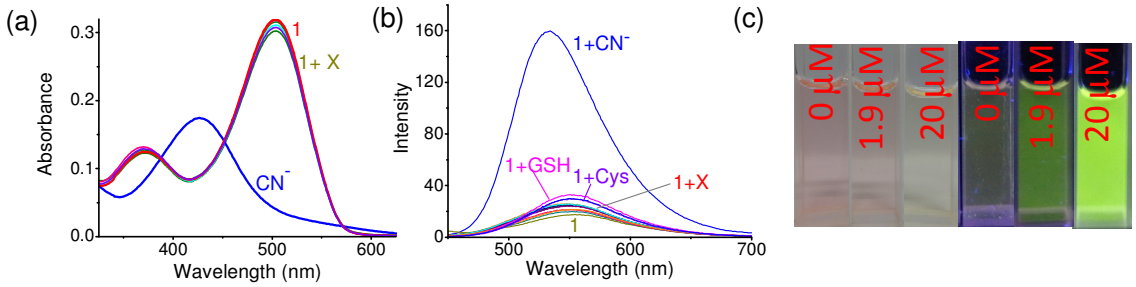

Figure 3.1. (a) Change in absorption and (b) emission spectra of **1** (20μM) in absence and presence of 10 equivalents of X (X= F^-, Cl^-, Br^-, I^-, CN^-, HSO_4^-, NO_2^-, NO_3^-, OAc^-, $H_2PO_4^-$), different AAs and 10 mole equivalents of GSH) λ_{Ext} of 430 nm was used for all luminescence studies. (c) Photograph showing the visually detectable changes in solution colour and fluorescence for **1** (10 μM) in presence of 1.9 μM (threshold concentration of CN^- for safe drinking water) and 20 μM of NaCN. All studies were performed in 10 mM aq. HEPES-DMSO (250:1, v/v) having 1.2 mM CTAB (pH 7.2) and a hand held 365 nm UV lamp was used for illumination.

Reaction of the aldehyde functionality of **1** with cyanide species (CN^- and/or HCN) was expected to yield the corresponding cyanohydrin derivative and this adversely influenced the ICT transition dipole, which was accounted for the observed blue shift. All other anions, biothiols and amino acids failed to induce such reaction and these results clearly revealed the specificity of the probe **1** towards CN^- and/or HCN in aq-buffer medium (pH = 7.2). An earlier report revealed that this reagent can be utilized for chemodosimetric detection of Cys and Hcy in acetonitrile-aq. HEPES buffer (10 mM, pH = 7.2) solution (3:7, v/v; RT) and no other amino acid was found to interfere in the detection process.[14] However, our studies revealed that the solution luminescence of **1**, trapped inside the micellar structure of the CTAB in aq. HEPES buffer medium (aq. buffer:DMSO of 250:1, v/v) remained practically invariant in presence of externally added 10 mole equivalent of various amino acids (AA: Ala, Ser, Trp, Met, Gln, Val, Arg, Phe, Pro, Thr, Gly, Lys, His, Asp, Ile, Asn, Leu, Glu, Tyr, Cys, Hcy, GSH) and all common anions (e.g. F^-, Cl^-, Br^-, I^-, CH_3COO^-, $H_2PO_4^-$, HSO_3^-, $P_4O_7^{4-}$, HSO_4^-, NO_2^- & NO_3^-) except HSO_3^- and CN^- (Figure 3.1). A *switch on* luminescence response was observed for CN^- with a blue shift of ~15 nm for the band maximum, while very little enhancement in emission intensity with emission maxima at 548 nm was observed for Cys or GSH. Hcy failed to induce any change in the spectral pattern

for probe **1** (Figure 3.1b). Presumably, the micellar structure of CTAB not only helped in solubilizing the probe **1** in aq. buffer medium, but the nano-compartments also provided a favourable hydrophobic environment for the interaction of the probe **1** and CN^-. Use of such micellar structures in the design of suitable sensors for cationic and anionic analytes has been reported recently. Interestingly, DLS studies with the solution after completion of reaction of the reagent **1** with CN^-/HCN revealed a small increase in the micellar diameter (from 4.1 to 5.3 nm), suggesting that the micellar structure remained intact even after the reaction of **1** with HCN/CN^-, though with a little broader diameter distribution (Figure 3.2). Analogous changes were also observed for HSO_3^-, although the extent of changes and detection limit were less as compared to that was observed for CN^- (Figure 3.2).

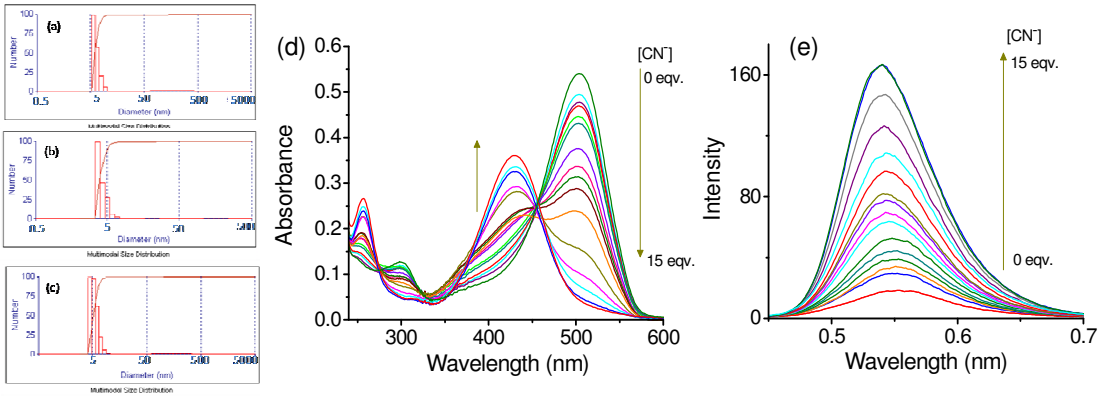

Figure 3.2. Dynamic light scattering study of (a) CTAB (1.2 mM) solution, (b) for solution with **1** (20 mM) in CTAB (1.2 μM) , and (c) **1** (20 μM) in CTAB (1.2 μM) + CN^- (200 mM). Changes in (d) absorption and (e) emission spectra of **1** (20 μM) in presence of 0-15 mole equivalents of $NaHSO_3$. Measurements were performed in 10 mM aq. HEPES-DMSO (250:1, v/v; pH 7.2) having 1.2 mM CTAB using λ_{Ext} of 430 nm.

Systematic absorption spectral titrations were carried out for varying [CN^-] (0 – 60 μM), while effective [**1**] was maintained at 20 μM. Upon gradual increase of [CN^-], the ICT band with maxima at 505 nm was found to bleach with concomitant increase of a new band with maximum at 425 nm (Figure 3.3). No further change in absorption spectral pattern was observed after 3 mole equivalents of [CN^-]. Titration spectral pattern also revealed three simultaneous isosbestic points at 272 nm, 340 nm and 447 nm, which indicated that reactant and product (absorbing species) existed in equilibrium.

As mentioned earlier, steady state emission studies showed a weak emission band with λ_{Ems}^{Max} of 548 nm ($\Phi = 0.009$; λ_{Ext} of 430 nm) for **1** (Figure 3.3). Systematic emission titration with 20 μM of **1** revealed an appreciable enhancement in emission intensity (Φ =

0.05, λ_{Ext} = 430 nm) with little blue shift in the band maximum (λ_{Ems}^{Max} = 535 nm) on gradual increase in [CN^-] (0 - 3 mole equivalent) (Figure 3.3). Relative luminescence quantum yield for **1** and **1**.CN^- were evaluated using coumarin-6 (Φ = 0.78) in ethanol solution as a standard. Excitation spectra of **1** in the presence of 3 mole equivalents of CN^- (λ_{Ems} = 535 nm) showed a maxima at ~425 nm and this implied that the final emission state for the cyanohydrin derivative was different from that of the reagent **1 (**Figure 3.3).

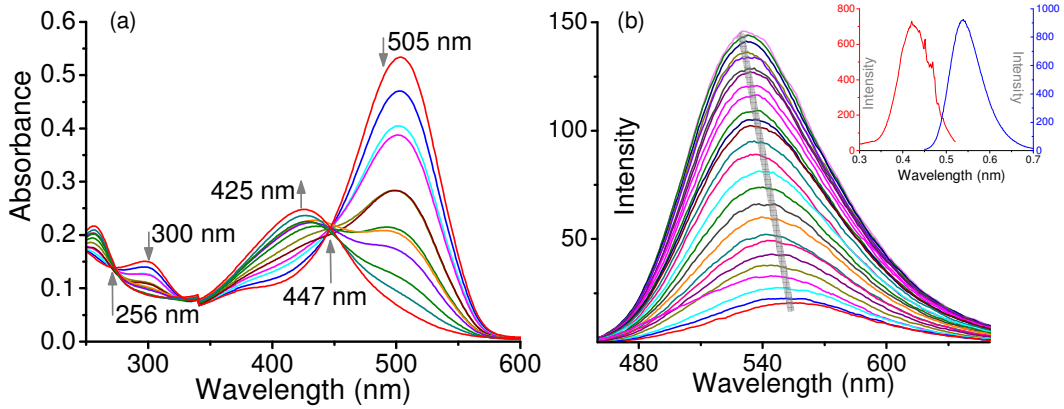

Figure 3.3. Changes in (a) absorption and (b) emission spectra of **1** (20 μM) in presence of 0-3 mole equivalents of NaCN [inset: Excitation (λ_{Ems} of 535 nm) and emission (λ_{Ext} of 430 nm) spectra of **1** (20 μM) in presence of 3 equivalents of CN^-.] Measurements were performed in 10 mM aq. HEPES-DMSO (250:1, v/v; pH 7.2) having 1.2 mM CTAB.

Results of interference studies carried out in the presence of 200 μM of all common anions and amino acids/biothiols (Figure 3.4) using 20 μM of **1** in 10 mM aq. HEPES buffer and 1.2 mM CTAB (pH = 7.2) clearly revealed that there was no interference from other anions and AAs, while interferences from GSH and Cys was kept to a bare minimum under the present experimental condition. As discussed earlier, interference was observed from only for hydrogen sulphite.

Analogous interference experiments were also performed with GSH or Cys in the presence of 50 mole equivalent of NEM (*N*-Ethylmaleimide), added prior to the addition of reagent **1**. The very small decrease in emission intensities that were earlier observed at 535 nm were restored (Figure 3.4). NEM is known to selectively block GSH or Cys and this confirmed that the interference from GSH and Cys in quantitative estimation of CN^- was truly minimal. Thus, these results clearly illustrate the specificity of the present reagent towards CN^- under the present experimental condition. Job plot analysis confirmed a 1:1 binding

stoichiometry (Figure 3.4) and the increase in emission intensity as a function of [CN^-] was found to be linear for [CN^-] of 0-8 μM region ([**1**] is 10 μM). This linear calibration plot could be used for quantitative estimation of CN^- and/or HCN in aq. buffer medium. The lowest detection limit of CN^- was evaluated as 2.86 × 10^{-7} M, which is much lower than the threshold limit set by WHO (1.9 μM) for safe drinking water.[5a] Visually detectable change in solution fluorescence was also observed for solution having [NaCN] of 1.9 μM (Figure 3.1) and this has made this reagent suitable for a "*yes-no*" type binary response for in-field detection of CN^- and/or HCN in pure aqueous medium. Examples of such fluorescence-based reagents are rather rare in the existing literature.[5b,c]

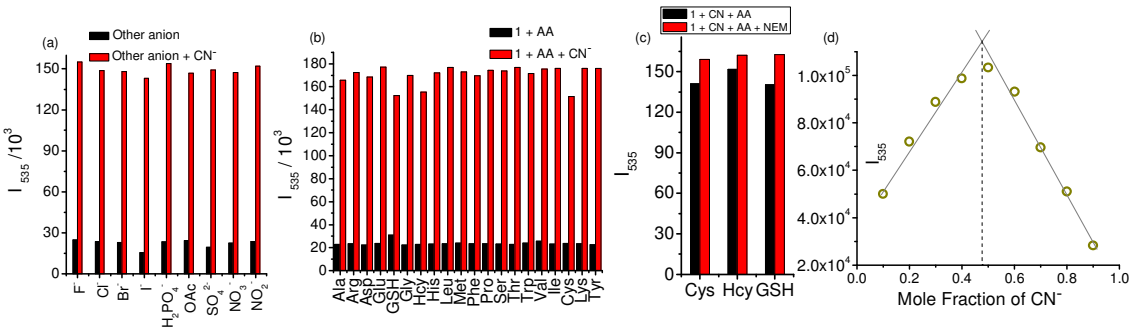

Figure 3.4. (a) Variation of relative fluorescence intensity at 535 nm of **1** (20 μM) in presence of 200 μM of competitive (a) anions F^-, Cl^-, Br^-, I^-, $H_2PO_4^-$, OAc^-, SO_4^-, NO_3^-, NO_2 (b) AA's and GSH in absence and presence of 100 μM of NaCN. (c) 5 equivalent of CN^-, 10 equivalents of Cys, Hcy, GSH in absence and presence of 50 equivalents of NEM, (d) Jobs plot analysis. Measurements were performed in 10 mM aq. HEPES-DMSO (250:1, v/v; pH 7.2) having 1.2 mM CTAB using λ_{Ext} of 430 nm.

The spectral response of the probe **1** (20 μM) in aq. HEPES medium having 1.2 mM CTAB solution were examined in absence and presence of 10 mole equiv. of NaCN at different pH (pH = 3-9). Results revealed that the absorbance at 425 nm as well as the steady state emission intensity at 535 nm for solution **1** remained practically invariant over the entire pH range that we studied. However, the reaction of **1** with the cyanide species was found to be efficient over the pH range of 5- 8 (Figure 3.5). Time dependent fluorescence at 535 nm was monitored with different concentration of CN^-, which revealed the reaction was completed within 10 minutes (Figure 3.6). Thus, results of all spectroscopic studies confirmed that probe **1** could preferentially react with cyanide species in aq. buffer medium within the pH range of 5-8, while the presence of the large excess of GSH, AAs and various anionic analytes failed to interfere with the detection processes. Furthermore, changes in electronic and luminescence spectral patterns in the visible region were large

enough for CN^- to induce a visually detectable change in the solution colour to allow its naked eye detection.

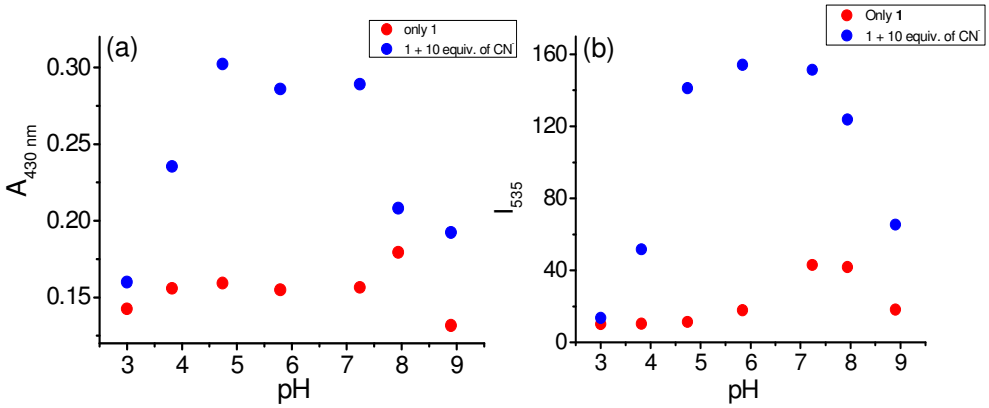

Figure 3.5. pH dependent (a) absorbance monitored at 430 nm (b) emission monitored at 535 nm of **1** (20 μM) in absence and presence of 10 equivalent of CN^-.

To ascertain the formation of corresponding cyanohydrin derivative, ^1H NMR spectra were recorded (in DMSO-d_6) in absence and presence of different concentration of CN^- (TBACN). On formation of the cyanohydrin, the sharp signal for H_{CHO} at 9.83 ppm disappeared with a simultaneous appearance of a new signal at δ = 8.33 ppm (Figure 3.6). This new signal was ascribed to be the $H_{CH(OH)(CN)}$ proton of the newly formed cyanohydrin derivative. Furthermore, anticipated upfield shifts were also observed for other aromatic protons of the reagent **1**. Formation of the corresponding cyanohydrin was also confirmed by the signal at *m/z* = 245.0784 (*m/z* calcd. is 245.08 for **1+** CN^-+H^+).

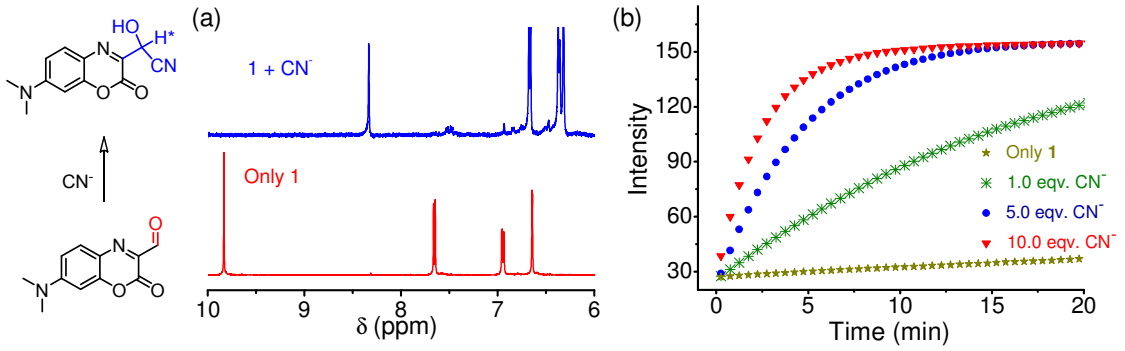

Figure 3.6. (a) Partial ^1H NMR spectra of **1** were recorded in DMSO-d_6 in absence and presence of different mole equivalents of TBACN. Plausible reaction of **1** with CN^- for the corresponding cyanohydrins formation was also shown. (b) Time dependent emission change in presence of CN^-.

3.3.2. Enzymatic studies

Having a molecular probe that could effectively detect CN^- and/or HCN under physiological conditions; we explored the possibility of developing a fluorescence-based assay for studying the hydrolysis of amygdalin by an important enzyme like β-glucosidase. β-glucosidase plays diverse and important roles in prokaryotes and eukaryotes.[16-18] This class of enzymes present in bacteria and fungi are crucial for biomass conversion,[16] while for animals these are essential for glycosphingolipid metabolism.[17] In higher plants, these are used in chemical defence against herbivores and pathogens through cyanogenesis in plants, lignifications and regulation of phytohormones by inducing hydrolysis of their inactive hormone-glucoside conjugates.[18] Considering the significance of the enzymatic activity of β-glucosidases, developing an effective and sensitive assay for this crucial enzyme is of vital importance. Enzyme assays are important to assess the performance of enzyme in high-throughput screening. Conventionally, chromatographic methodology or oligosaccharide substrates functionalized with an appropriate fluorophore moiety through an ether linkage is used for developing an assay for such enzyme.[19] However, synthesis of such functionalized oligosaccharide substrates generally involve intricate synthetic methodologies and above all, solubility of such reagent in aqueous medium or in physiological condition is limited. This means the use of such fluorogenic oligosaccharides is in slurry, which is barely homogeneous.[19] Considering these limitations, the possibility of using a small molecule that shows a *fluorescence turn-on* response on quantitative reaction with the hydrolyzed product of the β-glucosidase has significance for developing a more efficient assay. To explore such a possibility for **1**, this reagent was used to assay β-glucosidase activity on amygdalin, a well known cyanogenic glycoside found in bitter almond. Amygdalin is known to release CN^- and/or HCN depending on media pH upon metabolism by β-glucosidase (Scheme 3.2).[20]

Accordingly, the hydrolysis reaction of amygdalin by β-glucosidase in aqueous medium of pH 7.2 was monitored through the increase in luminescence intensity of **1** (20 μM) at 535 nm as a function of time as well as a function of the [β-glucosidase] (0 - 0.0176 UN/ml) in 10 mM HEPES/1.2 mM CTAB pH 7.2, with amygdalin (1 mM) (Figure 3.7). In the absence of β-glucosidase, fluorescence intensity at 535 nm remained unaltered; while a subsequent increase in emission intensity was observed as a function of [β-glucosidase]. At pH 7.2, cyanide (pK_a = 9.21) is expected to exist in solution predominantly as HCN (~ 99%). Thus, HCN produced through hydrolysis of amygdalin reacted with the probe

molecule (**1**) to generate the corresponding cyanohydrin compound with associated increase in emission intensity at 535 nm. For [β-glucosidase] of 0.0176 UN/ml, reaction was mostly complete (~90%) within 5 min.

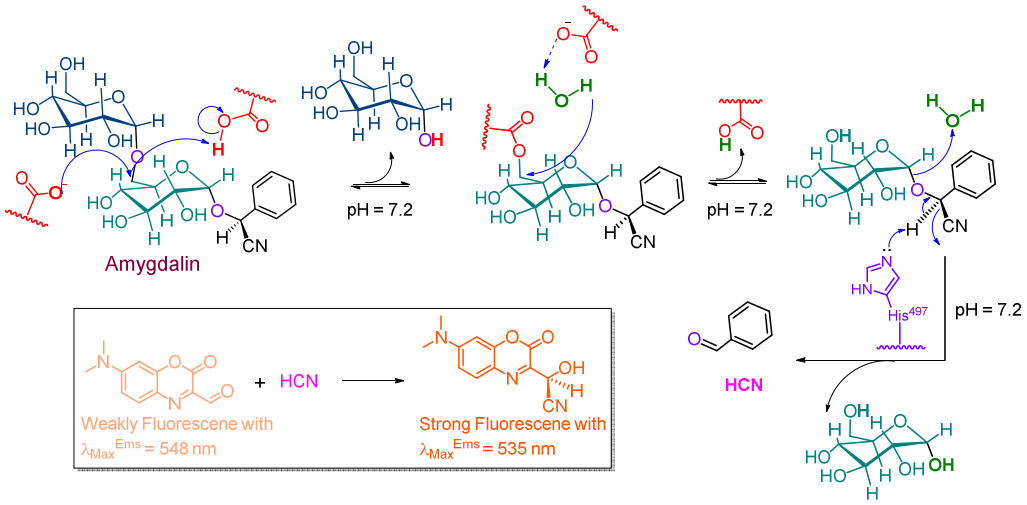

Scheme 3.2. Reaction Mechanism of of β-glucosidase with amygdalin.

To confirm that the emission enhancement was solely due to the reaction of HCN and/or CN^- that was produced through hydrolysis of amygdalin by β-glucosidase, control experiments in the absence of amygdalin under otherwise identical experimental condition were carried out and no enhancement in emission intensity was observed. This confirms that emission enhancement occurs only when both amygdalin and β-glucosidase are present and HCN/CN^- is produced by the hydrolysis of amygdalin by β-glucosidase (Figure 3.7). We have also performed control experiments under identical experimental conditions with other disaccharides that did not contain any cyano group, but are known to be hydrolysed by β-glucosidase to produce glucose and benzaldehyde. Accordingly, analogous studies with two different disaccharides (Maltose and lactose) and glucose did not show any change in luminescence intensity at 535 nm, compared to changes that were observed for amygdalin (Figure 3.7).[21] These results further confirm that other byproduct of the hydrolysis reaction, *i.e.*, glucose and benzaldehyde do not have any influence in emission enhancement. Thus, the above discussed methodology could be utilized for the development of an effective assay for a significant enzyme like β-glucosidase for studying the hydrolysis of amygdalin.

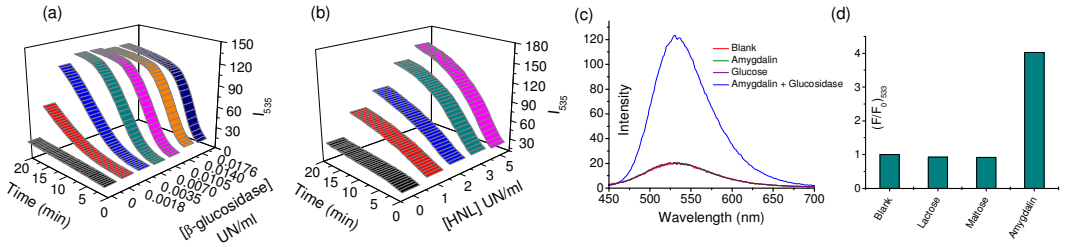

Figure 3.7. (a) amygdalin (1 mM) with varying concentration of β-glucosidase (0 - 0.0176 UN/ml) at pH 7.2 and (b) mandelonitrile (1 mM) with varying concentration of HNL (0 - 5 UN/ml) at pH 6.5. (c) control experiment with β-glucosidase and glucose. (d) Control experiment with disaccharides. All studies were performed in an essentially aq. buffer (10mM aq. HEPES-DMSO (250:1, v/v)) medium having 1.2 mM CTAB.

Michaelis constant (K_m) was evaluated from the time dependent luminescence studies of **1** (20 μM) and β-glucosidase (0.014 UN/ml) with varying [amygdalin] (0.4-1.0 mM) in solution. Initial rates were evaluated from the plot of Log [F_t-F_0] vs time (in sec), where F_t is the luminescence intensity for **1** at 535 nm (λ_{ext} = 430 nm) at time t and F_0 is the initial luminescence intensity. Initial rates (v) were calculated for the first five minutes and K_m (4.68×10^{-4} M) was evaluated from the slope of the plot of 1/v *vs* 1/[amygdalin] (Figure 3.8). Slight variation in the evaluated K_m value, from those reported in the literature,[8b,10a] could be ascribed to a slightly different assay condition. Thus, our studies confirmed that reagent (**1**) can be utilized as a fluorescence based assay for the industrially and biologically significant enzyme β-glucosidase and such example are scarce in the contemporary literature.

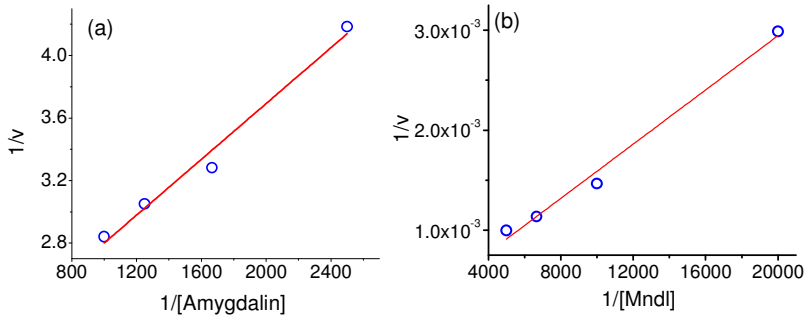

Figure 3.8. (a) (1/v) vs 1/[amygdalin] plot. (b) (1/v) vs 1/[Mandelonitrile] plot.

To illustrate the versatility of the probe **1,** as a reagent for developing luminescence based enzymatic assay, a similar enzymatic process, the hydrolysis of mandelonitrile (MNDL) by HNL (from *Arabidopsis thaliana*) into corresponding benzaldehyde and cyanide species,

was also examined (Figure 3.7). Luminescence enhancement was observed on hydrolysis of MNDL with HNL and this could be utilized for evaluating the Michaelis constant (5.76 x 10^{-4}) for HNL, (Figure 3.8), which was close to the value reported earlier for this reaction.[8a]

3.3.3. Cellular uptake and spatially resolved fluorescence spectroscopy

Finally, we have explored the possibility of detection and imaging of cellular uptake of cyanide ions in cellular environments using the apparent *switch on* fluorescence response of this reagent. For this purpose, human breast adenocarcinoma cells (MDA-MB-231 cells) were treated with **1** (10 μM) at 37℃. These cells were then washed twice with phosphate buffer saline solution (PBS) to remove excess adhered probe molecules. MDA-MB-231 cells, pre-treated with **1** were incubated with aq. solution of CN^- (200 μM) for 15 minutes and washed with PBS, following which both phase contrast and fluorescence intensity images were collected in the absence and presence of CN^- (Figure 3.9). Figures 3.9 B&C clearly demonstrate that probe molecule **1** is cell permeable, While MTT assay show nominal toxicity of the sensor molecule.

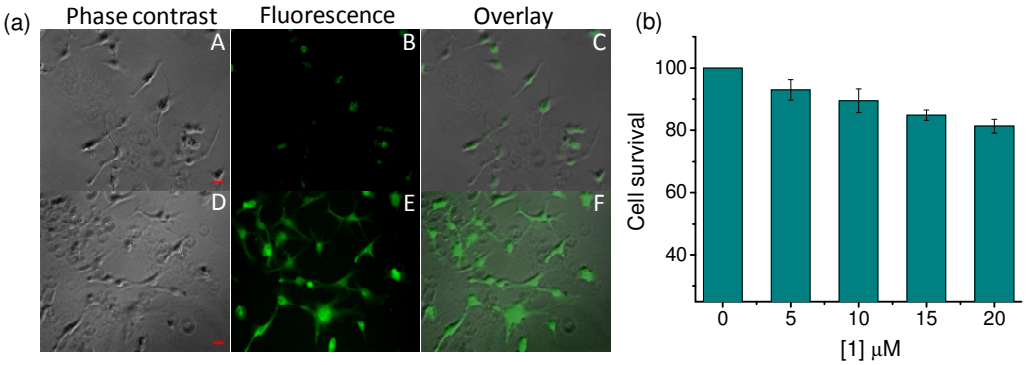

Figure 3.9. (a) Phase contrast (left panels), fluorescence microscopy (middle panels) at 10x magnification, and the overlay images (right panels) of the same lateral area for MDA-MB-231 cells incubated with**1** (10□M), in the absence (A, B, C) and presence (D, E, F) of NaCN (200 □M). Scale bar is 50 μm. (b) MTT assay.

These results suggest that the probe **1** could be utilized for detection of uptake of cyanide species in cells pre-exposed to an aq. solution of NaCN. Fluorescence intensity and overlay images (Figures 3.9 B, C, E and F) illustrate that cells treated with only **1** have very weak emission whereas those incubated with CN^-, showed considerable enhancement in the fluorescence intensity (Figure 3.9 E and F). We note however, that these intensity images (Figure 3.9 B, E) provide an average behaviour of intensity response of probe **1** in

an ensemble of cells, and it is inappropriate to comment on the spatial distribution of cyanide uptake from intensity measurements alone.

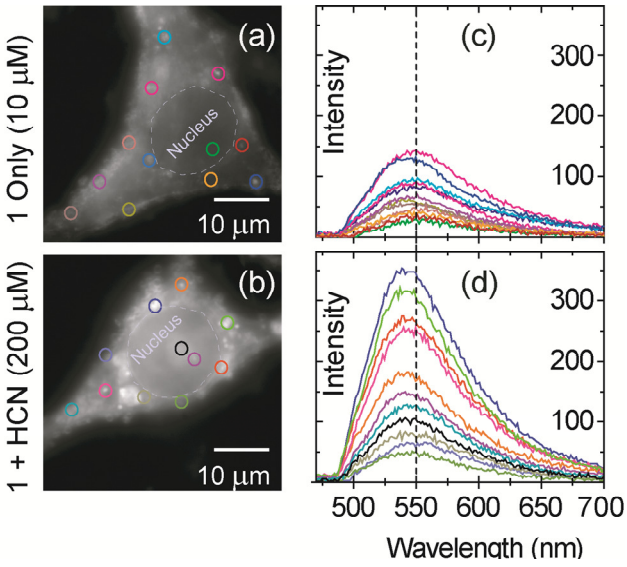

Figure 3.10. TIRF microscopy images (a, b) of single MDA-MB-231 cells treated with **1**, and representative spatially-resolved emission spectra (c, d) in the absence (a, c) and presence (b, d) of Cyanide. Circles within the images represent microscopic regions (~ 0.5 x 0.5 μm^2) within different locations of the cell from which fluorescence spectra were acquired (color matched with circles).

This is primarily due to non-uniform labelling of cells using probe **1**, and the resulting spatial variation in emission intensity can be easily noticed in the higher magnification TIRF (Total internal reflection fluorescence microscopy) images (Figures 3.10 a-b). Furthermore, a close inspection of individual cells revealed the existence of locally emissive bright spots over a relatively weak cytoplasmic background, suggesting accumulation of probe **1** in various microscopic sub-cellular domains within the cytoplasm of each cell even in the absence of cyanide (Figures 3.10 a). As a result, it was challenging to determine whether the enhancement of intensity within the sub-cellular regions arise from sensor accumulation in different microscopic spatial locations or due to the formation of strongly luminescent cyanohydrin derivative upon reaction with cyanide species. Therefore, using only emission intensity as a sole observable, it was not possible to determine the efficiency of probe **1** for cyanide detection in different sub-cellular regions. Since probe **1** also undergoes a blue shift in its emission spectral envelope upon cyanide binding, we surmised that colorimetric discrimination between various regions in individual cells might provide more insight into cyanide detection in cells. However, solution studies point out that the spectral blue-shift was not pronounced (~15 nm) and therefore it was

extremely challenging to detect the subtle color changes either visually or by dual-color imaging using energetically separated emission filters.

This prompted us to perform spatially-resolved fluorescence spectroscopy measurements on single cells labelled with probe **1**. Figures 3.10 c &d showed several characteristic emission spectra of probe **1** that were collected from different microscopic domains (0.5 x 0.5 μm^2) of a single cell, in the absence and presence of cyanide ions. It should be noted that these representative emission spectra shown in Figure 3.10 c, d are only a few of several hundreds of emission profiles collected from various local intracellular regions, over 15 different cells. Spatially-resolved spectroscopy revealed that the emission maxima of probe **1** in absence of cyanide were located close to ~550 nm, which shifted to slightly shorter wavelengths along with enhanced emission intensities (for a considerable fraction of spatial locations) in the presence of cyanide. We note however, that due to the non-homogeneous cellular medium, probe **1** exhibited a range of emission maxima, likely arising from fluctuations in local environmental polarity where the probes were embedded.

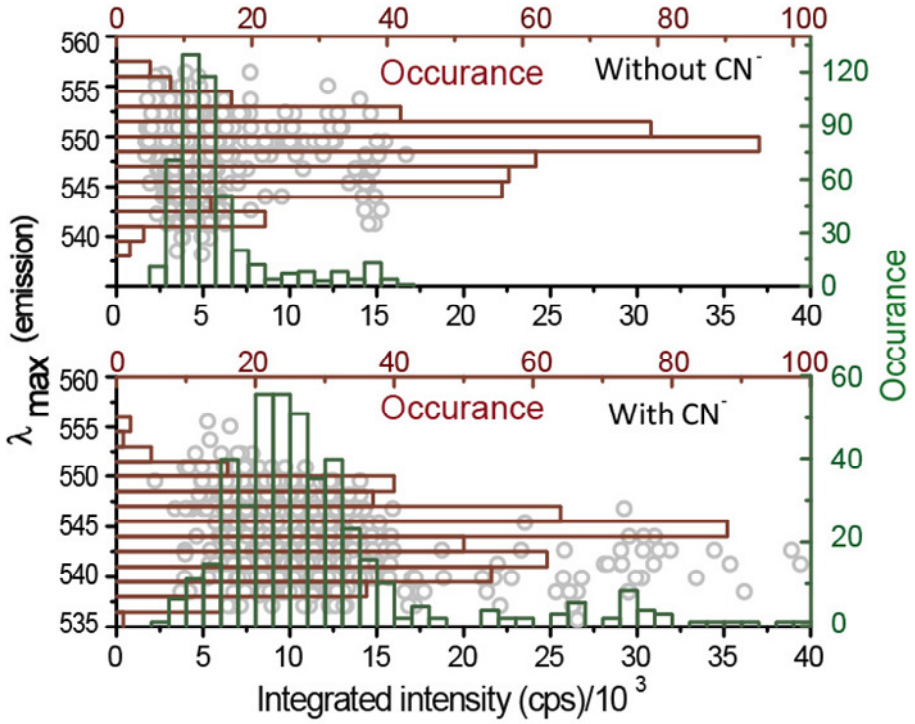

Figure 3.11. Scatter plots of emission spectral maxima against integrated intensity (circles) along with respective frequency distributions (bars) in absence (e) and presence (f) of cyanide species depicting the variation in sensing efficiency in cellular environments.

To understand whether an observed spectral shift was indeed due to detection of cyanide in a particular microscopic (sub-cellular) region, we extracted the integrated intensity and transition energy from each emission envelope, and generated a scatter plot considering a large number (~470) of such spatially-resolved emission spectra in the absence and presence of cyanide (Figure 3.11). In this scatter plot, we found several spots which have similar values of both intensity and transition energies in the absence and presence of cyanide. However, the qualitative change in the shape of the scatter plots indicated that a large fraction of spectra have relatively high values of intensity as well as transition energy, a signature of cyanide detection. Therefore, those spatial locations where there was a significant (>5 nm) blue-shift of spectral peak positions along with considerable intensity enhancement of probe **1** were likely to have more cyanide present as compared to other locations (with nominal shift) within the cellular environment. The observed heterogeneity in the emission spectra collected from different microscopic regions also indicates that, for a given (fixed) incubation concentration of cyanide ions, the proportion of cyanide-bound probe **1** present in different sub-cellular regions is likely to be non-uniform.

To illustrate the relative changes in spectral response in various microscopic sub-cellular regions; we have constructed distributions of both spectral peak positions (transition energies) and emission intensity, which are overlaid on the scatter plots (Figure 3.11). We find that the mean value (standard deviation) of transition energy shifts from ~549 nm (3.5 nm) to ~544 nm (4 nm) in the presence of cyanide, while the average emission intensity increases from 4995 cps to 11810 cps. The widths of distributions in the absence of cyanide can be used as a qualitative indicator for sensory response due to local environmental fluctuations within cells. Therefore, the relatively large change in both these distributions in the presence of cyanide suggests that the sensor's spectral response due to cyanide detection is greater than those arising from changes in the local environment. Attempts are currently being made to develop a methodology to further discriminate between spectral variations arising from local environmental fluctuations in the vicinity of probe **1** and the effect of cyanide binding/detection at different sub-cellular regions.

3.4. Conclusion

In summary, we have demonstrated that a simple luminophore could be used as chemodosimetric probe for specific recognition of cyanide species (CN^- and/or HCN) in an ensemble of all common anions, amino acids and GSH in an essentially aqueous buffer

medium at physiological pH. The *switch on* luminescence response at 535 nm could be utilized for achieving a lower detection limit of 0.286 μM for cyanide ion and this value was much lower than the threshold cyanide ion concentration of 1.9 μM for safe drinking water set by WHO. Specificity and the visually detectable change in solution luminescence at a [CN^-] of 1.9 μM offers the opportunity to use this reagent as an optical sensor for *in-field* application. Release of CN^- and/or HCN (at physiological pH) from amygdalin and mandelonitrile by important enzymes like β-glucosidase and, Hydroxynitrile lyase, respectively, could also be probed by monitoring the luminescence enhancement of probe **1** and this also helped us in developing an efficient and sensitive assay for two important enzymatic reactions. Importantly, this reagent showed insignificant toxicity towards live MDA-MB-231 cells and results of the imaging studies further revealed that this chemodosimetric reagent could be utilized for detection of cyanide ion uptake in live cells. Imaging studies using TIRF microscopy showed that the sole dependence on increase in luminescence intensity of the sensor within single cells studies might not provide all the necessary information while exploring cellular uptake of CN^-. On the contrary, spatially-resolved fluorescence spectroscopy measurements performed over a large number of microscopic domains (over several cells) reveal the overall shift in distribution of transition energies as well as integrated emission intensities. This demonstrates that a combination of both spectral shift and emission enhancement provides more conclusive evidence of cellular uptake of cyanide, and offers a way to probe changes in the sensory response due to variation in local environments within cells and that due to cyanide detection. We are exploring how such spatially-resolved spectral data can be better analyzed to extract more quantitative information on the non-uniformity in the relative proportion of analytes at various local sub-cellular regions.

3.5. References

1. Taylor, J.; Roney, N.; Harper, C.; Fransen, M.; Swarts, S. *Toxicological Profile for Cyanide*, US Department of Health and Human Services, Atlanta, GA, **2006**, 6–7.

2. (a) Muir, G. D. *Hazards in the chemical laboratory,* The Royal society of Chemistry, London, UK, **1977.** (b) Vennesland, B.; Conn, E. F.; Knownles, J.; Westly, J.; Wising, F. *Cyanide in Biology,* Academic London, **1981**.

3. (a) Dzombak, D. A.; Ghosh, R. S.; Wong-Chong, G. M. *Cyanide in Water and Soil: Chemistry, Risk, and Management,* CRC Press, Boca Raton, **2006**; (b) Young, C.; Tidwell, L.; Anderson, C. *Cyanide: Social Industrial and Economic Aspects*, TMS (The Minerals, Metals, and Materials Society), Warrendale, **2001**.

4. (a) Solomonson, L. P.; Vennesland, B.; Conn, E. E.; Knowles, C. J.; Westley, J.; Wissing, F. Eds.; In *Cyanide in Biology* Academic Press: London, **1981**; (b) O. S. A. Oluwole, A. O. Onabolu, K. Mtunda and N. Mlingi, *J. Food Compos. Anal.,* **2007**, *20*, 559.

5. (a) Sheffer, M. *Guidelines for Drinking-Water Quality, ed*. World Health Organization, Geneva, **1996**. (b) Kim, Y.; Huh, H.-S.; Lee, H. M.; Lenov, Y. I. L.; Zhao, H.; Gabbaï, F. P. *Chem. Eur. J.,* **2011**, *17*, 2057. (c) Lin, Q.; Liu, X.; Wei, T.-B.; Zhang, Y.-M.; *Chem. Asian J.,* **2013**, *8*, 3015.

6. (a) Xu, Z.; Chen, X.; Kim, H. N.; Yoon, J. *Chem. Soc. Rev*., **2010,** *39*, 127. (b) Kaur, K.; Saini, R.; Kumar, A.; Luxami, V.; Kaur, N.; Singh, P.; Kumar, S. *Coord. Chem. Rev*., **2012**, *256*, 1992.

7. (a) Wang, F.; Wang, Li.; Chen, X.; Yoon, J. *Chem. Soc. Rev*., **2014**, *43*, 4312. (b) Das, S.; Biswas, S.; Mukherjee, S.; Bandyopadhyay, J.; Samanta, S.; Bhowmick, I.; Hazra, D. K.; Ray, A.; Paruui, P. P. *RSC Advances*, **2014**, *4*, 9656. (c) Lee, C. H.; Yoon, H. J.; Shim, J. S.; Jang, W. D. *Chem. Euro. J.,* **2012**, *18*, 4513. (d) Saha, S.; Ghosh, A.; Mahato, P.; Mishra, S.; Mishra, S. K.; Suresh, E.; Das, S.; Das, A. *Org. Lett.,* **2010**, *12*, 3406. (e) Lee, K.; Kim, H.; Kim, G.; Shin, I.; Hong, J. *Org. Lett.,* **2008**, *10*, 49.

8. (a) Reddy, G. U.; Das, P.; Saha, S.; Baidya, M.; Ghosh, S. K.; Das, A. *Chem. Commun*., **2013**, *49*, 255. (b) Jose, D. A.; Elstner, M.; Schiller, A. *Chem. Eur. J*., **2013**, *19***,** 14451.

9. (a) Reymond, J. L.; Fluxá, V. S.; Maillard, N. *Chem. Commun*., **2009**, 34. (b) Desmet, T.; Soetaert, W.; Bojarov, P.; Křen, V.; Dijkhuizen, L.; Eastwick-Field, V.; Schiller, A. *Chem. Eur. J.,* **2012**, *18*, 10786.

10. (a) Yang, S.; Jiang, Z.; Yan, Q.; Zhu, H. *J. Agric. food Chem.,* **2008,** 56*,* 602. (b) Wallecha, A.; Mishra, S. *Biochim. Biophys. Acta,* **2003**, *1649*, 74.

11. Haisman, D. R.; Knight, D. J. *Biochem. J.,* **1967**, *103*, 528.

12. (a) Vetter, J. *Toxicon,* **2000**, *38*, 11. (b) Sharma, M.; Sharma, N. N.; Bhalla, T. C. *Enzyme and Microb. Tech.*, **2005**, *37*, 279.

13. Das, S.; Sharma, D. K.; Chakrabarty, S.; Chowdhury, A.; Gupta S. S. *Langmuir*, **2015**, *31*, 3402−3412.

14. Hu, M.; Fan, J.; Li, H.; Song, K.; Wang, S.; Cheng, G.; Peng, X. *Org. Biomol. Chem.,* **2011**, 9, 980.

15. (a) Hu, R.; Feng, J.; Hu, D.; Wang, S.; Li, S.; Li, Y.; Yang, G. *Angew. Chem.*, **2010**, *122*, 5035. (b) Manabe, K.; Iimura, S.; Sun, M. X.; Kobayashi, S**.** *J. Am. Chem. Soc.*; **2002**, *124*, 11971. (c) Wang, L. M.; Jiao, N.; Qiu, J.; Yu, J. J.; Liu, J. Q.; Guo, F. L.; Liu, Y. *Tetrahedron*, **2010**, *66*, 339.

16. (a) Béguin, P. *Annu. Rev. Microbiol.*, **1990**, *44*, 219. (b) Fowler, T. *Biochemistry and Molecular Biology, ACS Symposium Series*. American Chemical Society, Washington, DC, **1993**, *533,* 56.

17. Grabowski, G. A.; Berg-Fussman, A.; Grace, M. *Biochemistry and Molecular Biology, ACS Symposium Series* American Chemical Society, Washington, DC, **1993***, 533*, 66.

18. (a) Conn, E. E. *Cyanide and cyanogenic glycosides.* In GA Rosenthal, DH Janzen, eds, Herbivores, Their Interactions with Secondary Plant Metabolites. Academic Press, New York**, 1979,** 387. (b) Dharmawardhana, D. P.; Ellis, B. E.; Carlson, J. E. *Plant Physiol.*, **1995**, *107*, 331. (c) Falk, A.; Rask, L. *Plant Physiol.*, **1995**, *108*, 1369.

19. (a) McCleary, B. V.; Mangan, D.; Daly, R.; Fort, S.; Ivory, R.; McCormack, N. *Carbohydr Res.,* **2014,** *385*, 9. (b) Mangan, D.; McCleary, B. V.; Liadova, A.; Ivory, R.; McCormack, N. *Carbohydr Res.,* **2014,** *395*, 47.

20. Yamashita, T.; Sano, T.; Hashimoto, T.; Kanazawa, K. *Int. J. Food Sci. Technol.,* **2007**, *42*, 70.

21. (a) Tewari, Y. B.; Goldberg, R. N*. J. Biol. Chem.*, **1989**, *264*, 3966. (b) Zanoelo, F. F.; Polizeli, M. d. T. d. M. L.; Terenzi, H. F.; Jorge, J. A. *FEMS Microbiol. Lett.,* **2004**, *240*, 137.

CHAPTER 4

A FLUORESCENT PROBE FOR BISULFITE ION: ITS APPLICATIONS TO TWO-PHOTON TISSUE IMAGING AND ELECTROCHEMICAL DEVICE

Publication:
Under revision

4.1. Introduction

With the advent of industry in modern era, sulfur dioxide (SO_2) becomes an inevitable air pollutant originating from the combustion of fossil fuels and coal, as this has deleterious influences on the environment and human health.[1] On inhalation of SO_2, it is hydrated in respiratory tract to produce sulfite and bisulfite species, which are actually responsible for urticaria, hypotension, diarrhea, breathing problems, wheezing, hives and dermatitis.[2] Despite their adverse influence on human health and environment, bisulfites are widely used for their antioxidant, antimicrobial and preservative properties in pharmaceutical, food, and beverage industry.[3] Considering its adverse influences FAO/WHO have jointly suggested that the acceptable daily intake of SO_2 for a healthy human should not exceed 0.7 mg/kg of body weight.[4] US Food and Drug Administration (FDA) allows 10 ppm (125 μM) of SO_3^{2-} in food and beverages.[5]

Thus, there is a need to develop appropriate methodology capable of detecting SO_2 or SO_3^{2-}/HSO_3^- present at low concentrations in food/pharmaceutical products and also the environment. Many methods have been developed for quantification of sulfites/bisulfites in food and beverages such as Monier-Williams method,[6] spectrophotometry,[7] capillary electrophoresis,[8] and chromatography.[9] Among various methodologies, fluorescence based optical detection is preferred for specific recognition and sensing of these SO_2 derivatives. This is because of higher sensitivity in the detection process as well as the possibility of using such reagent for imaging application in mapping the distribution of intracellular sulfite/bisulfite species in live cells/tissue.[10]

Additionally it is also essential to develop a portable handheld device that allows specific and convenient infield analysis of the sulfite species. Along with optical, electrochemical techniques are best candidates for developing any portable device capable of offering digital output as a function of the effective concentration. Till date, there is no example of any ion-selective electrode (ISE) developed from appropriately modified bisulfite specific membrane, for specific detection and quantitative estimation of sulphite/bisulfite species in aqueous solution having appropriate pH. Such a process or methodology would be ideally suitable for developing low-cost, portable devices for in-field application.[11]

Thus there is a need for a sensitive and specific probe with fast response time and the above referred limitations alleviated. Significance of such a probe is more if it allows luminescence response in the red region of the spectrum—as this helps to reduce

interference due to autofluorescence from intrinsic biomolecules, which generally occur in the shorter wavelengths. Furthermore, it is more advantageous if such a probe can be used for two-photon imaging in the near-infrared wavelength region (~900 nm or so), which causes low phototoxcity, photobleaching, and autofluorescence while offering high spatial resolution in deep tissue imaging.[12]

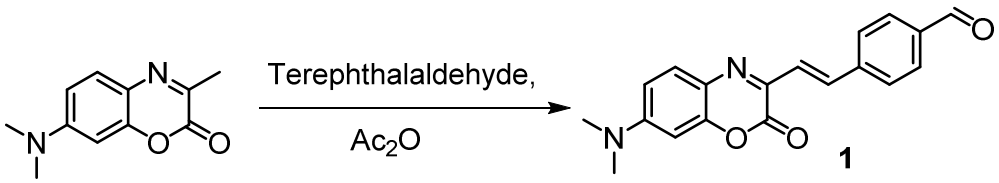

Scheme 4.1: Methodology adopted for synthesis of the probe **1.**

4.2. Experimental section

4.2.1. Materials

Terephthalaldehyde, ethyl pyruvate, Pd-charcoal (10%) were purchased from Sigma-Aldrich and were used as received. Acetic anhydride, dimethyl sulfoxide (DMSO, HPLC grade), $NaNO_2$, HCl, hydrazine hydrate, ethanol, selenium dioxide, 1,4-dioxane and salts of different anions were of reagent grade (S. D. Fine Chemical, India) and used as received.

4.2.2. Analytical Methods

^1H and ^{13}C NMR spectra were recorded on a Bruker 200/500 MHz FT NMR (Model: Avance-DPX 200/400/500) using trimethylsilane (TMS) as an internal standard. FTIR spectra were recorded as KBr pellets in a cell fitted with a KBr window, using a Perkin-Elmer Spectra GX 2000 spectrometer. ESI-Ms measurements were carried out on a Waters QTof-Micro instrument. Solution pH was evaluated using Mettler Toledo FEP20 pH meter. Absorption spectra were recorded using a Perkin Elmer Lambda 950 UV-Vis spectrophotometer equipped with cell holder having path length of 1 cm. Fluorescence spectra were recorded on PTI QuantaMaster 400 spectrophotometer.

4.2.3. Generalised methodology for spectroscopic studies

A solution of probe **1** (1 mM in DMSO) was prepared and used for all experiments after appropriate dilution with a buffer solution of Na_2HPO_4:citric acid (200 mM, pH 5.0) to make

a final concentration of **1** as 2.0×10^{-5} M. Stock solutions (100 mM) of different anions (sodium salts of F^-, Cl^-, Br^-, I^-, NO_3^-, SO_4^{2-}, OAc^-, CN^-, $S_2O_3^{2-}$, S^{2-}, N_3^-, HSO_3^-, SO_3^{2-}, and $H_2PO_4^-$) as well as solutions of cysteine (Cys), homocysteine (Hcy), and glutathione (GSH) were prepared in the Na_2HPO_4:citric acid buffer solution (200 mM, pH 5.0). Stock solutions were further diluted with the buffer solution as per requirement.

The relative fluorescence quantum yields (ϕ_f) were estimated using equation 1 by using the integrated emission intensity of Coumarin-6 in ethanol (Φ = 0.78 at RT) as a reference.

$$\Phi_f = \Phi_f'(I_{sample}/I_{std})(A_{std}/A_{sample})(\eta^2_{sample}/\eta^2_{std}) \quad \text{Equation 1}$$

where, Φ_f' is the absolute quantum yield for the Coumarin-6, used as standard; I_{sample} and I_{std} are the integrated emission intensities; A_{sample} and A_{std} are the absorbance at the excitation wavelength, and η_{sample} and η_{std} are the respective refractive indices of sample and standard.The lowest detection limit was calculated by following 2σ/k method; where σ is the standard deviation of blank measurement, k is the slope of intensity *vs.* [HSO_3^-] plot.

4.2.4. Membrane casting

Cellulose acetate granules (2.0 g) were dissolved in hot chloroform (25.0 mL) with constant stirring over a hot plate to make 8% cellulose acetate solution. A solution of probe 1 (10^{-3} M) was separately prepared by dissolving 8.0 mg of it in chloroform (25.0 mL). The probe 1 solution (12.5 mL) and the cellulose acetate solution (12.5 mL) were mixed together to make a casting solution. About 5.0 mL casting solution was dropped over a glass plate to cast the membrane with the help of a casting rod. The freshly prepared membrane was kept for 2–3 minutes over the glass plate and then it was peeled out from the glass plate by wet phase separation into water. The cellulose acetate membrane, so prepared, was preserved under folds of tissue paper for future use.

4.2.5. Ion selective electrode architecture

The cellulose acetate membrane was cut into small pieces and fitted tightly into the open mouth of a glass tube with Teflon tape. The other opening of the glass tube was sealed, leaving a small hole for inserting AgCl coated Ag wire. The cell was clamped and 1.0 mL of 10^{-2} M $NaHSO_3$ solution was filled into the glass tube. The assembled potentiometric cell can be represented as Ag/AgCl | 1.0×10^{-2} M $NaHSO_3$ solution | ion selective cellulose acetate || test solution || 3.0 M KCl | Ag/AgCl. Aqueous solutions of $NaHSO_3$ with varying

[$NaHSO_3$] (1.0×10^{-6} M–1.0×10^{-2} M) was prepared. The source meter unit was put in zero input current mode and the potential was measured. The equilibrium open circuit potential vs [$NaHSO_3$] curve was plotted as calibration curve.

4.2.6. Cell imaging

HeLa human cervical cancer cells were obtained from Korean Cell Line Bank. HeLa cells were incubated in DMEM supplemented with 10% (*v*/*v*) fetal bovine serum (FBS) and 1% (*w*/*v*) penicillin-streptomycin (PS) at 37 ˚C in a humidified atmosphere of 5% of CO_2 in the air. Cells were passaged when they reached approximately 80% confluence. Cells were seeded onto a cell culture dish at a density of 1.0×10^5 cells, which was incubated at 37 ˚C overnight under 5% CO_2 in the air. For imaging of endogenous bisulfite in cells, the cells in DMEM were incubated with the probe (10 μM) for 30 min and then subjected to imaging by two-photon microscopy (TPM). Both negative and positive control experiments were also conducted. For the negative control experiment, the cells were pre-incubated in DMEM contatining formaldehehyde (1 mM) for 30 min, washed with PBS (phosphate buffered saline) buffer for three times, and then incubated with the probe (10 μM) for 30 min. For the positive control experiment, the cells were incubated in DMEM contatining sodium bisulfite (1 mM) for 15 min, washed with PBS buffer solution for three times, and then incubated with the probe (10 μM) for 30 min. Those cells incubated finally with probe were washed with PBS buffer three times and then fixed with 4% formaldehyde solution for the microscopic imaging. Co-localization experiments were conducted similarly: the cells were incubated in DMEM containing 5 μM of the probe and then further incubated with 500 nM of LysoTracker Deep Red for 30 min at 37 ˚C under 5% CO_2 in the air. After the incubation, the cells were washed with PBS buffer three times to remove the remaining probe and then fixed with 4% formaldehyde solution. TPM imaging was performed using a Ti-Sapphire laser (Chameleon Vision II, Coherent) at 140 fs pulse width and 80 MHz pulse repetition rate (TCS SP5 II, Leica, Germany) and a 40× objective lens (obj. HCX PL APO 40×/ 1.10 W CORR CS, 506341, Leica, Germany). The two-photon excitation wavelength was tuned to 880 nm for the probe. Each emission light was spectrally resolved into multi-channels (λ_{em} = 500–550 nm, 565–605 nm) for the probe. The cells prepared as above were mounted on a tight-fitting holder. The excitation laser power was approximately 24.2 mW. The images were consisted of 1024×1024 pixels, and the scanning speed was maintained as 200 MHz. Cellular imaging by confocal microscopy was also performed using Leica TCS SP5 II Advanced System for LysoTracker Deep Red. This microscope

was equipped with multiple visible laser lines (405, 458, 476, 488, 496, 514, 561, 594, and 633 nm). For this one-photon imaging experiment, 633 nm laser line and an emission filter ranging from 660 to 700 nm were used. Acquired images were processed using LAS AF Lite (Leica, Germany), and all the images were covered with specific pseudo-colors: orange to red (probe) and cyan (LysoTracker Deep Red).

4.2.7. Tissue imaging

A Balb/C type mouse (6 weeks, female) was used for this experiment. Basically experiments were done under light protected conditions (in a dark-room and using aluminum foil). The mouse was dissected after dislocation of the cervical vertebra. Blood perfusion with phosphate buffered saline (PBS, 1X solution) was performed for elimination of blood. The organs were dissected, washed with PBS buffer, and then sliced with a vibrating blade microtome (VT1000S, Leica, Germany) to 400 μm thickness. The brain tissue slice samples were immersed in 4% aqueous paraformaldehyde for one week to fix the tissue and the other tissues were used without the fixation process. After the fixation, the tissues were immersed in the probe solution (10 μM) for 30 min at 37 ºC. The stained samples were placed on a slide glass for imaging, after washing with PBS three to four times. Experimental set-ups for tissue imaging were essentially the same as described above for the cellular imaging, except for the emission light collection both at 500–550 nm and 565–605 nm. The tissue slice samples were mounted on a tight-fitting holder. The excitation laser power was approximately 24.2 mW at the focal point, and the image depth was 80–100 μm from the surface. The imaging resolution was 1024×1024 pixels and the scanning speed was 200 Hz during the entire imaging. The acquired images were processed using LAS AF Lite (Leica, Germany).

4.2.8. Synthesis of Probe 1

Synthesis of probe **1**, 4-{(1*E*)-2-(7-(dimethylamino)-2-oxo-2H-benzo[b][1,4]oxazin-3-yl)vinyl}benzaldehyde, is shown in Scheme 1. The benzoxazinone intermediate, 7-(dimethylamino)-3-methyl-2H-benzo[*b*][1,4]oxazin-2-one, was prepared by following the previously reported method.[13] This was further used for the synthesis of probe **1**. 0.55 g (2.69 mmol) of the benzoxazinone intermediate was suspended in 3.5 mL of acetic anhydride. To this suspension, 0.54 g (4.04 mmol) of terephthaldehyde was added and temperature and the reaction mixture were maintained at 140 °C for 4 h. The mixture was then cooled to room temperature to give a red precipitate, which was filtered and the

residue was washed with cold diethyl ether to get the desired product in pure form. No further purification was required and an isolated yield of probe was 360 mg (41%). ^{1}H NMR (500 MHz, $CDCl_3$, 25 ^{o}C, TMS): 10.04 (s, 1H (H_{CHO})), 7.96 (d, 1H, J = 15 Hz (CH=CH)), 7.91 (d, 2H, J = 8 Hz (C_6H_4)), 7.78 (d, 2H, J = 8 Hz (C_6H_4)), 7.59 (d, 1H, J = 15 Hz (CH=CH)), 7.6 (d, 1H, J = 8.5 Hz (C_6H_3)), 6.75 (dd, 1H, J = 6.5 Hz, 2.5 Hz (C_6H_3)), 6.485 (s, 1H, (C_6H_3)), 3.14 (s, 6H ($N(CH_3)_2$)). ^{13}C NMR (100 MHz, $CDCl_3$, 25 ^{o}C, TMS): 214.56, 167.61, 165.57, 10.84, 153.33, 151.92, 145.1, 143.17, 137.85, 134.96, 132.14, 129.95, 113.02, 96.5, 25.59 IR (KBr) ν_{max}/cm^{-1}: 1718, 1688, 1609, 1382. ESI-Ms (*m/z*): 318.80 [M - H^+]. Elemental analysis: $C_{19}H_{16}N_2O_3$ calculated C (71.24), H (5.03), N (8.74); found C (71.5), H (4.97), N (8.8).

4.3. Results and Discussions

Probe **1** was synthesized following a general procedure in one step with moderate yield by following a condensation reaction between the benzoxazinone intermediate and terephthaldehyde (Scheme 4.1). The probe was characterized by spectroscopic (^{1}H, ^{13}C NMR and mass spectroscopy) and elemental analysis. All such data confirmed the desired purity of the probe. The probe was soluble in an essentially aqueous buffer medium (98:2 aq. buffer:DMSO, *v/v*) using 200 mM Na_2HPO_4:citric acid buffer (pH 5.0) solution. This solution was used or all other studies, unless mentioned otherwise.

4.3.1. Spectroscopic studies

Absorption spectra recorded for probe **1** showed a π–π* transition and a charge transfer transition with *N*,*N*′-dimethyl benzooxazine moiety as the donor fragment at 325 and 445 nm, respectively. A shoulder is observed at ~490 nm, which could also be attributed to ICT process (Figure 4.2). This was further confirmed from the shift of the absorption ([λ_{max}^{Abs}]~ 480 nm in toluene) and emission bands ([λ_{max}^{Ems}] ~555 nm in toluene) to longer wavelengths by ~20 nm and ~45 nm, respectively, on changing the solvent polarity from toluene to DMSO (Figure 4.1). Luminescence of probe **1** was essentially quenched possibly due to the non-radiative, lowest energy transition of n–π* from the formyl group. Luminescence spectra of the probe remained unaltered when recorded in the presence of all other anions (F^-, Cl^-, Br^-, I^-, NO_3^-, SO_4^{2-}, OAc^-, CN^-, $S_2O_3^{2-}$, S^{2-}, N_3^-, HSO_3^-, SO_3^{2-}, and $H_2PO_4^-$,) and biothiols (Cys, Hcy, and GSH), except sulfite/bisulfite (depending on the media pH). A switch-on type luminescence response was evident when spectrum for the probe was recorded in the presence of either of these two species (Figure 4.2).

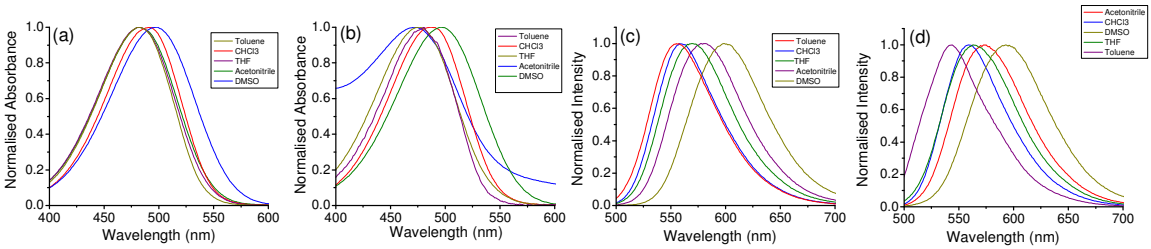

Figure 4.1. Normalised Absorption spectra of **1** (20 μM) in (a) absence (b) presence of 50 equivalent of HSO_3^- in solvents of different polarity. Normalised Emission spectra of **1** (20 μM) in (a) absence (b) presence of 50 equivalent of HSO_3^- in solvents of different polarity in aq. buffer:DMSO (98:2, *v*/*v*) using 200 mM Na_2HPO_4:citric acid buffer solution at pH 5.0 ($\lambda_{ex}/\lambda_{em}$: 490/600 nm).

When probe **1** was incubated with 100 equivalent of HSO_3^- for 5 min, the quantum yield (Φ) increased from 4.3×10^{-4} to 0.03 (75-fold). Respective Φ value was evaluated using coumarin-6 (Φ = 0.78 in ethanol) as reference. Interestingly, broad emission spectrum having a maximum at ~600 nm appeared with tail of the emission band extended beyond 700 nm (Figure 4.2). Further, fluorescence spectra of **1** (20 μM) were recorded with gradual increase in [HSO_3^-] (Figure 4.2). With increasing concentration of HSO_3^-, increase in luminescence intensity (λ_{ex} = 490 nm) was observed and this reached maximum at 8 mM of HSO_3^-. All fluorescence spectra were collected after 10 min ensuring completion of reaction. This luminescence response formed the basis of using this probe for specific detection of SO_3^{2-}/HSO_3^- in aq. buffer medium.

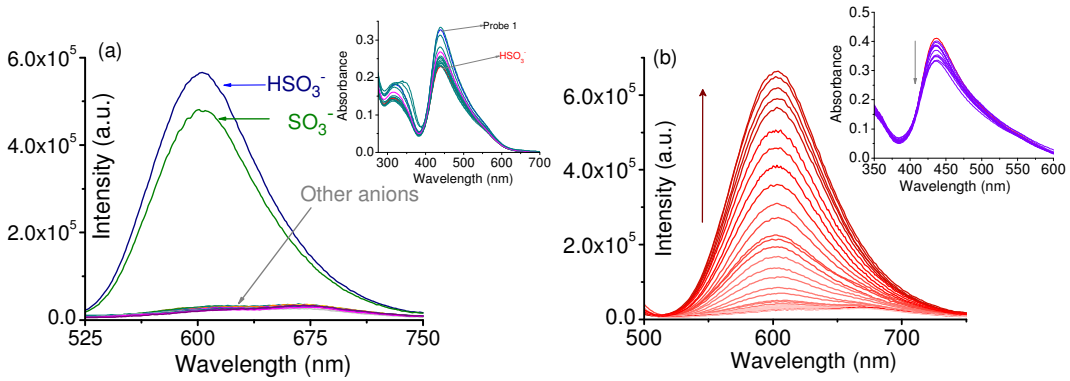

Figure 4.2. (a) Luminescence spectra for probe **1** (20 μM) in absence and presence of various ions (F^-, Cl^-, Br^-, I^-, NO_3^-, SO_4^{2-}, OAc^-, CN^-, $S_2O_3^{2-}$, S^{2-}, N_3^-, HSO_3^-, SO_3^{2-}, and $H_2PO_4^-$) and biothiols (Cys, Hcy, and GSH); (b) Changes in luminescence spectra for the probe (20 μM) in presence of varying [HSO_3^-] (0–8.0×10^{-3} M) using λ_{ex} of 490 nm. [inset: Absorption spectra in presence of different anions and with different concentration of HSO_3^-] All studies were performed in aq. buffer:DMSO (98:2, *v*/*v*) using 200 mM Na_2HPO_4:citric acid buffer solution at pH 5.0 ($\lambda_{ex}/\lambda_{em}$: 490/600 nm).

Interference studies in presence of large excess (200 molar equiv.) of various anions and biothiols were performed and the results clearly revealed that all such analytes failed to interfere with detection of SO_3^{2-}/HSO_3^- (Figure 4.3). As discussed above, sulfite can also exist as bisulfite ion depending on the media pH.[31] Accordingly, pH-dependent fluorescence spectra of **1** was measured in the absence and presence of HSO_3^-. No significant change in fluorescence spectra was evident for the pH range of 3–9. However, in the presence of HSO_3^-, distinct luminescence turn-on response was observed for the pH range of 4–6 and such change was the maximum at pH ~ 5. Relative changes in intensity as a function of time was found to be much more as well as found to reach the respective plateau much faster for a solution at pH 5 than that was observed for a solution at pH 7. This clearly revealed an efficient reaction and much better response at pH 5 (Figure 4.3). Hence pH 5.0 was chosen as preferred one, and at this pH bisulfite (pK_a ~6.97) is the reactive species.

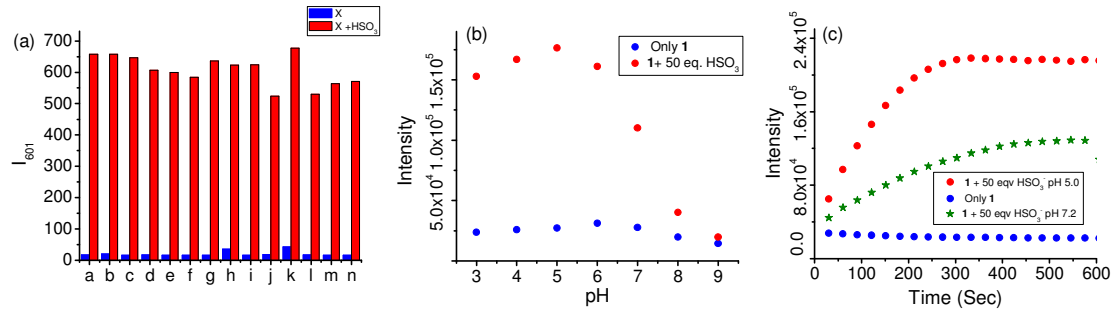

Figure 4.3. Change in emission profile of **1** (20 μM) for (a) in presence of 100 mole equivalent HSO_3^- and 200 mole equivalent of others [a=Cl^-, b= Br^-, c= F^-, d= I^-, e= OAc^-, f=NO_3^-, g= SO_4^-, h= $S_2O_3^{2-}$, i= $H_2PO_4^-$, j= N_3^-, k= Cys, l= Hcy, m=GSH, n= CN^-] (b) with different pH (c) with time in absence and presence of 50 equivalents of HSO_3^- in 200 mM Na_2HPO_4: citric acid aq. buffer solution pH 5.0 and pH 7.2 $\lambda_{Ext}/\lambda_{Em}$: 490/600nm.

Relative changes in luminescence intensities as a function of time for a specific concentration of HSO_3^- helped us to evaluate the observed pseudo first order rate constant (k_{obs}) for the reaction between **1** and HSO_3^- at pH 5 (Figure 4.4). A linear dependency of k_{obs} as a function of [HSO_3^-] ($k_{obs} = k_c [HSO_3^-] + c$, where k_c: rate constant for the overall reaction and *c* is an intercept; Figure 4.4f) yielded k_c of (18.9±0.3) s^{-1}. These results confirmed that the luminescence enhancement involved HSO_3^- in the slow step of the reaction. The results clearly revealed that relative changes in luminescence reached a plateau within 4.5 min and offered the possibility of the rapid hydrogen sulfite detection in an essentially aqueous buffer medium (Figure 4.3).

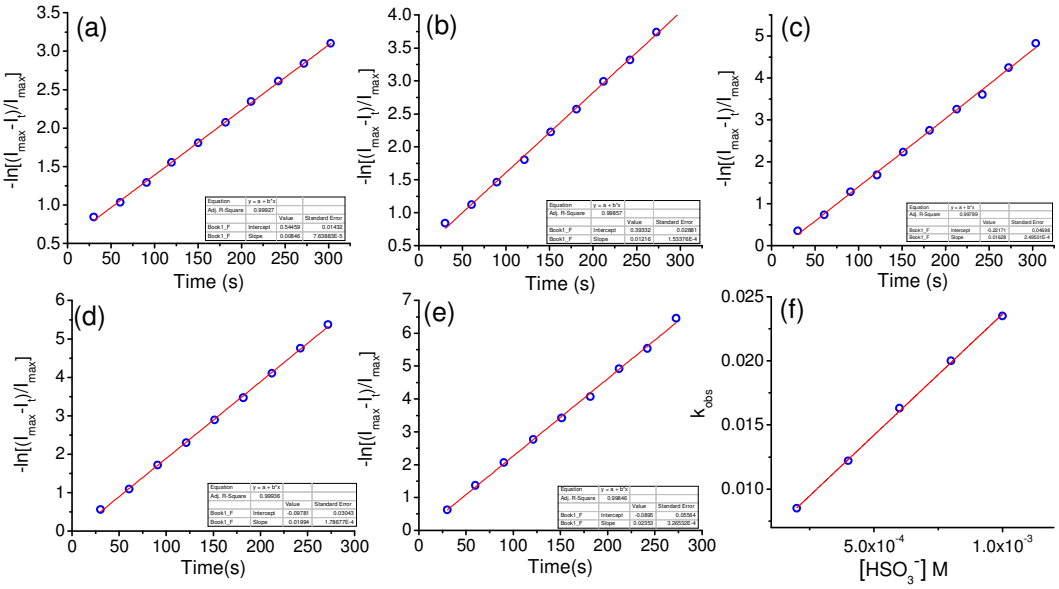

Figure 4.4. Plot of $-\ln[(I_{max}-I_t)/I_{max}]$ vs time with 20 μM of **1** in presence of different concentration of HSO_3^- (a) 2×10^{-4} M (b) 4×10^{-4} M (c) 6×10^{-4} M (d) 8×10^{-4} M (e) 10×10^{-4} M (f) k_{obs} vs HSO_3^- [in 200 mM Na_2HPO_4: citric acid aq. buffer solution pH 5.0.

An excellent linear relationship was observed for luminescence responses of probe **1** with varying concentration of HSO_3^- (from 0 to 200 μM), from which a lowest detection limit of 1.86×10^{-6} M was obtained. Significantly, this value is lower than the permitted level set by WHO, FAO and FDA in environmental, food and pharmaceutical samples, respectively. All these data confirmed that the present chemodosimetric probe helped us in sensing and quantitative estimation of bisulfite ion in an essentially aqueous buffer medium without any interference from all possible anions (including cyanide) and biothiols.

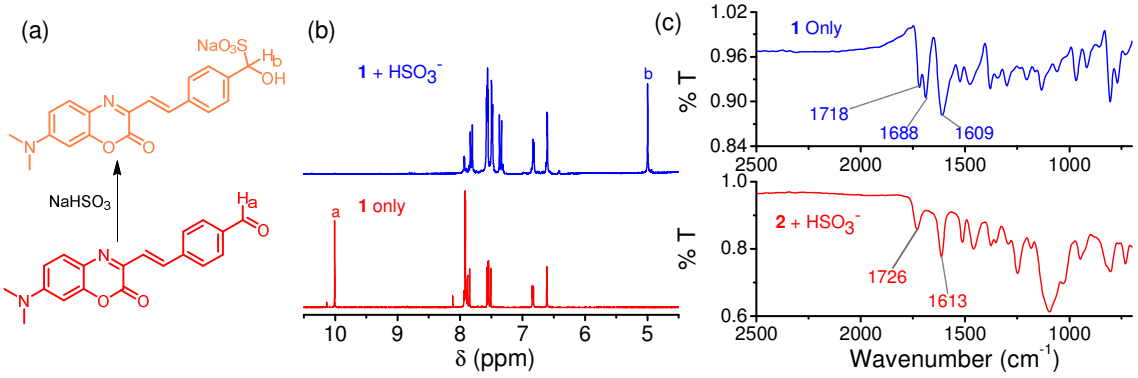

Figure 4.5. (a) Formation of bisulfite adduct with probe **1**. (b) Partial ^{1}H NMR spectra of **1** in DMSO-d_6. (c) IR spectra obtained in absence and presence of 10 equivalents of HSO_3^-.

The proposed reaction between probe **1** and HSO_3^- was also studied by ^1H NMR, IR and mass. ^1H NMR spectra of **1** showed a signal at 10.0 ppm (H_a) for H_{CHO} in DMSO-d_6 (Figure 4.5). On reaction with HSO_3^-, a new peak appeared at 4.99 ppm (H_b) with concomitant disappearance of the signal for H_{CHO} at 10.0 ppm (Figure 4.5). This confirmed the formation of the proposed adduct (Figure 4.5). Other aromatic protons also showed an obvious upfield shift compared to those of probe **1** due to the lowering of the extent of conjugation and the electron withdrawing influence. An IR signal responsible for the aldehyde functionality for probe **1** appeared at 1688 cm^{-1}, which completely disappeared on formation of the bisulfite adduct (Figure 4.5). A distinct signal at *m*/*z* of 402.69 (**1** + HSO_3^- + H^+) with anticipated isotope distribution further corroborated the proposed adduct formation.

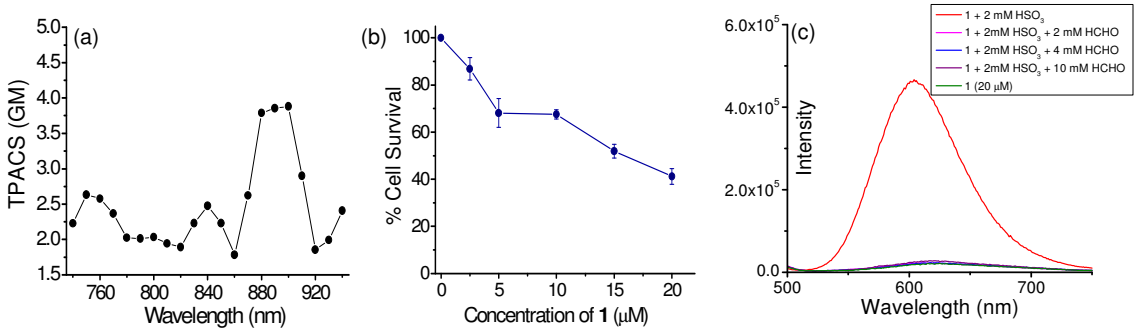

Figure 4.6. (a) TPACS value of probe **1** (10 μM in pH 5.6 HEPES buffer in the presence of 200 equivalent of sodium bisulfite) using Rhodamine B (100 μM in methanol) as a reference dye. (b) MTT assay (c) Control experiment in presence of different concentration of formaldehyde.

4.3.2. Two-photon imaging

Probe **1** and its bisulfite adduct have dipolar character owing to the presence of a donor (the amino group) and an acceptor (the formyl/lactone moiety). As such dipolar dyes generally have good two-photon excitable properties, we evaluated their two-photon absorbing property. The bisulfite adduct of probe **1** showed a marginal but sufficient two-photon action cross section (TPACS) value: the maximum two-photon action cross-section value was determined to be 3.9 GM at 900 nm (Figure 4.6). On the basis of the two-photon fluorescence data of the adduct, TPM imaging of bisulfite in cells and tissues was performed. Probe **1** was found to be substantially toxic to live Hct116 cells determined by MTT assay (Figure 4.6) and used further for imaging studies.

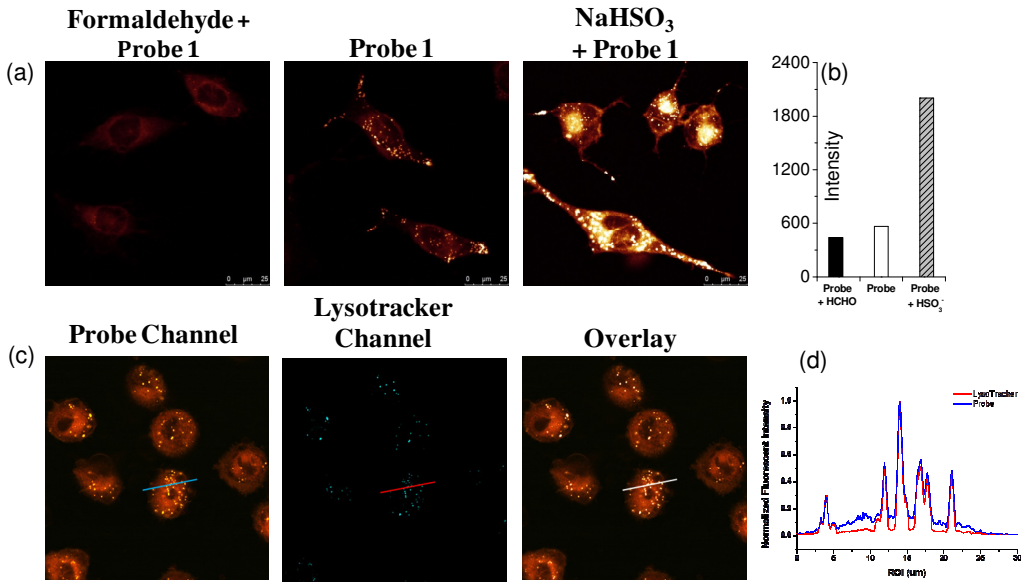

Figure 4.7. Fluorescence imaging of HeLa cells by TPM. (a) From the left: cells pre-incubated with formaldehyde (1 mM) followed by of probe **1** (10 μM), cells incubated only with probe **1** (10 μM), and cells pre-incubated with 1.0 mM of bisulfite followed by probe **1** (10 μM). (b) Relative fluorescence intensity of images of (a). (b) Cells co-incubated with probe **1** (5 μM) and LysoTracker Deep Red (500 nM): from the left, fluorescence collected from the probe channel (500–550 nm + 565–605 nm) under two-photon excitation at 880 nm, fluorescence collected from a LysoTracker channel (660–700 nm) under one-photon excitation by 688 nm. (d) Fluorescence intensity changes along with the line of interest (ROI) in Figure c images (marked with blue and red solid lines). Calculated colocalization factors are PCC = 0.628 and MOC = 0.897. The scale bar is 25 μm.

TPM imaging of HeLa cells with probe **1** alone shows bright, yellow-orange fluorescence, indicative of its imaging capability of endogenous cellular bisulfite.[14] Cells pre-treated with bisulfite (1 mM) (the positive control) show an increase in emission compared with that treated only with probe **1**, which indicates that our probe senses bisulfite in cells (Figure 4.7). A negative control experiment was also conducted in the presence of formaldehyde, which is known to consume bisulfite by forming an addition product. Indeed, the fluorescence spectra of probe **1** did not show any emission enhancement when sample was pre-treated with formaldehyde (Figure 4.7). As expected, the cells pre-incubated with formaldehyde did not show any notable emission (Figure 4.7), which confirms that bright emission was due to presence of endogenous bisulfite. Endogenous sulfite is known to be generated during the normal metabolism of sulfur-containing amino acids, and alterations in sulfur-containing amino acid metabolism occur in some neurodegenerative diseases. Sulfite is also an important intermediate in the metabolic pathway by which sulfur-containing amino acids is converted to the corresponding inorganic sulfate.[15]

A closer look at the patterns in images shown in Figure 4.7 clearly reveals that there are brighter particle-like spots over the dim background. By analyzing the patterns of the co-localization imaging with LysoTracker Deep Red, a commercially available lysosome specific dye, it is revealed that the brighter particles are overlaid with the distribution of lysosomes (Figures 4.7 c & d). Lysosomes, the terminal organelles on the endocytic pathway, digest macromolecules and make their components available to the cell as nutrients. Hydrolytic enzymes within the lysosome are activated by the highly acidic pH (4.5–5.0) in the organelles interior.[16] Lysosomes generate and maintain their pH gradients by using the activity of a proton-pumping V-type ATPase. As discussed earlier, the rate of our chemodosimetric reaction and the extent of emission intensity enhancement were higher for HSO_3^- than that of SO_3^{2-}, and the former species exists predominantly at pH ~5.0. This has presumably caused a faster response to give the brighter images of lysosomes over the dim background signal of cytosol where pH is around 7.4.

Given that the probe stains endogenous cellular bisulfite efficiently, next we move to *ex vivo* imaging of bisulfite in organ tissues by TPM. For this purpose, five different organs of mouse (brain, liver, lung, spleen and kidney) were prepared, which were incubated with probe **1** (10 μM) to sense endogenous bisulfite. The TPM image data given in Figure 4.8 clearly show bright fluorescence (with particle-wise brighter fluorescence) in brain, liver and lung tissues, suggestive of a high level of endogenous bisulfite in these organs and a very low level in spleen and kidney. As the image data is intensity based ones, at present it is difficult to estimate the probe penetration/distribution dependent on organs as well as the bisulfite concentration. A further look into bisulfite in the hippocampus region of brain, however, shows the presence of bisulfite in all of DG, CA1 and CA3 areas where neurons are located densely (Figure 4.8). Furthermore, along the neuronal pathway it also maintains particle-wise shape as does in the cellular level (yellow arrows in figure 4.8b). The results demonstrate that the probe can be used to fluorescence imaging of bisulfite in deep tissues of biological samples with high sensitivity and high resolution by TPM.

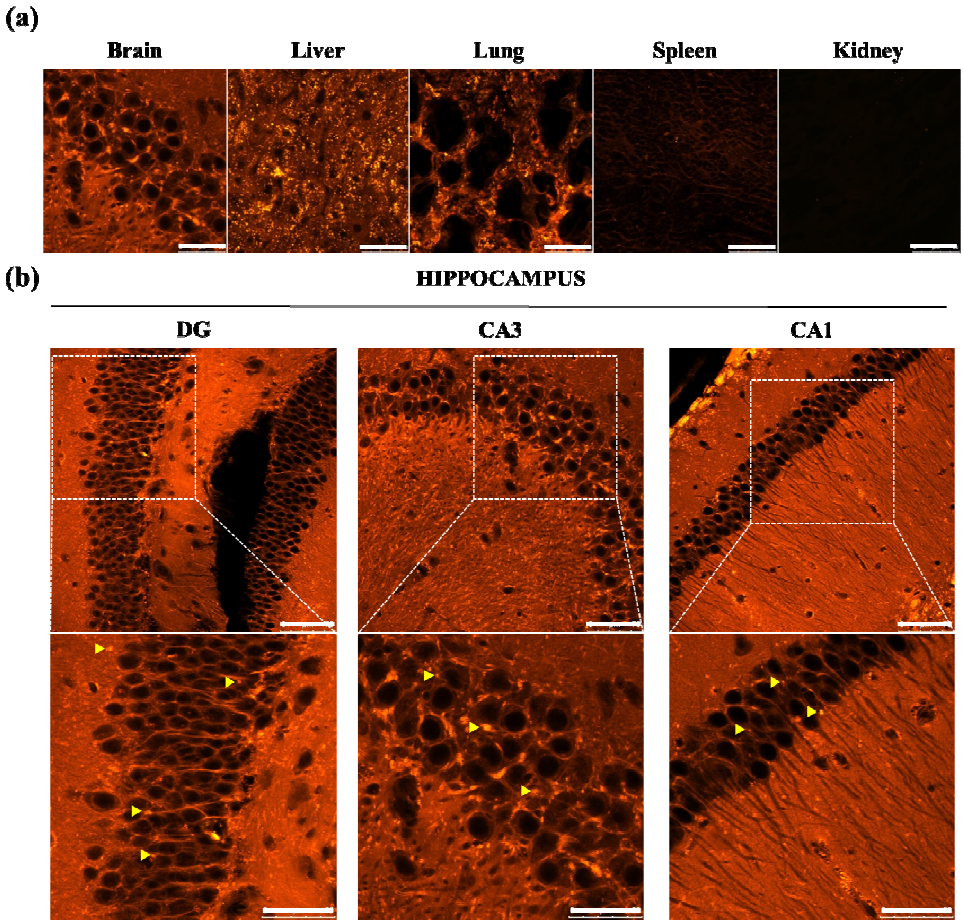

TPM tissue imaging data: (a) Fluorescence images of five different organs (brain, liver, lung, spleen and kidney); (b) Images of three different hippocampus regions of mouse brain (DG, CA3 and CA1). All of the tissues were incubated with 10 μM of probe **1** and images were obtained after 30 min incubation. The TPM imaging was conducted by exciting at 880 nm with 24.2 W laser power at the focal point and by collecting fluorescence emission through two overlaid channels (500–550 nm; 565–605 nm). Scale bar: 50 μm (in a), 75 μm (1st row in b), and 50 μm (2nd row in b). The depth of the tissue image is around 80–100 μm from the surface.

4.3.3. Electrochemical detection

ISEs are an important class of electrochemical sensors, which have significance due to their ease of fabrication, size tailorability, portability, economic viability and power efficiency. Recent advances in achieving improvement in the limit-of-detection (LOD) of ISE, discoveries of new membrane materials, new sensing concepts, deeper theoretical understanding and modeling studies have contributed a distinct surge of interest in ISEs.[17] It has been argued that for receptor-based efficient ISEs, appropriate choice of a membrane matrix depends upon the relative hydrophobic or hydrophilic nature of the receptor.[18,19] Typically, poly(vinyl chloride) (PVC) is used as the membrane matrix in ISEs

for the immobilization of hydrophobic receptors, while safe disposal of the discarded electrodes remained an issue and PVC-based membranes are of an environmental concern. To address this important issue, a biodegradable membrane, cellulose acetate was used as the matrix. Moreover, due to sufficient mechanical stability cellulose acetate does not need cross linking. We have utilized the hydrophobic nature of the probe 1 in developing the modified cellulose acetate membrane.

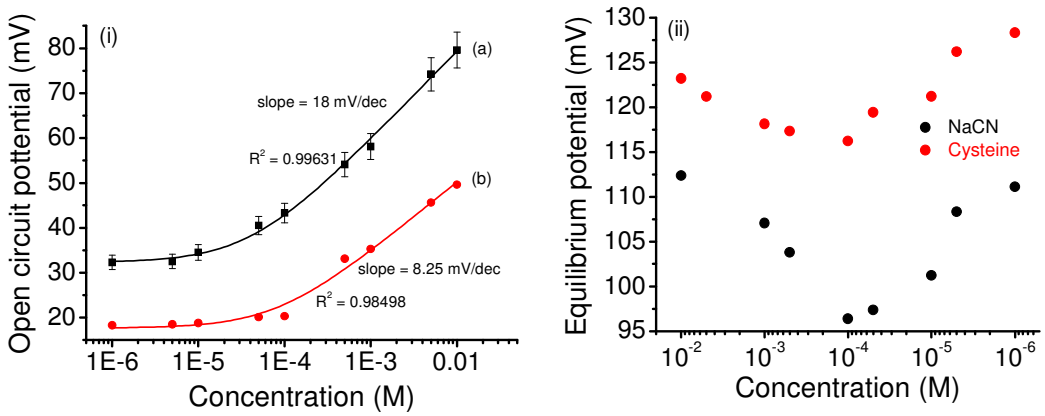

Figure 4.8. Potentiometric calibration curve of (i) probe **1** with HSO_3^- (a) having slope of 18 mV/dec and regression coefficient 0.99631 with 5% standard deviation. (b) Control experiments without ligand having slope of 8.25 mV/dec and regression coefficient 0.98498. (c) probe **1** with cyanide and cysteine.

The open circuit potentials for various concentrations of sulfite (predominant species for media pH 6.8) recorded. The limit of quantification for the sensor was found to be 1.0×10^{-4} M, whereas the linear range was found to extend from 1.0×10^{-4} M to 1.0×10^{-2} M with sub-Nernstian slope of 18 mV/dec and regression coefficient of 0.9914 (Figure 4.8). The limit of detection was found to be as low as 5.0×10^{-5} M. For control experiment (without using the probe **1)** the slope of 8.25 mV/dec and regression coefficient 0.9849 were observed. Sub-Nernstian slope, as it is observed for the present study, is not an uncommon phenomenon for anion sensing.[20] The response of chemical species like cyanide and cysteine on the ion selective electrode has been tested. Corresponding response curve is given in Figure 4.8. The linearity of the response curve is limited to small concentration windows contradictory to the response of HSO_3^-, where a regular trend has been observed in wider concentration window. The slopes were found between 6-7 mV/dec which is close to that of control experiment. This observation supports the selectivity of the sensor towards HSO_3^- ion.

The current work is just a proof-of-concept and we believe that present receptor-analyte combination fulfils above two requirements well. We are exploring the work further to improve the sensor response and to bring it to Nernstian level. This observation indicates the significance of sensor response even though it is sub-Nernstian and its efficiency over earlier reported bisulfite ion selective electrode.[17b]

4.4. Conclusion

We synthesized a molecular probe that can selectively detect bisulfite ion in an aqueous medium with turn-on type fluorescence response. The probe responds to bisulfite very fast with no interference from common interfering agents such as biothiols and cyanide ion. This emission on response was further utilized as an imaging reagent for cellular uptake of bisulfite. Furthermore, as the probe molecule is two-photon excitable, it was able to observe endogenous bisulfite not only in cells but also in different organ tissues with high resolution images of distinct morphology. Finally, we explored a possibility of preparation of a proof of concept, low-cost electrochemical device for detecting bisulfite ion in an aqueous medium for in-field detection.

4.5. References

1. (a) Iwasawa, S.; Kikuchi, Y.; Nishiwaki, Y.; Nakano, M.; Michikawa, T.; Tsuboi, T.; Tanaka, S.; Uemura, T. J. Occup. Health, **2009**, 51, 38–47. (b) Sang, N.; Yun, Y.; Li, H.; Hou, L.; Han, M.; Li, G. K. SO_2 Toxicol. Sci., **2010**, 114, 226–236.

2. (a) Meng, Z. Q.; Qin, G. H.; Zhang, B.; Bai, J. L. *Mutagenesis,***2004**, *19*, 465-468. (b) Vally, H.; Misso, N. L.; Madan, V. *Clin. Exp. Allergy*, **2009**, *39*, 1643-1651. (c) Li, G. K.; Sang, N. Ecotoxicol. Environ. Saf., **2009**, 72, 236-241. (d) Taylor, S. L.; Bush, R. K.; Selner, J. C.; Nordlee, J. A.; Wiener, M. B.; Holden, K.; Koepke, J. W.; Busse, W. W. J. Allergy Clin. Immunol., **1988**, 81, 1159-1167.

3. (a) Yang, X.; Guo, X.; Zhao, Y. *Anal. Chim. Acta*, **2002**, *456*, 121. (b) Fazio, T.; Warner, C. *Food Addit. Contam.*, **1990**, *7*, 433. (c) McFeeters, R. F. *J. Food Prot.*, **1998**, *61*, 885. (c) Azevedo, L. C. de; Reis, M. M.; Motta, L. F.; Rocha, G. O. da; Silva L. A.; Andeade, J. B. De. *J. Agric. Food Chem.*, **2007**, *55*, 8670. (d) Doty, J. R. *Anal. Chem.*, **1948**, *20*, 1166.

4. W. J. *FAO in WHO food additives series*, 60 (Ed.: World Health Organization), Geneva, **2009**.

5. Kalimuthu, P.; Tkac, J.; Kappler, U.; Davis, J. J.; Bernhardt, P. V. *Anal. Chem.*, **2010**, *82*, 7374.

6. Monier-Williams, G. W. *Analyst,* **1927**, *52*, 343.

7. (a) Abdel-Latifa, M. S. *Anal. Lett.*, **1994**, *27*, 2601. (b) Li, Y.; Zhao, M. *Food Control*, **2006**, *17*, 975.

8. (a) Daunoravicius, Z.; Padarauskas, *Electrophoresis*, **2002**, *23*, 2439. (b) Jankovskiene, G.; Daunoravicius, Z.; Padarauskas, A. *J. Chromatogr. A*, **2001**, *934*, 67.

9. (a) Pizzoferrato, L.; Lullo G. D.; Quattrucci, E. *Food Chem.*, **1998**, *63*, 275. (b) McFeeters, R. F.; Barish, A. O. *J. Agric. Food Chem.*, **2003**, *51*, 1513.

10. (a) Jung, H. S.; Chen, X. Q.; Kim, J. S.; Yoon, J. *Chem. Soc. Rev.*, **2013**, *42*, 6019. (b) Chen, X. Q.; Pradhan, T.; Wang, F.; Kim, J. S.; Yoon, *Chem. Rev.,* **2012,** *112*, 1910. (c) Ashton, T. D.; Jolliffe, K. A.; Pfeffer, F. M. *Chem. Soc. Rev.*, **2015**, *44*, 4547.

11. Buck, R. P.; Lindner, E. *Anal. Chem.*, **2001**, *73*, 88A.

12. (a) Kim, H. M.; Cho, B. R. *Chem. Rev.* **2015**, 115, 5014−5055. (b) Kim, D.; Ryu, H. G.; Ahn, K. H. *Org. Biomol. Chem.,* **2014**, *12*, 4550.

13. Hu, M.; Fan, J.; Li, H.; Song, K.; Wang, S.; Cheng, G.; Peng, X. *Org. Biomol. Chem.*, **2011**, *9*, 980.

14. (a) Sun, Y. Q.; Liu, J.; Zhang, J.; Yang, T.; Guo, W. *Chem. Commun.,* **2013**, *49*, 2637-2639. (b) Li, G.; Chen, Y.; Wang, J.; Wu, J.; Gasser, G.; Ji, L.; Chao, H. *Biomaterials*, **2015**, *63* 128. (b) Huang, Y.; Tang, C.; Du, J.; Jin, H. *Oxidative Med. Cellular Longevity*, **2016**, Article ID 8961951, DOI. 10.1155/2016/8961951.

15. (a) Lester, M. R. *J. Am. Coll. Nutr*, **1995**, *14*, 229. (b) Reist, M.; Marshall, K. A.; Jenner, P.; Halliwell, B. *J. Neurochem.*, **1998**, *71*, 2431.

16. Mindell, J. A. *Annu. Rev. Physiol.*, **2012**, *74*, 69.

17. (a) Bobacka, J.; Ivaska, A.; Lewenstam, A. *Chem. Rev.*, **2008**, *108*, 329. (b) Bakker, E.; Meyerhoff, M. E. *Anal. Chim. Acta*, **2000**, *416*, 121.

18. (a) Pedersen, C. J. *J. Am. Chem. Soc.*, **1967**, *89*, 7017. (b) Park, C. H.; Simmons, H. E. *J. Am. Chem. Soc.*, **1968**, *90*, 2431.

19. Antonisse, M. M. G.; Reinhoudt, D. N. *Electroanalysis*, **1999**, *11*, 1035.

20. Young, S. D.; Daunert, S.; Bachas, L. G. *Electroanaysis,* **1995**, *7*, 710.

CHAPTER 5

A SWITCH-ON NIR PROBE FOR SPECIFIC DETECTION OF Hg^{2+} ION IN AQUEOUS MEDIUM AND IN MITOCHONDRIA

Publication:
To Be Communicated

5.1. Introduction

Mercury is considered to be one of the most toxic heavy metal. Mercury in its various forms is known to be the most potent neurotoxin for human physiology and other living organisms.[1] Among various forms, Hg^{2+} is the most common form of ionic form of mercury that exists in the environment. Redox transformation between elemental Hg(0) and divalent Hg(II) is a key process that leads to the transport of mercury in ground water systems and this is actually induced by diverse anaerobic bacteria.[1] Bio-accumulation of Hg^{2+} in human body through food chain is a major source of serious neural disorder, Hunter-Russell syndrome, and diseases like Alzheimer's and Minamata.[2] Considering the deleterious effects of Hg^{+2} in human health, the Environmental Protection Agency (EPA) has set the maximum allowed level of Hg^{+2} in drinking water to be 2 ppb.[3] Therefore considerable efforts have been put together for developing appropriate reagent and the subsequent methodology for selective and sensitive detection of Hg^{2+}ion that could be present in an environmental or biological sample at a very low concentration.

Over the years, several methods have been developed *e.g.* Atomic absorption spectroscopy,[4] inductive coupled plasma mass spectroscopy (ICPMS),[5] inductively coupled plasma–atomic absorption spectroscopy (ICP-AES)[6] for detection of Hg^{+2} ion in environmental samples. However most of these methods are expensive; require tedious sample preparation and involvement of highly skilled manpower. On the other hand, use of molecular sensors that allow detection and quantitative estimation of the Hg^{2+} ion through measurable changes in optical responses have a distinct edge primarily due the ease in detection process/methodology as well as these methodologies allow detection of the Hg^{2+} ion present in the ultra trace quantity. Among various optical sensors, fluorescence based sensors are obviously preferred as these allow developing non-invasive methodologies with the possibility of using such reagent for *in-vitro* or *in-vivo* imaging application.[7] Such processes or methodologies are crucial for clinical diagnosis, assessing impact of the exposure of the living organisms to Hg^{2+} and studying biochemical processes associated with Hg^{2+} in living organisms.[8] There have been many previous attempts for developing fluorescence-based sensors for Hg^{2+} ion using small molecular probes, oligonucleotides, gold nanoparticles, etc.[9-11] Among such attempts, reagents that are capable of exhibiting modified luminescence response on binding to Hg^{2+} in the near infrared (NIR) region of the spectrum has a special significance for *in-vitro* or *in-vivo* imaging application and in clinical diagnosis. As, response in the NIR region (>650nm) helps in delineating the

response(s) from the background auto fluorescence from intrinsic biomolecules that generally occur in the visible region.[12] Moreover deep-red light allows minimum photo-bleaching of the probe/ photo-damage of the living tissues/cells, deeper tissue penetration and low light scattering.[13] Further, organelle specific dye localization also offers us the option to monitor Hg^{2+} localization in that specific cellular compartment and this is important for clinical impact assessment.[14,15] It is well documented that mitochondria are one of the major targets for localization of heavy metals. Several reports suggest mercury decreases mitochondrial membrane potential in hepatic and renal mitochondria.[16] It has been argued that mercury reacts with –SH group of proteins in the inner mitochondrial inner membrane and generates oxidative stress, which could lead to cell apoptosis.[17] However, the exact mechanism for this process is yet to be fully estanblished.[18] Considering these, there is a definite need and scope for developing an efficient NIR active molecular receptor that could effectively recognize and image the localization of Hg^{2+} in the mitochondrial region of live cells. Such examples are scare in contemporary literature.[19]

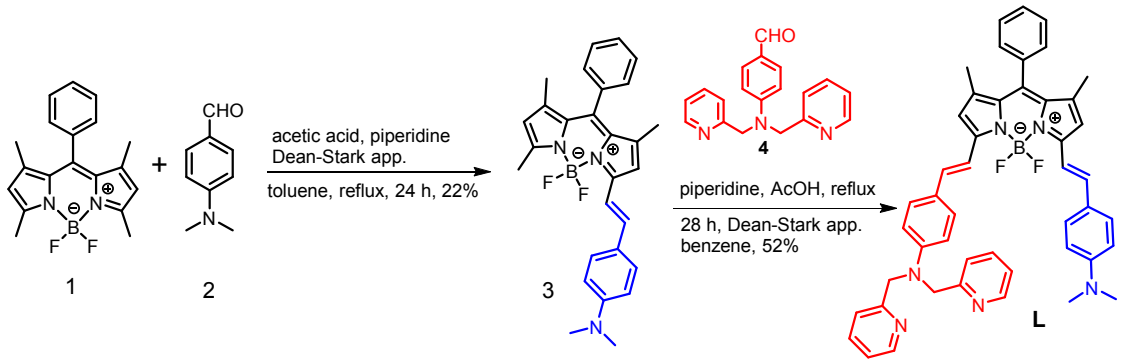

Scheme 5.1. Methodology adopted for synthesis of the reagent **L.**

5.2. Experimental section

5.2.1. Materials

Chloromethyl pyridine, aniline, benzoyl chloride, 2,4-dimethylpyrrole, N,N-dimethylaminobenzaldehyde and perchlorate salt of respective metal ion were purchased from Sigma Aldrich and were used as received. Other reagents and HPLC grade acetonitrile were procured from S. D. Fine Chemical (India) and were used without any further purification.

5.2.2. Analytical Methods

^{1}H and ^{13}C NMR spectra were recorded on a Bruker 200/500 MHz FT NMR (Model: Avance-DPX 200/400/500) using trimethylsilane (TMS) as an internal standard. FTIR spectra were recorded as KBr pellets in a cell fitted with a KBr window, using a Perkin-Elmer Spectra GX 2000 spectrometer. ESI-Ms measurements were carried out on a Waters QTof-Micro instrument. Solution pH was evaluated using Mettler Toledo FEP20 pH meter. Absorption spectra were recorded using a Perkin Elmer Lambda 950 UV-Vis spectrophotometer equipped with cell holder having path length of 1cm. Fluorescence spectra were recorded on PTI QuantaMaster 400 spectrophotometer.

5.2.3. Generalised methodology for spectroscopic studies

A solution of probe **L** (1.0 mM in acetonitrile) was prepared and used for all further studies after appropriate dilution with 10 mM HEPES buffer to make a final concentration of reagent as 2.0×10^{-6} M in 10 mM aq.HEPES buffer-CH_3CN (3:7, v/v; pH 7.2). Stock solutions of 100 mM of perchlorate salts of different metals, Na^{+}, K^{+}, Cs^{+}, Ba^{2+}, Ca^{2+}, Mg^{2+}, Cd^{2+}, Ni^{2+}, Cu^{2+}, Zn^{2+}, Pb^{2+}, Co^{3+}, Cr^{3+}, Fe^{2+}, $Fe^{3+}$and Hg^{2+} were prepared in a 10 mM aq.HEPES buffer-CH_3CN (7:3, v/v; pH 7.2) medium. Stock solutions were further diluted with buffer solution as per requirement for a specific experiment. All emission studies were performed in aq.- HEPES buffer-CH_3CN (3:7, v/v; pH 7.2) medium using λ_{Ext} = 620 nm, λ_{Mon} = 650 nm and a slit width of 2/2. The relative fluorescence quantum yields (ϕ_f) were estimated using equation 1 by using the integrated emission intensity of Cresyl violet perchlorate in ethanol (Φ = 0.54 at RT) as a reference.

$$\Phi_f = \Phi_f'(I_{sample}/I_{std})(A_{std}/A_{sample})(\eta^2_{sample}/\eta^2_{std}) \qquad \text{Equation 1}$$

where, Φ_f' is the absolute quantum yield for the Cresyl violet perchlorate, used as standard; I_{sample} and I_{std} are the integrated emission intensities; A_{sample} and A_{std} are the absorbance at the excitation wavelength, and η_{sample} and η_{std} are the respective refractive indices of sample and standard.

From luminescence titrations and their corresponding spectra, the association constant and binding stochiometry of **L** with Hg^{+2} was determined by using Benesi-Hildebrand analyses and related expression used for this purpose is shown in equation 2.[20].

$$1/(F-F_0) = 1/K(F_{max} - F_0)[M^{n+}] + 1/[F_{max} - F_0) \qquad \text{Equation 2}$$

Where F_0 is the luminescence intensity of **L** at a particular wavelength, F is the luminescence intensity obtained with externally added Hg^{+2} at that particular wavelength, F_{max} is the maximum intensity at the saturation point, *K* is the association constant (M^{-1}) and $[M^{n+}]$ is the concentration of the externally added Hg^{+2}. The lowest detection limit was calculated by following 3σ/k method; where σ is the standard deviation of blank measurement, k is the slope of intensity *vs.* $[Hg^{+2}]$ plot.

5.2.4. Computational Details

Full geometrical optimizations were carried out in the gas phase employing the M06-2X level[21] with standard 6-31G(d) basis set [22] for the non-metals (C, H, N, O, B, F and P) and LANL2DZ basis set[23] for metal ions (Hg^{2+}). The hybrid meta-functional M06-2X was considered as an excellent DFT functional considering the non-covalent interactions[24] and it predicted the accurate valence and Rydberg electronic excitation energies for main group chemistry.[21a] Frequency calculations were performed at the same level of theory to confirm that each stationary point was a local minimum (with zero imaginary frequency). The single point time-dependent DFT (TD-DFT) methods[25] were implemented with the same level of theory for evaluating the excitation energies from the ground state to the excited state. All the calculations were performed with GAUSSIAN 09 suite of program.[26]

5.2.5. Cell Culture and Confocal study

Hct116 cells (3.0×10^5) seeded on coverslips placed in 35mm petridishes and were maintained at 37℃ in a humidified 5% CO_2 atmosphere using DMEM (Dulbecco's modified Eagle's Medium) supplemented with 10% fetal Bovine serum and 100 units of penicillin streptomycin for 24 h. After 24 hours, cells were treated with **L** (2 μM) for 30 minutes. Cells were then washed thrice with phosphate buffer saline (1X PBS) and then stained cells were again treated with 20 μM of Hg^{2+} for 20 minutes, washed thrice with 1X PBS and fixed with 4% PFA for 20 minutes. Permeabilization of the cells was done using 0.2% Triton X 100 for 5 minutes. Coverslips were mounted with Fluoro shield mounting medium. Nail paints was used to seal the coverslips mounted on the glass slides. Confocal laser scanning images were acquired in Olympus Fluoview Microscope with a 60x objective lens with $\lambda_{Ext}/\lambda_{Ems}$ = 633/650 nm. For colocalisation experiment, cells were incubated with Mito-tracker green from life technologies before incubation with Hg^{2+} and images were taken at different channels.

5.2.6. Synthesis of Probe L

Intermediates **1**, **3** and **4** were synthesized following previously reported methods.[27] In a two necked round bottom flask equipped with a magnetic stirring bar, a Dean-Stark apparatus and a reflux condenser were added compound **3** (50 mg, 0.1 mmol) and aldehyde **4** (33.3 mg, 0.1mmol). The flask was flushed with argon, followed by addition of dry benzene (10 mL), piperidine (53 µL) and acetic acid (53 µL). The total volume of benzene was adjusted to 30 mL and the reaction mixture was set to reflux for next 28 h. After total consumption of aldehyde **4** (checked by TLC), the solvent was evaporated under vacuum and ethyl acetate (20 mL) was added. The organic layer was washed with water (10 mL × 3), separated and dried over sodium sulfate. Evaporation of the organic layer under vacuum yielded crude but desired product as a solid power, which was subjected to column chromatography for further purification using a gradient of MeOH-EtOAc (1:49, v/v) as eluent. Solvent was evaporated under reduced pressure and the desired product **L** was isolated as blue solid in pure form (42.3 mg, 52%). R_f for TLC: 0.2 (MeOH-EtOAc; 1:19, v/v), Yield; 42.3mg (52% with respect to starting reagents),^{1}H NMR (400 MHz, $CDCl_3$) δ:8.63 (d, J = 4.9, 2H), 7.70 (t, J = 7.8, 2H), 7.56-7.44 (m, 9H), 7.31 (d, J = 7.8, 4H), 7.26-7.09 (m, 4H), 6.72 (d, J = 8.3, 4H), 6.58 (d, J = 12.2, 2H), 4.92 (s, 4H), 3.04 (s, 6H), 1.42 (s, 3H), 1.41 (s, 3H); ^{13}C NMR (100 MHz, $CDCl_3$) δ:158.1, 153.2, 152.1, 150.8, 149.3, 148.4, 141.3, 140.7, 137.4, 136.64, 136.55, 135.6, 135.3, 133.1, 132.8, 129.09, 129.06, 128.9, 128.72, 128.65, 126.4, 125.1, 122.4, 121.1, 117.4, 117.1, 115.8, 114.9, 112.7, 112.1, 57.1, 40.3, 14.6, 14.5; HRMS-ESI (*m*/*z*): Calculated $[C_{47}H_{43}N_6BF_2+H]^+$ 741.3683 and found 741.3675.

5.3. Results and Discussions

We have prepared a new BODIPY derivative **L** having an appended dipicolylamine moiety (Scheme 5.1) for coordination to a metal ion. The purity of these intermediates was checked by standard analytical and spectroscopic techniques. Spectroscopic and analytical data confirmed the desired purity for the probe **L**. The newly synthesized probe **L** was found to have limited solubility in pure aqueous HEPES buffer medium. Accordingly, we had used a predominantly aq. buffer (10 mM aq. HEPES buffer-acetonitrile, 3:7 (v/v); pH 7.2) medium for all our studies.

5.3.1. Spectroscopic studies

Electronic spectrum recorded for the green coloured solution of the reagent **L** in aq. HEPES buffer-acetonitrile, 3:7 (v/v); pH 7.2 displayed an intense absorption band at 685 nm (ε = 5150 cm^{-1}), which was ascribed to a BODIPY based $S_0 \rightarrow S_1$ charge transfer (CT) transition (Figure 1). We anticipated that there would be an intra-molecular charge transfer (ICT) from donor dipicolylamine moiety to BODIPY chore as an acceptor. This was further supported by solvatochromic data, which showed distinct red shifted spectra with subsequent increase in solvent polarity (Figure 5.1a). We presumed that on interaction between the dipicolyl amine moiety and a metal ion, this ICT transition would be interrupted or disfavoured and accordingly a blue shift in the absorption band was anticipated. The metal ion recognition ability of the reagent **L** was systematically examined by recording Uv-Vis spectra in absence and presence (100 mole equivalents) of various metal ions in aq. HEPES buffer-acetonitrile, 3:7 (v/v) having pH 7.2 keeping [L] of 2 μM. Metal ions that are common for human physiology and are generally available in surface water, such as Na^+, K^+, Cs^+, Ba^{2+}, Ca^{2+}, Mg^{2+}, Cd^{2+}, Ni^{2+}, Cu^{2+}, Zn^{2+}, Pb^{2+}, Co^{3+}, Cr^{3+}, Fe^{2+}, Fe^{3+} and $Hg^{2+}$are utilized for our studies. Results revealed that barring Hg^{2+}, all other metal ions failed induce any detectable change in the observed electronic spectrum of the reagent **L**. For Hg^{2+} ion, a 15 nm blue shifted spectrum with little decrease in molar absorption coefficient (Figure 5.1b) was observed. The blue shift of the absorption band may be correlated to the interrupted or a disfavoured ICT process.

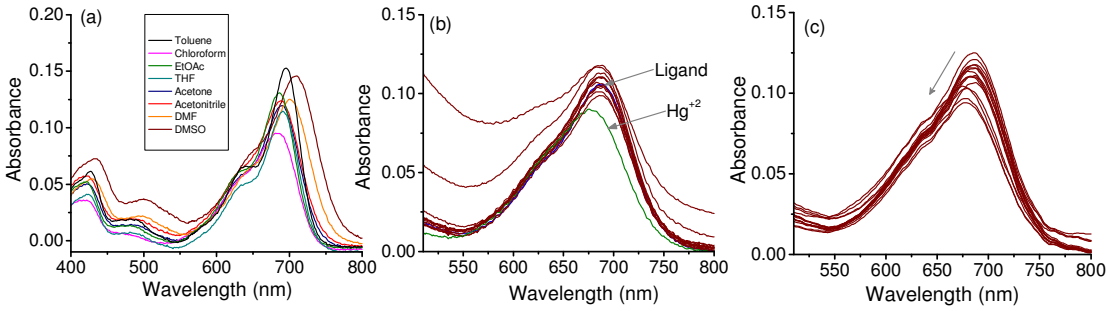

Figure 5.1. Absorption spectra of probe **L** (2 μM) in (a) solvents of different polarity (b) absence and presence of different metal ions (b) with different concentration of Hg^{2+} in CH_3CN-aq.HEPES buffer (10 mM, pH 7.2; 3:7, v/v).

However, changes were more prominent when steady state emission spectrum for **L** was recorded in absence and presence of various metal ions mentioned above. The emission spectrum of the reagent **L** (2 μM) in aq. HEPES buffer-acetonitrile, 3:7 (v/v) having pH 7.2

showed a weak band ~ 750 nm on excitation at 680 nm or 620 nm. This was attributed to an intra-molecular charge transfer (Figure 5.2b) and this was further substantiated by solvatochromic response of reagent in solvents of varying polarity (Figure 5.2a). On addition of 100 mole equivalents of different metal ions emission spectrum of reagent was considerably altered only in presence of Hg^{2+} and a new enhanced emission band appeared at 650 nm (λ_{Ext}= 620 nm) (Figure 5.2b). The excitation spectrum recorded in presence of Hg^{2+} showed a band at 620 nm and this implied that emission state of **L**. Hg^{2+} was different from the reagent (**L**) alone (Figure 5.2b). A little and insignificant enhancement of emission band intensity at 650 nm was observed in presence of Zn^{2+} (100 mole equivalents). The higher selectivity of Hg^{2+}over Zn^{2+} could be due to the high hydration enthalpy of Zn^{2+} (-2046 kJ mol^{-1}) than Hg^{2+} (-1824kJ mol^{-1}).[28] A significant increase in the emission quantum yield ($\mathbf{L}_{\Phi}$=0.026 and **L.**$Hg^{2+}{}_{\Phi}$ = 0.12; Cresyl violet perchlorate in ethanol (Φ = 0.54) was used as reference) was observed on binding of the reagent **L** to Hg^{2+}. This remarkable changes in the emission spectrum only in the presence of Hg^{2+} ions confirmed that the reagent showed highly specific binding towards Hg^{2+}. A little change in emission spectrum of **L** for Zn^{2+} or no detectable change in emission spectrum of **L** for other metal ions did not completely exclude the possibility of a weak coordination complex formation between **L** and Zn^{2+} or other metal ions in aq. HEPES buffer-acetonitrile, 3:7 (v/v) having pH 7.2.

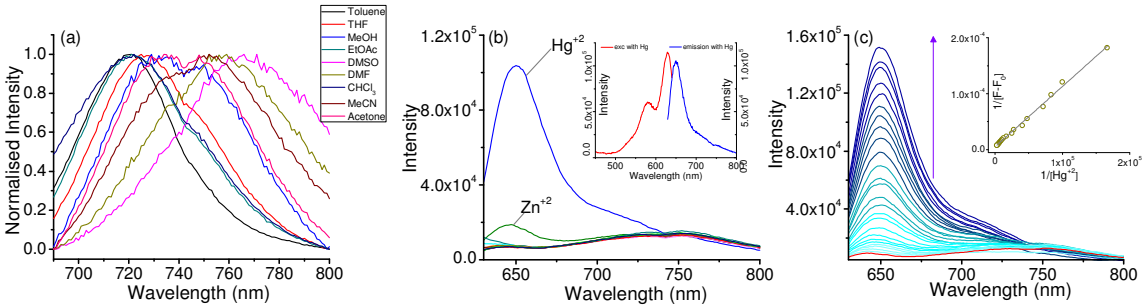

Figure 5.2. Emission spectra of probe **L** (2 μM) in (a) Solvents of different polarity (b) absence and presence of different metal ions [inset: excitation and emission after addition of Hg^{2+}] (c) with different concentration of Hg^{2+} [inset: Benesi-Hildebrand plot of L with Hg^{2+}] in CH_3CN-aq.HEPES buffer (10 mM, pH 7.2; 3:7, v/v) with λ_{exc}= 620 nm.

Fluorescence response was also examined in preference of the reagent **L** (2 μM) towards Hg^{2+} (100 μM) in presence of even larger (400 μM) excess of above mentioned cationic analytes (Figure 5.3a). Results of this interference study revealed that the spectral change observed for **L** on binding to Hg^{2+}, remained unaffected even in presence of large excess

of all other competing cations and this confirmed the specificity of the reagent towards Hg^{2+}.

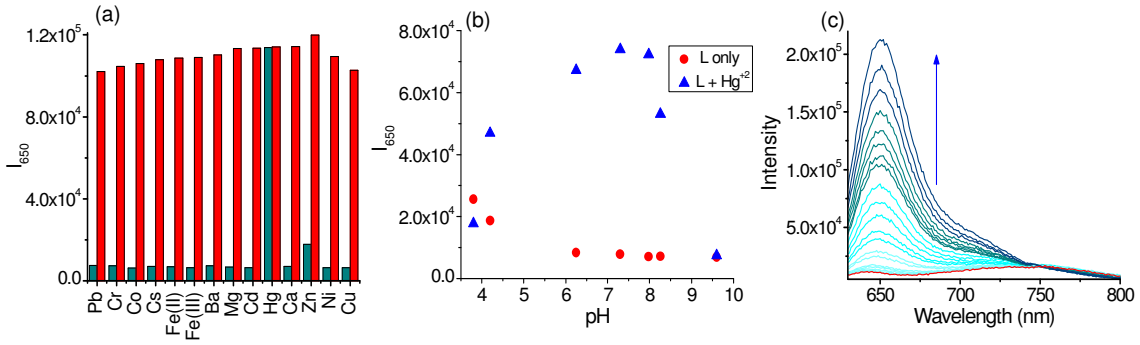

Figure 5.3. (a) Competitive graph of **L** (2 μM) in presence of 100 mole equivalent Hg^{2+} and 400 mole equivalent of other cations, (b) emission response at different pH, (c) Emission titration in presence of different concentration of $HgCl_2$.in CH_3CN-aq.HEPES buffer (10 mM, pH 7.2; 3:7, v/v) with λ_{exc}= 620 nm.

Binding affinity of the reagent **L** towards Hg^{2+} was studied by systematic emission titration studies using 2 μM of **L** and varying [Hg^{2+}] (0-150 mole equivalents) in aq. HEPES buffer-acetonitrile (3:7, v/v; pH 7.2) medium (Figure 5.2c). On addition of Hg^{2+}, a new emission band at 650 nm appeared. With increase in [Hg^{2+}], a gradual increase emission intensity at 650 nm was observed. Using parameters that were obtained from this titration plot, formation constant (K_a) for **L**. Hg^{2+} was evaluated using Benesi-Hildebrand equation and it was found to be (4.93 ± 0.2) $\times 10^3$ M^{-1}. A good linear fit of Benesi-Hildebrand plot was also confirmed the 1:1 binding stoichiometry for the complex formation between Hg^{2+} and **L**. Linear change in emission intensity at 650 nm was observed for the concentration range of 0-1.5$\times 10^{-5}$ M, while lowest detection limit (LOD) was evaluated as 1.7$\times 10^{-7}$ M by using 3σ/k method. Thus, this reagent could be used for quantitative estimation of Hg^{2+} that could be present in aq. environment in sub-micromolar region. Emission spectral responses were also examined in presence of varying [$HgCl_2$] for ascertaining the role of the effective acidity of the Hg-center in binding to **L**. This was important, as certain rhodamine based reagent showed luminescence *ON* response on binding to $Hg(ClO_4)_2$ or $Hg(NO_3)_2$, but failed to do so for Hg-center that is more covalent in nature (e.g. $HgCl_2$ or $HgBr_2$ or HgI_2).[9f] Systematic titration profile with varying [$HgCl_2$] helped us in evaluating the association constant (K_a^{HgCl2}= (2.96 ± 0.3)$\times 10^3$ M^{-1}) using B-H plot (Figure 5.3c), while LOD was evaluated as 4.7$\times 10^{-7}$ M. Slightly lower value for K_a^{HgCl2} presumably reflect relatively lower ionic character for Hg-center in $HgCl_2$. The pH influence of the reagent in sensing

was also investigated. This reagent showed higher sensitivity for the pH range of 6 – 8, just ideal for studies under physiological studies (Figure 5.3b).

The interaction and binding of the reagent **L** to Hg^{2+} was investigated by ^1H NMR and ESI-MS studies. The ^1H NMR spectra of the reagent **L** were recorded in absence and presence of Hg^{2+} ion. Appreciable downfield shifts for protons belonged to pyridine rings (Figure 5.4a) were observed **L** on binding to Hg^{2+}. Signal at 8.58 and 7.76 ppm for H_a and H_b protons, respectively, were found to shift to 8.60 and 8.36 ppm. Such downfield shift also supports coordination of pyridine moiety to Hg^{2+}-center. Downfield shift of 0.09 ppm (5.00 to 4.91 ppm) for H_c proton confirmed the coordination of the N_3 atom of the dipicolyl moiety to the Hg^{2+}-center. Results of the mass spectral studies further corroborated our proposition. ESI-MS studies performed with **L** and $Hg(ClO_4)_2$ showed *m/z* signal at 1140.7102 for [L+ Hg^{+2} + $2ClO_4^-$].

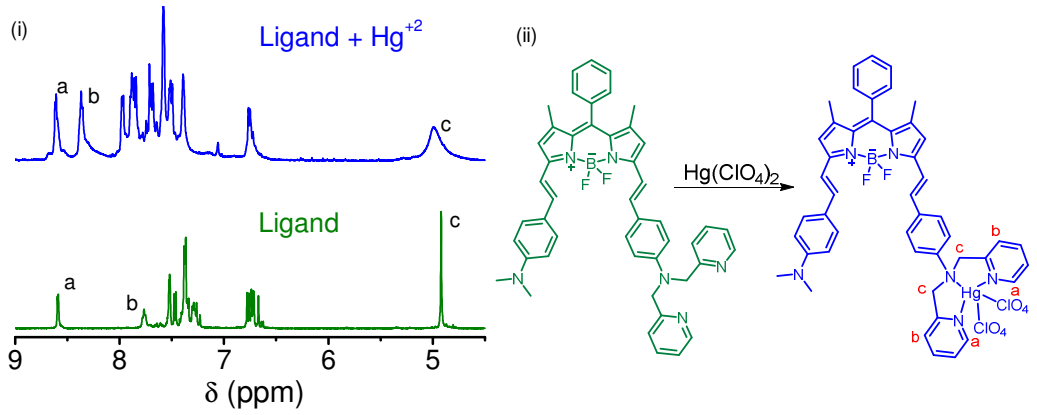

Figure 5.4: (a) ^1H NMR spectra for **L** recorded in absence and presence of Hg^{2+} in CD_3CN (b) Molecular structure for **L**.Hg^{2+}.

5.3.2. Computational Study

To explore the binding of Hg^{2+} with the reagent **L**, we have performed DFT calculations using (M06-2X) functional. We have examined the probable complex formation between **L** and Hg^{2+} by varying stoichiometry of coordinating water or/and ClO_4^-. Geometry of the reagent **L** was first optimized at M06-2X/6-31G(d) level of theory. The complexation between Hg^{2+} and the optimized structure for **L** was studied with different coordinating ligands/anions (H_2O or/and ClO_4^-). First, the coordination of two H_2O molecules to Hg^{2+} (abbreviated as [**L**+ Hg^{2+} +$2H_2O$**]**) was considered (Figure 5.5). In the next calculation, we

have examined the complex formation involving coordination of one H_2O and one ClO_4^- to the Hg^{2+} ion ([**L**+ Hg^{2+} +H_2O+ClO_4^-]). Finally, the coordination of either one or two ClO_4^- to the Hg^{2+} ion, ([**L**+ Hg^{2+} +ClO_4^-] and [**L**+ Hg^{2+} +2ClO_4^-]) was examined. Relative complexation energies ($\mathbf{E_{rel}}$) for all the above referred complexes were evaluated (Figure 5.5).The calculated results revealed that Hg^{2+} complex with two coordinated ClO_4^-, apart from the coordinated **L** (**L** + Hg^{2+} + 2ClO_4^-) has the lowest energy (Figure 5.5). This lowest energy complex agreed well with the results of the mass spectral analysis described previously.

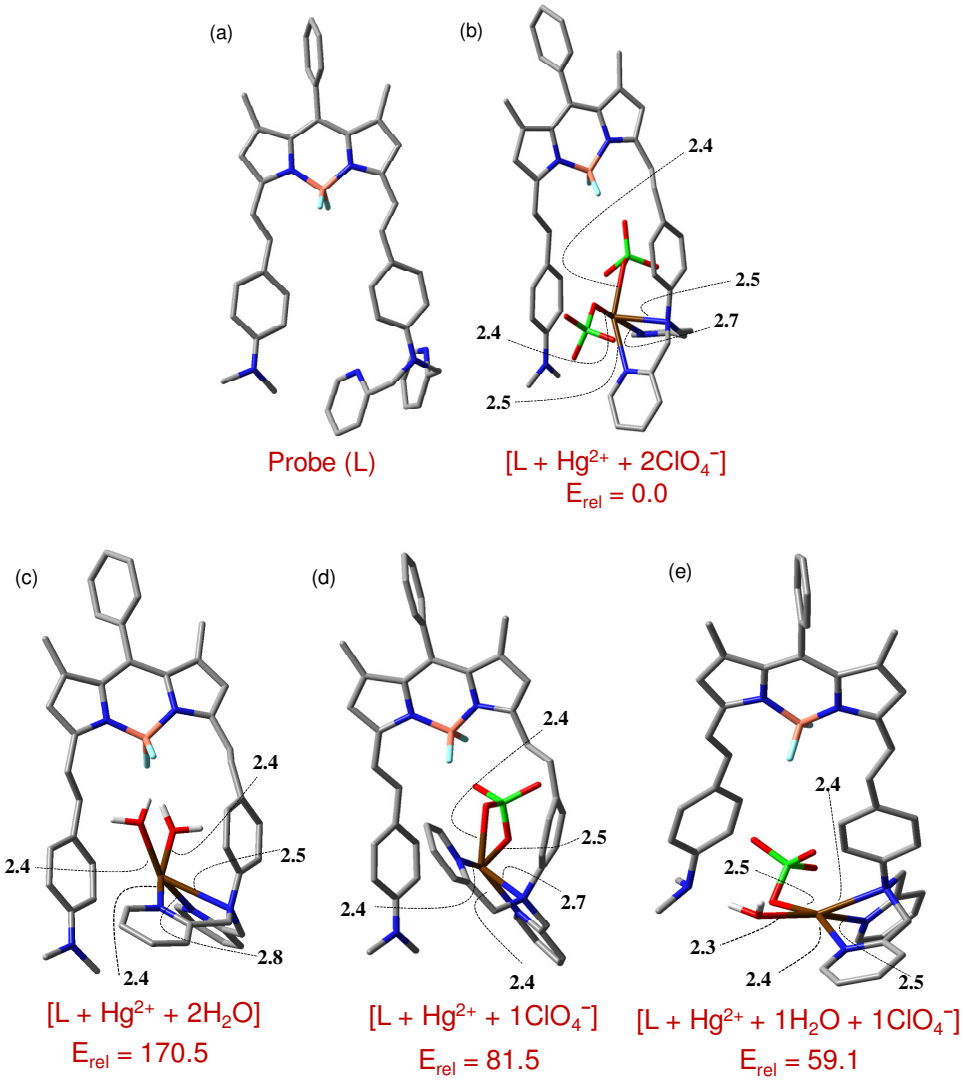

Figure 5.5. M06-2X optimized geometries with their relative energies (E_{rel}). The energies are in kcal/mol and the distances are in Å. Key: gray, C; green, Cl; orange, B; blue, N; white, H; red, O; cyano blue, F;deep maroon, Hg^{2+}.

To get a better insight in the transitions associated with **L** and **L** + Hg^{2+} + $2ClO_4^-$ (lowest energy form of the complex) and the spectroscopic behaviour, we have simulated the UV-Vis spectrum for both species using TD-DFT calculations. The highest occupied molecular orbital (HOMO) and the lowest unoccupied molecular orbital (LUMO) for two species are shown in Figure 5.6. Figure 5.6a reveals that the HOMO orbital coefficients of the reagent **L** are delocalized over the π framework of the BODIPY and extended up to the styryl group. In the case of LUMO, the electron densities are mainly localized in the BODIPY core, which indicates a charge transfer transition from styryl to BODIPY moieties. On complexation with Hg^{2+}, electron densities for HOMO are located mainly on the dimethylamino arm and the BODIPY core with less electron density at dipicolylamine arm. The redistribution of electron density on binding to Hg^{+2} indicates a disfavored ICT process, which also supports our observation for the experimental UV-Vis spectra.

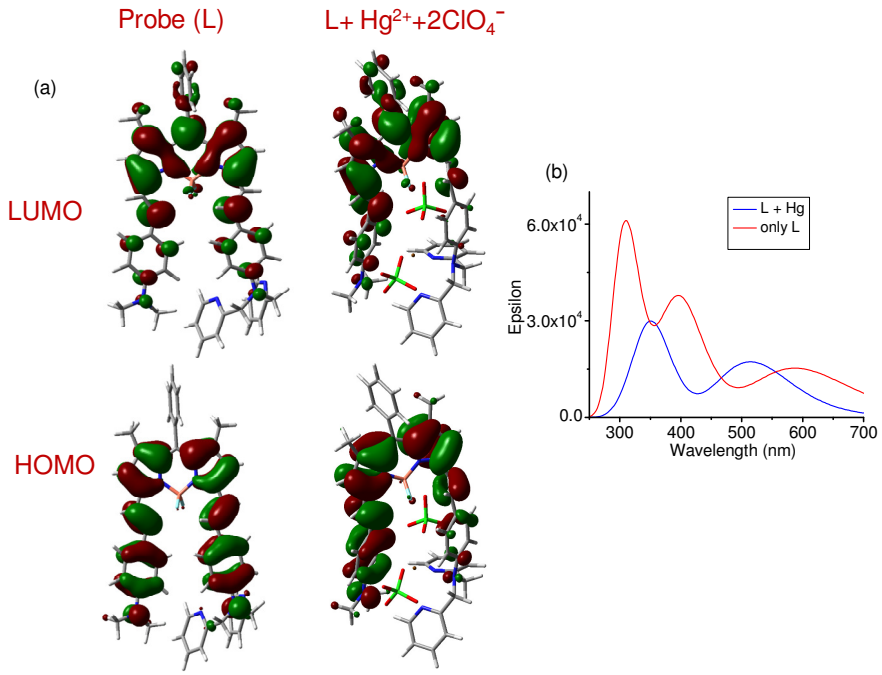

Figure 5.6. (a) M06-2X calculated HOMO, LUMO of probe (**L**) and [**L**+Hg^{2+}+$2ClO_4^-$] and (b) UV-Vis spectra.

The first excited states of **L** (oscillator strength, f= 0.3756) and the complex, [**L**+Hg^{2+}+$2ClO_4^-$] (oscillator strength, f = 0.4245) are characterized as the HOMO–LUMO one-electron excited states. The theoretical vertical excitation wavelengths for the reagent **L** and the complex, [**L**+Hg^{2+}+$2ClO_4^-$] in the gas phase are at 588 and 514 nm, respectively

(Figure 5.6b). The calculated blue shift in the UV-Vis spectra also corroborates well with experimental UV-Vis spectra discussed previously.

5.3.3. Cellular imaging Study

For evaluating the feasibility of using the reagent **L** as an imaging agent for mapping the cellular uptake of Hg^{2+}, cytotoxicity of **L** toward human colon cancer cells (Hct116 cells) was examined by MTT assay methodology. Experimental results revealed that 85% of cells survived even in presence of 50 μM of reagent (Figure 5.7), which confirmed the insignificant toxicity of the reagent towards these live cells used for study and thus, the complex was ideally suited for use as an imaging reagent. For mapping the cellular uptake of Hg^{2+} ion in live colon cancer cells (Hct116 cells), live cells were incubated with the reagent **L** (2 μM) for 30 min and then were thoroughly washed with PBS buffer for removing any surface adhered reagent. Then it was incubated with 20 μM of Hg^{2+} for 10 min and images were recorded using scanning confocal laser microscope (SCLM). The DIC and SCLM image of same lateral area of live cells with reagent obtained using 621nm laser illuminations. These images in combination with overlay image revealed emission arose from cells where the reagents were located. It also confirmed that the reagent was cell membrane permeable and was specifically localized in cytoplasm. On incubation with Hg^{2+} the emission intensity from the cell are found to be enhanced (Figure 5.7). Nonetheless this contrast of confocal images indicates efficient cellular uptake of reagent and allows us to test the imaging of Hg^{2+} in cellular environment.

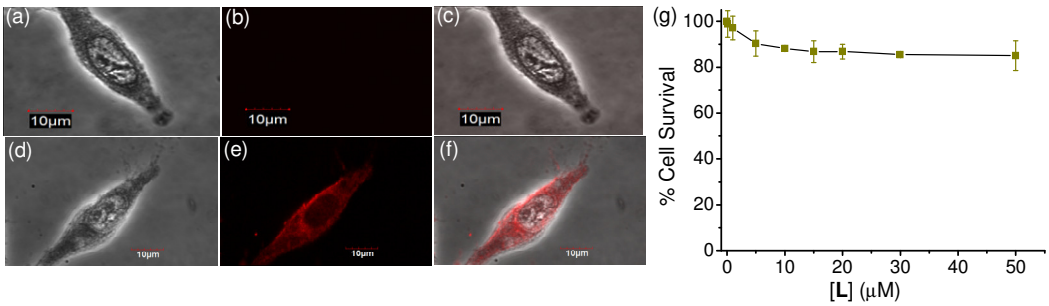

Figure 5.7: Cellular uptake of **L** (2 μM) by live Hct116 cells in the absence of (a–c) and in presence of 20 μM of Hg^{2+} (d–f). (a,d) bright field (b,e) dark field, and (c,f) overlay images of the same lateral area. SLCM fluorescence images were collected using the same emission filter (BP 621–647 nm). Scale bar in the images is 10 μm. (g) MTT assay of probe **L**.

Image of cell in presence of Hg^{2+} indicates intensity from the cell is not uniform and it may be due non-uniform localization of the reagent in particular organelle of the cells. As discussed earlier it is well known that mercury causes severe toxicity in mitochondria.[17-18] This prompted us to explore the colocalisation study with commercial available Mito tracker Green FM, a mitochondria specific dye for examining the extent of localization of the reagent **L** and thus, formation of the complex **L**. Hg^{2+} in mitochondrial region of the cells. The overlay images of probe (in absence and presence of Hg^{2+}) and Mitotracker Green showed well merged emission and intensity profile in the linear region of interest was synchronous. Moreover, co-localization was also quantified by Pearson's correlation factor which was found to be 0.92. This confirmed that the reagent was localized in mitochondria of Hct116 cells and could detect localization of Hg^{2+} in that region. NIR probe for detection of mitochondrial mercury is scarce in contemporary literature.[19]

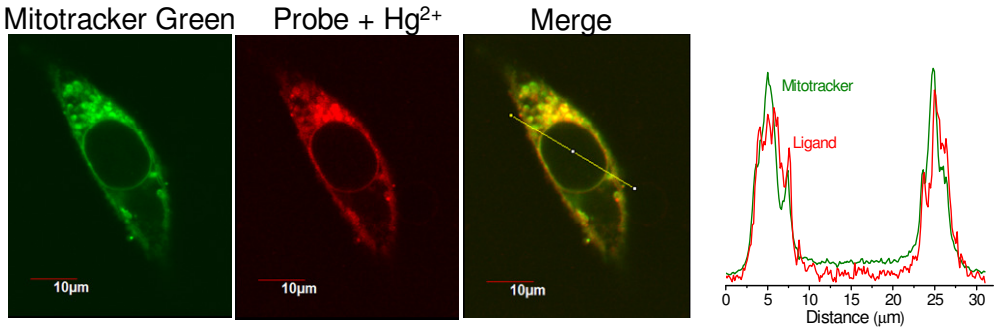

Figure 5.8. Colocalization experiment with Hct116 cells stained with (a) Mitotracker green. (b) 2 µM of probe + 20 µM of Hg^{2+} (c) Merged image of green and red channel (d) Intensity profile of region of interest across the cell.

5.4. Conclusion

In summary, an ICT based NIR probe for switch on detection Of Hg^{2+} ion in aqueous medium was synthesised. The reagent was found to highly selective towards Hg^{2+} ion with low detection limit. On interaction with Hg^{2+}, ICT band of the molecule is disturbed and a new blue shifted band observed in Uv-Vis spectra. From DFT studies the structure of the stable complex [**L**+Hg^{2+}+2ClO_4^-] was found which was also confirmed by Mass spectroscopy. Further theoretical absorption spectra also shows blue shift on complex formation as found in experimental studies. At last probe was found to less toxic and cell permeable, and also shows emission enhancement in presence of Hg^{2+} in live cells. Further co-localization studies indicate that probe specifically locates at mitochondria of the cell and can be used to detect mitochondrial Hg^{2+} ion.

5.5. References

1. (a) Shotyk, W.; Weiss, D.; Appleby, P. G.; Cheburkin, A. K.; Frei, R.; Gloor, M.; Kramers, J. D.; Reese, S.; Vanderknaap, W. O. *Science,* **1998**, *281*, 1635. (b) Que, E. L.; Domaille, D. W.; Chang, C. J. *Chem. Rev.,* **2008**, *108*, 1517. (c) Colombo, M. J.; Ha, J.; Reinfelder, J. R.; Barkay, T.; Yee, N. *Chemical Geology*, **2014**, *363*, 334.

2. (a) Mutter, J.; Naumann, J.; Sadaghiani, C.; Schneider R.; Wallach, H. *Neuroendocrin. Lett.,* **2004**, *25*, 331. (b) Stefansson, E. S.; Heyes, A.; Rowe, C. L. *Environ. Sci. Technol.,* **2014**, *48*, 1957−1963. (c) Clarkson, T. W.; Magos, L.; Myers, G. J. N. *Engl. J. Med.,* **2003**, *349*, 1731.

3. *Mercury Update: Impact of Fish Advisories*. EPA Fact Sheet EPA-823-F-01-011; EPA, Office of Water: Washington, DC, **2001**.

4. (a) Silva, M. J. da; Paim, A. P. S.; Pimentel, M. F.; Cervera, M. L.; Guardia, M. de la. *Anal. Chim. Acta,* **2010**, *667*, 43. (b) Kunkel, R.; Manahan, S. E. *Anal. Chem.,* **1973**, *45*, 1465.

5. Bings, N. H.; Bogaerts, A.; Broekaert, J. A. C. *Anal. Chem.,* **2006**, *78*, 3917.

6. Chai, X.; Chang, X.; Hu, Z.; He, Q.; Tu, Z.; Li, Z. *Talanta,* **2010**, *82*, 1791.

7. (a) Prodi, L.; Bolletta, F.; Montalti, M.; Zaccheroni, N. *Coord. Chem. Rev.,* **2000**, *205*, 59. (b) Valeur, B.; Leray, I. *Coord. Chem. Rev.,* **2000**, *205*, 3.

8. (a) Domaille, D. W.; Que, E. L.; Chang, C. J. *Nat. Chem. Biol.,* **2008**, *4*,168. (b) Carter, K. P.; Young, A. M.; Palmer, A. E. *Chem. Rev.,* **2014**, *114*, 8, 4564.

9. (a) Quang, D. T.; Kim; J. S. *Chem. Rev.,* **2010**, *110*, 6280. (b) Mahato, P.; Saha, S.; Das, P.; Agarwalla, H.; Das, A. *RSC Adv.,* **2014**, *4*, 36140. (c) Srivastava, P.; Razi, S, S.; Ali, R.; Gupta, R. C.; Yadav, S. S.; Narayan, G.; Misra, A. *Anal. Chem*., **2014**, *86*, 8693. (d) Reddy, U. G.; Ramu, V.; Roy, S.; Taye, N.; Chattopadhyay, S.; Das, A. *Chem. Commun*., **2014**, *50*, 14421. (e) Lee, M. H.; Lee, S. W. Kim,; S. H.; Kang, C.; Kim, J. S. *Org. Lett.,* **2009**, *11*, 10, 2101. (f) Nolan, E. M.; Lippard, S. J. *J. Am. Chem. Soc.,* **2007**, *129*, 5910. (g) Ding, J.; Li, H.; Wang, C.; Yang, J.; Xie, Y.; Peng, Q.; Li, Q.; Li, Z. *ACS Appl. Mater. Interfaces,* **2015**, *7*, 11369. (h) Saha, S.; Mahato, P.; Reddy, U. G.; Suresh, E.; Chakrabarty, A.; Baidya, M.; Ghosh, S. K.; Das, A. *Inorg. Chem*. **2012**, *51*, 336.

10. (a) Chiang, C. K.; Huang, C. C.; Liu, C. W.; Chang, H. T. *Anal. Chem.,* **2008**, *80*, 3716. (b) Ren, X.; Xu, Q.-H. *Langmuir,* **2009**, *25*, 29.

11. (a) Lee, J.-S.; Han, M. S.; Mirkin, C. A. *Angew. Chem., Int. Ed.,* **2007**, *46*, 4093. (b) Chen, L.; Li, J.; Chen, L. *ACS Appl. Mater. Interfaces*, **2014**, *6*, 18, 15897.

12. (a) Guo, Z. Q.; Park, S.; Yoon, J.; Shin, I. *Chem. Soc. Rev.,* **2014**, *43*, 16. (b) Frangioni, J. V. *Curr. Opin. Chem. Biol.*, **2003**, *7*, 626.

13. (a) Yuan, L.; Lin, W.; Zheng, K.; He, L.; Huang, W. *Chem. Soc. Rev.,* **2013**, *42*, 622. (b) Kiyose, K.; Kojima, H.; Nagano, T. *Chem.–Asian J.,* **2008**, *3*, 506.

14. (a) Appelqvist, H.; Waster, P.; Kagedal, K.; Ollinger, K. *J. Mol. Cell Biol.,* **2013**, *5*, 214. (b) Luzio, J. P.; Pryor, P. R.; Bright, N. A.; *Nat. Rev. Mol. Cell Biol.,* **2007**, *8*, 622.

15. (a) McBride, H. M.; Neuspiel, M.; Wasiak, *Curr. Biol.,* **2006**, *16*, R551. (b) Glancy, B.; Balaban, R. S. *Biochemistry,* **2012**, *51*, 2959.

16. (a) Santos, A. C.; Uyemura, S. A.; Santos, N. A. G.; Mingatto, F. E.; Curti, C. *Mol. Cell. Biochem.,* **1997**; *177*, 53. (b) Weinberg, J. M.; Harding, P. G.; Humes, H. D. *J. Biol. Chem.* **1982**; *257*, 60.

17. Königsberg, M.; Edith, N.; Díazguerrero, L.; Bucio, L.; Concepción, M.; Ruiz, G. *J. Appl. Toxicol.,* **2001**, *21*, 323.

18. (a) Belyaeva, E. A.; Dymkowska, D.; Wieckowski, M. R.; Wojtczak, L. *Toxicology and Applied Pharmacology*, **2008**, *231*, 1, 34. (b) Belyaeva, E. A.; Sokolova, T. V.; Emelyanova, L. V.; Zakharova, I. O. *The Scientific World Journal,* **2012**, Article ID 136063.

19. (a) Chen, J.; Liu, W.; Zhou, B.; Niu, G.; Zhang, H.; Wu, J.; Wang, Y.; Ju, W.; Wang, P. *J. Org. Chem.,* **2013**, *78*, 6121. (b) Taki, M.; Akaoka, K.; yoshi, S.; Yamamoto, Y. *Inorg. Chem.,* **2012**, *51*, 13075.

20. Shiraishi, Y.; Sumiya, S.; Kohono, Y.; Hirai, T. *J. Org. Chem*. **2008**, *74*, 8571.

21. (a) Zhao, Y.; Truhlar, D. G. *Acc. Chem. Res.,* **2008**, *41*, 157. (b) Zhao, Y.; Truhlar, D. G. *J. Chem. Theory Comput.,* **2008**, *4*, 1849. (c) Hohenstein, E. G.; Chill, S. T.; Sherrill, C. D. *J. Chem. Theory Comput.,* **2008**, *4*, 1996.

22. Francl, M. M. *J. Chem. Phys.,* **1982**, *77*, 3654.

23. (a) Dunning Jr., T. H.; Hay, P. J. In *Modern Theoretical Chemistry*; Plenum, New York, **1977**; Vol. 3, pp. 1–28. (b) Hay, P. J.; Wadt, W. R. *J. Chem. Phys.,* **1985**, *82*, 299. (c) Wadt, W. R.; Hay, P. J. *J. Chem. Phys.,* **1985**, *82*, 284. (d) Hay, P. J.; Wadt, W. R. *J. Chem. Phys.,* **1985**, *82*, 270.

24. Zhao, Y.; Truhlar, D. *Theor. Chem. Accounts: Theory, Comput. Model.,* **2008**, *120*, 215.

25. (a) Casida, M. E.; Jamorski, C.; Casida, K. C.; Salahub, D. R. *J. Chem. Phys.,* **1998**, *108*, 4439. (b) Bauernschmitt, R.; Ahlrichs, R. *Chem. Phys. Lett.,* **1996**, *256*, 454. (c) Caillie, C. V.; Amos, R. D. *Chem. Phys. Lett.,* **2000**, *317*, 159. (d) Caillie, C. V.; Amos, R. D. *Chem. Phys. Lett.* **1999**, *308*, 249. (e) Furche, F.; Ahlrichs, R. *J. Chem. Phys.,* **2002**, *117*, 7433. (f) Scalmani, G.; Frisch, M. J.; Mennucci, B.; Tomasi, J.; Cammi, R.; Barone, V. *J. Chem. Phys.,* **2006**, *124*, 094107.

26. Frisch, M. J.; Trucks, G. W.; Schlegel, H. B.; Scuseria, G. E.; Robb, M. A.; Cheeseman, J. R.; Scalmani, G.; et al. *Gaussian 09, Revis. B01, Gaussian, Inc., Wallingford, CT,* **2010**.

27. (a) Saha, S.; Agarwalla, H.; Gupta, H.; Baidya, M.; Suresh, E.; Ghosh, S. K.; Das, A. *Dalton Trans.*, **2013**, **42**, 15097. (b) Choi, H.; Lee, J. H.; Jung, J. H. *Analyst,* **2014**, *139*, 3866. (c) Wang, Z.; Xie, Y.; Xu, K.; Zhao, J.; Glusac, K. D. *J. Phys. Chem., A,* **2015**, *119*, 6791.

28. Smith, D. W. *J. Chem. Edu.,* **1977**, *54*, 9, 540.

CHAPTER 6

A TURN-ON FLUORESCENT PROBE FOR DETECTION OF BIO-THIOLS WITH LARGE STOKES SHIFT IN AQUEOUS MEDIUM

Publication:
To Be Communicated

6.1. Introduction

Cysteine (Cys), Homocysteine (Hcy), and Glutathione (GSH) are the most important biological thiols, as they play essential roles for regulating the redox balance of various biological processes.[1] The intracellular pool of Cys is relatively much smaller than the metabolically active pool of GSH in cells.[2] It has been argued that Cys is generally the limiting amino acid for GSH synthesis in humans.[2c] Abnormal level of biothiols associated to various dysfunctions and diseases. Deficiency of Cys induces various diseases such as, slow growth, hair depigmentation, liver damage, skin lesions, hematopoiesis decrease, leukocyte loss, psoriasis, etc.[3] On other hand Hcy is linked to different clinical conditions including Alzheimer's disease, schizophrenia, renal disease, cardiovascular disease, and diabetes.[4] Increase in the supply of Cys or its precursors (e.g., cystine and N-acetylcysteine) via oral or intravenous intervention improves GSH synthesis and prevents GSH deficiency in humans under various nutritional and pathological conditions, such as protein malnutrition, adult respiratory distress syndrome, HIV, and AIDS.[5] Thus, effective quantification of biothiols in biological medium is expected to assist in early diagnosis of such crucial diseases. Accordingly, considerable efforts have been made for developing efficient reagent and appropriate methodology for quantitative detection of biothiols in physiological condition and in biofluids. Numerous analytical methods have been employed for detection of biothiols which include high-performance liquid chromatography (HPLC),[6] electrochemical assay,[7] capillary electrophoresis,[8] mass spectrometry.[9] Most of these methods involve tiresome sample preparation and not suitable for mapping distribution of either of these biothiols in live cells or tissues. Considering such limitations, reagents that allow fluorescence on response either on binding or reaction with these biothiols have significance for developing efficient methodology that are relevant for clinical diagnosis, cell biology and assessing analytical samples. Fluorescence based methodology also provides high sensitivity and reliability. Importantly, non-invasive methodology is ideally suited for use as an imaging reagent as well as for in-vitro studies.[10] In recent past, significant efforts have been made for developing efficient fluorescence-based reagents for recognition and quantitative estimation in bio-fluids for diagnostic application as well as for mapping its distribution in live cells.[11] A majority of these relies on certain reaction of biothiols, such as cyclization with aldehyde,[12] cleavage reactions by thiols,[13] metal displacement,[14] and Michael addition.[15] However, examples of reagents which could detect/ estimate any one of these free biothiols as well as thiols in a protein residue are important as this would provide better idea of thiol pool in biological system,

and are rare in the contemporary literature. Larger Stokes shift, high emission quantum yield and emission at longer wavelength are the desired criteria for using a reagent for imaging application. Benzoxazine dyes are important class of dyes as they show very high stokes shift in comparison to the parent coumarins owing to their large dipole moment in excited state.[16] Large stokes shift minimizes self-absorption and background noise due to auto-fluorescence while using the reagent for in-vitro or in-vivo imaging applications.[17]

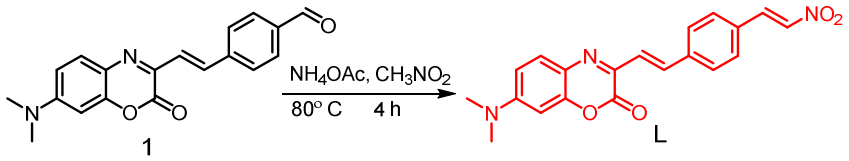

Scheme 6.1: Methodology adopted for synthesis of the reagent **L.**

6.2. Experimental section

6.2.1. Materials

Terephthaladehyde and ammonium acetate were purchased from Sigma Aldrich. Acetic anhydride, Acetonitrile (DMSO, HPLC grade), nitro methane and different amino acids were of reagent grade (S. D. Fine Chemical, India) and used as received without any further purification.

6.2.2. Analytical Methods

^{1}H and ^{13}C NMR spectra were recorded on a Bruker 200/500 MHz FT NMR (Model: Avance-DPX 200/400/500) using trimethylsilane (TMS) as an internal standard. FTIR spectra were recorded as KBr pellets in a cell fitted with a KBr window, using a Perkin-Elmer Spectra GX 2000 spectrometer. ESI-Ms measurements were carried out on a Waters QTof-Micro instrument. Solution pH was evaluated using Mettler Toledo FEP20 pH meter. Absorption spectra were recorded using a Perkin Elmer Lambda 950 UV-Vis spectrophotometer equipped with cell holder having path length of 1cm. Fluorescence spectra were recorded on PTI QuantaMaster 400 spectrophotometer.

6.2.3. Generalised methodology for spectroscopic studies

1.0 mM stock solution of in probe **L** acetonitrile was prepared and used for further studies after appropriate dilution using 10 mM HEPES buffer achieving the effective concentration of 1.0×10^{-5} M in 10 mM aq. HEPES buffer-CH_3CN (7:3, v/v; pH 7.2). Stock solutions of

100 mM of different amino acids were prepared in a 10 mM aq. HEPES buffer-CH_3CN (7:3, v/v; pH 7.2) medium. Stock solutions were further diluted with buffer solution as per requirement for a specific experiment.

The relative fluorescence quantum yields (Φ_f) were estimated using equation 1 by using the integrated emission intensity of Coumarine-343 in ethanol (Φ = 0.63 at RT) as a reference.

$$\Phi_f = \Phi_f'(I_{sample}/I_{std})(A_{std}/A_{sample})(\eta^2_{sample}/\eta^2_{std}) \quad \text{Equation 1}$$

where, Φ_f' is the absolute quantum yield for the Coumarine-343, used as standard; I_{sample} and I_{std} are the integrated emission intensities; A_{sample} and A_{std} are the absorbance at the excitation wavelength, and η_{sample} and η_{std} are the respective refractive indices of sample and standard.

The lowest detection limit was calculated by following 3σ/k method; where σ is the standard deviation of blank measurement, k is the slope of intensity *vs.* $[Hg^{+2}]$ plot.

6.2.4. Cell Culture and Confocal study

HeLa cells were incubated in DMEM supplemented with 10% (v/v) fetal bovine serum (FBS) and 1% (w/v) penicillin-streptomycin (PS) at 37 °C in a humidified atmosphere of 5% of CO_2 in the air. Cells were passaged when they reached approximately 80% confluence. Cells were seeded onto a cell culture dish at a density of 1.0×10^5 cells, which was incubated at 37 °C overnight under 5% CO_2 in the air. For the negative control experiment, the cells were pre-incubated in NEM (1 mM) for 30 min, washed with PBS (phosphate buffered saline) buffer for three times, and then incubated with the probe (10 μM) for 30 min. For the positive control experiment, the cells were incubated in N-acetyl Cystiene(NAC, 0.7 mM) for 15 min, washed with PBS buffer solution for three times, and then incubated with the probe (10 μM) for 30 min. Finally incubated cells, with probe were washed with PBS buffer three times and then fixed with 4% formaldehyde solution for the microscopic imaging.

6.2.5. Synthesis of Probe L

The preparation of intermediate **1** was described in Chapter 4. To prepare probe **L**, 160 mg (0.5 mmol) of **1** was dissolved in 10 ml of nitromethane. To it 385 mg (5 mmol) of

ammonium acetate was added to it and heated at 80 °C for 4 h. On cooling to room temperature precipitate appeared, which was washed with water and then with 10 ml of diethyl ether. Residue was further extracted from DCM/water and the DCM layer was dried for isolating the desired pure product as brown solid. Yield; 130 mg (71%),^{1}H NMR (400 MHz, $CDCl_3$) δ:8.27 (d, *J* = 13.2Hz, 1H), 8.14 (d, *J* = 13.6Hz, 1H), 7.88 (m, 2H), 7.81 (m, 2H), 7.56 (d, *J*=9.2Hz, 1H), 7.50 (d, *J*=16Hz, 1H), 6.83 (dd, *J*=2.4, 8.8 Hz, 1H), 6.61 (d, *J*=2.4, 1H), 3.08 (s, 3H). ^{13}C NMR (300 MHz, CPMAS, 8 kHz) δ:153.1, 151.2, 147.9, 140.5, 136.4, 130.1, 127.3, 124.1, 109.6, 94.5, 39.53. IR ν_{max}/cm^{-1}: 2914, 1728, 1616, 1467. HRMS (*m*/*z*): Calculated $[C_{20}H_{17}N_3O_4+H]^+$364.1292 and found 364.1285.

6.3. Results and Discussions

Probe **L** was readily synthesized from a condensation reaction of **1** with nitromethane as shown in scheme 6.1. Probe and intermediates were characterized by standard spectroscopic techniques and found to be of desired purity. Designed probe **L** contains a nitroolefin group in conjugation with benzooxazine group which acts as Michael acceptor and provides a reaction site for biothiols. Being in conjugation, $–NO_2$ and $–N(CH_3)_2$ functionalities favored a strong push-pull effect and this accounted for a relatively narrower HOMO-LUMO energy gap. This is expected to be directly linked to the effective deactivation of the excited state through a non-radiative pathway and attributed to a poor emission quantum yield. This push-pull effect is effectively interrupted due to the 1,4-addition reaction of biothiols with this reagent and this is expected to enhance the gap for the HOMO-LUMO energy levels and cause a hypsochromic shift in the electronic spectra.

6.3.1. Spectroscopic studies

Considering the possible applications in real sample and biology, all the experiments were carried out in aq. HEPES buffer:CH_3CN medium (7:3, v/v; pH 7.2). The absorption spectrum of **L** (10 μM) in an aq. HEPES buffer:CH_3CN medium (7:3, v/v; pH 7.2) shows a strong band at 505 nm (ε = 24100 $M^{-1}cm^{-1}$) and a weak band at 360 nm (8200 $M^{-1}cm^{-1}$) (Figure 6.1). Being the part of the extended conjugation, $-NO_2$ and $–N(CH_3)_2$ functionalities favored a strong push pull effect as well as a facile ICT process. This account for the ICT band at 505 nm of **L**. Charge transfer nature of this band was also ensured by the observed shift of the band maxima to longer wavelength with increase in solvent polarity (Figure 6.1). The absorption spectrum of **L** was recorded in absence and presence of 100 mole equivalent of different common anions (X: $F^–$,$Cl^–$, $Br^–$, $H_2PO_2^–$, $OAc^–$, $HSO_4^–$, $CN^–$),

cations (Na^+, Ca^{2+}, Mg^{2+},Fe^{2+}, Fe^{3+}, Cu^{2+}, Cr^{3+}, Ni^{2+}, Zn^{2+}) and natural amino acids(AAs: histidine (His), leucine (Leu), methionine (Met), isoleucine(Ile), phenylalanine (Phe), tryptophon (Trp), tyrosine (Tyr), valine (Val), serine (Ser), alanine (Ala), arginine (Arg), glycine (Gly), glutamine (Gln), proline (Pro), aspartic acid (Asp), glutamic acid (Glu), threonine (Thr), lysine (Lys), methionine (Met)), and biothiols like glutathione (GSH), Homocysteine (Hcy) and Cysteine (Cys) (Figure 6.1b). A hypsochromic shift of ~25nm was observed for the 505 nm band only when spectra were recorded in presence of Cys and Hcy and this attributed to a visually detectable change in solution colour from red to orange. Other analytes failed to induce any detectable change in absorption spectra. Observed hypsochromic shift in absorption spectra supports the formation of Michael adducts with Cys and Hcy which interrupted the extended conjugation as well as disfavor the push-pull effect and the ICT process. Electronic spectra for the probe molecule **L** (10 μM) were recorded for increasing concentration of Cys or Hcy (0.0 – 1.0 mM), which showed appearance of two new bands at 480 nm and 315 nm with concomitant decrease in band intensities at 505 nm and 360 nm (Figure 6.1c,d). Titration profile also revealed three isosbestic points at 285 nm, 330 nm, 400 nm which reflects reaction is proceeding without forming an intermediate.

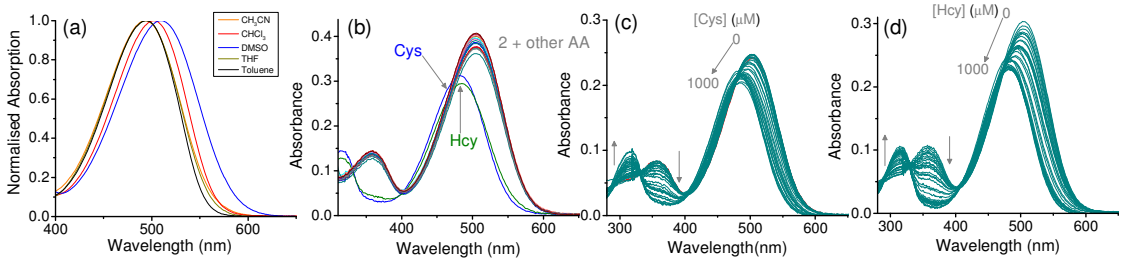

Figure 6.1. Absorption spectra of probe **L** (10 μM) (a) in solvent of different polarity, (b) in absence and presence of different amino acids, anions and cations, (c) in varying amount of Cys (0-1 mM) (d) in varying amount of Hcy (0-1 mM) in aq. HEPES buffer:CH_3CN medium (7:3, v/v; pH 7.2).

Emission spectra for **L** revealed a weak emission in aq. HEPES buffer:CH_3CN medium (7:3, v/v; pH 7.2) when excited at 480 nm. This weak emission could be attributed to a narrow HOMO-LUMO energy gap owing to the facile ICT process that is discussed earlier (*vide supra*). Emission spectra for **L** were recorded in absence and presence of 100 mole equivalents of different anions, cations and natural amino acids following excitation at 480 nm. Apparently a switch ON emission response with λ_{max} of 585 nm was observed for **L** only in presence of Cys, and Hcy (Figure 6.2). Other analytes including GSH did not show

any detectable change in the emission spectra. Probe **L** shows a large stokes shift of ~105 nm, which was highly desirable as it would help in reduction of the self-absorption and background noise for improved fluorescence responses. Quantum yield for **L** ($\Phi_{\mathbf{L}}$ = 0.01; $\Phi_{\text{Coumarin 343}}$ = 0.63 in ethanol is used for evaluating the relative Φ values) was found to increase on reaction with either Cys ($\Phi_{\mathbf{L}\text{-Cys}}$ = 0.23) or Hcy ($\Phi_{\mathbf{L}\text{-Hcy}}$ = 0.22). This significant increase in fluorescence enhancement in presence of Cys and Hcy is attributed to the 1,4-addition that leads to the formation of **L**-Cys/Hcy adduct. Lack of extended conjugation in these adducts has contributed in achieving the enhanced HOMO-LUMO energy gap and this favors the radiative deactivation of the CT-based excited state, which results in the appreciable increase in emission quantum yield.

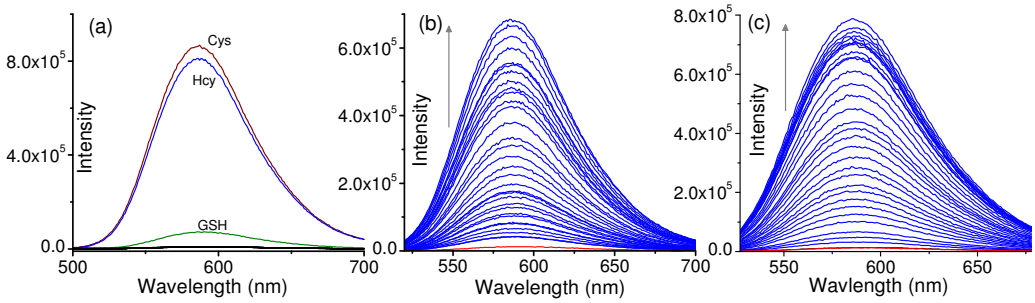

Figure 6.2. Emission spectra of probe **L** (10 μM) (a) in absence and presence of different amino acids, anions and cations, (b) in varying amount of Cys (0-1 mM) (c) in varying amount of Hcy (0-1 mM) in aq. HEPES buffer:CH_3CN medium (7:3, v/v; pH 7.2) with λ_{exc}= 480 nm.

Systematic changes in the emission spectra were recorded in HEPES buffer:CH_3CN medium (7:3, v/v; pH 7.2) with increasing [Cys] or [Hcy] (0 to 100 mole equivalent) and these spectra are shown in Figures 6.2b and 6.2c, respectively. A linear relationship of emission intensity (after a delay time of 5 and 20 min after mixing **L** with Cys or Hcy, respectively) in the concentration range of 0-25 μM of Cys/Hcy was also observed and this enabled us to evaluate the lowest detection limit of 2.05×10^{-8} M for Cys and 0.93×10^{-8} M for Hcy.

To validate the selectivity of **L** for any practical application, interference studies were performed. Emission responses were recorded for **L** (10 μM) after incubating with 100 mole equivalent of Cys (recorded after 5 min) or Hcy (recorded after 20 min in presence of excess (200 equivalent) of other amino acids. Even after one hr incubation of these resultant solutions, no further change in emission intensities was observed. This clearly

nullified any interference other competing amino acids, including potential interfering agent GSH (Figure 6.3). These results indicate that probe **L** can be used as a turn-on probe for selective detection of Cys/Hcy selectively even in presence other common interfering agents.

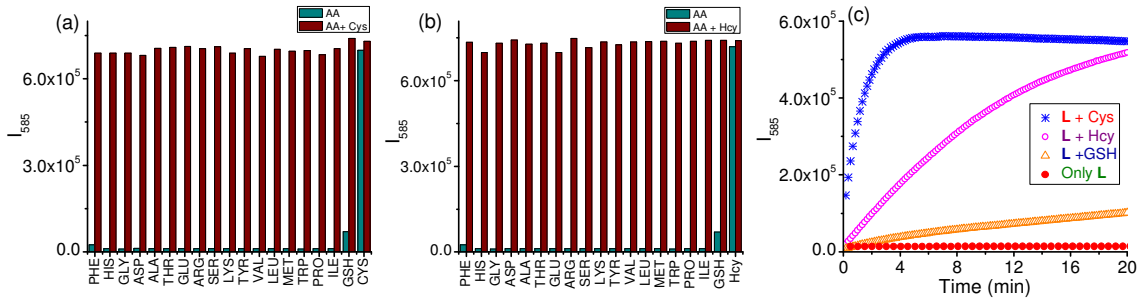

Figure 6.3. Interference study of **L** (10 μM) in presence of (a) 100 mole equivalent of Cys (b) 100 mole equivalent of Hcy, and in absence and presence of 200 mole equivalent of other aminoacids (c) Time dependent spectra in presence of Cys, Hcy and GSH; in 10 mM HEPES aq. Buffer: acetonitrile (7:3, v/v) pH 7.2 using $\lambda_{Ext}/\lambda_{Em}$: 480/585nm.

6.3.2. Time dependent studies

Short response time was also a very important criterion for developing an analytical reagent for quantitative and estimation of a biomarkers for any possible practical application, especially for chemodosimetric probes. To examine the time response of probe **L**, emission was monitored at 585 nm as a function of time in absence and presence of Cys/Hcy. Probe **L** did not show any detectable change in emission intensity with time (Figure 6.3c). However, in presence of Cys and Hcy emission increase with time, for Cys it takes only ~4 min to reach plateau whereas for Hcy it takes 15 min. As anticipated, GSH shows a very weak emission response with time even after 20 min (Figure 6.3c).

Kinetics for the reactions between **L** and Cys and Hcy were studied in details. Relative changes in emission intensities as a function of time for a definite concentration of **L** and Cys or Hcy (used in excess for ensuring the pseudo first order rate constant) in aq. HEPES buffer:CH_3CN medium (7:3, v/v; pH 7.2 using λ_{Ext} of 480 nm at 25°C) helped us in evaluating the pseudo first order rate constant (k_{obs}) for particular analytes (Cys or Hcy). A plot of k_{obs} as a function of [Cys] or [Hcy] was found to be linear and followed the equation $k_{obs} = k_c[\text{Analyte}] + C$ (Analyte is Cys or Hcy), where k_c is the intrinsic rate constant. k_c evaluated for reaction with Cys and Hcy are $32.2 \pm 1.7\ s^{-1}$ and $11.1 \pm 1.1\ s^{-1}$, respectively (Figure 6.4).

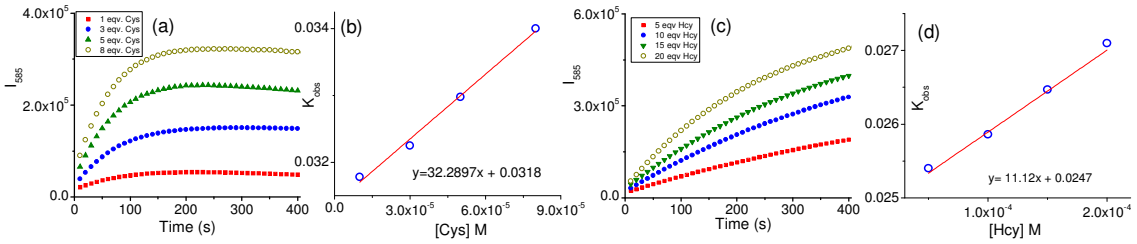

Figure 6.4. Time dependent spectra of **L** (10 μM) in presence of different concentration of (a) Cys (c) Hcy; and K_{obs} vs Concentration plot of (b) Cys and (d) Hcy, in aq. HEPES buffer:CH_3CN medium (7:3, v/v; pH 7.2), λ_{exc}/ λ_{mon} =480/585 nm.

6.3.3. Effect of pH

pH of the medium is also a determining factor for nucleophilic reaction for sulfahydryl group on Michael acceptor. To examine the effect of pH on response of probe **L**, emission response was recorded at different pH medium (Figure 6.5). It shows that emission of probe **L** was not influence by wide range of pH, however in presence of Cys/Hcy it shows maximum intensity at pH ≥ 7. pK_a of Cys, Hcy and GSH is 8.30, 8.87 and 9.2 respectively.[15b] Fast response with Cys at pH 7.2 can be explained by the fact that at this pH thiolate/thiol ratio will be higher for Cys. Hcy shows slower reaction than Cys and insignificant interaction of GSH may attribute to high pK_a value and also steric factor. At lower pH relatively little fluorescence enhancement were observed due to formation less nucleophilic thiol form, whereas at higher pH Cys/Hcy shows similar response. The reactivity order of Cys>Hcy>GSH can be rationalized by pK_a value and steric factor of thiols on Michael addition reaction.

6.3.4. Sensing mechanism

For establishing the sensing mechanism i.e.; Michael addition, we recorded ^{1}H NMR spectra of probe **L** in presence of 100 equivalents of Cys and Hcy in DMSO-d_6. Probe **L** shows peaks at 8.14 and 8.27 ppm due to nitroolefin peaks (H_a, H_b). On addition of Cys this peaks disappeared and a new set of peak appeared at 4.79 and 5.19 ppm. Similarly, for Hcy new set of peaks appears at 4.64 and 5.18 ppm (Figure 6.5). This definitely proves that 1,4 addition reaction of thiolate occurs at nitroolefin centre. Other aromatic protons show an upfield shift which can be attributed to the decrease in intramolecular charge transfer. The adduct formation was further corroborated by high resolution mass spectroscopy, peak corresponding to Cys adduct was found at *m/z*= 485.1483 [**L**+ Cys + H]$^+$ and for Hcy adduct at 499.1645 [**L**+ Hcy+ H]$^+$ which further confirms the 1,4 addition

reaction. Thus our probe can detect Cys/Hcy specifically and in aqueous medium with a large stokes shift and low detection limit.

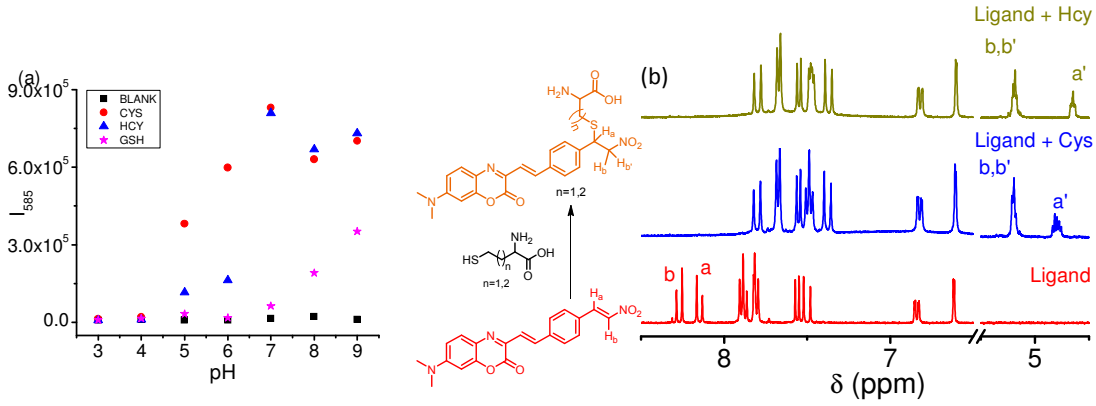

Figure 6.5. (a) pH dependent spectra of L in absence and presence of 100 mole equivalent of Cys, Hcy and GSH; in in aq. HEPESbuffer:CH_3CN medium (7:3, v/v; pH 7.2), λ_{exc}/ λ_{mon} =480/585 nm (b) Partial ^{1}H NMR spectra of probe **L** in absence and presence of 100 mole equivalents of Cys and Hcy. Mechanism of reaction of Cys/Hcy with probe **L**.

6.3.5. Detection of HSA

Considering these favorable properties, probe **L** was further utilized for detection of free Cys residue in proteins. We have employed Human Serum Albumin (HSA) as template protein because it is a major component of blood plasma [18] and also as it contains only one free Cys residue (Cys 34).[19] First, sensing of HSA was tested by addition of different concentration of protein with probe **L**. As shown in figure 5, with increasing concentration of HSA from (0.5 μM to 20 μM), fluorescence intensity at 585 nm increase, with naked eye colour change from red to orange. This indicates that probe **L** reacts with the free Cys 34 residue of the protein. Next, we checked the time course of the reaction, and found it takes ~10 min to complete the reaction which is greater than the time taken for Cys. The pK_a value of Cys residue of HSA is 5.0 which is quiet low than the Cys/Hcy, so it is expected to react better than them.[20] However, the slow reactivity of HSA can be attributed to the microenvironment of the protein residue which makes it difficult to undergo substitution reaction.

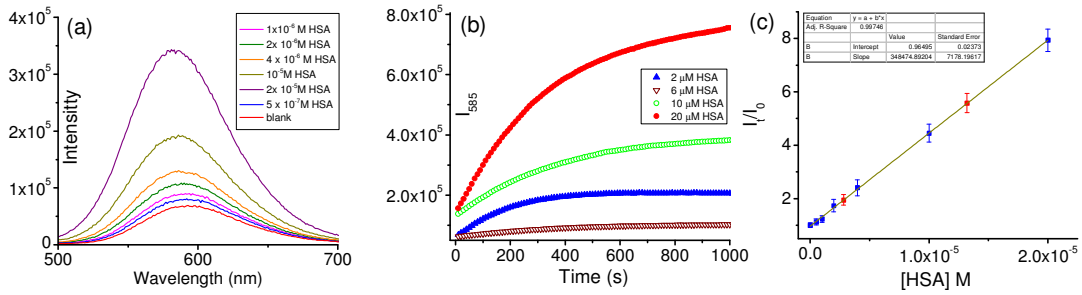

Figure 6.6. (a) Fluorescence spectra of probe **L** (5 μM) in presence of different concentration of HSA (0-20 μM). (b) Change in emission intensity in presence of different concentration of HSA. (c) Calibration plot and quantification of HSA in human urine.

Considering above results we now wished to establish its efficacy of detection of HSA in biological system. Healthy human urine contains less than 30 mg L^{-1} of HSA, but in kidney disease, HSA concentration in urine increases which cause proteinurea.[21] So HSA detection in urine can be useful in early detection of kidney disease and cardiovascular disease. Fresh urine sample from healthy donor was collected and diluted 10 times before use. Different concentration of HSA (0.5-20 μM) in HEPES buffer was prepared and then incubated with probe **L** (5 μM). Emission intensity at 585 nm shows a good linear relationship with HSA concentration and used as standard curve. Two known concentration of HSA (3 and 14 μM) were spiked with urine sample and then incubated with probe **L**. Results from the calibration curve, seems to be in good agreement with high recovery rate using this method (Table 6.1). Thus, this provides a very simple method for detection of HSA in human urine.

Table 6.1. Determination of HSA in healthy human urine.

Sample no	HSA added (μM)	HSA found (μM)	Recovery (%)
1	3.0	2.81 ± 0.2	93.6
2	14.0	13.2 ± 0.3	94.2

6.3.6. Cellular imaging Study

As we know cells contain high level of thiols, and they also play important roles in cancer cells. Since biothiols in cancer cells are responsible for signal transduction, tumor invasion and metastasis, cancer cell proliferation and tumor growth,[22] it is of great significance to

detect and monitor cellular biothiols. Our probe shows highly sensitive turn-on fluorescence for biothiols in aqueous medium with low detection limit. Moreover, a large stokes shift and emission in red region of the spectrum bestow probe **L**, as a promising probe for imaging studies. To use this probe as cellular imaging of biothiols, HeLa cells were incubated with 10 μM of probe for 30 min and then washed with PBS buffer. Confocal images with probe **L** shows bright fluorescence from cells due to reaction of biothiols with probe within the cells (Figure 6.7a). To ascertain that emission originates due to presence of biothiols a control experiment were carried out in presence of N-ethylmaleimide (NEM) a thiol blocking agent. Cells pre-incubated with NEM (1 mM) shows week fluorescence compared to the only probes (Figure 6.7b) which proves that emission in the cells were due to presence of biothiols. Further, experiment were also carried out in presence of N-acetyl cysteine (NAC) which reacts with probe, emission enhancement can be seen in Figure 6.7c , which is in line with solution study (Figure 6.7d). Thus these results revealed that probe **L** is cell permeable and can react with bithiols within cells which proves its efficacy as reagent for monitoring cellular thiols.

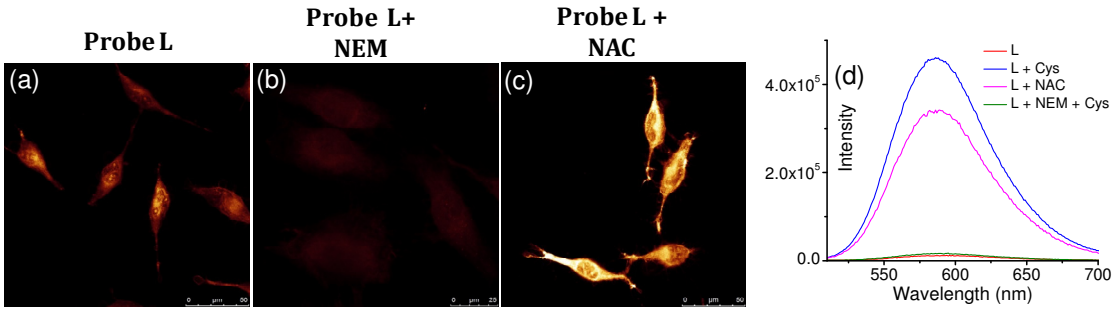

Figure 6.7. Confocal microscope images of HeLa cells with (a) only probe **L**(10 μM) (b) probe **L**(10 μM) with NEM (1 mM) (c) probe **L** (10 μM) with NAC (0.7 mM) and (d) Emission spectra of probe **L** (10 μM) in presence of Cys (50 equivalent), Cys (50 equivalent) and pre-incubated with NEM (50 equivalent) and NAC (50 equivalent).

6.4. Conclusion

In a nutshell we are able to design a fluorescent turn-on probe for specific detection of biothiol in aqueous medium. Probe displays an emission enhancement on reaction with thiols, which break the conjugation between nitroolefin and benzooxazine group. Interruption of Conjugation leads to alteration in the ICT character as well as blocked the PET process which results in high quantum yield. Moreover, our probe can bind with free SH group of HSA with increase in emission. This has been used to detect HSA in human

urine. Further probe can also be used to detect and monitor cellular thiols by using confocal microscope.

6.5. References

1. (a) Wood, Z. A.; Schröder, E.; Harris, J. R.; Poole, L. B. *Trends Biochem. Sci.,* **2003**, *28*, 32. (b) Mathews, C. K.; Holde, van K. E.; Ahern, K. G. *Biochemistry, Addison-Wesley,* San Francisco, **2000**.

2. (a) Stipanuk, M. H. *Annu. Rev. Nutr.,* **2004**, *24*, 539. (b) Wu, G.; Fang, Y.-Z.; Yang, S.; Lupton, J. R.; Turner, N. D. *J. Nutr.,* **2004**, *134*, 489. (c) Lyons, J.; Rauh-Pfeiffer, A.; Yu, Y. M.; Lu, X. M.; Zurakowski, D.; Tompkins, R. G.; Ajami, A. M.; Young, V. R.; Castillo, L. *Proc. Natl. Acad. Sci. USA,* **2000**, *97*, 5071.

3. (a) Shahrokhian, S. *Anal. Chem.,* **2001**, 73, 5972. (b) Borowich, K. K.; Swiader, M.; Kamiński, R.; Kuźńiar, H.; Kleinrok, Z.; Czuczwar, S. J. *Pol. J. Pharmacol.,* **2000**, *52*, 345.

4. (a) Mills, J. L.; McPartlin, J. M.; Kirke, P. N.; Lee, Y. J.; Conley, M. R.; Weir, D. G.; Scott, J. M. *Lancet,* **1995,** *345*, 149. (b) Guldener, C.; Stehouwer, C. D. *Clin. Chem. Lab. Med.*, **2003**, *41*, 1412. (c) Luis, De D. A.; Fernandez, N.; Arranz, M. L.; Aller, R.; Izaola, O.; Romero, E. J. *J. Diabetes Complicat.,* **2005**, *19*, 42. (d) Seshadri, S.; Beiser, A.; Selhub, J.; Jacques, P. F.; Rosenberg, I. H.; D'Agostino, R. B.; Wilson, P. W. F. *New Engl. J. Med.,* **2002**, *346*, 476.

5. (a) Townsend, D. M.; Tew, K. D.; Tapiero, H. *Biomed. Pharmacother.,* **2003**, *57*, 145. (b) Lu, S. C. *Curr. Top. Cell Regul.,* **2000**, *36*, 95. (c) Griffith, O. W. *Free Radic. Biol. Med.*, **1999**, *27*, 922.

6. (a) Chwatko, G.; Bald, E. *Talanta,* **2000**, *52*, 509. (b) Tcherkas, Y. V.; Denisenko, A. D. *J. Chromatogr. A*, **2001**, *913*, 309. (c) Nolin, T. D.; McMenamin, M. E.; Himmelfarb, J. *J. Chromatogr. B,* **2007**, *852*, 554.

7. (a) Inoue, T.; Kirchhoff, J. R. *Anal. Chem.,* **2000**, *72*, 5755. (b) Potesil, D.; Petrlova, J.; Adam, V.; Vacek, J.; Klejdus, B.; Zehnalek, J.; Trnkova, L.; Havel, L.; Kizek, R. *J. Chromatogr. A*, **2005**, *1084*, 134.

8. Inoue,T.; Kirchhoff, J. R. *Anal. Chem*. **2002**, *74*, 1349.

9. Rafii, M.; Elango, R.; Courtney- Martin, G.; House, J. D.; Fisher, L.; Pencharz, P. B. *Anal. Biochem.,* **2007**, *371*, 71.

10. (a) Shao, J.; Guo, H.; Ji, S.; Zhao, J. *Biosens. Bioelectron.*, **2011**, *26*, 3012. (b) Zhang, M.; Yu, M.; Li, F.; Zhu, M.; Li, M.; Gao, Y.; Li, L.; Liu, Z.; Zhang, J.; Zhang, D.; Yi, T.; Haung, C. *J. Am. Chem. Soc.,* **2007**, *129*, 10322.(a) Chen, X.; Zhou, Y.; Peng, X.; Yoon, *J. Chem. Soc. Rev.,* **2010**, *39*, 2120. (b) Niu, L. Y.; Chen, Y. Z.; Zheng, H. R.; Wu, L. Z.; Tung, C. H.; Yang, Q. Z. *Chem. Soc. Rev.*, **2015**, *44*, 6143.

11. (a) Lin, L.; Long, L.; Yuan, Z; .Cao, B. C.; Tan, W. *Org. Lett.,* **2008**, *10*, 5577. (b) Hu, J.; Fan, H.; Li, K.; Song, S.; Wang, G. C.; Peng, X. *Org. Biomol. Chem.*, **2011**, *9*, 980. (c) Rusin, O.; Luce, N. N. St.; Agbaria, R. A.; Escobedo, J. O.; Jiang, S.; Warner, I. M.; Dawan, F. B.; Lian, K.; Strongin, R. M. *J. Am. Chem. Soc.,* **2004**, *126*, 438. (d) Das, P.; Mandal, A. K.; Chandar, N. B.; Baidya, M.; Bhatt, H. B.; Ganguly, B.; Ghosh, S. K.; Das, A. *Chem. Eur. J.,* **2012**, *18*, 15382.

12. (a) Lee, J. H.; Lim, C. S.; Tian, Y. S.; Han, J. H.; Cho, B. R. *J. Am. Chem. Soc.,* **2010**, *132*, 1216. (b) Yang, Y. L.; Zhang, F. M.; Wang, Y. W.; Zhang, B. X.; Fang, R.; Fang, J. G.; Peng, Y. *Chem. Asian J.,* **2015**, *10*, 422. (c) Yin, J.; Kwon, Y.; Kim, D.; Lee, D.; Kim, G.; Hu, Y.; Ryu, J. H.; Yoon, J. *J. Am. Chem. Soc.,* **2014**, *136*, 5351. (d) Liu, X. D.; Sun, R.; Ge, J. F.; Xu, Y. J.; Xu, Y.; Lu, J. M. *Org. Biomol. Chem.,* **2013**, *11*, 4258.

13. (a) Shao, N.; Jin, J. Y.; Cheung, S. M.; Yang, R. H.; Chan W. H.; Mo, T. *Angew. Chem., Int. Ed.*, **2006**, *45*, 4944. (b) Reddy, U. G.; Agarwalla, H.; Taye, N.; Ghorai, S.; Chattopadhyay, S.; Das, A. *Chem. Commun.,* **2014**, *50*, 9899. (c) Yang, X.-F.; Liu, P.; Wang, L.; Zhao, M. *J. Fluoresc.,* **2008**, *18*, 453–459.

14. (a) Sreejith, S.; Divya, K. P.; Ajayaghosh, A. *Angew. Chem., Int. Ed.*, **2008**, *47*, 7883. (b) Jung, H. S.; Ko, K. C.; Kim, G. H.; Lee, A. R.; Na, Y. C.; Kang, C.; Lee, J. Y.; Kim, J. S. *Org. Lett.,* **2011**, *13*, 6, 1498. (c) Kim, G. J.; Lee, K.; Kwon, H.; Kim, H. J. *Org. Lett.,* **2011**, *13*, 11, 2799. (d) Ali, F.; Anila H. A.; Taye, N.; Gonnade, R. G.; Chattopadhyay, S.; Das, A. *Chem. Commun.,* **2015**, *51*, 16932. (e) Liu, J.; Sun, Y. Q.; Huo, Y.; Zhang, H.; Wang, L.; Zhang,P.; Song, D.; Shi, Y.; Guo, W. *J. Am. Chem. Soc.,* **2014**, *136*, 574. (f) Liu, Y.; Yu, D.; Ding, S.; Xiao, Q.; Guo, J.; Feng, G. *ACS Appl. Mater. Interfaces,* **2014**, *6*, 17543.

15. (a) Bris, M.-T. L. *J. Heterocycl. Chem.*, **1985**, *22*, 1275. (b) Trebaul, C.; Roncali, J.; Garnier, F.; Guglielmetti, R. *Bull. Chem. Soc. Jpn.,* **1987**, *60*, 2657.

16. Lakowicz, J. R. *Principles of Fluorescence Microscopy*; Springer: New York, **2006**.

17. (a) Kumar, C. V.; Buranaprapuk, A.; Opiteck, G. J.; Moyer, M. B.; Jockusch, S.; Turro, N. J. *Proc. Natl. Acad. Sci. U. S. A.,***1998**, *95*, 10361. (b) Fan, J.; Sun, W.; Wang, Z.; Peng, X.; Li, Y.; Cao, J. *Chem. Commun.,* **2014**, *50*, 9573.

18. Sugio, S.; Kashima, A.; Mochizuki, S.; Noda, M.; Kobayashi, K. *Protein Eng.,* **1999**, *12*, 6, 439.

19. Narazaki, R.; Hamada, M.; Harada, K.; Otagiri, M. *Pharm. Res.,* **1996**, *13*, 1317.

20. (a) Hoogenberg, K.; Sluiter W. J.; Dullaart, R. P. *Acta Endocrinol.,* **1993**, *129*, 151. (b) Zeeuw, D.; Parving, H. H.; Henning, R. *J. Am. Soc. Nephrol.*, **2006**, *17*, 2100.

21. (a) Shi, H.; Zhang, C. J.; Chen, G. Y.; Yao, S. Q. *J. Am. Chem. Soc.*, **2012**, *134*, 3001. (b) Tozer, R. G.; Tai, P.; Falconer, W.; Ducruet, T.; Karabadjian, A.; Bounous, G.; Molson, J. H.; Droge, W. *Antioxid. Redox Signaling,* **2008**, *10*, 395. (c) Caglic, D.; Globisch, A.; Kindermann, M.; Lim, N. H.; Jeske, V.; Juretschke, H. P.; Bartnik, E.; Weithmann, K. U.; Nagase, H.; Turk, B.; Wendt, K. U. *Bioorg. Med. Chem.,* **2011**, *19*, 1055.

Conclusion of the Thesis

The thesis entitled "*Design and Synthesis of Molecular Probes For Detection of Biological and Environmental Significant Ions*" describes the design and synthesis of new molecules for specific detection of analytes along with their recognition studies which have implications in various biological processes and environmental monitoring. The thesis contains overall six chapters. The first chapter is the introductory chapter, which describes significance of important analytes in biology and environment and briefly discusses about existing literature report and scopes present in designing new receptor molecules for detection process. The Aim of this thesis is to design molecules which can efficiently detect important analytes.

Our earlier studies revealed that subtle difference in the relative special orientations could actually influence hydrogen bonding interaction of methylene hydrogen atoms and the fluoride ion. So in Chapter 2, we demonstrate that the presence of the positively charged phosphonium ion also contribute to the overall binding of F^- and OAc^- to the methylene functionality. To envisage the role of the acidity of the active methylene hydrogen atoms, while maintaining the identical relative spatial arrangement, a corresponding Ru(II)-bis terpyridyl complex was synthesized and used for hydrogen bonding interaction studies with different anionic analytes. Both the receptors show Hydrogen bonding interactions at lower concentrations and deprotonation equilibrium at higher concentration of F^- and OAc^-. This is evident from observed electronic spectral changes and from ^{1}H and ^{31}P NMR. Further DFT calculations substantiated the efficient hydrogen bonding interactions of F^- and OAc^- with receptor molecules and experimental results were rationalized based on the results of the detailed computational studies.

Cyanide is one of the most toxic anions, and in Chapter 3, we described a simple molecule as a chemodosimetric probe for specific recognition of cyanide species (CN^- and/or HCN) in an ensemble of all common anions, amino acids and GSH in an essentially aqueous buffer medium at physiological pH. The *switch on* luminescence response could be utilized for achieving a lower detection limit of 0.286 μM for cyanide ion and this value was much lower than the threshold cyanide ion concentration of 1.9 μM for safe drinking water set by WHO. Moreover, visually detectable change in solution luminescence at a [CN^-] of 1.9 μM offers the opportunity to use this reagent as an optical sensor for *in-field* application. Release of CN^- and/or HCN (at physiological pH) from amygdalin and mandelonitrile by

important enzymes like β-glucosidase and, Hydroxynitrile lyase, respectively, could also be probed by monitoring the luminescence enhancement and this helped us in developing an efficient and sensitive assay for two important enzymatic reactions. Spatially-resolved fluorescence spectroscopy measurements performed over a large number of microscopic domains (over several cells) reveal the overall shift in distribution of transition energies as well as integrated emission intensities. This demonstrates that a combination of both spectral shift and emission enhancement provides more conclusive evidence of cellular uptake of cyanide, and offers a way to probe changes in the sensory response due to variation in local environments within cells and that due to cyanide detection.

In Chapter 4, we discuss specific recognition of an important analyte bisulfite which is common in pharmaceuticals and food industry and also a environmental pollutant. Here we synthesised a benzooxazinone based molecule that can selectively detect bisulfite ion in an aqueous medium with turn-on type fluorescence response in the red region of the spectrum which is important as it minimizes the auto-fluorescence from intrinsic biomolecules. The probe responds to bisulfite very fast with no interference from common interfering agents such as biothiols and cyanide ion. This emission on response was further utilized as an imaging reagent for cellular uptake of bisulfite. Furthermore, as the probe molecule is two-photon excitable, it was able to observe endogenous bisulfite not only in cells but also in different organ tissues with high resolution images of distinct morphology. Finally, we explored a possibility of preparation of a proof of concept, low-cost electrochemical device for detecting bisulfite ion in an aqueous medium for in-field detection.

Among different metals ions, Mercury in its various forms is known to be the most potent neurotoxin for human physiology and other living organisms. In Chapter 5, we have designed BODIPY derivative appended with dipicolylamine moiety as an ICT based NIR probe for switch on detection Hg^{+2} ion in aqueous medium. The reagent was found to highly selective towards Hg^{+2} ion with low detection limit. On interaction with Hg^{+2}, ICT band of the molecule is disturbed and a new blue shifted band observed in Uv-Vis spectra. From DFT studies the structure of the stable complex [$L+Hg^{2+}+2ClO_4^-$] was found which is also confirmed by Mass spectroscopy. Further theoretical absorption spectra also shows blue shift on complex formation as found in experimental studies. At last probe was found to less toxic and cell permeable, and also shows emission enhancement in presence of

Hg^{+2} in live cells. Further, co-localization studies indicate that probe specifically locates at mitochondria of the cell and can be used to detect mitochondrial Hg^{+2} ion.

Among biological important analytes, Biothiols (Cys, Hcy and GSH) are the most important one plays crucial role in regulating redox balance in various biological processes. In Chapter 6, we attempt to prepare a molecular probe for specific detection of biothiols. A benzooxazine derivative conjugated with a nitroolefin group was synthesised and used for detection of thiols in aqueous medium. Probe displays an emission enhancement on reaction with thiols, which break the conjugation between nitroolefin and benzooxazine group. Interruption of Conjugation leads to alteration in the ICT character as well as blocked the PET process which results in high quantum yield. Moreover, the probe can bind with free Cys present in HSA and has been used to detect HSA in human urine, which could be used in diagnostics. Further, the probe can also be used to detect and monitor cellular thiols by using confocal microscope.

In a nut-shell attempt has been made to design and synthesis new molecules for specific and efficient detection of important anions like fluoride, Cyanide, Bisulfite, cations like mercury and neutral analytes like Cys/Hcy in aqueous medium. Changes in optical properties due to receptor analyte interaction were studied. Wherever possible, we tried to explore the application in different aspects like bioimaging of analytes in cells and tissues, enzymatic assay, diagnostics or infield detection. We hope that reagent and strategies discussed in this thesis will certainly be useful in designing better and efficient molecules for specific detection of analytes.

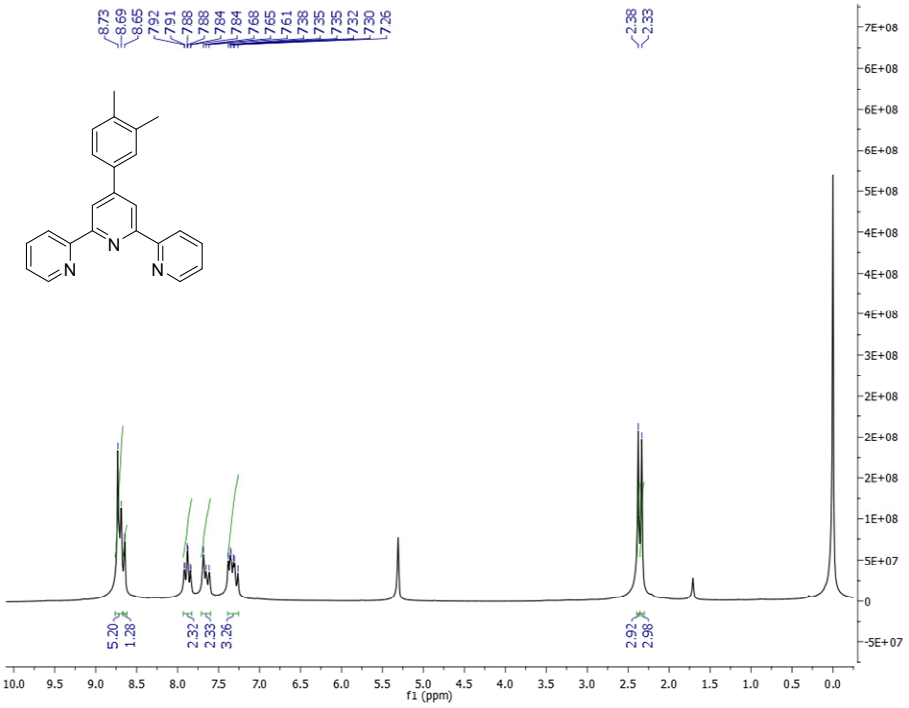

Figure 1. ^{1}H NMR spectra recorded in CD_2Cl_2.

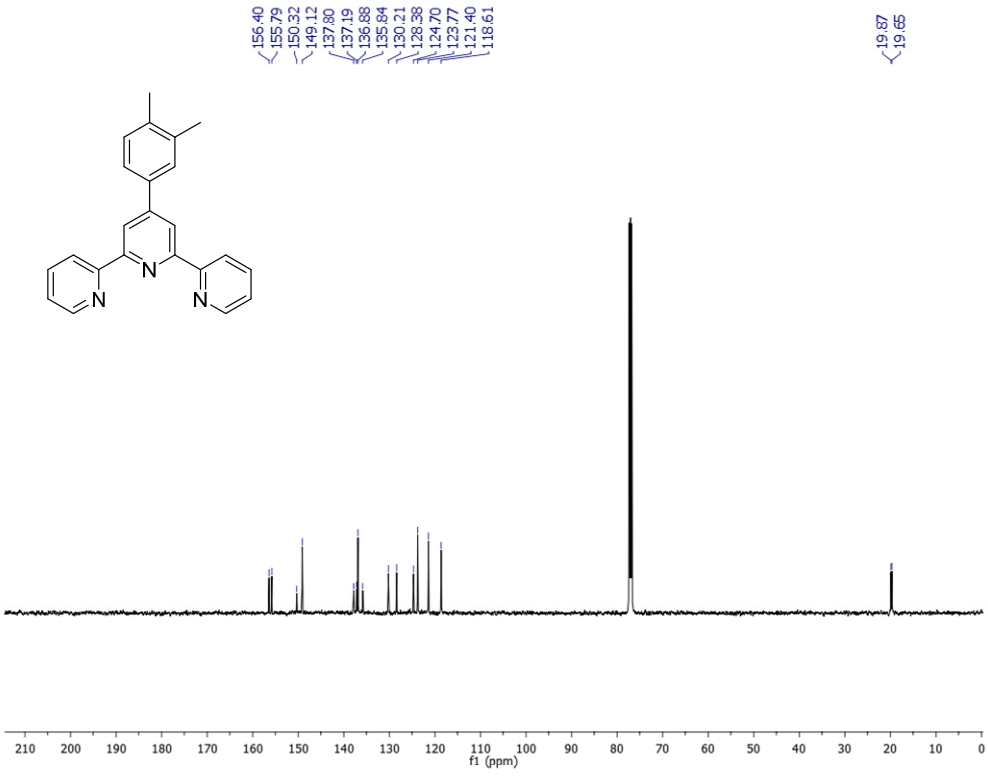

Figure 2. ^{13}C NMR spectra recorded in $CDCl_3$.

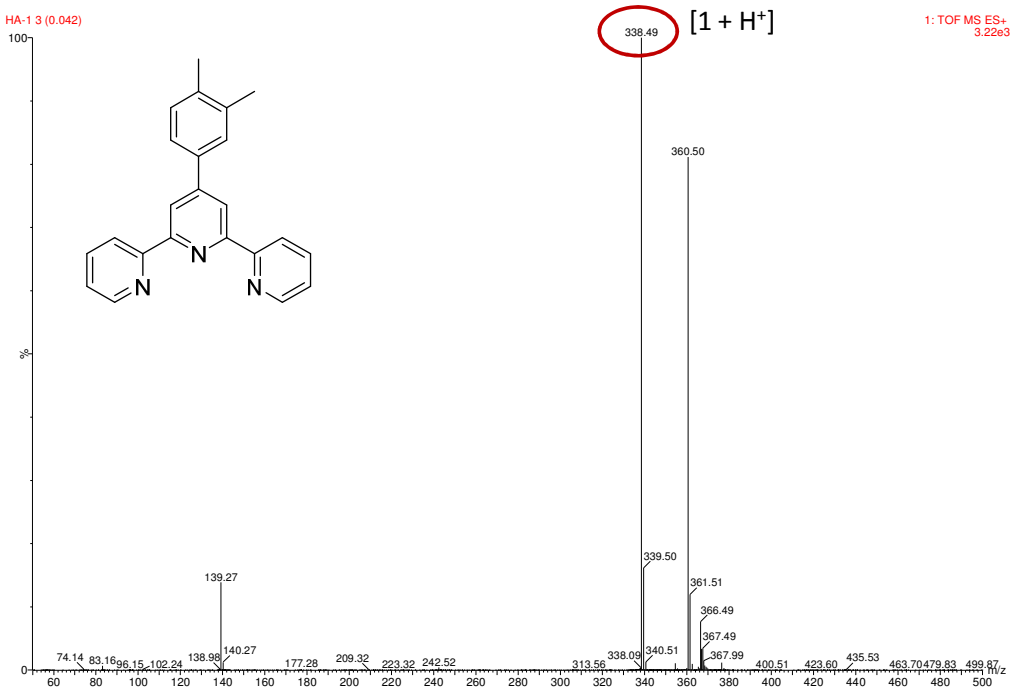

Figure 3. ESI-Ms spectra recorded in MeOH.

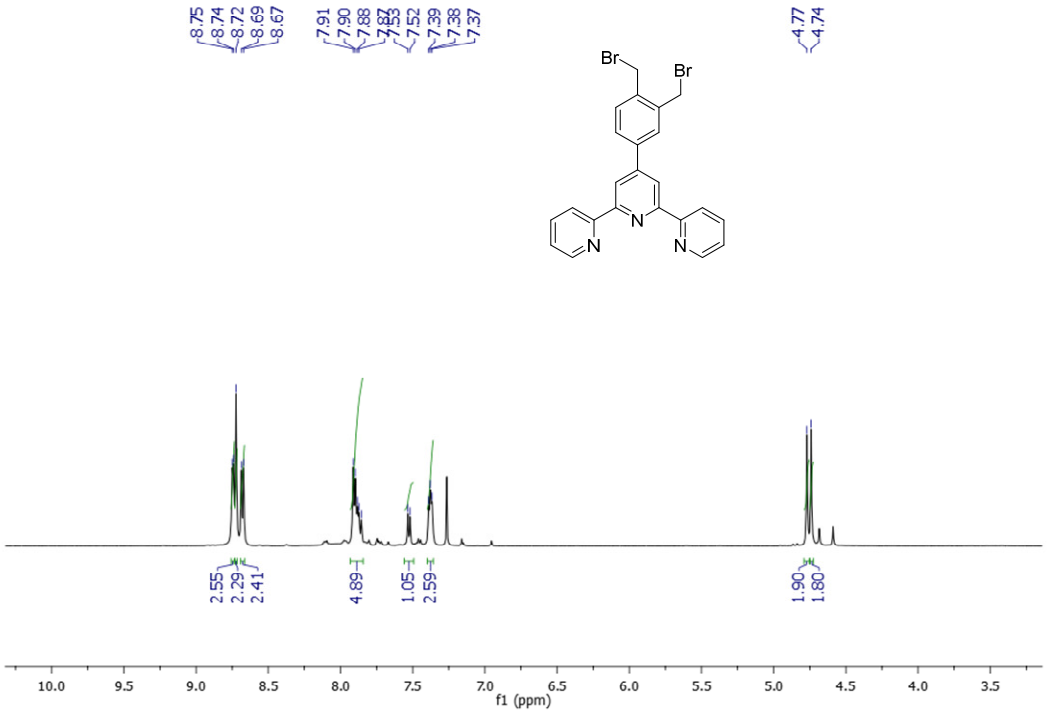

Figure 4. ^{1}H NMR spectra recorded in $CDCl_3$.

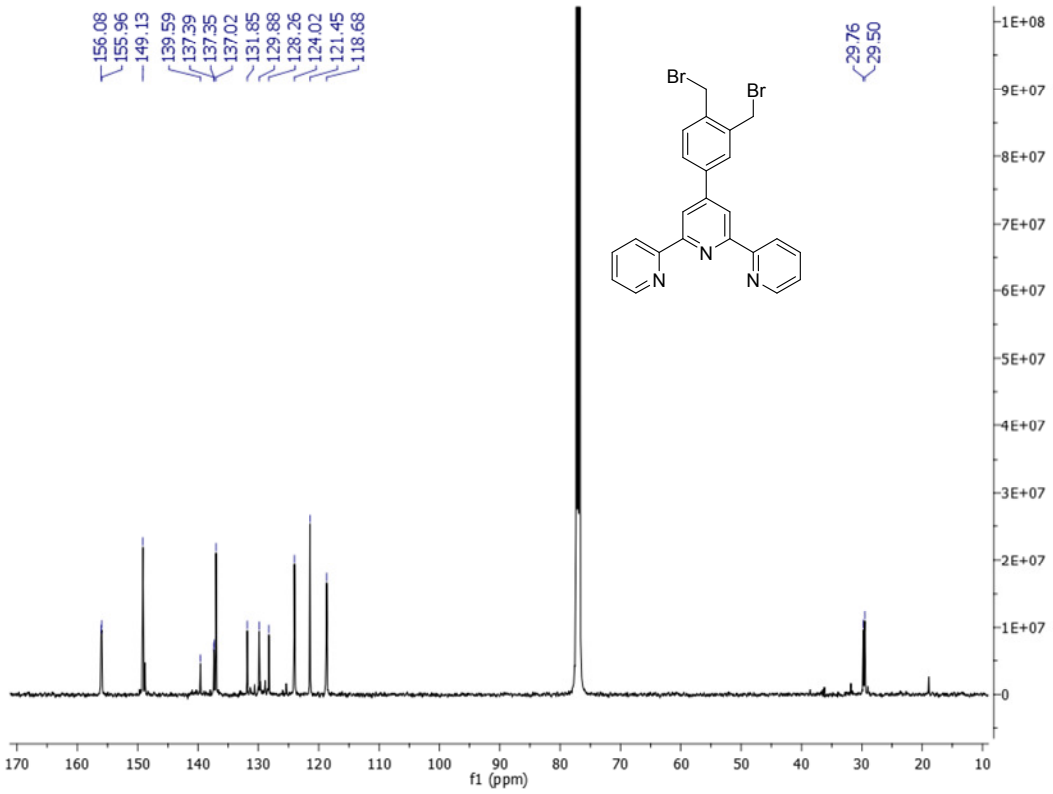

Figure 5. ^{13}C NMR spectra recorded in $CDCl_3$.

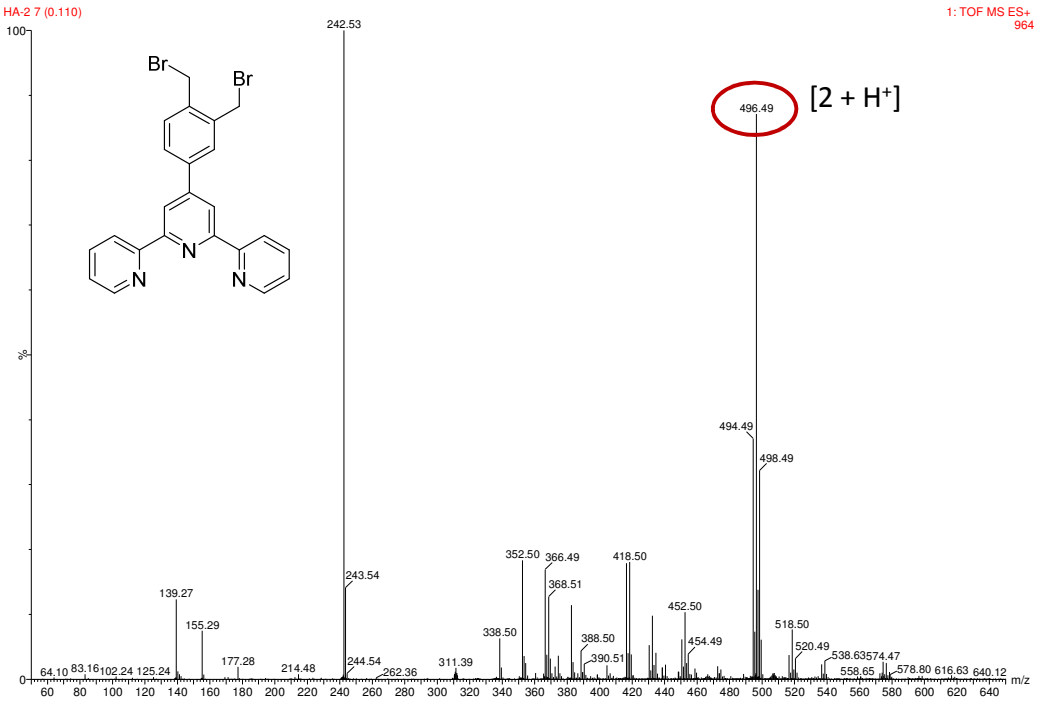

Figure 6. ESI-Ms spectra recorded in MeOH.

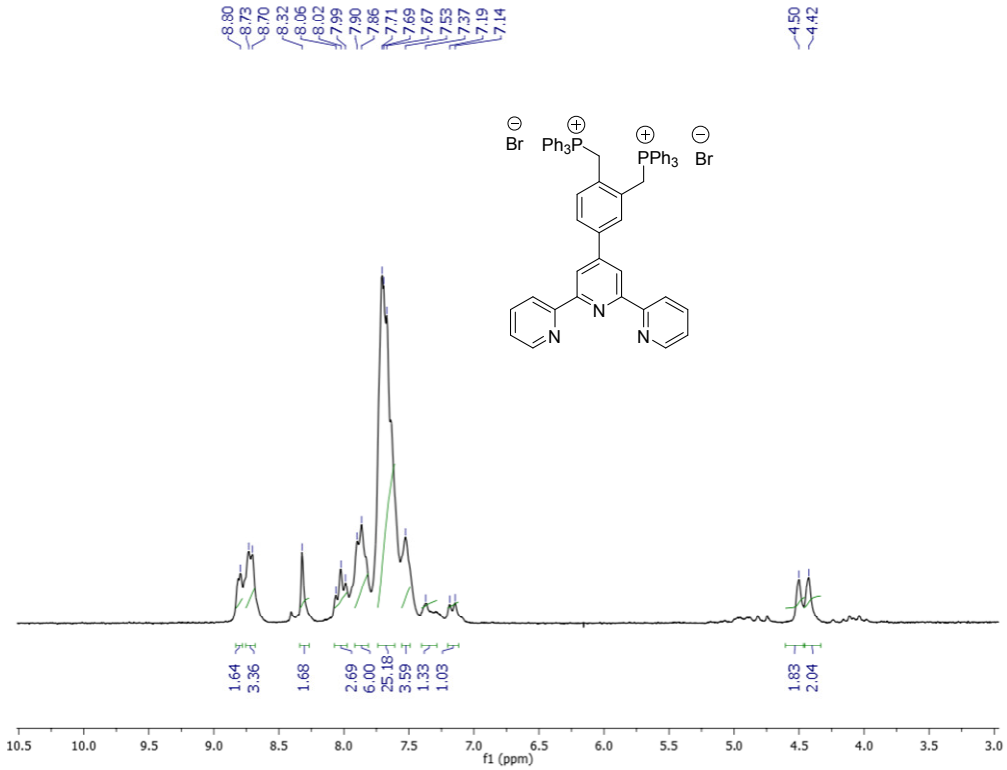

Figure 7. ^{1}H NMR spectra recorded in $CDCl_3$.

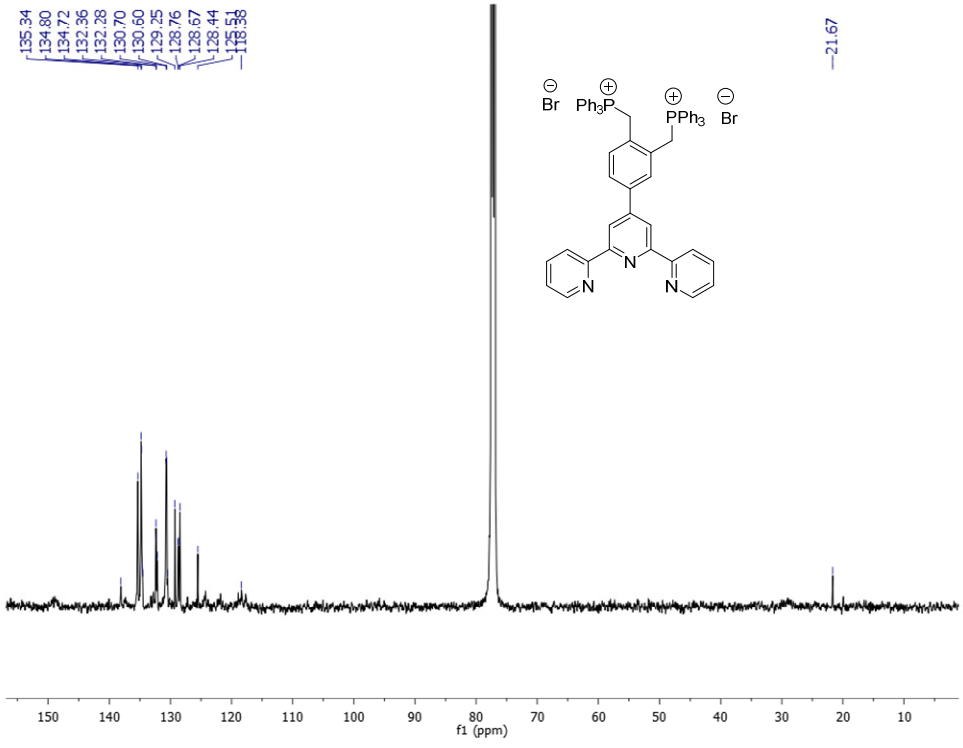

Figure 8. ^{13}C NMR spectra recorded in $CDCl_3$.

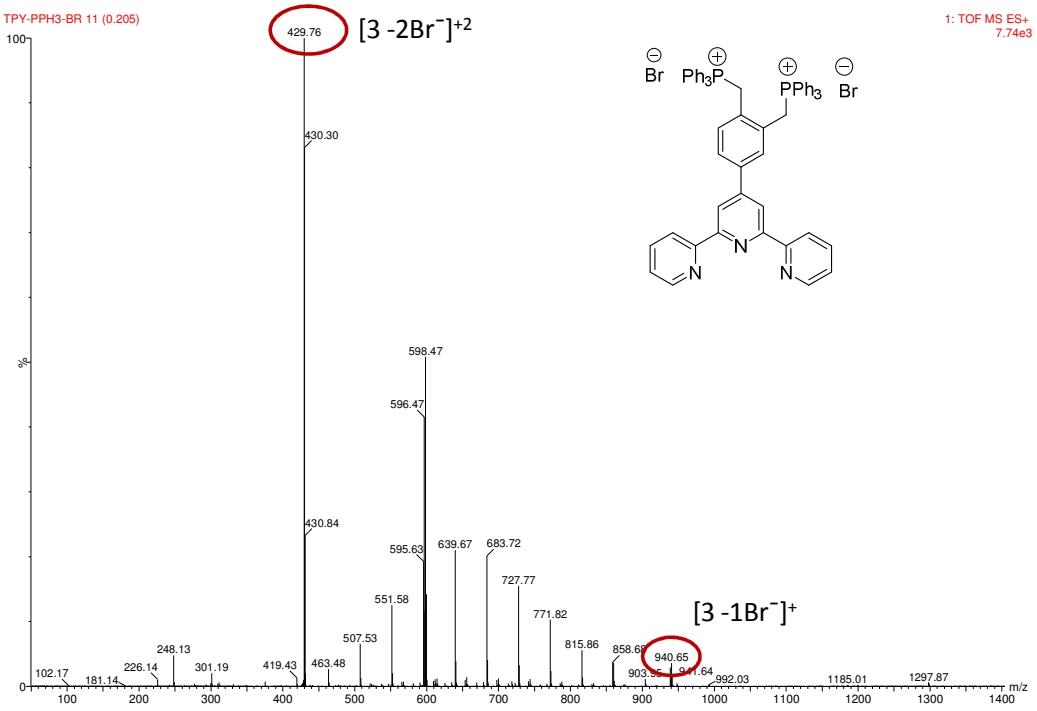

Figure 9. ESI-Ms spectra recorded in MeOH.

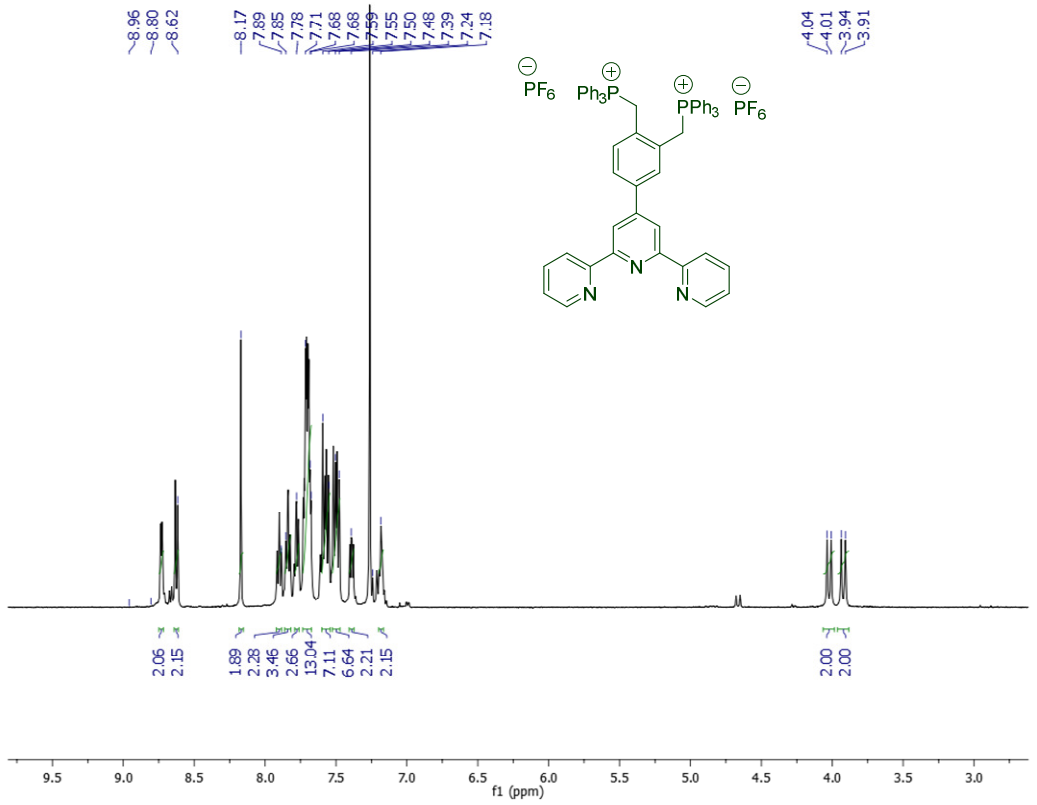

Figure 10. ^{1}H NMR spectra recorded in $CDCl_3$.

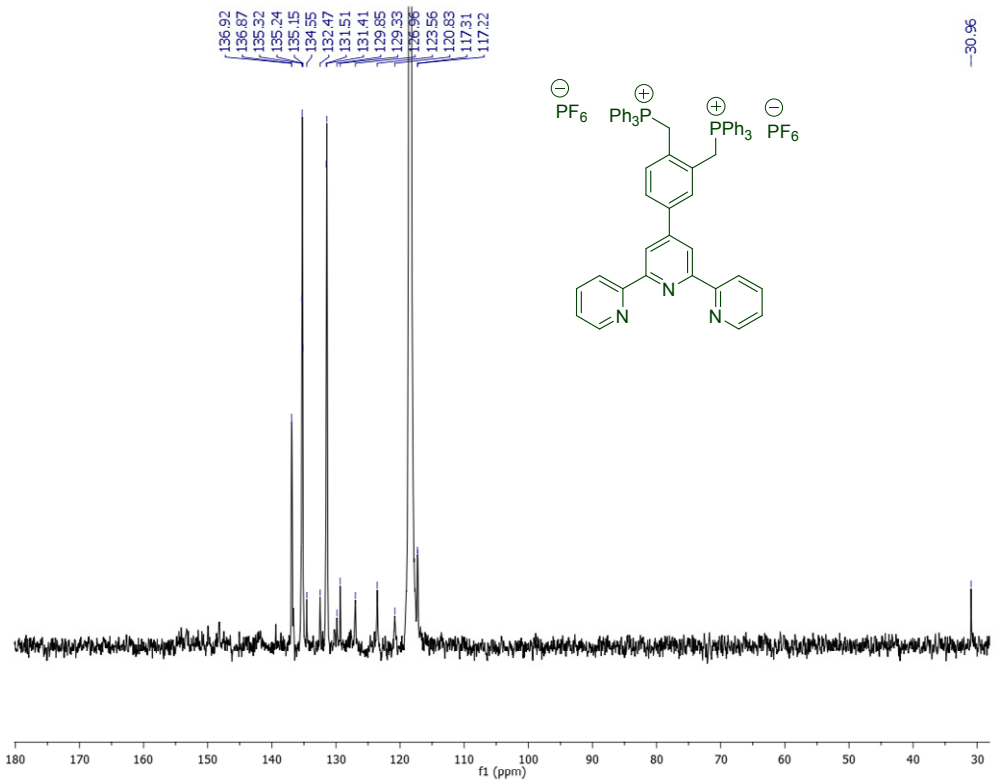

Figure 11. ^{13}C NMR spectra recorded in CD_3CN.

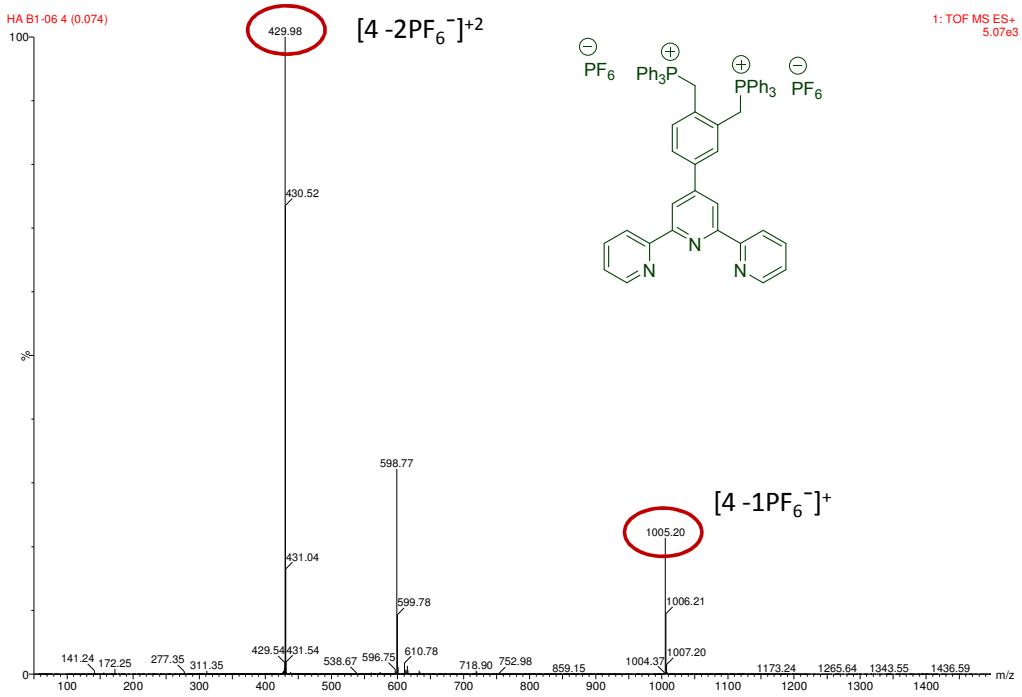

Figure 12. ESI-Ms spectra recorded in MeOH.

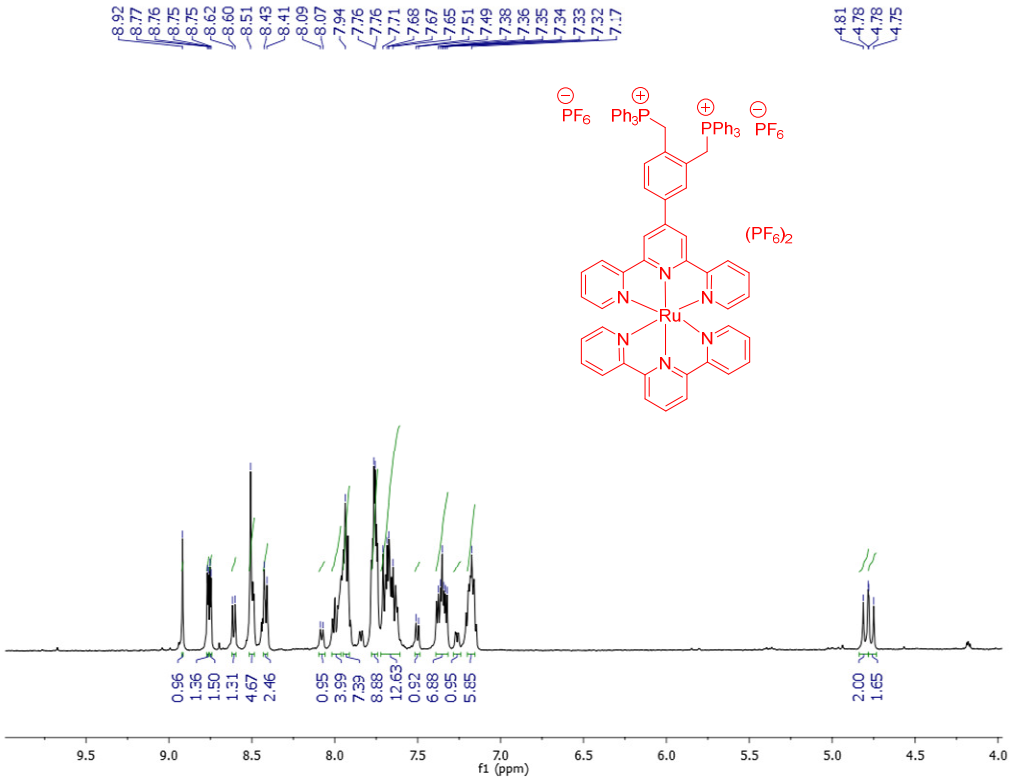

Figure 13. ^{1}H NMR spectra recorded in CD_3CN.

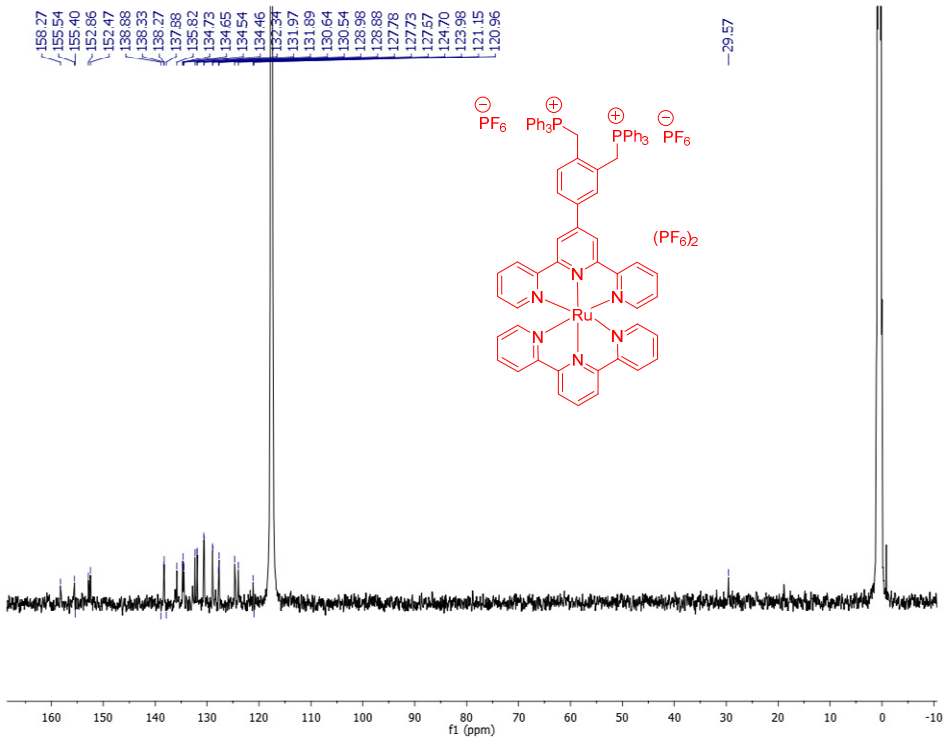

Figure 14. ^{13}C NMR spectra recorded in CD_3CN.

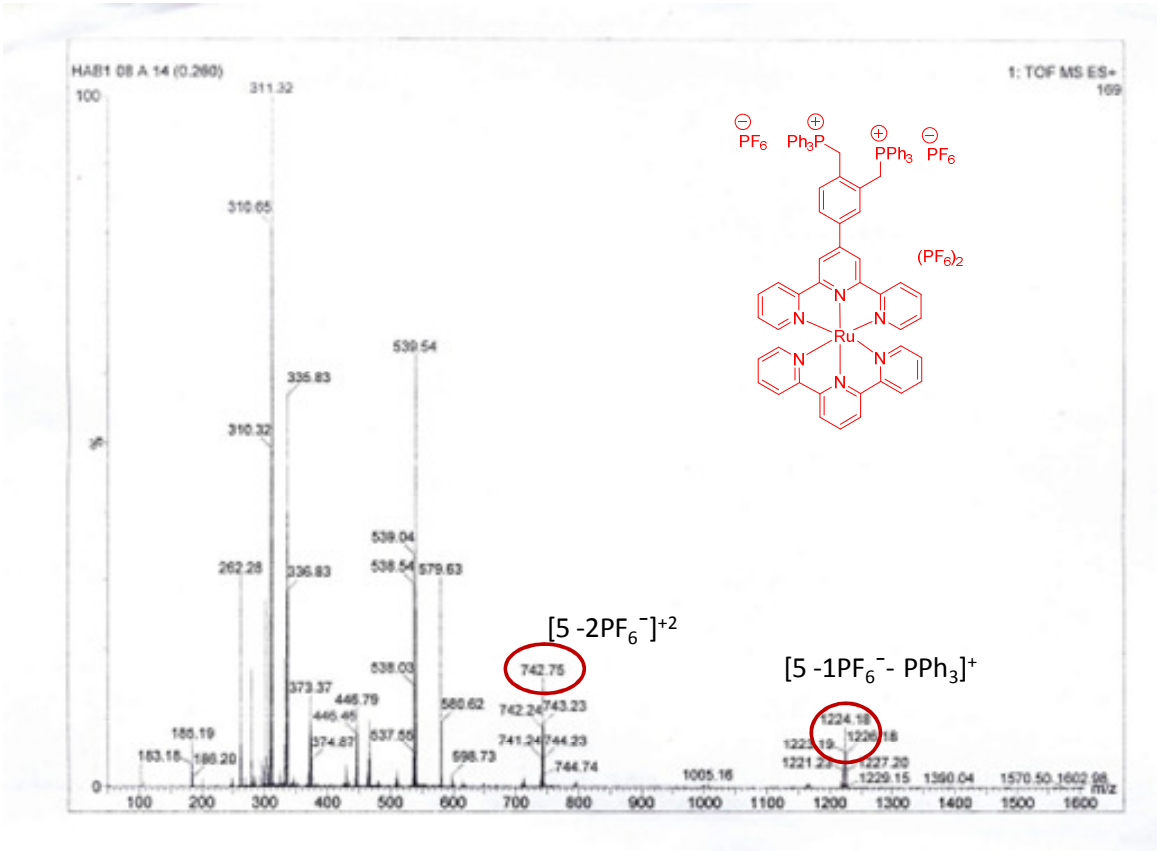

Figure 15. ESI-Ms spectra recorded in Acetonitrile.

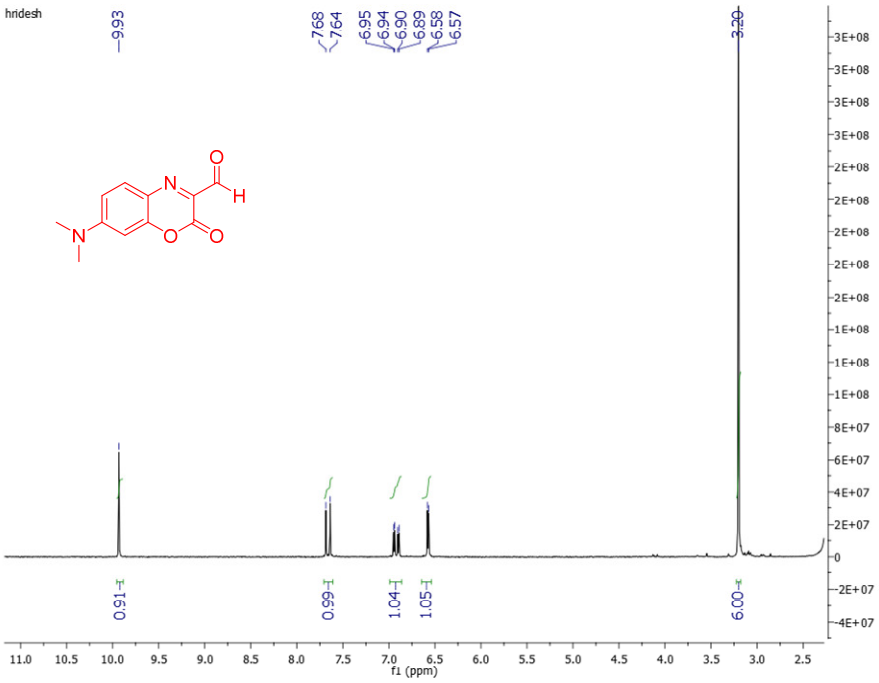

Figure 16. ^{1}H NMR spectra recorded in CD_3CN.

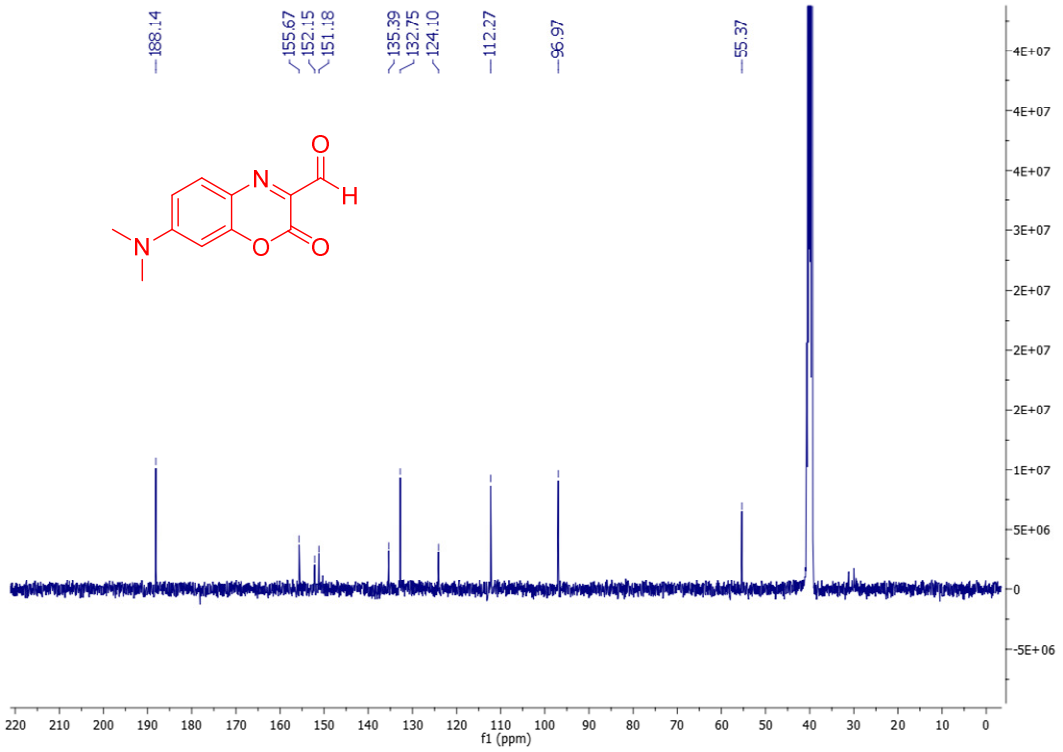

Figure 17. ^{13}C NMR spectra recorded in DMSO-d_6.

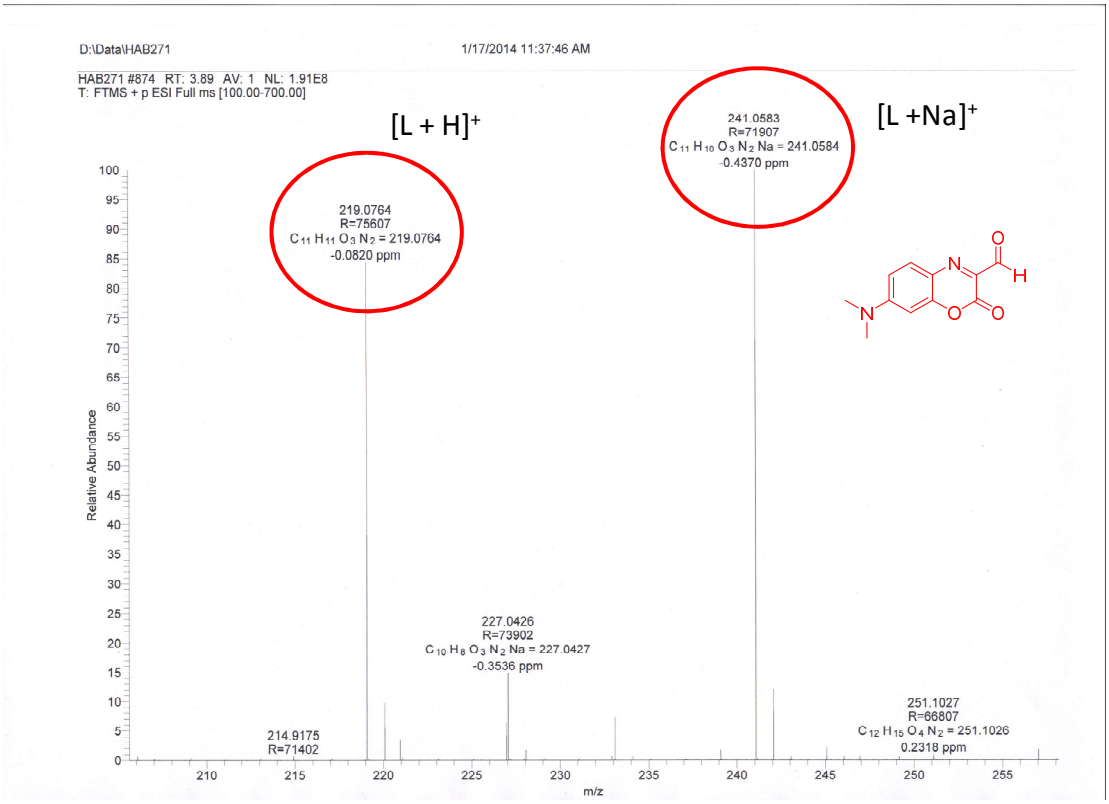

Figure 18. HRMS spectra recorded in Acetonitrile.

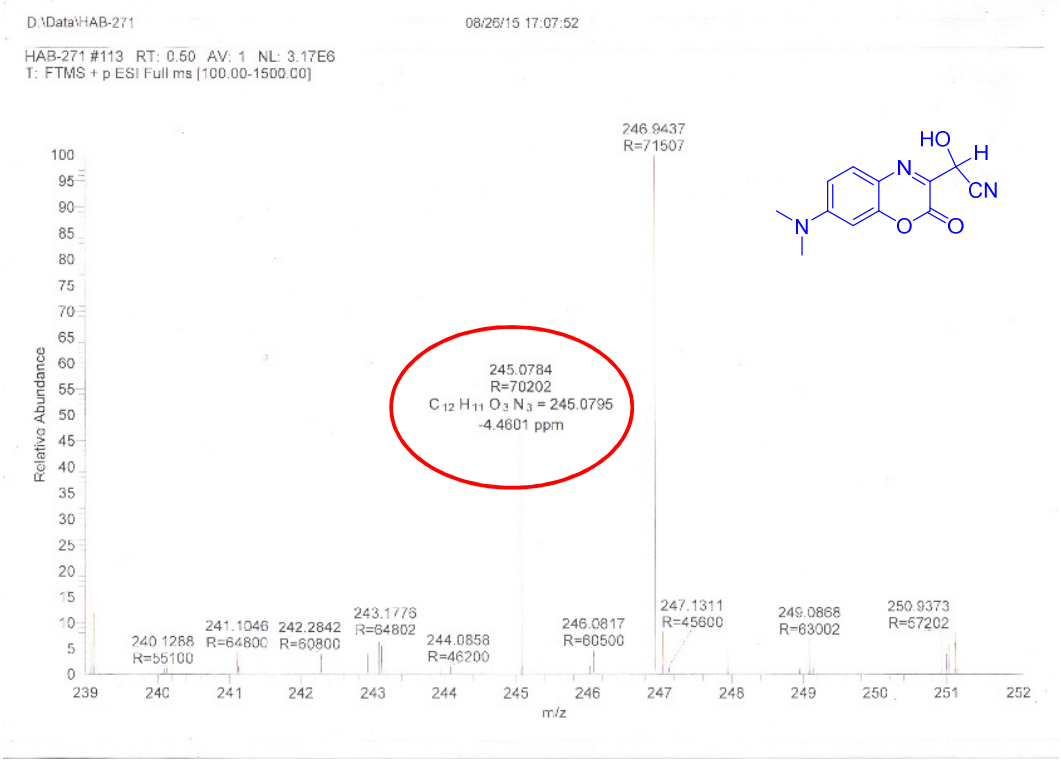

Figure 19. HRMS spectra recorded in Acetonitrile.

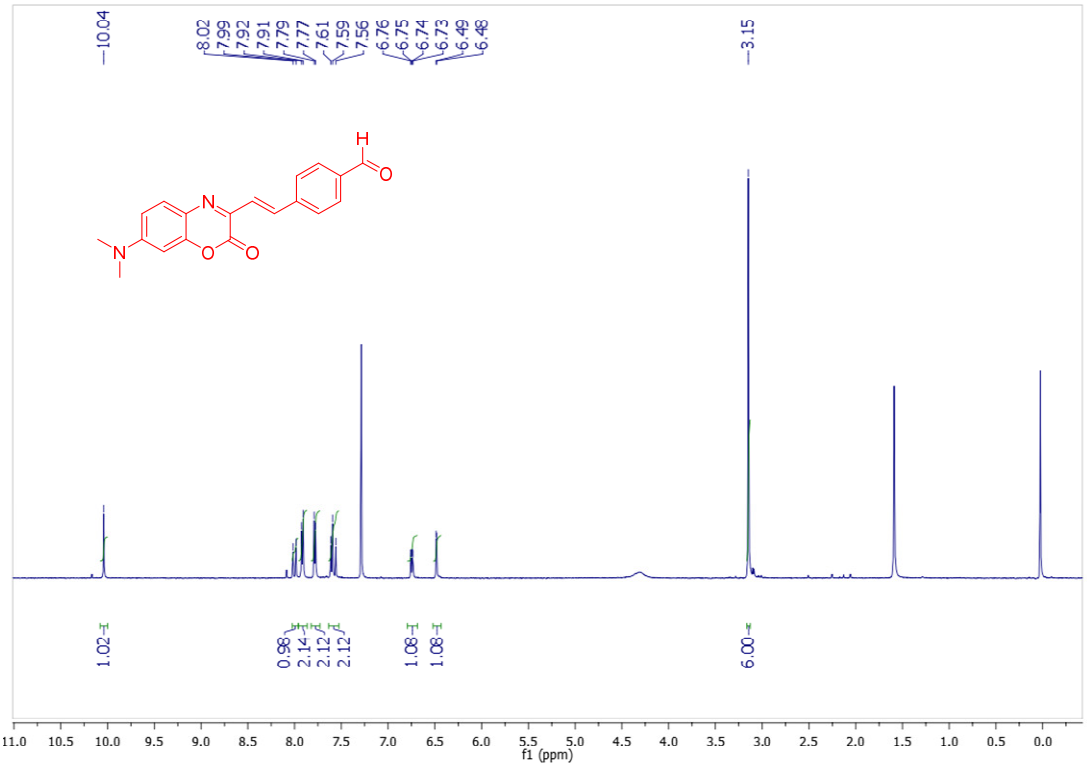

Figure 20. ^{1}H NMR spectra recorded in $CDCl_3$.

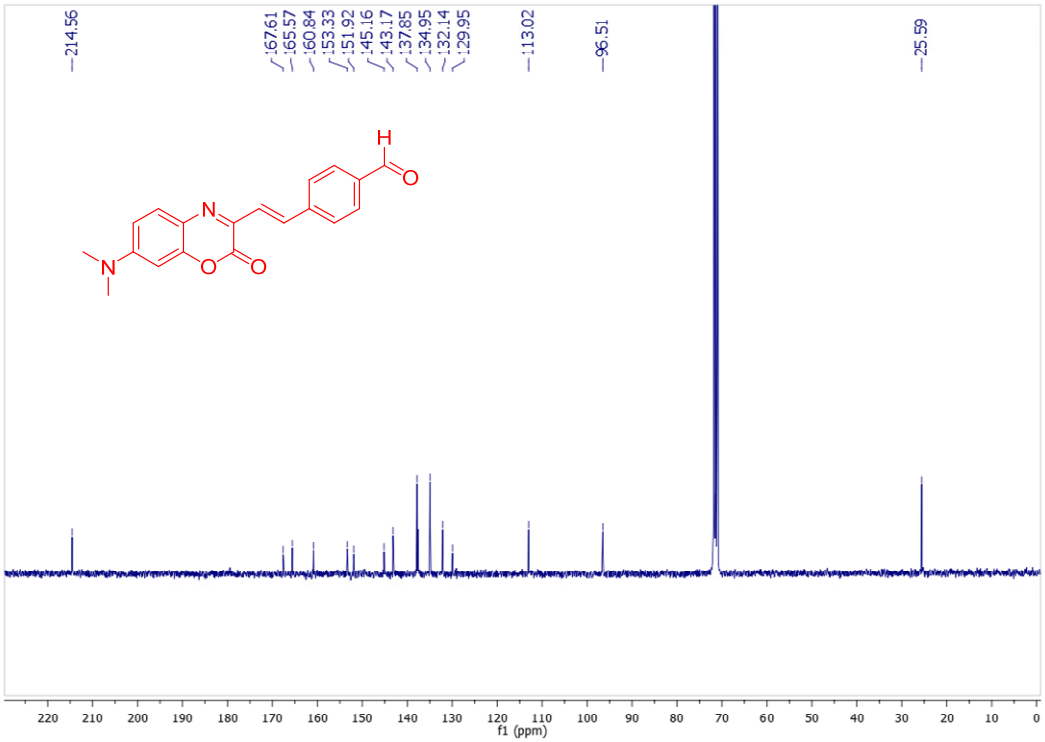

Figure 21. ^{13}C NMR spectra recorded in $CDCl_3$.

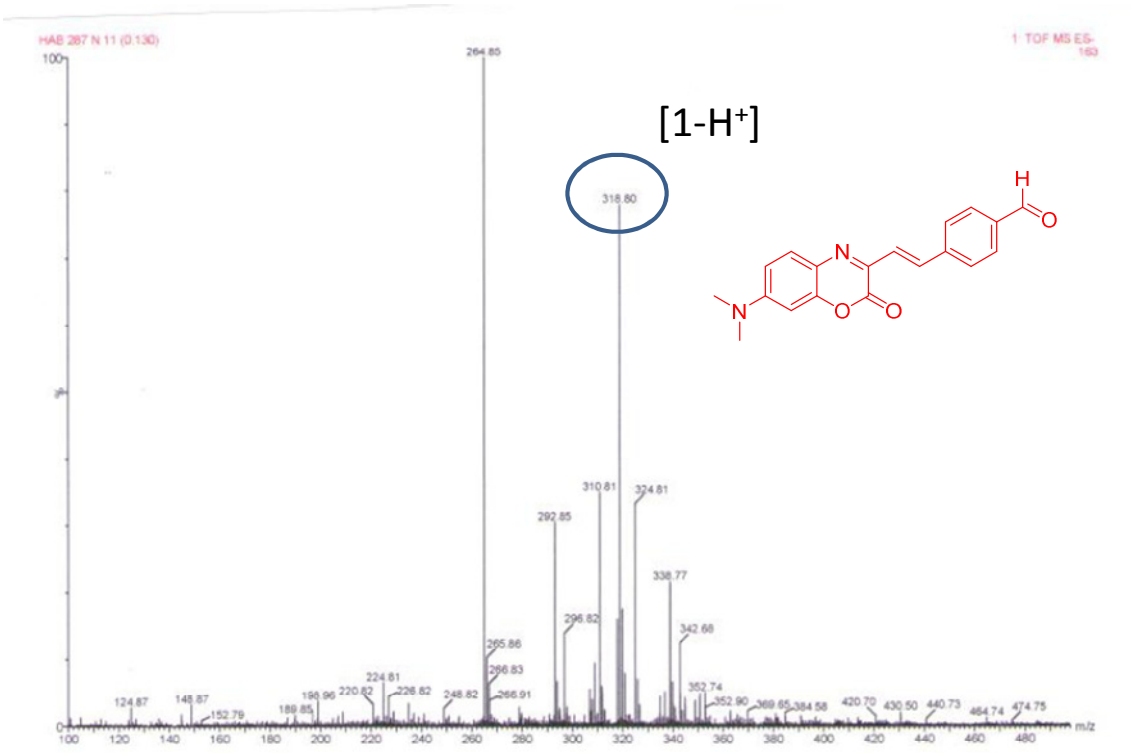

Figure 22. ESI-MS spectra recorded in Acetonitrile.

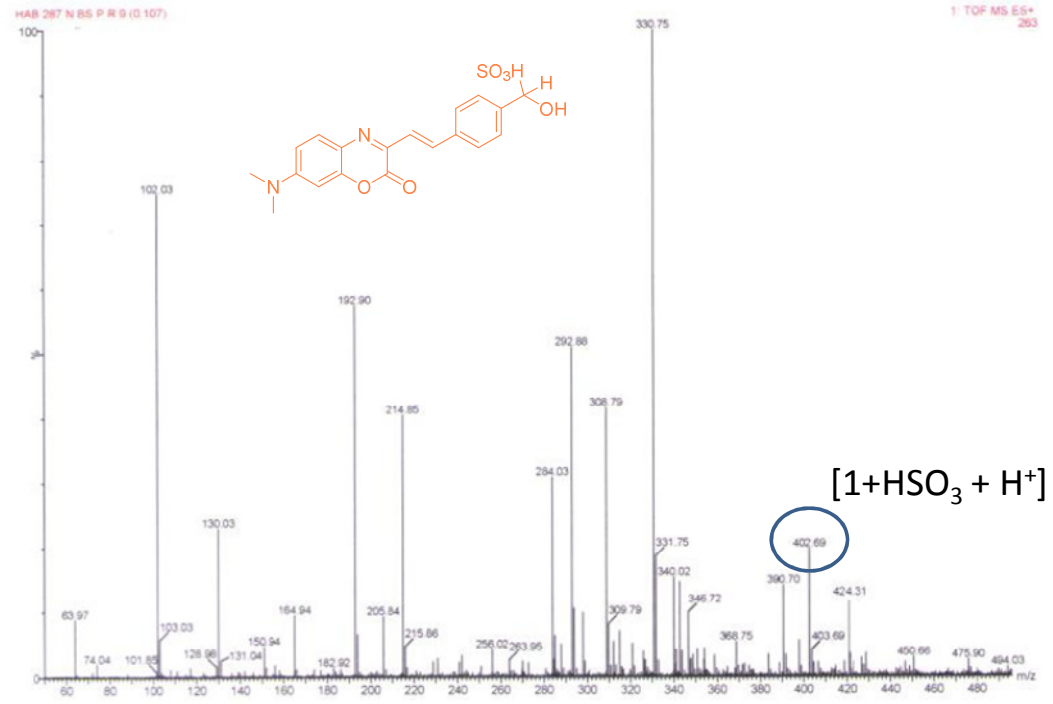

Figure 23. ESI-MS spectra recorded in Acetonitrile.

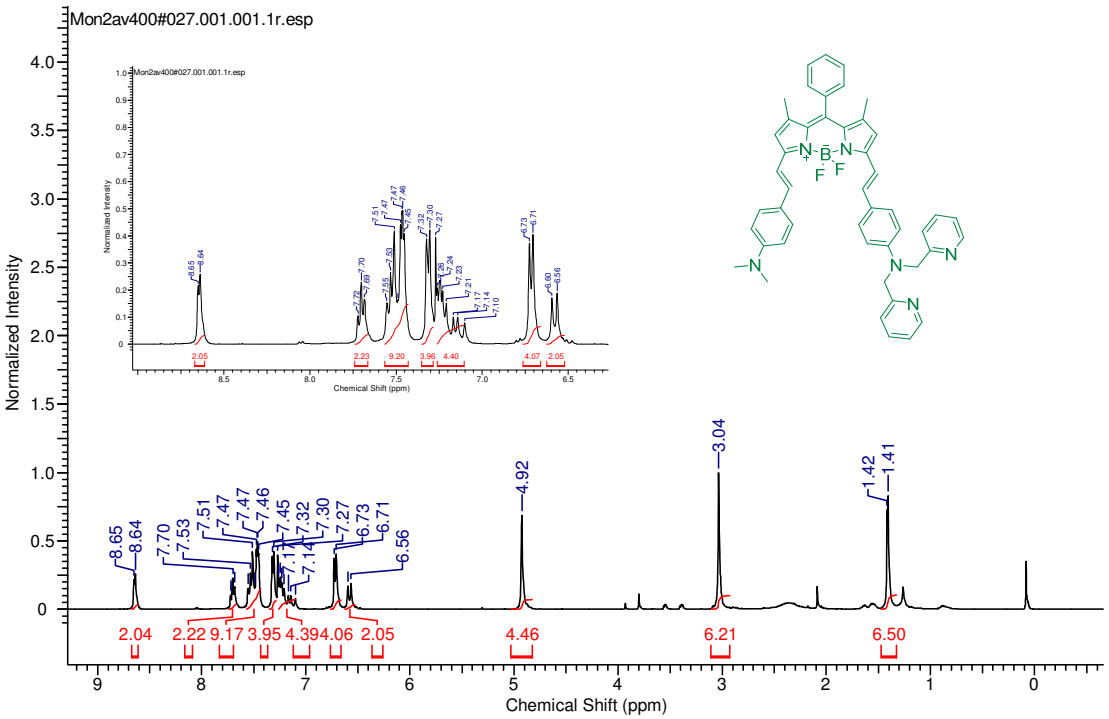

Figure 24. ^{1}H NMR spectra recorded in $CDCl_3$.

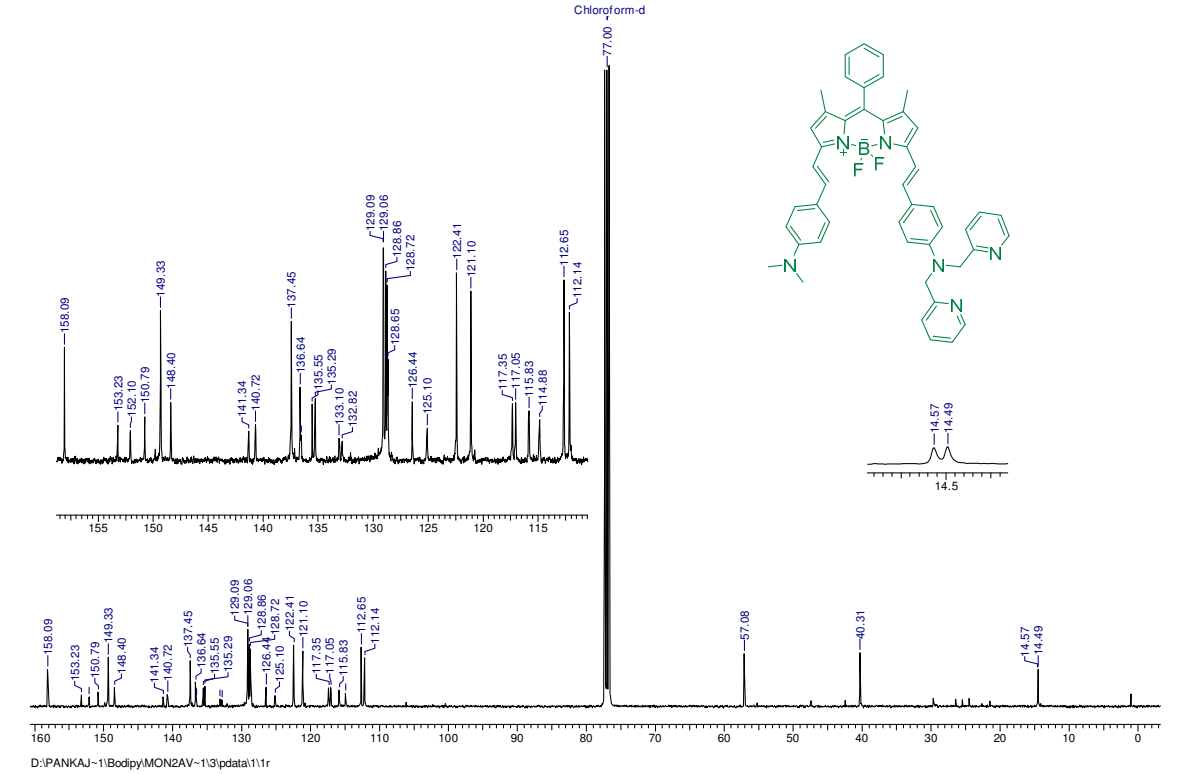

Figure 25. ^{13}C NMR spectra recorded in $CDCl_3$.

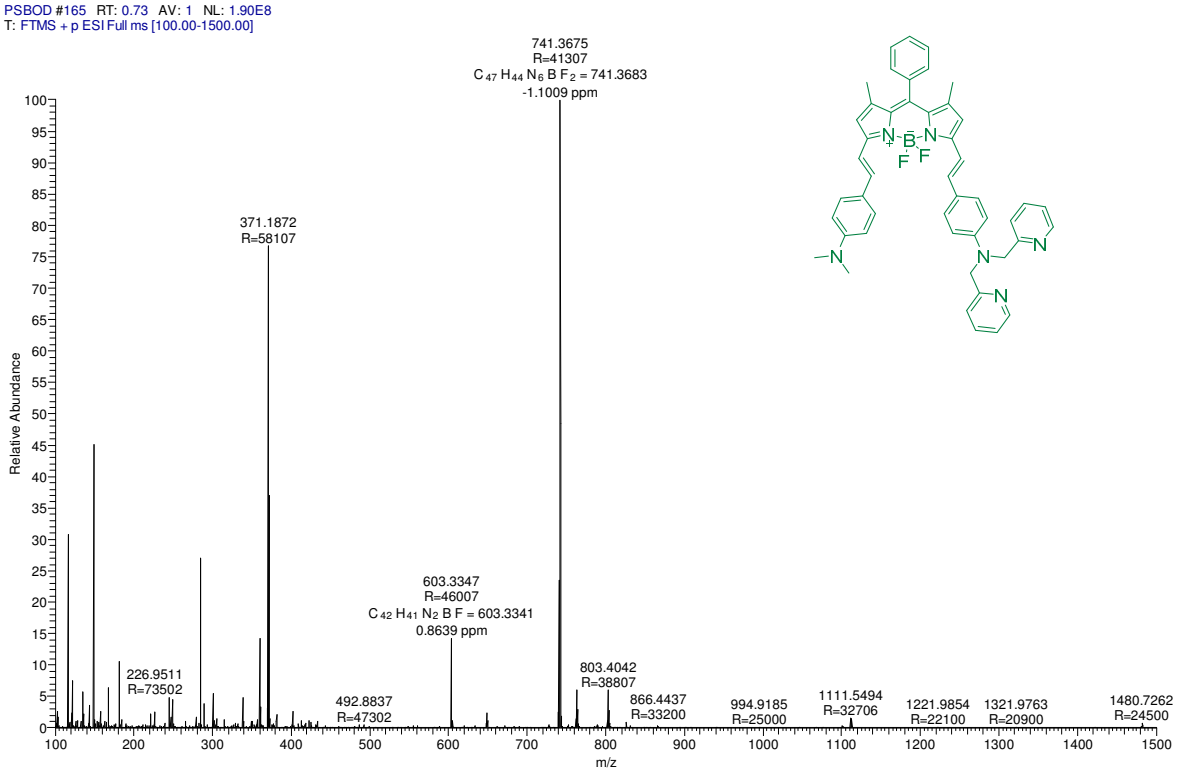

Figure 26. HRMS spectra recorded in Acetonitrile.

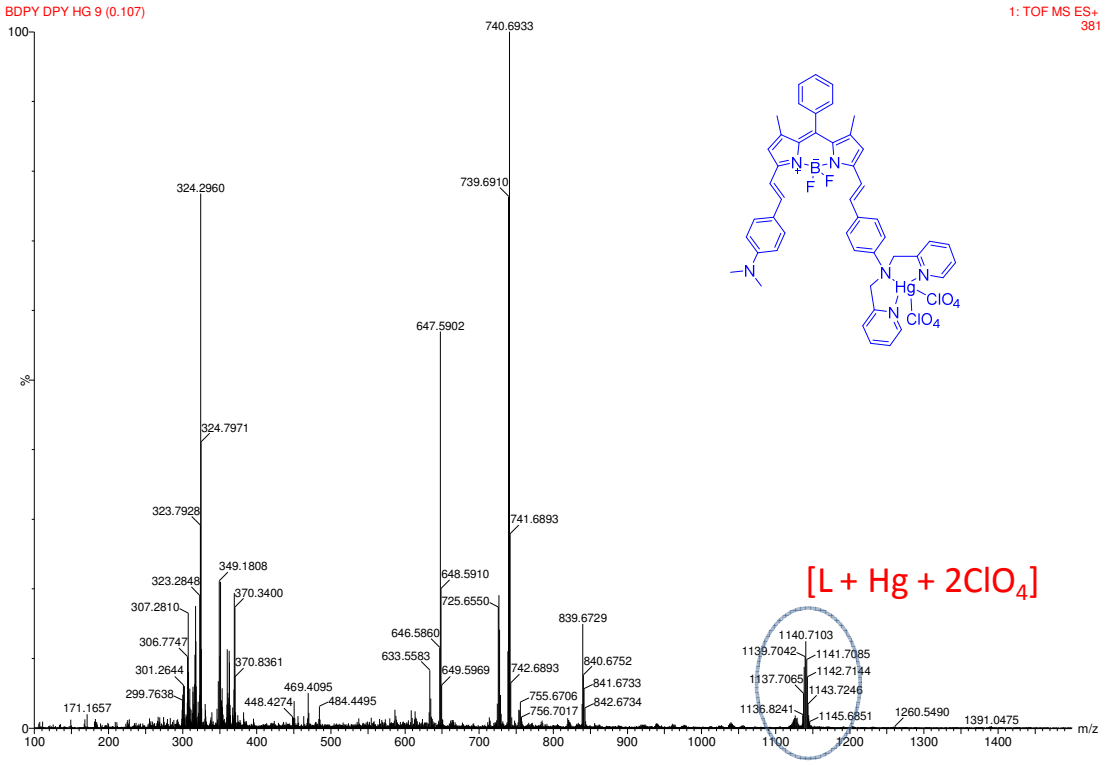

Figure 27. ESI-MS spectra recorded in Acetonitrile.

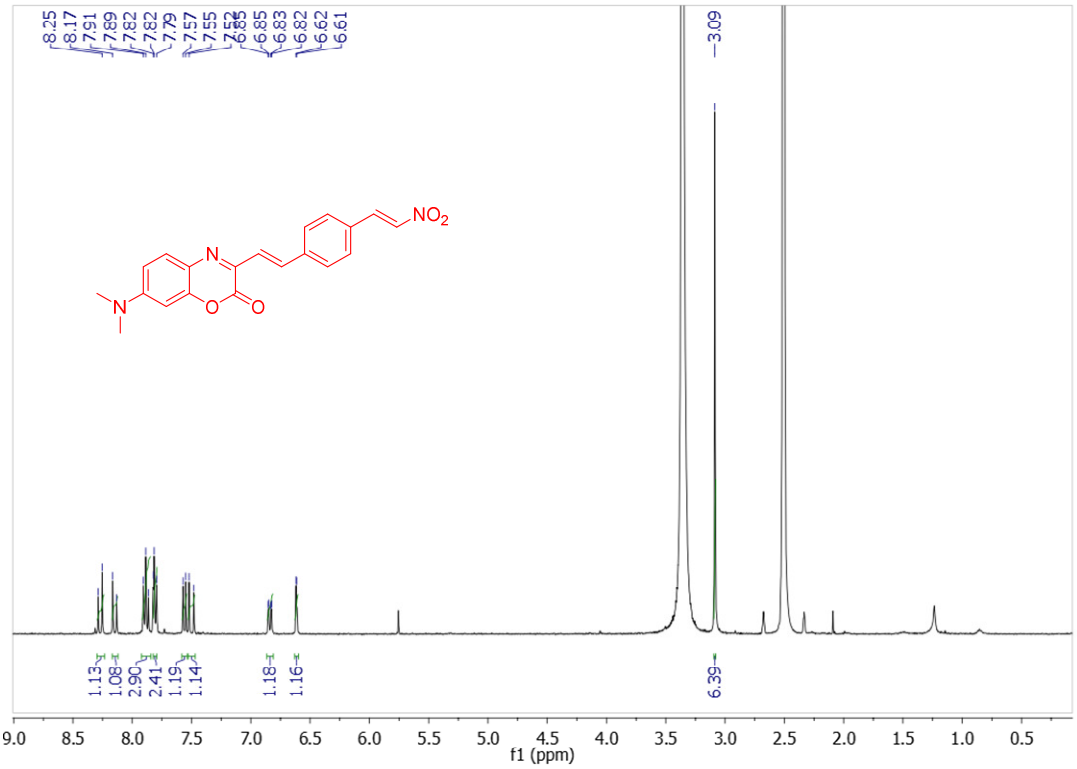

Figure 28. ^{1}H NMR spectra recorded in DMSO-d_6.

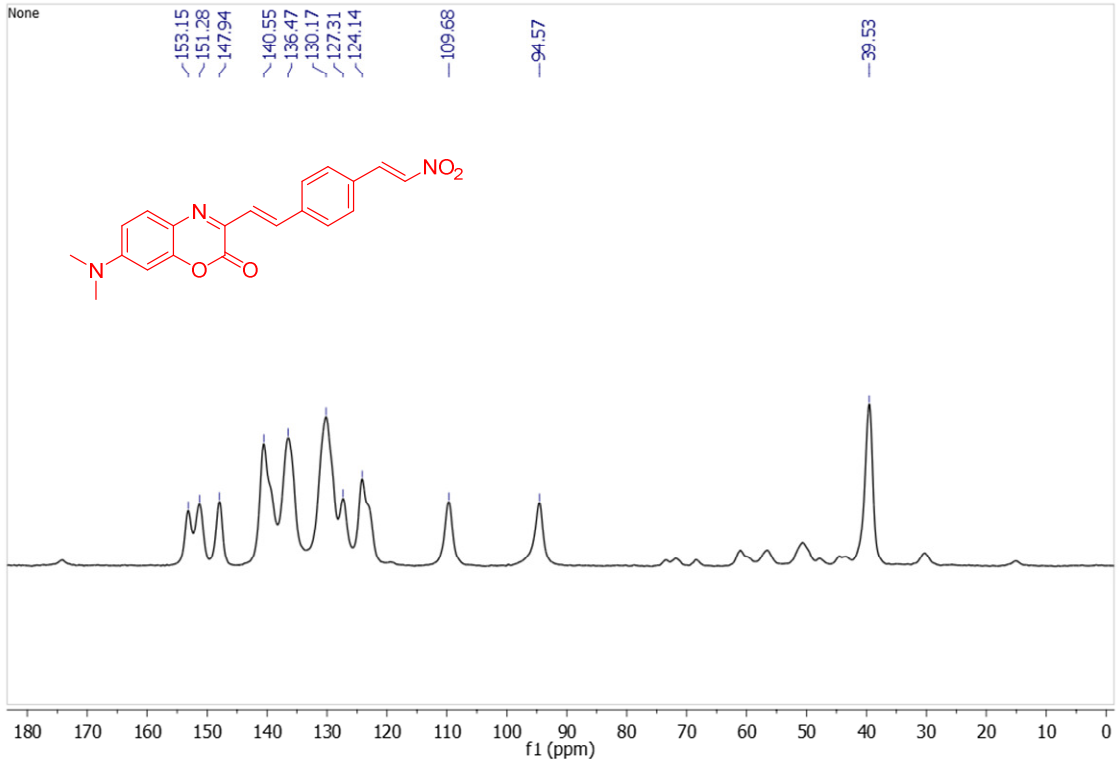

Figure 29. ^{13}C NMR spectra recorded in solid state.

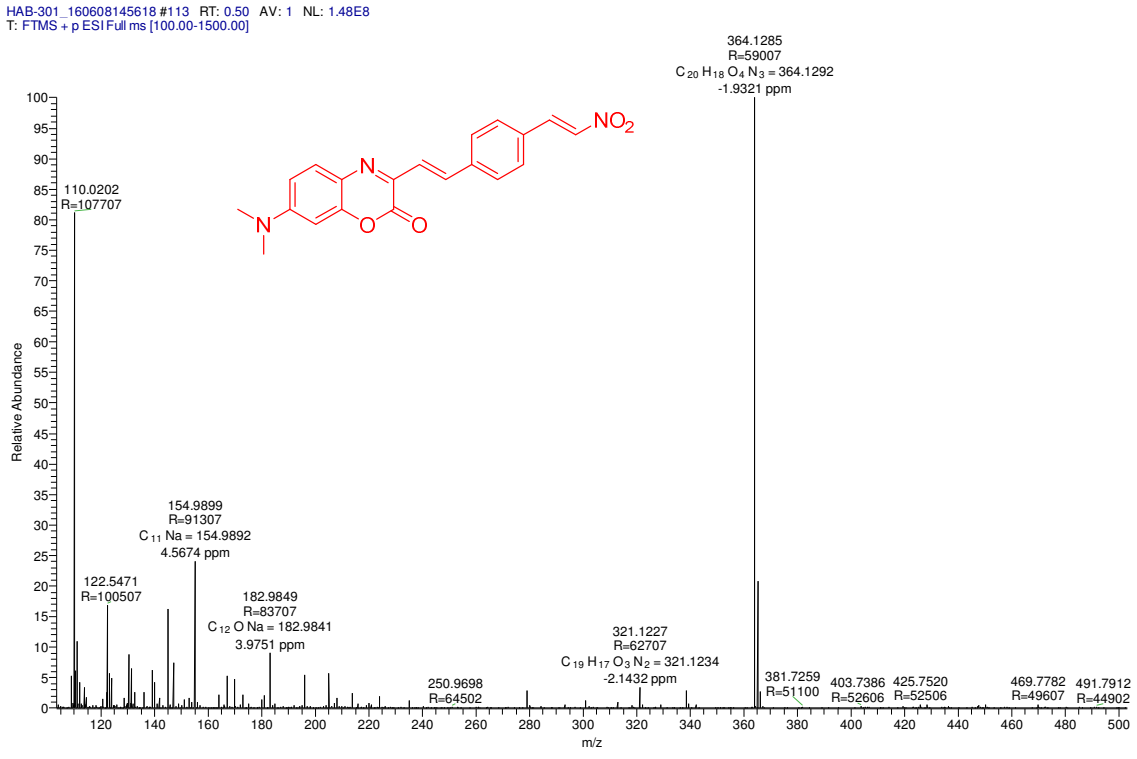

Figure 30. HRMS spectra recorded in Acetonitrile.

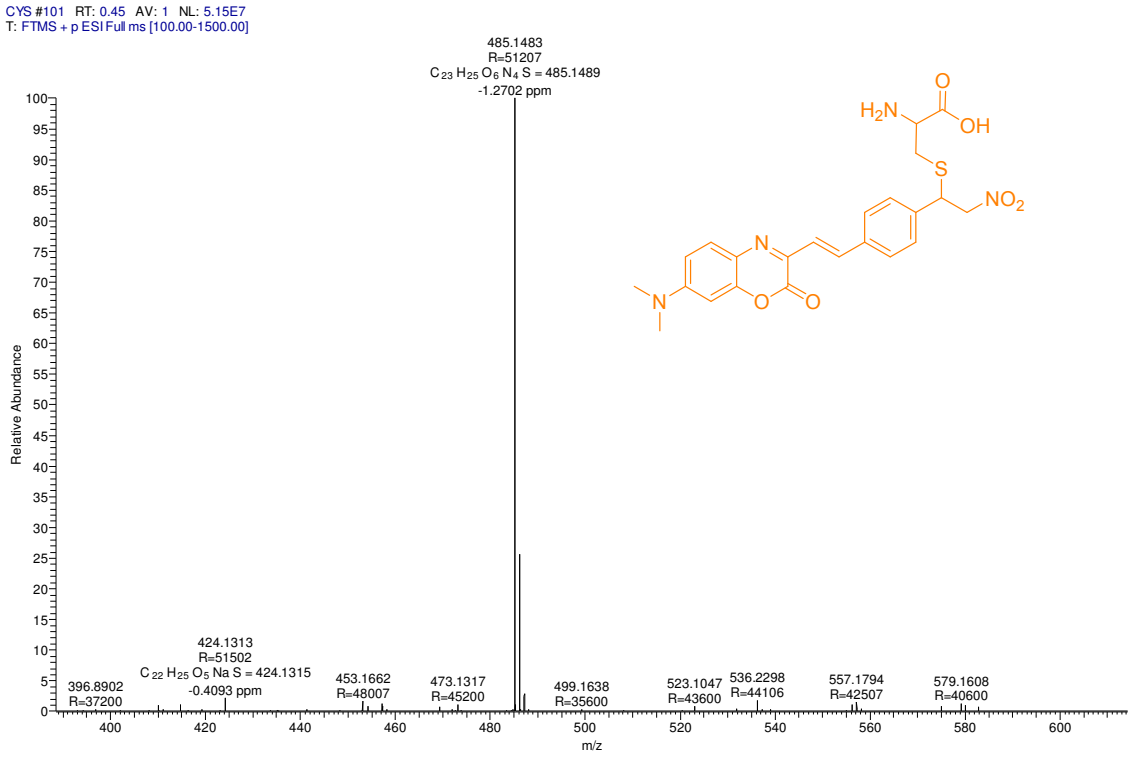

Figure 31. HRMS spectra recorded in Acetonitrile.

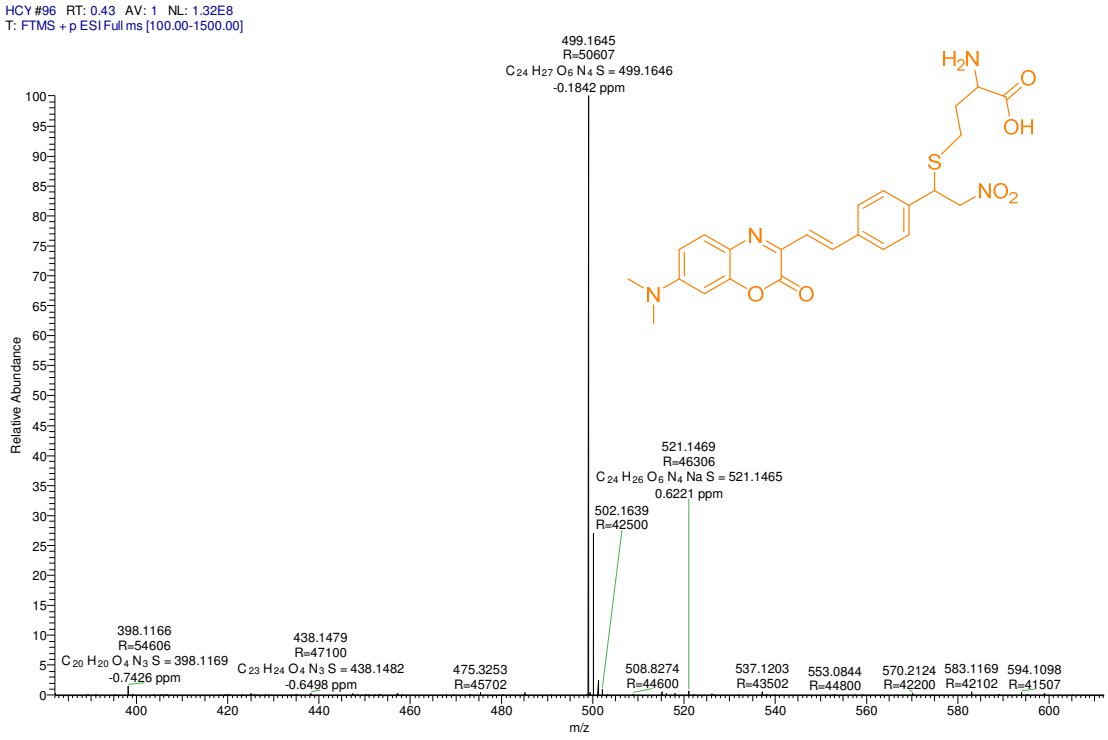

Figure 32. HRMS spectra recorded in Acetonitrile.

List of Publications Related To The Thesis

1. **Hridesh Agarwalla** , Kalyanashis Jana , Arunava Maity , Manoj K. Kesharwani , Bishwajit Ganguly and Amitava Das, Hydrogen Bonding Interaction between Active Methylene Hydrogen Atoms and an Anion as a Binding Motif for Anion Recognition: Experimental Studies and Theoretical Rationalization*, J. Phys. Chem. A, **2014,** 118, 14, 2656–2666.*

2. **Hridesh Agarwalla,** Monalisa Gangopadhyay, Dharmendar Kr. Sharma, Santanu Kr. Basu, Sameer Jadhav, Arindam Chowdhury and Amitava Das, Fluorescent Probe for Detection of Cyanide Ion in Aqueous Medium: Cellular Uptake and Assay for β-Glucosidase and HydroxynitrileLyase**.** *J. Mat. Chem. B**, 2015, 3,*** 9148-9156**.**

3. **Hridesh Agarwalla**, Suman Pal, Anirban Paul, Jun Yong woong, Bae Juryang, Divesh N. Srivastava, Kyo Han Ahn and Amitava Das, A Two-Photon Fluorescent Probe for Bisulfite Ion: Tissue Imaging. (**Under Revision in Analytical Chemistry**)

4. **Hridesh Agarwalla,** Pankaj S. Mahajan, Debashis Sahu, Nandaraj Taye, Biswajit Ganguly, Santosh B. Mhaske, Samit Chattopadhyay and Amitava Das, A Switch-On NIR Probe for Specific Detection of Hg^{2+} Ion in Aqueous Medium and in Mitochondria. (**To be communicated**).

5. **Hridesh Agarwalla,** Nandaraj Taye, Samit Chattopadhyay and Amitava Das, A Turn-on Fluorescent Probe for Detection of Bio-thiols With Large Stokes Shift in Aqueous Medium. (**To be communicated**).

List of other Publications

1. Sukdeb Saha, **Hridesh Agarwalla,** Hariom Gupta, Mithu Baidya, E. Suresh, Sudip K. Ghosh and Amitava Das, New chemodosimetric probe for the specific detection of Hg^{2+} in physiological condition and its utilisation for cell imaging studies. *Dalton Trans.***, 2013**, *42*, 15097-15105.

2. Upendar Reddy G., **Hridesh Agarwalla**, Nandaraj Taye, Suvankar Ghorai, Samit Chattopadhyay and Amitava Das, *Chem. Commun.,* **2014**, *50*, 9899-9902.

3. Arunava Maity, Firoj Ali, **Hridesh Agarwalla**, Bihag Anothumakkool and Amitava Das, *Chem. Commun.,* **2015**, *51*, 2130-2133.

4. Priyadip Das, Nellore Bhanu Chandar, Shishir Chourey, **Hridesh Agarwalla**, Bishwajit Ganguly, and Amitava Das, *Inorg. Chem.*, **2013**, *52,* 19, 11034–11041.

5. Prasenjit Mahato, Sukdeb Saha, Priyadip Das, **Hridesh Agarwalla** and Amitava Das, recognition. *RSC Adv.***, 2014**, *4*, 36140-36174.

List of Patents

1. SELECTIVE DETECTION AND ESTIMATION OF HISTIDINE AND CYSTEINE, Amitava Das, Samit Chattopadhyay, Upendar Reddy Gandra; **Hridesh Agarwalla**; Application Number Appl. no –PCT/IN2015/000250.

List of Conferences Attended

1. Poster presented in "**16th International Symposium on Modern Trends in Inorganic Chemistry**" which is held at Department of Chemistry, Jadavpur University 3rd Dec to 5th Dec 2015. (**Awarded Dalton Trans. Poster Prize**)

2. Poster Presented in "**17th CRSI National Symposium in Chemistry**" which is held at National Chemical Laboratory, Pune 6-8 Feb 2015.

3. Participated in "**International Conference on Structural and Inorganic Chemistry"** which held at National Chemical Laboratory, Pune on 4th – 5th Dec 2014.

4. Poster Presented in "National Science Day Celebration 2015" at CSIR-National Chemical Laboratory, Pune on 25-26th of February 2015.

5. Poster Presented in "National Science Day 2014 Celebration 2014" at CSIR-National Chemical Laboratory, Pune on 25-26th of February 2014.

THE JOURNAL OF PHYSICAL CHEMISTRY A

Article

pubs.acs.org/JPCA

Hydrogen Bonding Interaction between Active Methylene Hydrogen Atoms and an Anion as a Binding Motif for Anion Recognition: Experimental Studies and Theoretical Rationalization

Hridesh Agarwalla,[†] Kalyanashis Jana,[‡] Arunava Maity,[†] Manoj K. Kesharwani,[‡] Bishwajit Ganguly,*[,‡] and Amitava Das*[,†]

[†]Organic Chemistry Division, CSIR-National Chemical Laboratory, Pune 411008, Maharashtra, India

[‡]CSIR-Central Salt & Marine Chemicals Research Institute, Bhavnagar 364002, Gujarat, India

Supporting Information

ABSTRACT: Two new reagents, having similar spatial arrangements for hydrogen atoms of the active methylene functionalities, were synthesized and interactions of such reagents with different anionic analytes were studied using electronic spectroscopy as well as by using ^{1}H and ^{31}P NMR spectroscopic methods. Experimental studies revealed that these two reagents showed preference for binding to F^- and OAc^-. Detailed theoretical studies along with the above-mentioned spectroscopic studies were carried out to understand the contribution of the positively charged phosphonium ion, along with methylene functionality, in achieving the observed preference of these two receptors for binding to F^- and OAc^-. Observed differences in the binding affinities of these two reagents toward fluoride and acetate ions also reflected the role of acidity of such methylene hydrogen atoms in controlling the efficiencies of the hydrogen bonding in anion$-H_{methylene}$ interactions. Hydrogen bonding interactions at lower concentrations of these two anionic analytes and deprotonation equilibrium at higher concentration were observed with associated electronic spectral changes as well as visually detectable change in solution color, an observation that is generally common for other strong hydrogen bond donor functionalities like urea and thiourea. DFT calculations performed with the M06/6-31+G**//M05-2X/6-31G* level of theory showed that F^- binds more strongly than OAc^- with the reagent molecules. The deprotonation of methylene hydrogen atom of receptors with F^- ion was observed computationally. The metal complex as reagent showed even stronger binding energies with these analytes, which corroborated the experimental results.

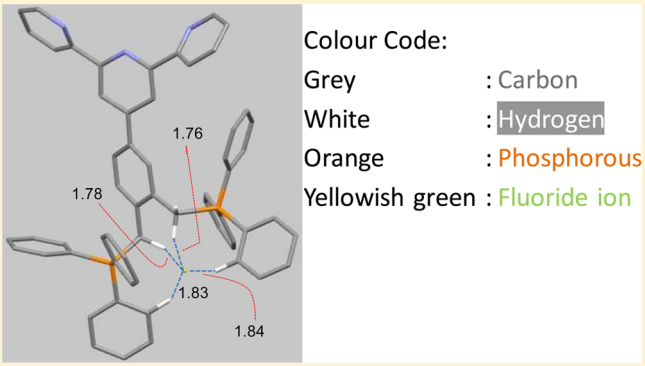

INTRODUCTION

Specific recognition and sensing of anions are important due to the diverse roles that anions play in chemical and biological events. It is crucial to develop insights for understanding the various interactions or binding motifs that one can actually use for recognition of such anionic analytes.[1,2] Consequently, there is a large interest for specific and selective recognition of anions that have adverse influences on human physiology.[3] Among the vast family of anions the most explored individual is the F^- ion owing to its duplicitous nature. F^- is essential for the prevention of dental caries and treatment of osteoporosis[4] and it is used in anesthetic, hypnotic, and psychiatric drugs and military nerve gases.[5] Fluorosis and neurological and metabolic disorders are reported to be caused by an exposure to a higher amount of F^- and this can even lead to cancer.[6] A more recent report suggests that higher F^- may also cause osteosarcoma.[7] All these have contributed to an exponential growth in research for specific recognition of fluoride ion, which is generally achieved through ion−dipole interaction (hydrogen bonding interaction),[8] electrostatic interaction,[9] binding induced perturbation of the π-conjugation framework,[10] or the F^- triggered chemical reaction (chemodosimetric pathway) to bring about change in the optical signal of the molecule.[11] Among these, the most common methodology that is adopted for designing receptor molecule for reversible binding and recognition of fluoride ion is based on hydrogen bonding interactions. For such interactions, geometry and spatial orientation(s) of the hydrogen bond donor fragment(s) with respect to the fluoride ion play a very crucial role.[12] Despite several reports, the basic understanding that governs such interaction and thus the binding efficiency is not very well understood. Recently, it has been argued that a dual approach, having a H-bond donor group along with a nearby positively charge center would enhance the recognition process. Positive charge increases the acidity of the protons and, thus, is expected to enhance the hydrogen bond donating ability as well as to provide an additional electrostatic interaction for anions.[13] Two

Received: December 20, 2013
Published: March 20, 2014

Journal of
Materials Chemistry B

PAPER

View Article Online
View Journal | View Issue

Cite this: J. Mater. Chem. B, 2015, 3, 9148

Fluorescent probes for the detection of cyanide ions in aqueous medium: cellular uptake and assay for β-glucosidase and hydroxynitrile lyase†

Hridesh Agarwalla,[a] Monalisa Gangopadhyay,[a] Dharmendar Kumar Sharma,[b] Santanu Kumar Basu,[c] Sameer Jadhav,[c] Arindam Chowdhury*[b] and Amitava Das*[a]

Received 7th September 2015,
Accepted 29th October 2015

DOI: 10.1039/c5tb01853f

www.rsc.org/MaterialsB

A chemodosimteric reagent (**1**) for the efficient detection of cyanide species (CN^- and/or HCN) in aq. medium as well as under physiological conditions has been described. Selective reaction of the cyanide species with this reagent in the presence of all common interfering anions, amino acids and glutathione (GSH) led to the generation of the corresponding cyanohydrin derivative. The formation of the cyanohydrin derivative of the probe is associated with a visually detectable change in solution fluorescence in aq. buffer medium with 1.9 μM NaCN, the threshold limit set by WHO for the safe drinking water and this makes this fluorogenic sensor an ideal candidate for in-field applications. An apparent switch on the luminescence response, ultralow detection limit, low response time, cell membrane permeability and insignificant toxicity are key features of a probe molecule, which gives it a distinct edge over previously reported chemodosimetric reagents for the detection of cyanide species (CN^- or HCN) in an aqueous environment. This methodology could be used for developing a generalized and efficient fluorescence-based assay for crucial enzymes like β-glucosidase and hydroxynitrile lyase. Furthermore, spectrally-resolved fluorescence microscopy measurements on single-cells revealed that this sensor molecule could also be used for imaging the cellular uptake of cyanide species from aq. solution contaminated with NaCN. Our results confirmed that statistical analysis of integrated intensity and transition energy obtained from the emission spectra collected over various microscopic sub-cellular regions can potentially be used to discriminate the effects of local cellular environments and that due to cyanide detection.

Introduction

The design and synthesis of new chemosensors for the recognition of specific anions that have serious biological effects is of immense importance for chemists and biologists who are active in the area of diagnostics as well as in studies involving biological and environmental events.[1] Among various toxic anions, the cyanide ion (CN^-) is considered to be the most toxic and its acute toxicity towards mammals primarily arises from its adverse influences on the central nervous system.[2] Cyanide primarily binds to metallic cofactors in metalloenzymes, adversely influencing the enzyme and cell function. It inhibits the activity of Cytochrome-*c* oxidase and causes histotoxic hypoxia, which further adds to the toxicity by reducing the unloading gradient of oxyhemoglobin.[3] Cyanide is also known to inhibit the activity of enzymes like catalase, peroxidase, hydroxocobalamin, phosphatase, tyrosinase, ascorbic acid oxidase, xanthine oxidase, and succinic dehydrogenase. These also contribute to cyanide's acute toxicity.[4,5,9] Despite influences on living organisms, cyanide is extensively used in various industries like metal gold mining, electroplating, petrochemical, synthetic fibers and the resin industry.[6] Regardless of environmental consciousness, a certain amount of this toxic ion escapes into the environment either as water soluble cyanide species or as HCN. Some fruits and vegetables such as cassava, lima beans, and bitter almond also contain high levels of cyanogenic glycosides which are potential sources of cyanide in the presence of certain enzymes and can be lethal if not processed properly before consumption.[7] The World Health Organization (WHO) has set the maximum allowed cyanide contaminant in drinking water to be 1.9 μM.[8] Due to its extreme physiological toxicities, a suitable reagent for the efficient and preferential recognition of cyanide species in

[a] Organic Chemistry Division, CSIR-National Chemical Laboratory, Pune 411008, India. E-mail: a.das@ncl.res.in; Fax: +91(0)25902629; Tel: +91(0)25902385
[b] Department of Chemistry, Indian Institute of Technology Bombay, Powai, Mumbai 400 076, India
[c] Chemical Engineering, Indian Institute of Technology Bombay, Powai, Mumbai 400 076, India. E-mail: arindam@chem.iitb.ac.in; Fax: +91(0)22-2576 7152; Tel: +91(0)22-2576 7154

† Electronic supplementary information (ESI) available. See DOI: 10.1039/c5tb01853f